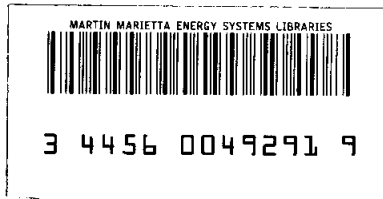


ornl

OAK
RIDGE
NATIONAL
LABORATORY

UNION
CARBIDE

OPERATED BY
UNION CARBIDE CORPORATION
FOR THE UNITED STATES
DEPARTMENT OF ENERGY



ORNL/TM-7755

Iodine Sorption on Low-Chromium Alloy Steel

M. F. Osborne
R. B. Briggs
R. P. Wichner

OAK RIDGE NATIONAL LABORATORY

CENTRAL RESEARCH LIBRARY

CIRCULATION SECTION

4500N ROOM 175

LIBRARY LOAN COPY

DO NOT TRANSFER TO ANOTHER PERSON

If you wish someone else to see this
report, send in name with report and
the library will arrange a loan.

UCN-7969 3 9-77

Printed in the United States of America. Available from
National Technical Information Service
U.S. Department of Commerce
5285 Port Royal Road, Springfield, Virginia 22161
NTIS price codes—Printed Copy: A09 Microfiche: A01

This report was prepared as an account of work sponsored by an agency of the United States Government. Neither the United States Government nor any agency thereof, nor any of their employees, makes any warranty, express or implied, or assumes any legal liability or responsibility for the accuracy, completeness, or usefulness of any information, apparatus, product, or process disclosed, or represents that its use would not infringe privately owned rights. Reference herein to any specific commercial product, process, or service by trade name, trademark, manufacturer, or otherwise, does not necessarily constitute or imply its endorsement, recommendation, or favoring by the United States Government or any agency thereof. The views and opinions of authors expressed herein do not necessarily state or reflect those of the United States Government or any agency thereof.

ORNL/TM-7755
Dist. Category UC-77

Contract No. W-7405-eng-26

CHEMICAL TECHNOLOGY DIVISION

HTGR BASE TECHNOLOGY PROGRAM
HTGR Chemistry Studies (189a 01329)

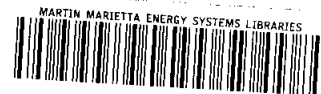
IODINE SORPTION ON LOW-CHROMIUM ALLOY STEEL

M. F. Osborne
R. B. Briggs*
R. P. Wichner

*Consultant.

Date Published: January 1982

Prepared by the
OAK RIDGE NATIONAL LABORATORY
Oak Ridge, Tennessee 37830
operated by
UNION CARBIDE CORPORATION
for the
DEPARTMENT OF ENERGY



3 4456 0049291 9

CONTENTS

	<u>Page</u>
ABSTRACT	1
1. SUMMARY	1
2. INTRODUCTION	5
2.1 Purpose of Work	5
2.2 Scope of Investigation	5
2.3 Applications for Data	6
3. REVIEW OF PREVIOUS STUDIES OF IODINE SORPTION ON STEEL	8
4. PREDOMINANT IODINE SPECIES IN THE GAS PHASE	11
5. EXPERIMENTAL APPARATUS AND PROCEDURE	14
5.1 Test Apparatus	14
5.2 Metal Sorption Specimens	19
5.3 Instrumentation	20
5.4 Iodine Source and Saturator	22
5.5 Operating Procedure	23
5.6 Experiment Disassembly and Posttest Measurements	25
6. RESULTS AND ANALYSIS	26
6.1 Equilibrium Adsorption Measurements	26
6.2 Adsorption and Desorption Rates	36
6.3 Conclusions	55
7. FUTURE WORK	57
8. ACKNOWLEDGMENTS	58
9. REFERENCES	59
10. APPENDIXES	63
Appendix A. THERMODYNAMIC EQUILIBRIUM CALCULATIONS	65
Appendix B. CHARACTERIZATION OF METAL ADSORPTION SPECIMENS	83
Appendix C. PREPARATION OF ELEMENTAL IODINE SOURCE MATERIAL	89
Appendix D. DETECTOR CALIBRATIONS AND ACTIVITY PROFILES FOR SPECIMENS	91
Appendix E. BRIEF DESCRIPTIONS OF EXPERIMENTS	99
E.1 Experiment A-4	99
E.2 Experiment A-5	105
E.3 Experiment A-6	112

E.4	Experiment A-7	119
E.5	Experiment A-8	126
E.6	Experiment A-9	134
E.7	Experiment A-10	140
E.8	Experiment A-11	141
E.9	Experiment A-12	143
E.10	Experiment A-13	153

Appendix F.	CALCULATION OF THE CONCENTRATION OF IODINE IN THE GAS AND ON THE SURFACES OF THE SPECIMENS FOR THE CONDITION THAT THE EQUILIBRIUM CONCENTRATION ON THE SURFACE IS PROPORTIONAL TO THE CONCENTRATION IN THE GAS	179
-------------	--	-----

Appendix G.	MASS TRANSPORT ANALYSIS FOR ADSORPTION SPECIMENS	183
-------------	---	-----

IODINE SORPTION ON LOW-CHROMIUM ALLOY STEEL

M. F. Osborne
R. B. Briggs*
R. P. Wichner

ABSTRACT

Studies of iodine sorption on low-alloy steel in helium atmosphere included both computer calculations and experimental measurements under conditions that could be related to the high-temperature gas-cooled reactor (HTGR). Adsorption measurements provide data on the potentially releasable inventory of iodine (a major radiological hazard) stored on surfaces in the coolant circuit during normal operation. Measurements of the rate and extent of iodine desorption when test conditions were changed are useful for evaluating the consequences of accidents.

The results of calculations with the SOLGASMIX-PV computer program indicated that HI is the dominant iodine species in the system and that the deposition of $\text{CrI}_2(\text{s})$ or $\text{FeI}_2(\text{s})$ in the cooler regions will effectively limit the amount of iodine in the gas phase. Experimental measurements were obtained on 2-1/4% Cr-1% Mo steel specimens at iodine burdens as low as 10^{-6} Pa (10^{-11} atm), about 100 times lower than any previous work. Equilibrium iodine loadings were very sensitive to specimen surface condition, being reduced with oxidation. Loadings on unoxidized specimens ranged from ~ 0.001 $\mu\text{g I/cm}^2$ at 10^{-4} Pa (10^{-9} atm) and 800°C to ~ 4 $\mu\text{g I/cm}^2$ at 3×10^{-5} Pa (3×10^{-10} atm) and 400°C . Temperature increases of 100 to 200°C caused rapid desorption of large fractions of the absorbed iodine, and sites with a spectrum of activation energies for desorption were indicated.

1. SUMMARY

The equilibrium sorption of iodine on 2-1/4% Cr-1% Mo steel in flowing helium was investigated at conditions that could be compared to those in the coolant circuit of a high-temperature gas-cooled reactor (HTGR).

*Consultant.

The purpose of this work was to provide data on adsorption and subsequent desorption which could be used in the assessment of HTGR safety. The results of our investigations to date — about two years of a three-year program — are presented in this report. A final report will be prepared upon completion of additional work. Efforts included computer calculations to determine the partial pressures of the various iodine species as functions of temperature, hydrogen pressure, and oxygen pressure. Whereas most of the earlier experimental studies had examined iodine sorption on low-alloy steels at iodine burdens (defined as the partial pressure if all iodine in the gas phase were converted to the monatomic form) greater than $\sim 10^{-2}$ Pa ($\sim 10^{-7}$ atm)*, these experiments were concentrated in the range 10^{-6} to 10^{-3} Pa (10^{-11} to 10^{-8} atm). Iodine burdens in an operating HTGR are expected to be $\leq 10^{-5}$ Pa. Test temperatures were 400 to 800°C, and test atmospheres were 1.1×10^5 Pa (~ 1.1 atm) helium containing 50 Pa (5×10^{-4} atm) hydrogen in most cases.

The computer program SOLGASMIX-PV uses standard thermodynamic data to calculate the equilibrium relationships in complex chemical systems. Calculations were made on an isothermal system at 5×10^6 Pa (50 atm) helium pressure with constant amounts of iron and chromium available. System temperature and the amounts of iodine, hydrogen, and oxygen were varied. The results showed that, in all realistic cases, the dominant iodine species in the gas phase was hydrogen iodide. Depending on the amount of iodine available and the temperature, $\text{CrI}_2(\text{s})$ or $\text{FeI}_2(\text{s})$ may form to effectively limit the amount of iodine in the gas phase.

An experimental apparatus and procedure were developed to measure iodine sorption on metal specimens using the transpiration, or flowing gas, method. Purified helium passed over elemental iodine which contained ^{131}I tracer in a low-temperature (-80 to -50°C) saturator. The helium-iodine stream was diluted with helium containing the desired amount of hydrogen before passing over the specimens in a quartz furnace tube. The accumulation of iodine on the specimens was measured and

* Since $1.00 \text{ atm} = 1.01325 \times 10^5 \text{ Pa}$, we use the approximation $1.0 \text{ atm} = 1.0 \times 10^5 \text{ Pa}$ throughout this report.

recorded continuously with NaI (Tl) crystal detectors connected to single-channel analyzers. The iodine source temperature and the helium flow rates were controlled to supply the desired iodine burden in the mixed helium stream, which was monitored by measuring the iodine collected from a small side stream ($\sim 5\%$ of the total mixed helium stream). The iodine collected on the metal specimens and on a charcoal trap downstream from the specimens was integrated to determine the average iodine burden in the helium over stable periods of operation. Each experiment consisted of several successive phases; where practical, the equilibrium loading at a constant temperature and iodine burden was measured, then conditions were changed either to allow more iodine to adsorb or to cause desorption to a new equilibrium loading on the same specimens. Each test phase required from 1 to >10 d, and test durations were up to 45 d. After completion of a test, the specimens were removed and the apparatus was disassembled. The amounts of iodine on all components were determined with a multichannel analyzer to verify both the on-line measurements with single-channel analyzers and the material balance for the test. The test specimens were examined visually and metallographically to evaluate changes in surface character, such as oxidation.

Equilibrium loading data were found to be quite variable and sensitive to specimen oxidation. At 400°C , the most thoroughly tested temperature, equilibrium loadings of ~ 1 to $5 \mu\text{g I/cm}^2$ were obtained on relatively clean specimens at iodine burdens of 10^{-5} to 10^{-3} Pa (10^{-10} to 10^{-8} atm); at lower iodine burdens, the loadings were reduced. In several tests where the specimens were heavily oxidized ($<1 \times 10^{-2}$ Pa hydrogen in the helium), the loading was reduced about one order of magnitude at all iodine burdens. As specimen temperature was increased, the iodine loadings decreased, roughly one order of magnitude for each 200°C in the 400 to 800°C interval. At 600°C the loading varied from ~ 0.003 to $\sim 0.3 \mu\text{g I/cm}^2$ at iodine burdens of 3×10^{-6} and 1×10^{-3} Pa (3×10^{-11} and 1×10^{-8} atm) respectively. Measurements at 800°C were near the limit of detection, $\sim 0.001 \mu\text{g I/cm}^2$ at $\sim 1 \times 10^{-4}$ Pa (10^{-9} atm). Data scatter prevented correlation with a particular isotherm, but some agreement with the Temkin isotherm was apparent.

Analysis of the rates of adsorption and desorption revealed some interesting results. The adsorption of iodine on steel is not a thermally activated process. The adsorption rate decreases with increasing temperature, and the adsorption reactions are not understood. If the adsorption rate is taken as the product of the rate of impingement of iodine on the surface and a sticking coefficient, the sticking coefficient in our experiments decreased from $\sim 10^{-3}$ at 400 to $\sim 10^{-4}$ at 700°C.

The desorption of iodine is thermally activated, however. Desorption rate data indicate that the iodine adsorbed on sites having a spectrum of activation energies for desorption that ranged from 2.2×10^5 to 3.3×10^5 J/mol. Some evidence indicates that iodine resides on the metal surface as FeI_2 . The form in which it desorbs appears to depend on such factors as temperature, composition of the environment, and amount and rate of desorption.

2. INTRODUCTION

Iodine is an important element in the safety evaluation of all reactor systems. It is of particular interest in the high-temperature gas-cooled reactor (HTGR) because its combination of chemical and physical properties make it a potential hazard under both normal operation and accident conditions.¹ Among the more significant of these characteristics are (1) iodine is produced in relatively large fission yields; (2) it is highly volatile at all HTGR coolant circuit temperatures and migrates rapidly through graphite; (3) several isotopes are radiologically significant because they decay with energetic beta and gamma rays with half-lives of hours or days; and (4) a variety of chemical forms -- all readily transportable -- are possible, depending on temperature and the level of impurities (H₂, H₂O, CH₄, etc.) in the helium coolant. Moreover, changes in coolant circuit conditions, such as temperature increase or water ingress, would be expected to increase the potential for release in a depressurization accident.

2.1 Purpose of Work

The limited amount of applicable data on iodine sorption and desorption under HTGR conditions, as emphasized by safety studies, dictated a need for additional work in this area.² The specific objectives of this program were (1) to determine equilibrium loadings of iodine on low-chromium alloy steel, specifically 2-1/4% Cr-1% Mo, called T-22, which is a major component of the HTGR coolant circuit, at conditions representative of an operating HTGR, and (2) to investigate the rate of desorption under conditions that could be related to hypothetical accident situations in an HTGR. General information about the behavior of various chemical species of iodine was pursued also.

2.2 Scope of Investigation

Because most of the previous experimental work (to be discussed in more detail in Sect. 3) had been conducted at iodine burdens* $\geq 10^{-2}$ Pa

*Iodine burden (P_T) is defined as the partial pressure of iodine with all iodine species in the gas phase converted to monoatomic I:

$$P_T = P_I = 2P_{I_2} + P_{HI} + 2P_{FeI_2} + 4P_{Fe_2I_4} + 2P_{CrI_2}$$

(10^{-7} atm) compared to an expected burden of no more than $\sim 10^{-5}$ Pa ($\sim 10^{-10}$ atm) in the HTGR,³ equilibrium loading measurements at iodine burdens of 10^{-6} to 10^{-3} Pa (10^{-11} to $\sim 10^{-8}$ atm) were of primary interest. During normal operation, the temperatures of metal surfaces in the HTGR coolant circuit should range between ~ 300 and 800°C , thereby setting the bounds for our experimental studies. The coolant in the HTGR is high-purity helium at 48×10^5 Pa (48 atm). Use of a glass/fused silica test apparatus, which was highly desirable for ease of construction and for minimizing iodine sorption and/or reaction, limited the test pressure to a maximum of about 1.2×10^5 Pa (1.2 atm) of helium. As with coolant pressure, there was no possibility of simulating the high flow rates in the HTGR; in our tests the flow rates were typically 200 to 400 std cm^3/min , which corresponds to 4.5 to 9.0 cm/s at 400°C and 7.3 or 14.4 cm/s at 800°C across the specimens. A temperature of 400°C was chosen for the major emphasis in the adsorption measurements.

Desorption data were obtained during phases of the equilibrium loading tests when changes in conditions caused iodine to desorb from partly or fully loaded specimens. Such changes involved (1) reducing the iodine burden in the gas while holding the specimen temperature constant, (2) increasing the temperature of the specimen while holding the iodine burden constant, or (3) reducing the iodine burden and increasing the temperature simultaneously.

2.3 Applications for Data

Assessments of HTGR safety utilize computer programs to make comprehensive calculations of the conditions (temperature, atmospheric properties, surface deposits, etc.) at various points around the coolant circuit. In this manner estimates of the circulating versus deposited inventories of the released fission products, and their distribution within the system, are obtained. The usefulness of such programs as PAD⁴ and PADLOC,⁵ which have been developed and used to make these calculations, is limited by the precision of input data. Equilibrium iodine loading measurements at significantly lower iodine burdens [$<10^{-5}$ Pa ($<10^{-10}$ atm)] were needed to reduce the uncertainties associated with extrapolations of previously available data. Similarly,

additional, more applicable data were needed to better evaluate iodine desorption and release during accidents including system depressurization.

3. REVIEW OF PREVIOUS STUDIES OF IODINE SORPTION ON STEEL

Several experimenters have studied the sorption of iodine on steels; the review and evaluation by Hoinkis⁶ were particularly helpful. Minor differences in alloy should not have a significant effect on the results since the major component (>90%) was iron in all cases, but differences in experimental technique, atmospheric impurities (especially O₂ and H₂O), and iodine burden are more important.

Some sorptions have been carried out in vacuum, called the pseudoisopiestic method, and others in flowing helium, called the transpiration method. The latter method better simulates behavior in the HTGR coolant circuit. Some tests using the transpiration method were conducted in a closed loop (as in the HTGR), but the majority operated in a once-through mode, as in our experiments.

Milstead, Bell, and Norman⁷ reported the results of pseudoisopiestic tests wherein the sorption of iodine on 1% Cr-1/4% Mo steel at 400°C was measured at iodine burdens of $\sim 2 \times 10^{-4}$ to ~ 2 Pa ($\sim 2 \times 10^{-9}$ to $\sim 2 \times 10^{-5}$ atm). They also evaluated and compared previous work at the General Atomic Company which utilized the transpiration method. With one exception, these tests were conducted at iodine burdens >0.1 Pa. The results of thermodynamic equilibrium calculations, reported in Fig. A.14 of Sect. 9, indicate that most of the iodine would have been in the form of iron iodides. More recent experiments at the General Atomic Company using the pseudoisopiestic technique have concentrated on even higher iodine burdens,⁸ such as might occur in some accident situations.

A series of pseudoisopiestic tests of iodine sorption on mild steel at 316 to 538°C was reported by Neill.⁹ The iodine burdens in these experiments were either $\sim 1 \times 10^{-4}$ or ~ 10 Pa, and both adsorption and desorption rates were measured. Data from Neill⁹ and Milstead et al.⁷ are plotted in Fig. 3.1 to illustrate the need for additional measurements at the lower iodine burdens. Although fairly consistent iodine coverages of ~ 10 $\mu\text{g}/\text{cm}^2$ are indicated at high iodine burdens (0.01 to 10 Pa), the large uncertainties of extrapolation to an iodine burden of

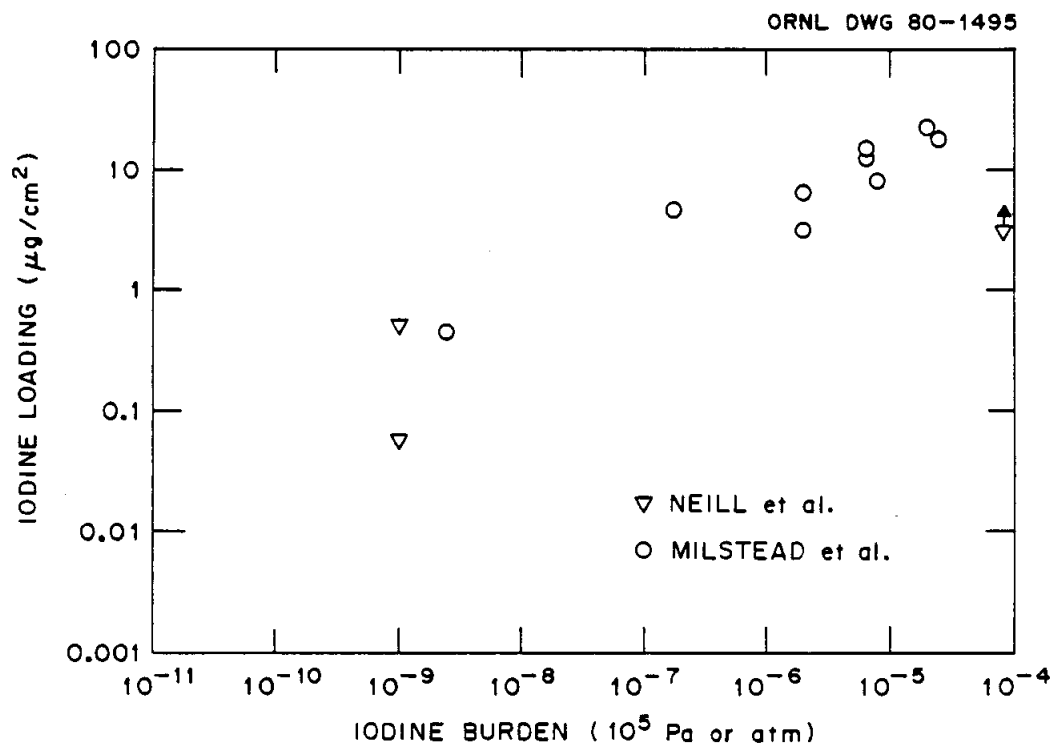


Fig. 3.1. Measurements of iodine sorption on low-alloy steel at 400°C, assuming that the iodine burden was equal to twice the reported source pressure of iodine.

$\sim 10^{-5}$ Pa are apparent. In addition to the obvious data scatter, most of the plotted values were derived from experiments in which $\text{FeI}_2(\text{s})$ was stable,⁶ thereby adding further uncertainty to extrapolations into regions where $\text{FeI}_2(\text{s})$ would not exist. An additional uncertainty in comparing data from different experiments is the ratio of true-to-geometric surface area. Only Neill⁹ reported any consideration of this parameter, and his value of 1.25 seems unreasonably low because the specimens did not receive the special polishing necessary to obtain a particularly smooth surface. The work of Watanabe et al.¹⁰ and of Strehlow¹¹ shows that even highly polished surfaces have roughness factors of ~ 2.5 .

Chemisorption of iodine on a metal surface, which should be the dominant mode of deposition at the low iodine burdens of interest, predicts iodine loadings much below those indicated by the above data, as

discussed by Compere et al.³ Assuming an ionic radius of 2.16×10^{-10} m (2.16 Å) and association of each iodine atom with a particular iron atom to form Fe-I bonds, Compere et al. concluded that monolayer coverage should be about $0.086 \mu\text{g I/cm}^2$ (4.1×10^{14} I atoms/cm²). This calculation, however, was based on the true surface area available for gas adsorption, whereas the data in Fig. 3.1 are based on geometric area. As noted above, surface roughness factors, the ratio of true-to-geometric surface area, vary widely; depending on the method used to fabricate the specimens, roughness factors as high as 10 may exist.

Other studies of iodine sorption on metals do not appear particularly useful for comparison. Neill, Gray, and Kress¹² conducted tests of iodine behavior in a stainless steel loop containing helium at 2.76×10^6 Pa (400 psig). Test temperatures were 200 to 260°C, and neither the iodine burdens in the circulating helium nor the surface coverages were accurately determined. Genco and co-workers¹³ reported transpiration experiments of iodine deposition on preoxidized stainless steel in air-steam and hydrogen-steam atmospheres in the temperature range 150 to 750°C. Iodine burdens, injected as I₂ or HI, were in the 10^{-3} to 10 Pa (10^{-3} to 10^{-4} atm) range. Maximum reported loadings were less than $1 \mu\text{g I/cm}^2$ at 150°C. The deposition of iodine on a variety of metal surfaces was investigated by Davis et al.¹⁴ in atmospheres of helium, hydrogen, air, and steam. This work, which was actually several different types of experiments, was intended more to establish limits of iodine behavior under a broad range of conditions than to measure specific loadings under clearly defined conditions.

A study of iodine sorption on Fe₃O₄ powder in vacuum (the pseudo-isopiestic method) at 200 to 450°C and 10^{-6} to 10^{-2} Pa (10^{-11} to 10^{-7} atm) was initiated by Hoinkis¹⁵ and continued by Osborne and co-workers.¹⁶ Differences in experimental methods and specimen surface characteristics make data comparisons difficult to interpret even for oxidized metal specimens, but the previous experience proved very helpful in planning and conducting the recent experiments using steel specimens.

4. PREDOMINANT IODINE SPECIES IN THE GAS PHASE

Recognizing that the various chemical species in the Fe-Cr-I-He system would vary in concentration with temperature and with the concentration of such impurities as hydrogen and oxygen, we employed the computer program SOLGASMIX-PV¹⁷ to investigate the equilibrium relationships. This program considered an isothermal system with a constant total pressure and used the thermodynamic data to compute the equilibrium compositions of all species by minimization of the system free energy. The temperature range investigated was 100 to 800°C, and the quantities of the various elements input for the several series of calculations are listed here.

<u>Element and state</u>	<u>Quantity or partial pressure</u>
Fe(s)	100 mol
Cr(s)	0 to 2 mol
He(g)	5×10^6 Pa (50 atm)
I(g)	1×10^{-7} to 1 Pa (10^{-12} to 10^{-5} atm)
H(g)	0 to 2×10^2 Pa (0 to 2×10^{-3} atm)
O(g)	0 to 5 Pa (0 to 5×10^{-5} atm)

Since a large fraction of the HTGR coolant circuit — especially in the temperature region where a large fraction of the fission product iodine is expected to deposit — is composed of 2-1/4% Cr-1% Mo steel, we assumed essentially unlimited availability of this alloy. Some uncertainty about the availability of unoxidized chromium dictated that cases with and without chromium be considered, as shown above. The ranges of partial pressures of iodine, hydrogen, and oxygen were chosen to span any expected coolant conditions. Other possible coolant impurities, such as carbon, were ignored because they would not be expected to significantly affect the behavior of iodine in this system.

The results of these calculations showed that where hydrogen was present, the dominant iodine species was hydrogen iodide, with monoatomic iodine concentrations some two orders of magnitude lower, as shown in Fig. 4.1. Gaseous metal iodides (CrI_2 , FeI_2 , FeI_3 , and Fe_2I_4)

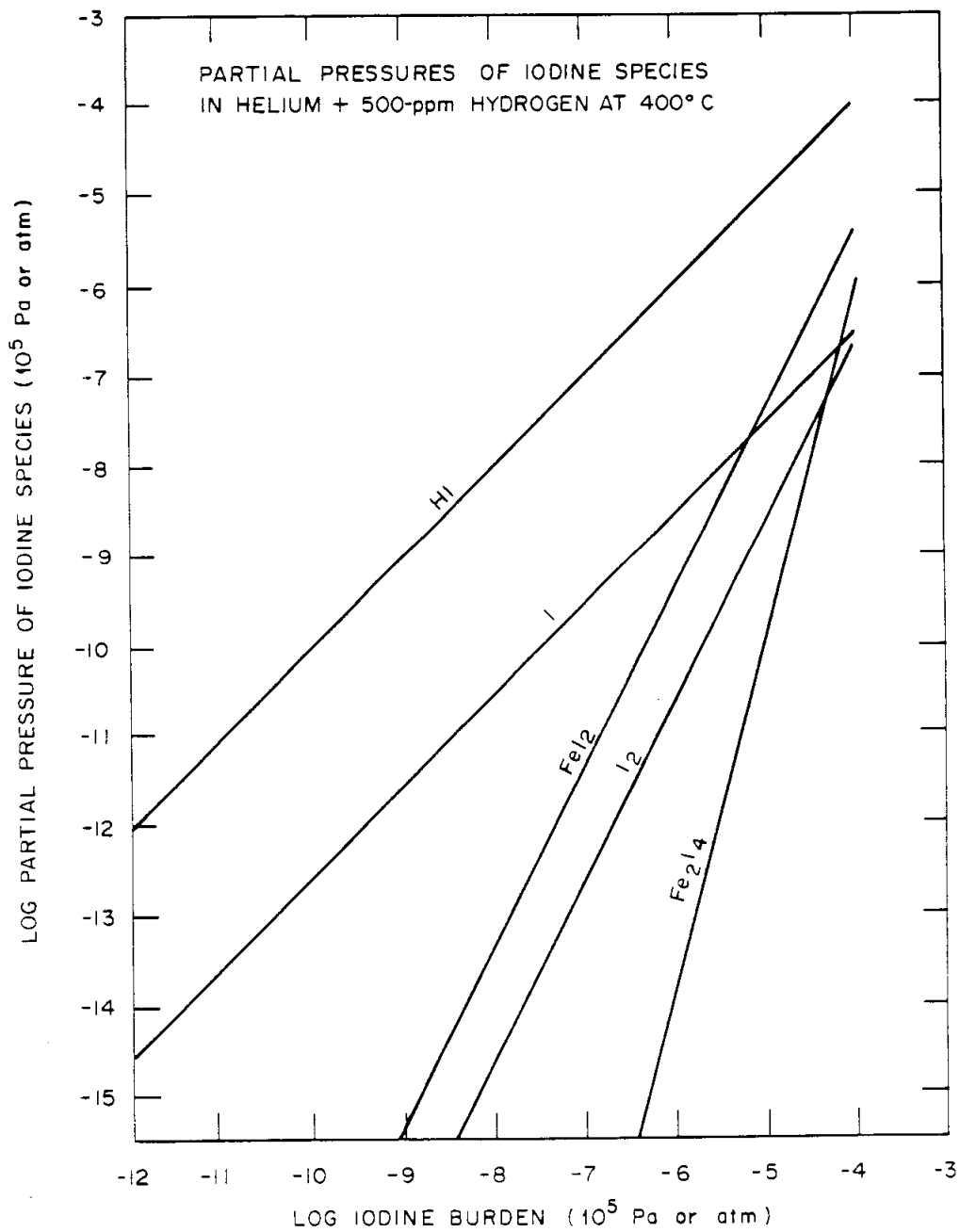


Fig. 4.1. The equilibrium distribution of the iodine species in the Fe-I-H system at 400°C, as calculated by the computer program SOLGASMIX-PV.

appeared in comparable concentrations only at the higher iodine input levels and were limited by deposition of $\text{CrI}_2(\text{s})$ and/or $\text{FeI}_2(\text{s})$. These results are discussed further and are illustrated in a series of figures in Appendix A.

5. EXPERIMENTAL APPARATUS AND PROCEDURE

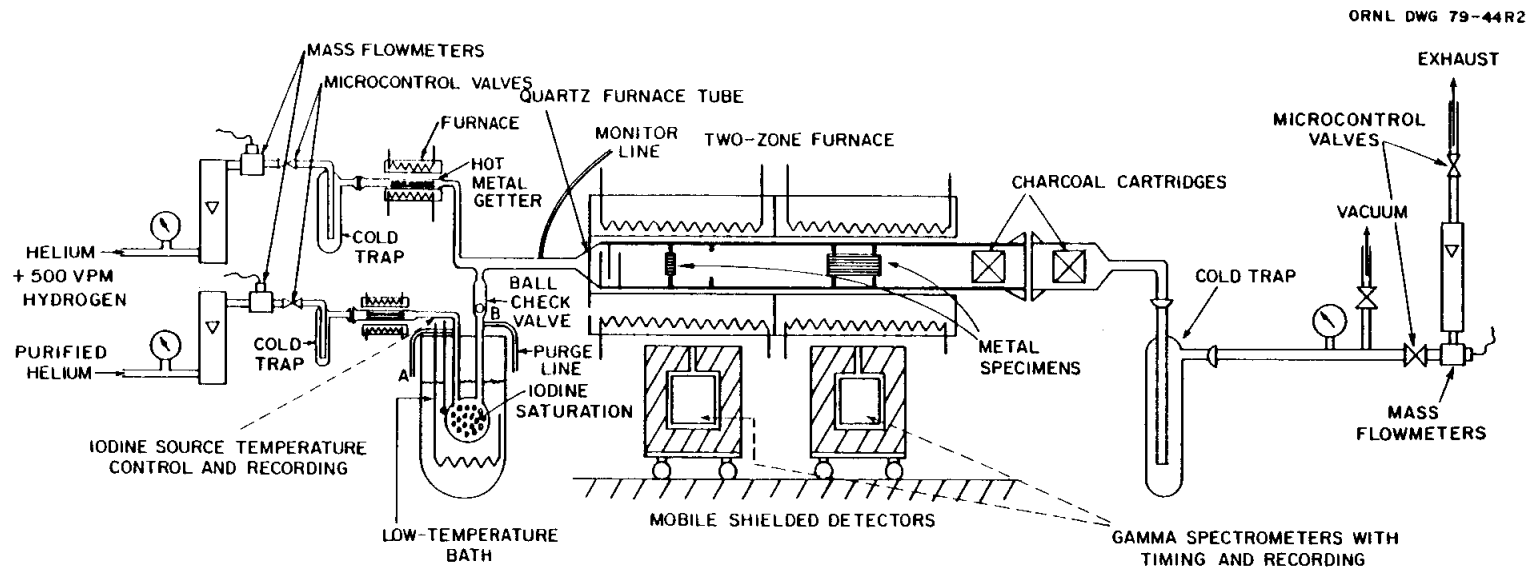
The primary requirements for the test apparatus were that it be relatively (1) impervious to gaseous contaminants (especially oxygen and water vapor) over the temperature range -100 to 800°C, (2) unreactive with both iodine and the steel specimens, and (3) simple to fabricate and operate. In order to attain good counting precision at the low iodine burdens, specimens of a high surface-to-mass/volume ratio, an iodine source of high specific activity, and an arrangement for locating the detectors close to the specimens (but well shielded from the source) were required.

5.1 Test Apparatus

The apparatus was composed of a fused silica furnace tube to which the other components made of Pyrex glass (Fig. 5.1) could be readily attached. Several minor modifications were made to the apparatus during the test series. The apparatus shown in Fig. 5.1 is the final version, as was used in the last several tests; details of the development are discussed in the preliminary reports of individual tests,¹⁸⁻²⁷ and the more significant changes will be mentioned later along with experimental results.

Helium was supplied, typically in two separate, standard cylinders. Cylinder 1 was of highest available purity and was connected to the saturator. Cylinder 2 supplied a special mix, containing 0.05 vol % hydrogen, to provide a partial pressure of 50 Pa (5×10^{-4} atm) in the ~ 1.1 atm tests, the same as the predicted hydrogen pressure in the 48-atm HTGR coolant. Analyses of the helium used in these tests are listed in Table 5.1. The helium supply lines, pressure gauges, mass flowmeters, and microcontrol valves were all standard metal components. The connections to the Pyrex cold traps were ground ball joints, sealed with vacuum grease.

The apparatus, from the cold traps designed to freeze out water vapor or any other impurity condensable at -196°C (liquid nitrogen temperature) to the large ball joint connection at the downstream end of the



ORNL DWG 79-44R2

Fig. 5.1. Experimental apparatus for iodine adsorption/desorption studies.

Table 5.1. Mass spectrometric analysis of helium used in sorption tests

Cylinder No.	Test No.	Impurity contents (ppm)					
		H ₂	O ₂	H ₂ O	CO	CO ₂	CH ₄
1							
(Saturator flow)	A-5, A-6	0.06	<0.02	1.3		0.02	<0.005
	A-7 through A-13	0.01	0.01	0.9		0.02	<0.005
2							
(Primary flow)	A-5, A-6	0.06	<0.02	1.3		0.02	<0.005
	A-7	600	<1	1		<1	
	A-8	510	0.8	<0.1	<0.1	<0.2	
	A-9	490	0.7	<0.1	<0.1	<0.2	
	A-10	530	0.1	0.1		0.3	
	A-11	500	3.6	1		1	
	A-12	500	1-3	<3		<1	
	A-13	510	1-3	<1		<1	

furnace tube, was a single unit. After assembly in situ, it was filled with helium to $\sim 1.2 \times 10^5$ Pa (~ 1.2 atm) pressure, and all components were checked for leakage with a leak detector.

The parallel inlet helium streams served a dual function. Purified helium passed through the saturator at a low flow rate (2 to 10 std cm³/min) to entrain the desired amount of iodine in the inert gas stream. The larger primary flow rate (200 to 400 std cm³/min) provided both dilution to reduce the iodine burden and also the desired mix of impurities (primarily hydrogen) to simulate HTGR coolant (Fig. 5.2).

Both helium streams were passed through clusters of T-22 strips (the same material as used for adsorption specimens) maintained at 400°C. This step was intended to reduce the content of any remaining oxidants in the helium to a level at which no oxidation of the specimens could occur. (As shown in Fig. 5.2, the helium supplied to the saturator stream was passed through a purification trap, a bed of zirconium chips at 700°C, prior to reaching the flow measurement and control equipment.)

The saturator was a U-tube with a ~ 2.0 -cm-diam bulb at the bend immersed in a propanol bath, which was cooled to the desired temperature

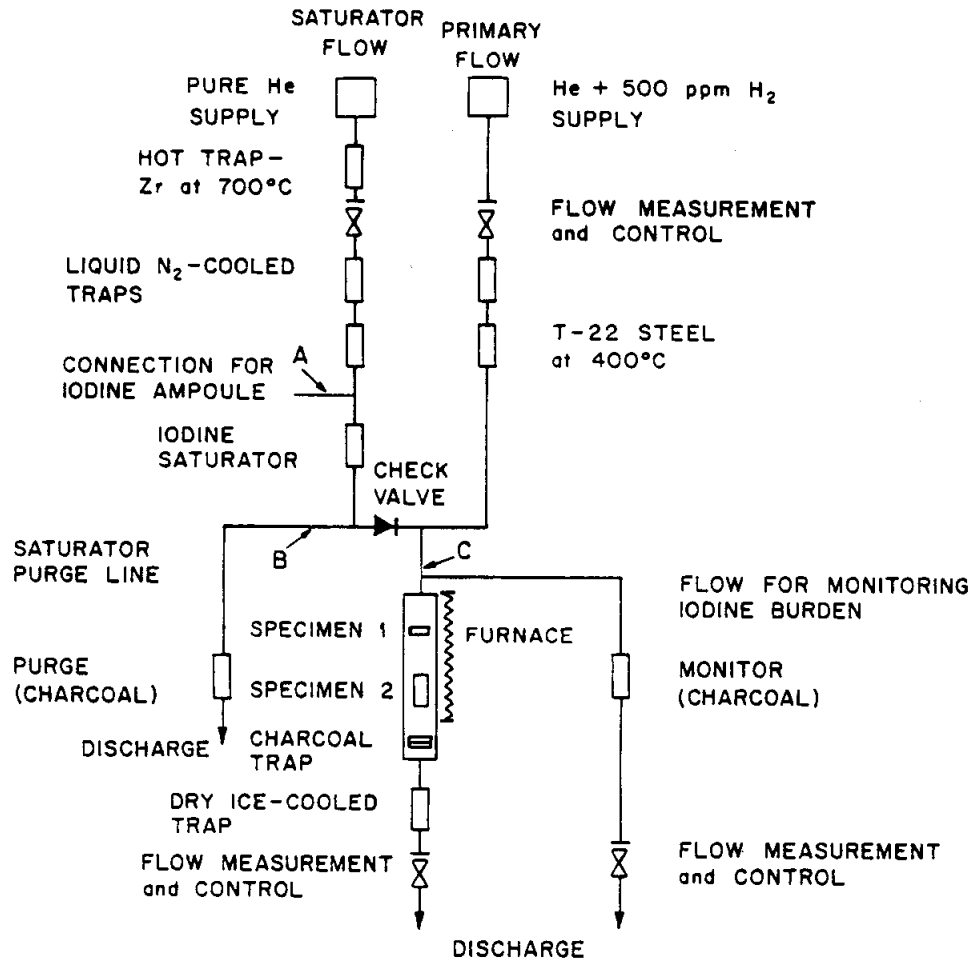


Fig. 5.2. Flow diagram for adsorption experiment.

(-80 to -50°C) by a mechanical cooler (FTS Systems Multicool Model MC-1-90). A ball check valve was located in the outlet from the saturator to impede iodine diffusion into the primary stream when no helium was flowing through the saturator. A small side tube, called the purge line, was attached to the outlet from the saturator immediately before the ball check valve. The purpose of this purge line was to allow helium to be discharged from the saturator through a small charcoal trap, without any flow to the furnace tube and specimens, during the transfer of iodine from the preparation ampoule to the saturator. (In some of the early

experiments, some iodine was inadvertently deposited on the specimens during this transfer operation.) The charcoal trap in the purge line, which was composed of Teflon, was temporarily mounted at detector 2, allowing the collection of iodine during transfer and monitoring for a period thereafter. After iodine transfer into the saturator and purging to a constant, predictable flow rate, the Pyrex purge line was fused at point B (Fig. 5.2).

Immediately downstream from the junction of the primary and saturator lines, a small side line was attached (point C, Fig. 5.2). This monitor line allowed a small fraction (typically 3-6%) of the mixed gas to bypass the furnace tube and flow through another small charcoal cartridge (called the monitor trap). This monitor trap was mounted at a third detector (not shown in Fig. 5.1), which enabled us to continuously monitor independently the rate of iodine flow to the specimens.

The furnace tube was a 30-mm-diam \times 1.5-mm-wall fused silica tube, 50 cm long. The inlet end was reduced to 8 mm diam and contained three baffles to mix the incoming gas. The outlet end terminated in a large ground glass joint to facilitate loading the specimens and charcoal trap. The specimens were mounted in bulkheads with 15-mm² cutouts, assuring gas flow through the array of thin plates. Two independently controlled furnaces surrounding the furnace tube were capable of heating the specimens to 1000°C with rapid heating rates (\sim 100°C/min) and stable control (\pm 5°C). A cylindrical cartridge of activated charcoal capable of adsorbing all of the iodine source was mounted in the downstream end of the furnace tube, and a similar cartridge was mounted as a backup in the connection between the furnace tube and the cold trap. This trap, cooled in a solid CO₂-acetone bath, protected the furnace tube from back-diffusion of impurities during evacuation at the beginning of an experiment and also served as a third collector for any iodine that might penetrate the charcoal traps during the experiments.

Downstream from the cold trap were (1) a connection to a vacuum system, plus the valves and vacuum gauges needed for system evacuation; and (2) a mass flowmeter, rotometer, and microcontrol valve for regulating and measuring outlet gas flow.

5.2 Metal Sorption Specimens

The 2-1/4% Cr-1% Mo steel specimens were rectangular arrays of 0.24-mm-thick plates, as shown in Fig. 5.3. The thin plates were mounted in slots in thicker side pieces of the same alloy. The gas stream flowed through the array parallel to the plates, 2 mm and 51 mm, respectively, for specimens 1 and 2.

ORNL-DWG 78-355R2

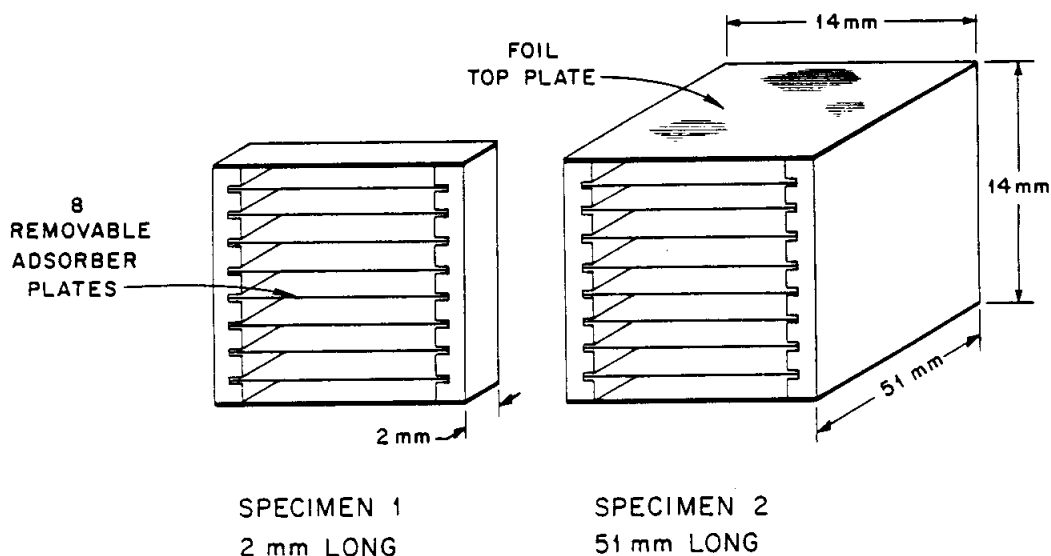


Fig. 5.3. Low chromium alloy steel adsorption specimens.

The thin plates were produced by successively rolling and annealing strips²⁸ of 4.76-mm-thick (3/16-in.) plate.* Chemical analysis and mechanical characteristics of the material are listed in Table 5.2. The individual plates were sheared to the proper size. Because this low-alloy steel tends to rust in room air, the protective oil film was not removed until immediately before loading into the apparatus. The assembled specimens were cleaned by washing in CCl₄ and acetone, then dried at 125°C.

* Obtained from Alloy and Carbon Steel Co., North Bergen, NJ 07047.

Table 5.2. Chemical analysis and characteristics
of specimen material^a

Element	Content per manufacturer (%)
C	0.13
Mn	0.45
P	0.012
S	0.017
Si	0.021
Cr	2.37
Mo	0.92
Fe	Balance

Mechanical test results

Yield point (0.2%)	33.3 ksi (2.30×10^8 Pa)
Tensile strength	66.3 ksi (4.57×10^8 Pa)
Elongation	28% in 2 in. (5.08 cm)
Reduction of area	62%

^aAlloy and Carbon Steel Co., North Bergen, NJ
07047, 2-1/4% Cr-1% Mo steel, heat no. 3P796.

Surface characterization of the specimens included surface roughness (6.8 times geometric) by the diamond stylus method,²⁹ surface area (~ 140 times geometric) by the BET gas adsorption method,³⁰ and metallographic examination at 250 to 1000 \times ,³¹ as reported in Appendix B. The latter revealed numerous small cracks, apparently caused by shearing, which tended to corroborate the very high surface area indicated by gas adsorption. However, this surface area measurement must be considered a relatively low confidence value because the total area was marginal for measurement.

5.3 Instrumentation

A variety of instruments were used to (1) record helium flow rates; (2) control and record temperatures of hot metal getters, the iodine source, and the specimens; (3) regulate the supply of liquid nitrogen to the cold trap; and (4) count and record the radioiodine collected on the

specimens and charcoal traps. Gas flow rates were set and occasionally readjusted manually, but all temperatures were controlled automatically.

The counting system was composed of three similar channels feeding data to a printout control, as shown in Fig. 5.4. At predetermined time

ORNL DWG 80-1505

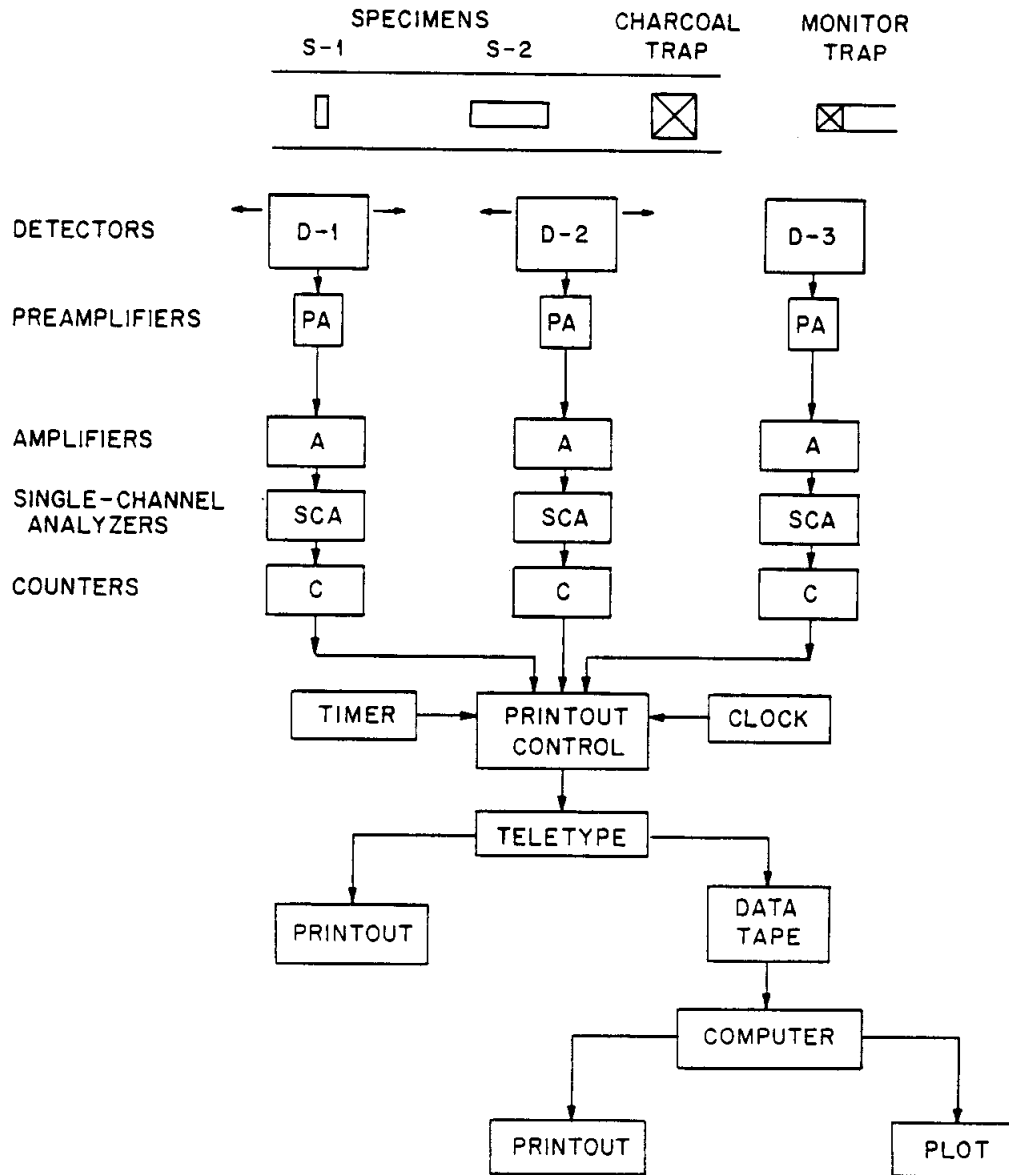


Fig. 5.4. Schematic diagram of data collection system.

intervals, the number of counts collected in each channel, the length of the time interval, and the accumulated time from the beginning of the experiment were printed by a teletype and recorded on paper tape. The printout was used to monitor the progress of the experiment, and the data on tape were transferred for computer processing; corrections for background and radioactive decay, relative and maximum count rates, specimen loadings, etc., were calculated and selected data were plotted.

5.4 Iodine Source and Saturator

The ^{131}I source material (typically 5 mCi) was obtained as carrier-free NaI in aqueous solution. After adding a small amount of natural iodine (as NaI) and the extraction of standard samples, elemental iodine was prepared by the decomposition of PdI_2 in vacuum. The detailed procedure for this operation, which was carried out in a separate laboratory, is listed in Appendix C. In order to obtain high specific activities, the amount of carrier (natural) iodine was limited to ~ 1 mg.

About 1% of the total solution was withdrawn, divided into small samples adsorbed on silver zeolite beads, and sealed in 3-mm-diam \times 15-mm-long Pyrex tubes for use as standards in calibrating the detectors prior to an experiment. Beginning with the original ^{131}I source material, each specific fraction (ampoule, standards, etc.) was measured by a multi-channel analyzer. Two of these small standards, which were essentially line sources ~ 1 cm long, were placed in the furnace tube at the positions of the leading edges of the sorption specimens to determine the counting efficiency for an accurately known amount of ^{131}I before each experiment. They were also counted at the entrance to the collimator of each detector. The same standards were recounted at the collimators several times per week during the experiment as verification of the counting system stability. Details of these calibrations are discussed in Appendix D.

During preparation the elemental iodine (I_2) was deposited in an ampoule equipped with a magnetically operated breakseal. This ampoule was attached to the experimental apparatus at point A, Fig. 5.1. With a helium flow of about 5 std cm^3/min through the cold (-80°C) saturator and purge line, the breakseal was broken and the iodine was warmed to

40 to 50°C, permitting it to diffuse slowly into the helium stream and be carried to the saturator where it condensed on the inlet leg. After a few hours, most of the iodine was transferred to the saturator, as verified by radioactivity measurements with a survey meter, and the source ampoule was fused closed and removed.

In all cases, a small amount of radioiodine was collected on the purge trap during this transfer operation, thus indicating the presence of a small fraction of an iodine species with much higher vapor pressure at -80°C than I₂. We speculate, but cannot demonstrate, that a small amount of organic impurity reacted to form CH₃I (or some other organic iodide) with such a vapor pressure. Other experimenters,^{13,32} while conducting similar tests, have observed similar high vapor pressures of an unidentified iodine species at the beginning of experiments.

In order to establish the desired iodine burden, P_T, in the helium stream, we set the temperature of the saturator to provide a vapor pressure, P_{I₂}, according to the work of Honig and Hook,³³ then adjusted the helium flow rates to obtain the desired total flow rate and dilution factor, using the expression

$$P_{I_2} = \left(\frac{F_1 + F_2}{2F_1} \right) P_T, \quad (1)$$

where

F₁ = flow rate through saturator,

F₂ = flow rate in primary stream.

Flow rates through the saturator, F₁, were kept very low (2 to 10 std cm³/min) to ensure saturation of the helium.

Depending somewhat on sorption test conditions, the effective useful lifetime of a typical ¹³¹I source (~2-5 μCi/μg I) was about 6 weeks, at which point the count rates for most loadings were approaching marginal usefulness.

5.5 Operating Procedure

The procedure for conducting an experiment included apparatus construction, specimen preparation, iodine source preparation, detector

calibration and background counting, and leak-testing of the apparatus with specimens in place, all before opening the iodine source ampoule, which was defined as time zero for each experiment. After transferring the iodine into the saturator, the source was purged at $\sim 50^{\circ}\text{C}$ for several hours to discharge any highly volatile species to the purge trap. The iodine flow rate was measured at two or more saturator temperatures over a period of several days to verify that the source was behaving according to the temperature-flow relationship.

Once predictable behavior of the iodine source had been established, the purge line was sealed, and flow of the mixed gas through the furnace tube and the monitor line was initiated. Since the specific activity of the iodine was highest at the beginning of an experiment, the conditions usually were chosen so that relatively low loadings were measured early, with higher loadings obtained later in the test sequence. To achieve an equilibrium loading on specimen 1, the conditions (temperature, flow, and P_T) were held constant until the count rate (corrected for decay) stopped increasing or until, as in some cases, we concluded that an unreasonably long period (>2 weeks) would be required to approach the desired equilibrium. The counting system collected data continuously and printed at intervals of 1000 to 5000 s.

Upon reaching equilibrium (or nearly so) iodine coverage on specimen 1, conditions were changed to begin the next phase of the experiment. The conditions for the various phases of each experiment are tabulated in Appendix E, and calculations of the concentration of iodine on the surfaces are given in Appendix F. Desorptions were begun from an equilibrium loading by either reducing the iodine burden (normally to 0), which resulted in very slow desorption, or by increasing specimen temperature 100 or 200°C , which caused rapid desorption. The counting intervals were adjusted to reflect the rate of desorption.

The total amount and the distribution of iodine adsorbed on the specimens, the outlet end of the furnace tube (generally insignificant), and the charcoal trap were determined through periodic profile measurements. Detectors 1 and 2 were moved in increments of 2 to 10 mm with 100-s counts at each position, and the data were plotted versus position.

Comparison of these plots with the detector calibration curves (Appendix D) enabled us to make reliable estimates of the total amount of iodine on specimen 2 and the charcoal trap. These data were useful in verifying the average iodine burden at the specimens and in determining loading ($\mu\text{g I}/\text{cm}^2$) on specimen 2.

5.6 Experiment Disassembly and Posttest Measurements

At the conclusion of each experiment, the temperatures were reduced, the specimens and charcoal traps were removed into individual containers, and the apparatus was disassembled into sealed sections (saturator, furnace tube, and connecting tube) under continued helium flow. All components were inspected visually, and the iodine content of each component was measured by a multichannel analyzer and found to agree acceptably with in situ measurements. (In some cases the detector calibrations were reverified with standards before disassembly.) The iodine material balance was determined, as tabulated in Appendix E, and the results usually indicated the recovery of >90% of the original iodine.

6. RESULTS AND ANALYSIS

As noted previously, the first priority of these experiments was to determine the equilibrium iodine loading on the steel specimens as functions of iodine burden and temperature. The influence of small amounts of oxidizing impurities (O_2 and H_2O) in the helium was investigated also and is included in the discussion. In planning the sequence of experimental phases, we tried to obtain as much additional data on adsorption and desorption rates as possible. These data were examined, and although somewhat incomplete, some interesting results were obtained.

6.1 Equilibrium Adsorption Measurements

Our specific objective in measuring the equilibrium loadings of iodine on low-alloy steel was to obtain a series of adsorption isotherms at iodine burdens of $\sim 10^{-6}$ to 10^{-3} Pa ($\sim 10^{-11}$ to 10^{-8} atm) and temperatures of 400 to 800°C. Test conditions and adsorption data are summarized in Table 6.1. On comparison of the data from different experiments, however, we found a disturbing lack of consistency. All data at 400°C are plotted in Fig. 6.1, which shows ranges of iodine loadings up to >100 at iodine burdens of $\sim 10^{-5}$ Pa ($\sim 10^{-10}$ atm). It was readily apparent that iodine loading was sensitive to specimen oxidation. The measurements obtained from tests A-4-4, A-5-1, and A-6-1 in pure helium, which was known to be slightly oxidizing, fall well below other values at similar iodine burdens. In addition, posttest examination of these specimens verified that they were heavily oxidized. Thus, these three measurements may be more representative of iodine sorption on iron oxide than on steel, but comparisons with earlier measurements on Fe_3O_4 (ref. 16) are limited by uncertainties in the true surface area.

The remaining equilibrium sorption data at 400°C indicate iodine coverages in the range 0.5 to 5 $\mu\text{g}/\text{cm}^2$ (geometric area) for iodine burdens of 10^{-5} to 10^{-3} Pa (10^{-10} to 10^{-8} atm) and decreasing to ~ 0.05 $\mu\text{g}/\text{cm}^2$ at 10^{-6} to 10^{-5} Pa (10^{-11} to 10^{-10} atm). The width of this data band is about one order of magnitude. Typical uncertainties in these data include measurement of iodine concentration ($\pm 10\%$) and

Table 6.1. Summary of adsorption and desorption data from all experiments

Experiment	Test phase	Specimen	Steady state iodine concentration ($\mu\text{g}/\text{cm}^2$)	Iodine burden (10^{-5} Pa or 10^{-10} atm)	Temperature ($^{\circ}\text{C}$)	P_{H_2} (Pa or 10^{-5} atm)	Remarks
A-4	1 and 2 (adsorption)	1 (51 mm)	2 to 3	20 to 30	400	1200	Steady state concentration estimated from analyses of profiles for long specimen.
	3 and 4 (adsorption)	1 (51 mm)	0.1 to 0.2	20	400	3	When P_{H_2} was reduced, iodine neither adsorbed or desorbed at entrance of specimen. Concentrations are steady values reached on specimen downstream of 4 to 8 mm at entrance. Specimen was considerably oxidized. Blistered near entrance
A-5	1 (adsorption)	1 (2 mm)	0.4	500 to 600	400	~ 0.001	Activity was continuing to rise slowly at end of phase 1. Severe oxidation.
		2 (51 mm)	0.4 to 2	500 to 600	200	~ 0.001	Activity was steady at entrance of specimen. Concentration was obtained from profile.
	4 (desorption)	1	0.1	0	600	~ 0.001	No desorption when burden was reduced at 400°C . Steady state reached at 600°C .
A-6	1 (adsorption)	1	0.013	0.8 to 1.7	400	~ 0.001	Steady value reached early in phase 1.
		2	>0.034	0.8 to 1.7	200	~ 0.001	Determined from profile. No indication that it was at steady state.
	11, 12, 13 (adsorption)	1	0.003	0.4 to 14	400	~ 0.001	No adsorption on specimen 1 after iodine was desorbed at 600 and 800°C . Specimen was severely oxidized.
A-7	1 (adsorption)	1	0.04 to 0.05	0.4 to 2.0	400	50	No adsorption or desorption of iodine sorbed on specimens during charging of saturator.
	2 (adsorption)	1	0.4	10 to 19	400	50	Concentration of $0.4 \mu\text{g}/\text{cm}^2$ was not quite at steady state for burden of 19×10^{-5} Pa when burden decreased to 10×10^{-5} Pa. Iodine desorbed slowly and was not yet at equilibrium when concentration had decreased to $0.3 \mu\text{g}/\text{cm}^2$.
	3 (adsorption)	1	>2.1	140	400	50	At end of phase 3, <0.15 of iodine was being adsorbed on specimen 1, but there was no indication that rate of adsorption was decreasing.
		2	>4	140	400	50	Determined from profile. No indication that concentration had reached steady value.

Table 6.1 (continued)

Experiment	Test phase	Specimen	Steady state iodine concentration ($\mu\text{g}/\text{cm}^2$)	Iodine burden (10^{-5} Pa or 10^{-10} atm)	Temperature ($^{\circ}\text{C}$)	P_{H_2} (Pa or 10^{-5} atm)	Remarks
	4 (adsorption)	1	>2.3	4.0	400	50	Iodine on specimen 1 continued to increase when saturator temperature was lowered. Burden calculated from rate of increase on specimen 1. No indication of being near steady state.
A-8	2 (desorption)	1A 1B	0.011 0.007	0 0	600 600	50 50	At beginning of phase 2, there was $0.093 \mu\text{g}/\text{cm}^2$ on 1A and $0.053 \mu\text{g}/\text{cm}^2$ on 1B. Iodine did not desorb at 400°C in phase 1, but burden might have been as high as 7×10^{-6} Pa from desorption of iodine from wall of furnace tube. Activity very close to background.
	3 (desorption)	1A 1B	0.001 <0.001	0 0	800 800	50 50	
	5 (adsorption)	1A 1B	1.4 0.81	90 to 170 90 to 170	400 400	50 50	These values were steady or very nearly so.
	6 (desorption)	1A 1B	0.3 0.2	130 to 140 130 to 140	600 600	50 50	Desorption to steady state with iodine burden held constant.
	7 (adsorption)	1A 1B	1.0 0.6	90 to 190 90 to 190	400 400	50 50	These values were steady.
	8 (desorption)	1A 1B	<0.5 <0.4	0 to 4 0 to 4	400 400	50	Temperature of saturator was reduced and flow was stopped to reduce burden to 0. Bypass flow could have maintained burden at 4×10^{-5} Pa. Concentrations appeared to be nearing, but had not reached steady values.
A-9	2 (adsorption)	1A	0.087	0.2 to 0.4	400	50	Iodine was put on specimen when burden was $\sim 2 \times 10^{-5}$ Pa for short time. Iodine concentration was still increasing when burden had fallen to 4×10^{-6} Pa but was steady at 2×10^{-6} Pa.
	3 (desorption)	1A 1B	0.003 0.002	0.2 to 0.4 0.2 to 0.4	600 600	50 50	Reached steady values during desorption.
	5 (adsorption)	1A 1B	0.064 0.056	0.4 to 0.6 0.4 to 0.6	400 400	50 50	Iodine concentrations were steady, but lower than at end of phase 1.

Table 6.1 (continued)

Experiment	Test phase	Specimen	Steady state iodine concentration ($\mu\text{g}/\text{cm}^2$)	Iodine burden (10^{-5} Pa or 10^{-10} atm)	Temperature ($^{\circ}\text{C}$)	P_{H_2} (Pa or 10^{-5} atm)	Remarks
	6 (desorption)	1A 1B	<0.046 0.056	0 to 0.07 0.12 to 0.19	400	50 50	Saturator temperature was reduced and flow was stopped. Material balance indicated that burden at entrance of specimen 1A might have been as high as 0.7×10^{-6} Pa. Iodine desorbed from specimen 1A and was continuing to desorb at end of phase. Iodine on specimen 2 did not change.
A-11	1 (adsorption)	1	>0.034	0.060 to 0.096	400	50	Run was ended by crack in helium line. Activity was rising at steady rate and almost all the iodine was adsorbing on specimen 1 at end.
A-12	1-9 (adsorption)	1	≤ 3.2	0.7 to 1.2	400	50	Iodine neither adsorbed nor desorbed when burden was reduced from 17×10^{-5} Pa.
	1-12 (adsorption)	1	≥ 3.5	2.2 to 3.0	400	50	Iodine was continuing to adsorb although 0.45 fraction was passing specimen 1.
	14 (desorption)	1	<0.4 (0.1-0.2)	2.2 to 3.0	600	50	Desorption was not carried to steady state. Steady value estimated to be 0.1-0.2 $\mu\text{g}/\text{cm}^2$.
A-13	1 (adsorption)	1	>0.83 (~ 4)	2.6 to 3.0	400	50	Adsorption was normal. Phase was ended while specimen was still adsorbing 0.69 of iodine in gas. ($\sim 4 \mu\text{g}/\text{cm}^2$) estimated by method of Hougen and Marshall.
	2 (desorption)	1	<0.64 (0.3-0.5)	3.0	500	50	Phase was ended before reaching steady state. Steady state value of 0.3 to 0.5 $\mu\text{g}/\text{cm}^2$ was estimated from shape of desorption curve. Steady state value.
	3 (desorption)	1	0.091	3.0	600	50	Steady state value.
	4 (desorption)	1 2	0.0060 0.0065	3.0 3.0	700 700	50 50	Steady state value. Assumes uniform concentration on surface.
	5 (desorption)	1	0.0012	3.0	800	50	Steady state value, but activity was hardly distinguishable from background.
	6 (adsorption)	2 1	0.0007 0.0014	3.0 20 to 30	800 800	50 50	Steady state value. Assumes uniform concentration. Steady state value, but activity was hardly distinguishable from background.
		2	0.0009	20 to 30	800	50	Steady state value. Assumes uniform concentration.

Table 6.1 (continued)

Experiment	Test phase	Specimen	Steady state iodine concentration ($\mu\text{g}/\text{cm}^2$)	Iodine burden (10^{-5} Pa or 10^{-10} atm)	Temperature ($^{\circ}\text{C}$)	P_{H_2} (Pa or 10^{-5} atm)	Remarks
7		1	0.010	20 to 30	700	50	Steady state value.
(adsorption)		2	>0.010	20 to 30	700	50	Steady state had not been reached.
8		1	0.046	20 to 30	600	50	Steady state value.
(adsorption)		2	0.065	20 to 30	600	50	At or near steady state.
9		1	0.015	3.0 to 6.0	600	50	Steady state. High burden based on monitor.
(desorption)		2	<0.044	3.0 to 6.0	600	50	Far from steady state at end of phase.
11		1	>1.4 (>4)	3.1	400	50	Far from steady state. Appeared that steady state value would be greater than the $14 \mu\text{g}/\text{cm}^2$ estimated for phase 1.
(adsorption)							
12		1	<1.36	0	400	50	Not at steady state when phase ended.
(desorption)							
13		1	<0.086 (0.06-0.07)	2.0 to 3.0	600	50	Not quite at steady state. Estimate based on shape of desorption curve.
(desorption)		2	<0.046	2.0 to 3.0	600	50	Not at steady state.

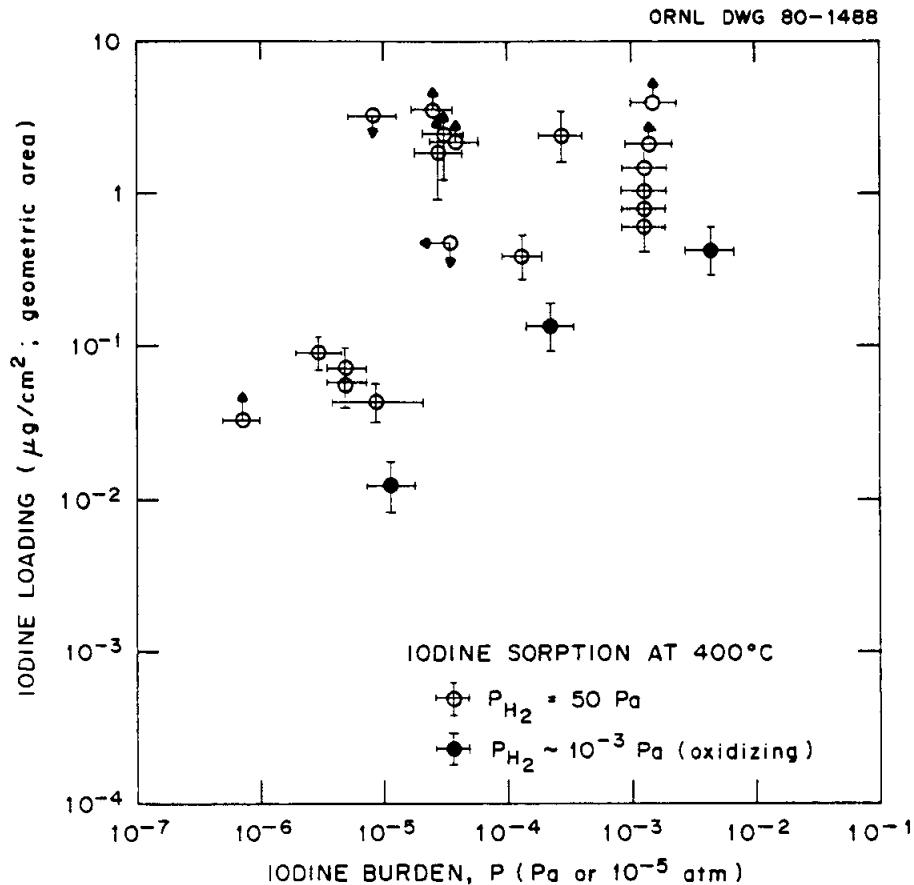


Fig. 6.1. Equilibrium sorption measurements of iodine on low-alloy steel at 400°C. Points with arrows denote near-equilibrium measurements, with arrow indicating direction of true value.

iodine burden ($\pm 30\%$), but the major contributor to this data scatter is thought to be variation in the surface characteristics of the specimens, both from one experiment to another and during the course of an experiment. The apparent change in specimen adsorptive capacities during experiments A-11, A-12, and A-13 is discussed in detail in Appendix E, and uncertainties in the true surface area of specimens are considered in Appendix B. In addition, variation in the stability of FeI_2 with changes in experimental conditions may be a factor in the wide range of data.

If we accept the previously calculated value¹⁶ for monolayer coverage of iodine on iron ($0.086 \mu\text{g I/cm}^2$ true surface area) and assume that

3 to 5 $\mu\text{g I/cm}^2$ geometric area corresponds to monolayer coverage on our specimens, the true surface area should be 30 to 60 times geometric. Since measurements of the ratio of true-to-geometric surface area were 6.8 (by surface roughness) and ~ 140 (by gas adsorption), as discussed in Appendix B, the ratio of 30 to 60 seems reasonably compatible. These widely varying values, about a factor of 20, are roughly comparable to the range in iodine loading values and could account for most of the data scatter.

Another factor that cannot be discounted is the variation in the stability of FeI_2 with changes in temperature, iodine burden, and partial pressure of hydrogen in the helium. If conditions were suitable for FeI_2 formation and condensation (see Appendix A), the amount of iodine deposited at a particular location would be limited only by the amount available, and would be totally unrelated to monolayer coverage of iodine in the form of I or HI. The equilibrium partial pressures of the various iodine species are shown for a wide variety of test conditions in Appendix A.

Although the specimens tested in helium containing 50 Pa (500 volumes/million) hydrogen were never heavily oxidized, as in tests A-4, A-5, and A-6, some evidence of oxidation was frequently apparent. Thus, it appears likely that limited and variable oxidation of the specimens in tests A-7 through A-13 may have contributed to the wide range of equilibrium sorption values. The apparent changes in specimen adsorptive capacities during experiments A-11, A-12, and A-13 could have been the result of changes in oxidation.

Comparable data from other investigators are presented along with our data in Fig. 6.2, thereby illustrating iodine loading on steel at 400°C over seven orders of magnitude in iodine burden. In the absence of information about the surface area of specimens in the data from Milstead et al., we assumed that the values were based on geometric area, as were our data. Since Neill et al. reported a true-to-geometric area ratio of only 1.25, the difference in his data is insignificant.

The equilibrium sorption measurements obtained at higher temperatures (500 to 800°C) are shown in Fig. 6.3. All of these values were

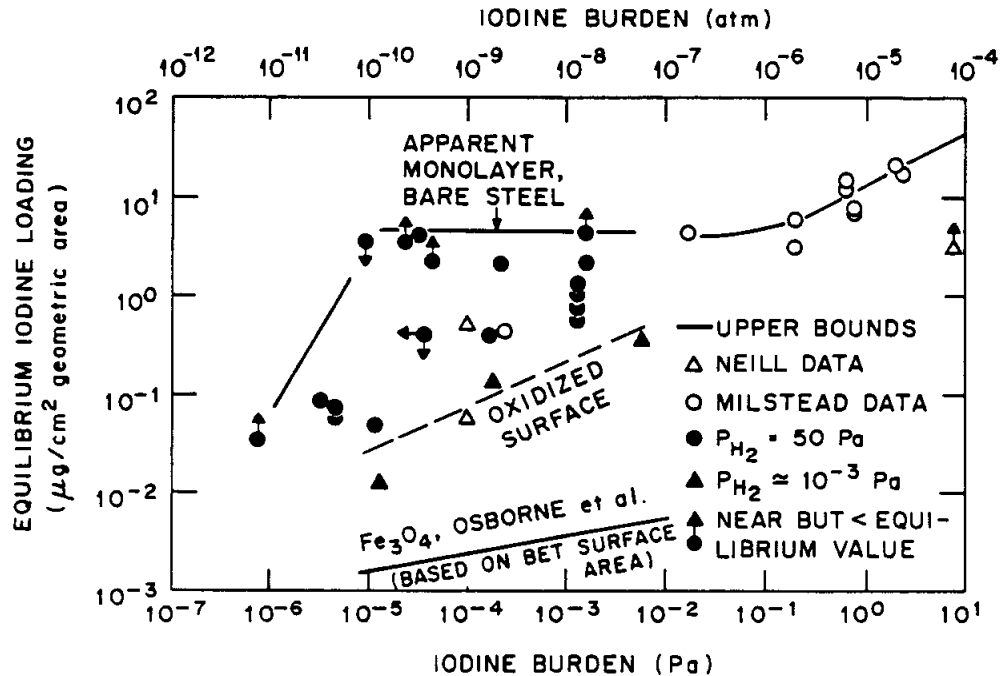


Fig. 6.2. Comparison of all measurements of iodine sorption on steel at 400°C. For the data of Milstead et al.⁷ and Neill,⁹ we assume that the iodine burden was equal to twice the reported source pressure of iodine.

derived from tests in helium containing 50 Pa (500 volumes/million) hydrogen. Although relatively few higher temperature measurements were made, the data appear reasonably consistent, both between different experiments at the same temperature and between different temperatures. For iodine burdens of 10^{-6} to 10^{-3} Pa (10^{-11} to 10^{-8} atm), the iodine coverage decreased by a factor of ≈ 8 for each 100°C increase in temperature. The three filled points in Fig. 6.4 represent data from Milstead et al.⁷ and Neill et al.⁹ at intermediate temperatures, the only comparisons available. All these data indicate that, at constant temperature in the 600 to 800°C range, equilibrium iodine loading increases with iodine burden with a slope of ≈ 1 . The same effects that caused data scatter at 400°C, particularly uncertainty in true surface area and the effect of oxidation, would be expected to influence measurements at higher temperatures. In addition, the lower iodine loadings at higher temperatures can be measured with somewhat less precision.

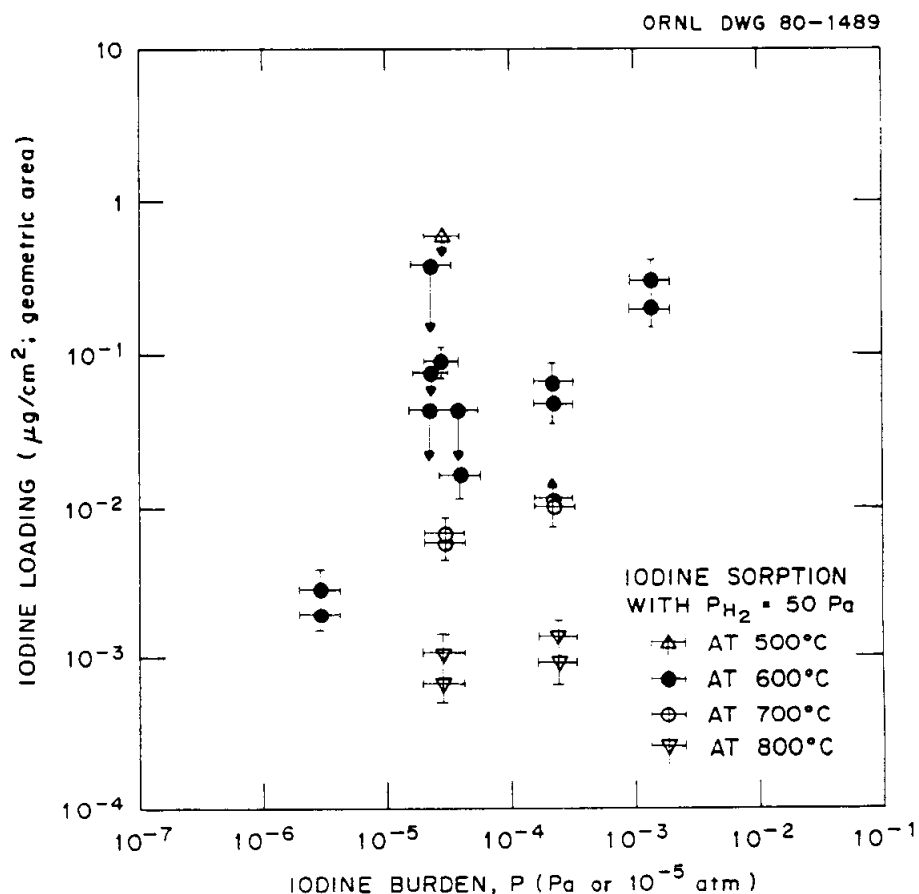


Fig. 6.3. Equilibrium sorption measurements of iodine on low-alloy steel at 500 and 800°C. Points with arrows denote near-equilibrium measurements, with arrow indicating direction of true value.

Interpretation of the data in Figs. 6.2 and 6.4 is complicated by the previously discussed scatter. At 400°C, a straight line of slope $\sim 1/2$ appears to fit the data reasonably well but is difficult to correlate with theory. Let us assume that monolayer coverage is $\sim 3 \mu\text{g I}/\text{cm}^2$, as suggested by the data between 10^{-5} and 10^{-1} Pa (10^{-10} and 10^{-6} atm) iodine burden in Fig. 6.2, and that the higher loadings at iodine burdens of ~ 1 Pa ($\sim 10^{-5}$ atm) were the result of FeI_2 condensation. Then the lower iodine loadings at 10^{-5} Pa (10^{-10} atm) and below would represent a sharp decline in loading with iodine burden. Since several adsorption isotherms are of this general shape, we tested data for iodine burdens below 10^{-4} Pa for correlation with three simple isotherms.

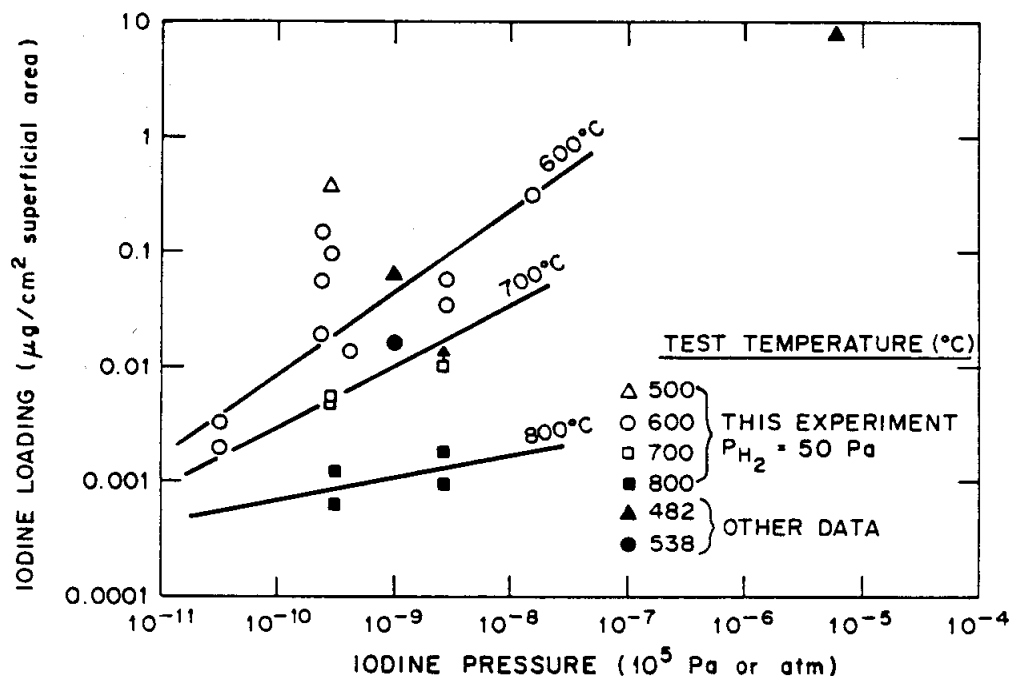


Fig. 6.4. Comparison of measurements of iodine sorption on steel at higher temperatures.

The Langmuir isotherm is of the general form

$$\theta = \frac{aP}{1 + aP}, \quad (2)$$

where

θ = fraction of monolayer coverage,

a = a constant,

P = iodine burden.

According to Hayward and Trapnell,³⁴ plotting P/θ versus P should yield a straight line if the process is Langmuir in character; that is, the heat of adsorption, q , is independent of the extent of coverage, θ . Similarly, the general form of the Freundlich isotherm, which assumes that q falls logarithmically with increasing coverage, is

$$\theta = (a_0 P)^{RT/q_m}, \quad (3)$$

where

a_o = a constant

R = the ideal gas constant,

T = absolute temperature,

q_m = heat of adsorption at monolayer coverage.

A plot of $\log \theta$ versus $\log P$ should produce a family of straight lines converging to a common point at $\theta = 1$. The Temkin isotherm assumes that q falls linearly with increasing coverage and, in the region of intermediate coverage ($0.2 < \theta < 0.8$), is of the form

$$\theta = \frac{RT}{q_o a} \ln A_o P, \quad (4)$$

where q_o is heat of adsorption at $\theta = 0$, and a and A_o are constants independent of θ . If a process follows Temkin behavior, a plot of $\ln P$ versus θ yields a straight line with the slope proportional to the absolute temperature.

When the equilibrium sorption data were plotted as above, the results were inconclusive. In all three cases, the data fell in bands that were too broad to clearly indicate correlation with a particular isotherm, but the data bands were narrower in the Freundlich and Temkin plots than in the Langmuir plot. In addition, there was an apparent increase in slope with increasing temperature on the Temkin plots (shown in Fig. 6.5) in agreement with the theory. Based on other considerations which are discussed under desorption behavior, a spectrum of adsorption site energies, leading to a spectrum of heats of adsorption, appears to exist. Consequently, either the Freundlich or the Temkin isotherm (and perhaps both) would be expected to fit the data better than the Langmuir isotherm. Thus, we are inclined to conclude that iodine sorption on steel follows Temkin isotherm behavior.

6.2 Adsorption and Desorption Rates

The adsorption of iodine from the helium carrier can be described by an equation in which the adsorption rate is set equal to the product

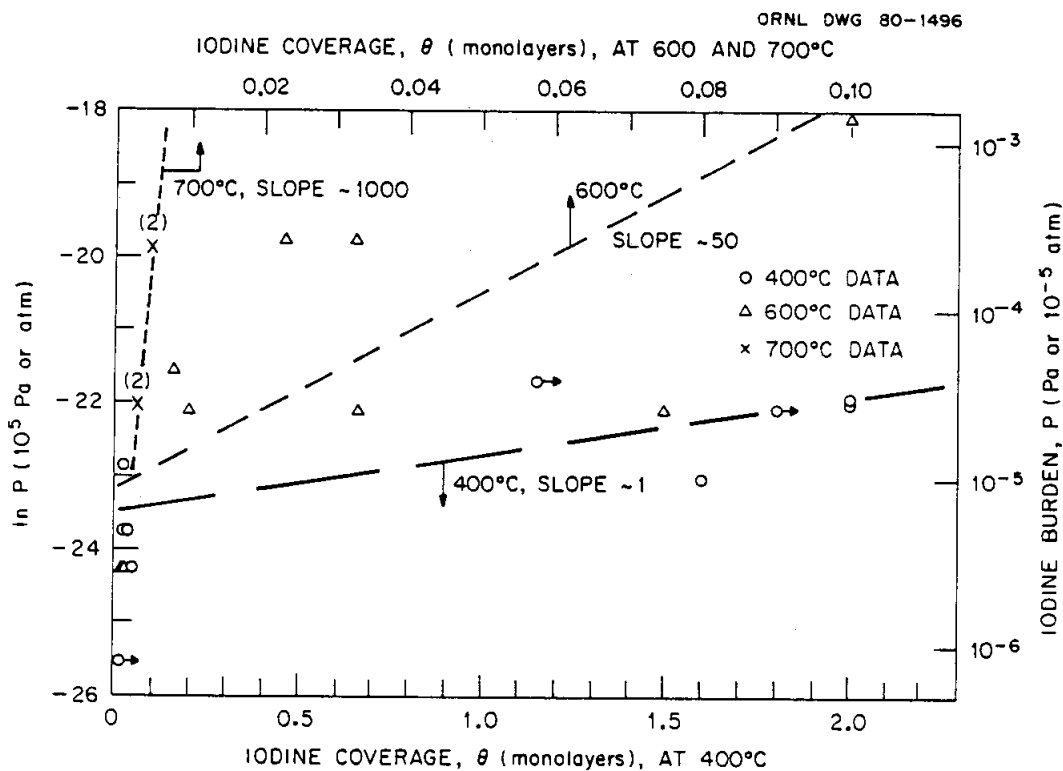


Fig. 6.5. Relationship of iodine burden and equilibrium coverage to test for Temkin isotherm behavior.

of the rate of collision of iodine species with the surface and a sticking coefficient.*³²

$$u = \frac{p}{\sqrt{2\pi mkT}} S, \quad (5)$$

where

u = adsorption rate, atoms or molecules/ m^2s ;

S = sticking coefficient;

p = partial pressure of iodine species, Pa;

m = mass of iodine species, kg (2.11×10^{-25} kg for an iodine atom);

k = Boltzmann constant (1.374×10^{-23} J/K);

T = temperature, K.

* This section is based primarily on information from Chaps. III and IV of ref. 34.

For direct activation adsorption

$$S = \sigma f(\theta) e^{-E(\theta)/RT}, \quad (6)$$

where

σ = condensation coefficient;

θ = fractional coverage of the adsorption sites;

$f(\theta)$ = a function of θ ;

$E(\theta)$ = activation energy for adsorption, which may depend on θ ,
J/mol;

R = gas constant [8.313 J/(mol·K)].

For desorption, which is always activated,

$$u' = K_D f'(\theta) e^{-E'(\theta)/RT}, \quad (7)$$

where

u' = desorption rate, atoms or molecules/m²s;

K_D = a desorption rate constant, atoms or molecules/m²s;

$f'(\theta)$ = a function of θ ;

$E'(\theta)$ = activation energy for desorption, which may depend on θ ,
J/mol.

The net rate of adsorption (or desorption) can be obtained by combining equations (5), (6), and (7) to give

$$\frac{dn}{dt} = u - u' = \frac{p\sigma}{\sqrt{2\pi mkT}} f(\theta) e^{-E(\theta)/RT} - K_D f'(\theta) e^{-E'(\theta)/RT}. \quad (8)$$

According to the system equilibrium calculations described earlier, practically all the iodine in the helium in contact with the specimens in these experiments was in the form of monatomic iodine or hydrogen iodide molecules. We assume that the adsorption and desorption of iodine involved only single adsorption sites. In that case, the rate of adsorption is proportional to the fraction of the surface not covered by adsorbate, $f(\theta) = (1 - \theta)$, and the rate of desorption is proportional to the fraction of the surface that is covered, $f'(\theta) = \theta$. By definition

$$\theta = n/n_s, \quad (9)$$

where

n = number of atoms or molecules adsorbed/m²,

n_s = number of adsorption sites/m².

Also,

$$K_D = \nu n_s, \quad (10)$$

where

ν = vibration frequency perpendicular to surface of atoms or molecules having sufficient energy to desorb, s⁻¹.

Substitution of these relationships into Eq. (8) yields

$$\frac{dn}{dt} = \frac{p\sigma}{\sqrt{2\pi mkT}} \left(1 - \frac{n}{n_s}\right) e^{-E(n/n_s)/RT} - \nu n e^{-E'(n/n_s)/RT}. \quad (11)$$

The data from our experiments were expressed most conveniently in units of $\mu\text{g I/cm}^2$ of geometrical area. Also, the data were not sufficient for determining a relationship between the activation energies and θ . For our purposes, Eq. (11) became

$$\frac{dw}{dt} = \frac{4947\sigma p}{T^{3/2}} \left(1 - \frac{w}{w_s}\right) e^{-E/RT} - \nu w e^{-E'/RT}, \quad (12)$$

where

w = concentration of adsorbed iodine, $\mu\text{g/cm}^2$;

w_s = concentration of adsorbed iodine with all sites filled, $\mu\text{g/cm}^2$;

E and E' = "average" activation energies.

Preferably, values for the product $\sigma \exp(-E/RT)$ are obtained from measurements of dw/dt under conditions where w/w_s is small, and values for the product $\nu \exp(E'/RT)$ are obtained from such measurements when $p = 0$. These conditions were not often present in the experiments. Consequently, the effects of adsorption and desorption usually had to be considered simultaneously when calculating values for the parameters.

During the adsorption phases of the experiments,

$$\frac{dw}{dt} = k_M(C_G - C^*), \quad (13)$$

where

k_M = overall mass transfer coefficient, cm/s;

C_G = local or bulk gas concentration of iodine species in gas,
 $\mu\text{g}/\text{cm}^3$;

C^* = concentration of iodine in gas in equilibrium with the concentration of adsorbed iodine on the surfaces, $\mu\text{g}/\text{cm}^3$.

When the concentration of iodine on the surface was low and $C_G \gg C^*$,

$$\frac{dw}{dt} \approx k_M C_G = 15.5 \frac{k_M p}{T} . \quad (14)$$

Values for k_M were obtained directly from the experimental data by use of the relationship

$$k_M = \frac{-3.66 \times 10^{-3} FT}{A} \ln \frac{p_e}{p_o} , \quad (15)$$

where

F = helium flow rate, std cm^3/s ;

A = surface area of specimen, cm^2 (7 cm^2 for specimen 1);

p_e, p_o = iodine burden in gas at exit and inlet, respectively, Pa;

p_e/p_o = fraction of inlet iodine in exit gas.

The adsorption rate for a constant pressure, p_o , was obtained by substituting values for k_M and p_o in Eq. (14).

The adsorption rate data obtained from the experiments are reported in Table 6.2. In some cases, the concentration of iodine on the specimen at the end of the interval, over which the measurement was made, was large enough that the criterion $C_G \gg C^*$ would not have been satisfied. For those cases, the derived k_M values are low.

The conditions during phase 1 of experiment A-13 were such that a method described by Hougen and Marshall³⁵ could be used to estimate k_M . The method involves the use of charts, presented in their paper, to obtain k_M from the rate of change in the fraction of the iodine in the gas leaving the specimen. An important assumption in the method is that the concentration of adsorbed iodine is directly proportional to the concentration in the gas at the surface over the range involved in the calculation. We cannot be certain that the assumption is valid for our

Table 6.2. Adsorption rate data

Experiment	Test phase	Time at end of interval (10 ⁶ s)	Temperature (°C)	Gas flow (std cm ³ /s)	Iodine burden in inlet gas (Pa)	Fraction of iodine in exit gas	Measured iodine adsorption rate (μg/cm ² s)	Iodine on specimen at end of interval (μg/cm ²)	Steady state concentration of iodine (μg/cm ²)	k _M (cm/s)	σ exp(-E/RT)		ν exp(-E'/RT)	
											No desorption w/w _s = 0	Desorption w _a = 5 and 10 μg/cm ²	w _s = 5 μg/cm ² (1/10 ⁶ s)	w _s = 10 μg/cm ² (1/10 ⁶ s)
A-5	1	0.35	400	3.3	5.6E-3	0.81	3.2E-5	0.11	(0.4) ^a	0.3	4E-5	5E-5	12	13
A-7	2	6.50	400	3.3	1.9E-4	0.51	2.4E-6	0.24	(>0.4)	0.8	1E-4			
	3	9.50	400	3.3	8.0E-4	0.45	1.1E-5	0.50	(>?)	0.9	1E-4			
A-8	4	3.34	400	3.3	4.0E-6	0.12	1.1E-7	0.01	(>0.02)	3	4E-4			
	5	10.28	400	3.3	1.2E-3	0.49	1.7E-5	1.2	1.4	0.8	1E-4	7E-4	8	10
	7	13.65	400	3.3	1.2E-3	0.37	2.7E-5	0.66	1.0	1	1E-4	4E-4	7	7
A-9	1	6.77	400	3.3	2.0E-6	0.19	4.6E-8	0.016	(>0.02)	2	2E-4			
	2	8.49	400	3.3	2.0E-5	0.14	5.6E-7	0.081	(>0.10)	2	2E-4			
	5	22.40	400	3.3	4.0E-6	0.12	7.3E-8	0.034	0.06	3	4E-4	8E-4	1	1
A-11	1	9.98	400	6.7	7.9E-7	0.51	2.0E-8	0.0035	(>>0.03)	2	2E-4			
	2	14.45	400	3.3	1.3E-6	0.050	3.3E-8	0.018	(>>0.03)	4	5E-4			
	3	18.00	400	6.7	6.0E-7	0.031	3.0E-8	0.029	(>>0.03)	8	10E-4			
A-12	1a	3.70	400	6.5	2.4E-5	0.50	6.3E-7	0.063	(>1)	2	2E-4			
	1b	8.50	400	6.3	2.7E-5	0.034	1.3E-6	0.62	(>1)	8	10E-4			
	3	11.20	400	6.3	5.7E-5	0.015	1.9E-6	1.2	(>2)	9	10E-4			
	8	23.10	400	6.3	1.5E-4	0.038	7.1E-6	3.2	(>4)	7	8E-4			
A-13	1	5.50	400	6.5	1.8E-5	0.043	9.0E-7	0.068	(4)	7	8E-4	9E-4	0.02	0.04
	7	18.95	700	6.5	3.0E-4	0.90	1.6E-5	0.005	0.01	0.4	4E-5	8E-5	40	40
	8	19.95	600	6.5	3.0E-4	0.73	4.3E-6	0.029	0.046	0.9	1E-4	3E-4	30	30
	11	25.83	400	6.3	4.7E-5	0.44	1.4E-6	0.26	(4)	2	2E-4	3E-4	0.01	0.04
	11	29.41	400	6.3	3.1E-5	0.041	1.4E-6	0.73	(4)	7	8E-4	10E-4	0.03	0.06

^a Values in parentheses are estimated. Steady state was not reached during the phase of the experiment.

case, but a value of 7.4 cm/s was obtained for k_M . This compares with the 7 cm/s given in Table 6.2.

The values of k_M range from 0.3 cm/s in experiment A-5 to 9 cm/s in experiments A-12 and A-13. In Appendix G, we estimated that the coefficient, k_G , for transport of iodine atoms and HI molecules through the gas to the surface is about 50 cm/s at 400°C and increases with temperature. The much lower values obtained from the experiments show that the transport of the iodine through the gas to the surface provided only a minor part of the resistance to adsorption of the iodine.

In experiment A-5, the carrier for the iodine was "pure" helium. The helium contained some oxygen, and specimen 1 was severely oxidized during the experiment. Helium containing hydrogen at a partial pressure of 50 Pa was the carrier in experiments A-12 and A-13. By the time of those experiments, the apparatus had been modified to almost eliminate oxidation of the specimen. We attribute the lower value of k_M in experiment A-5 to an effect of oxidation.

The value obtained for k_M depends on the number of sites per square centimeter available to the iodine and the "resistance" that must be overcome to reach the sites. The data seem to indicate that the primary effect of the oxygen was to reduce the number of sites. The steady state concentration of iodine on the surfaces estimated for experiment A-5, when the iodine burden was 5.6×10^{-3} Pa, was about one-tenth of that estimated for experiments A-12 and A-13, when the burden was only 3 to 5×10^{-5} Pa. Also, at the beginning of experiments A-11 and A-12, and in phase 11 of A-13 after some moisture had passed over the specimens, k_M was only 2 cm/s but increased over a few days to 7 to 9 cm/s.

Having values for k_M , the relationship obtained by combining Eqs. (12) and (14) was used to derive estimates for the values of other parameters:

$$15.5 \frac{k_m p_o}{T} = 4947 \sigma p_o e^{-E/RT} \left(1 - \frac{w}{w_s} \right) - v w e^{-E'/RT} . \quad (16)$$

Based on the assumptions that $w \ll w_s$ and the effect of desorption was negligible, values of $\sigma \exp(-E/RT)$ were calculated for all the adsorptions. The results are listed in Table 6.2.

Some of the adsorptions were carried to steady state, or we were able to extrapolate from the shape of the adsorption curve what the steady state loading would have been. For those cases, values for $\sigma \exp(-E/RT)$ and $\nu \exp(E'/RT)$ were obtained by solving a pair of Eq. (16)'s — one for an adsorption interval and another for the steady state condition. A value for w_s was required in order to solve the equations. For experiments A-12 and A-13, the steady state concentration of iodine was estimated to have been about $4 \mu\text{g}/\text{cm}^2$ at 400°C . For those experiments, at least, w_s must have been greater than $4 \mu\text{g}/\text{cm}^2$. We assumed values of 5 and $10 \mu\text{g}/\text{cm}^2$ for use in the calculations. The results of these calculations are included in Table 6.2.

The values for $\sigma \exp(-E/RT)$ at 400°C range from 4×10^{-5} to 1×10^{-3} at 400°C . Since they depend primarily on k_M , the causes for the variation are the same: the effects of oxidation, method of analysis, and others as yet unidentified. Only in a few cases, where a comparison could be made, did including the effect of desorption produce large increases in the values. The values of $\sigma \exp(-E/RT)$ were insensitive to the choice of values for $w_s > 5 \mu\text{g}/\text{cm}^2$.

Values for $\nu \exp(-E'/RT)$ that were derived from the calculations are included in Table 6.2. They will be considered later along with other desorption data.

In experiment A-13, data were obtained from adsorptions at 600 and 700°C as well as 400°C . The values for $\sigma \exp(-E/RT)$, from calculations that included the effect of desorption, are plotted versus $1000/T$ in Fig. 6.6.

Because of the few data points and the uncertainty in their values, it is difficult to draw an acceptable line through them for use in calculating values for the activation energy and the condensation coefficient. A single straight line would imply constant values for those parameters. If the iodine were adsorbed on sites having a range of activation energies, the "average" energy could change with temperature, and such a line would not truly represent the data.

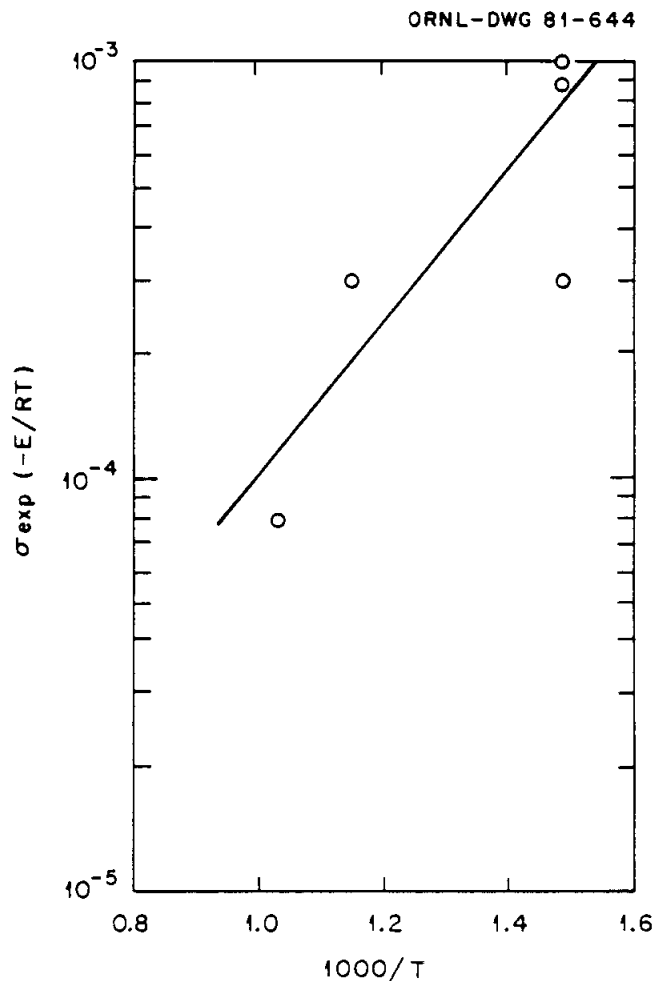


Fig. 6.6. Effect of temperature on $\sigma \exp[-E/RT]$.

Despite these considerations, we have drawn a straight line of arbitrary position and slope through the data points. Based on that representation of the data, $E = -36,000$ J/mol and $\sigma = 1.4 \times 10^{-6}$.

Rates of adsorption of iodine on mild steel were measured by Neill.³ He obtained net adsorption rates of 7.5×10^{-8} to 775×10^{-8} mg/cm² h (2×10^{-8} to 215×10^{-8} $\mu\text{g}/\text{cm}^2$ s) at 400°C when the iodine source pressure was 4.9×10^{-5} Pa and the iodine burden at the specimens was about 9×10^{-5} Pa. At 400°C we measured adsorption rates of similar magnitude, 240×10^{-8} and 710×10^{-8} $\mu\text{g}/\text{cm}^2$ s when the average iodine burdens were

about 1.5×10^{-4} and 8×10^{-5} Pa respectively (experiment A-7, phase 2 and experiment A-12, phase 8).

Neill derived values for the activation energy for adsorption and the condensation coefficient from data taken at temperatures from 316 to 538°C when the iodine source pressure was 4.9 Pa. The activation energy was -27.5 kcal/mol (-115,000 J/mol), and the condensation coefficient was 5.53×10^{-18} .

Inspection of Neill's data⁹ indicates that the activation energy would have been near the -36,000 J/mol that we obtained, if only the data at 400°C and above had been available for the determination. His value for the condensation coefficient is much less than the 1.4×10^{-6} that we obtained. Part of the difference is a consequence of the difference in activation energies. The remainder seems to be a result of Neill's value being based on data obtained when the iodine source pressure was 4.9 Pa. It appears that the adsorption rate in Neill's experiments increased by a factor of less than 40 when the source pressure was increased by a factor of 10^5 (from 4.9×10^{-5} Pa to 4.9 Pa). Since the adsorption rate did not increase in proportion to the pressure, the apparent value of the condensation coefficient would have been much smaller at the higher pressure.

Since the activation energy derived from the experiments has a negative value, the adsorption process is not thermally activated. According to Hayward and Trapnell,³⁴ there is no established theory that can account for the kinetics of nonactivated adsorption in detail. Precursor states are important, so the kinetics cannot be described adequately in terms of collisions with vacant sites by substituting $E = 0$ into the equations for direct activated adsorption. The significance of values for E and σ , derived from plots such as Fig. 6.6, is uncertain.

If one considers the adsorption data in terms of Eq. (5), the sticking coefficient, S , has the value of $\sigma \exp(-E/RT)(1 - w/w_s)$. At the times that adsorption rates were measured in our experiments, w/w_s was small enough to be neglected. Therefore, S had approximately the values of $\sigma \exp(-E/RT)$ in Table 6.2 and Fig. 6.6. Those values, 4×10^{-5} to

1×10^{-3} , are much lower than the 0.1 to 0.5 that have been reported for other systems,³⁴ but such low values are not uncommon. Rapid desorption of iodine from the precursor state or volatilization of FeI_2 , if it was a product of the adsorption, are possible causes for the low sticking coefficients in our experiments.

The experiments to measure the steady state concentration of iodine on metal specimens included desorption phases. In some, the iodine burden was reduced while the specimen was held at the adsorption temperature. In others, the temperature was raised while the iodine burden was held constant in order to obtain steady state loadings at higher temperature. In a few, the iodine burden was reduced and the temperature was raised. Data obtained from all the desorptions are presented in Table 6.3.

Early in the experiment, we observed that iodine adsorbed at 400°C desorbed slowly, or not at all, at 400°C when the iodine burden was reduced to 0. Raising the temperature to 600°C , with the burden at 0, resulted in rapid desorption of 60 to 90% of the iodine before the rate slowed to near 0. Practically all the remaining iodine desorbed rapidly when the temperature was raised further to 800°C . This behavior is shown by the data from experiments A-5, A-6, and A-8 in Table 6.3.

Kelly³⁶ reported on experiments in which gas "attached" to various materials was released by heating in steps to 800°C , where the last of the attached material was released. With each increase in temperature, some of the gas was released rapidly. Then, the rate of release slowed greatly until the temperature was raised again. Kelly showed that such behavior is a consequence of a spectrum of activation energies for release. The analysis of data from our experiments is consistent with such a conclusion.

For each desorption in our experiments, the logarithm of the amount of iodine on specimen 1 was plotted versus time. It developed that the desorption curves could be resolved, with good fits to the data, into component curves, each of the form

$$\ln\left(\frac{m_n}{m_{no}}\right) = \lambda_n(t - t_o) , \quad (17)$$

Table 6.3. Desorption data

Experiment	Test phase	Temperature (°C)	Helium flow (std cm ³ /s)	Iodine burden at inlet of specimen		Iodine loading on specimen		Duration of desorption phase (10 ³ s)	$-\lambda_n$ (1/10 ³ s)	m_{no} (μg)	Δp^a (10 ⁻⁶ Pa)	$\frac{1}{T} (87,200 \text{ KPa s} / T^{1/2} \text{ K})$		$v_e^{-E_n'/RT}$		E_n' for $v = 10^3$	
				Desorption phase (10 ⁻⁶ Pa)	Preceding phase (10 ⁻⁶ Pa)	Beginning (μg)	End (μg)					$\text{Pa} \cdot 10^{-3}$	$\text{Pa} \cdot 10^{-4}$	$\text{Pa} \cdot 10^{-3}$	$\text{Pa} \cdot 10^{-4}$	$\text{Pa} \cdot 10^{-3}$	$\text{Pa} \cdot 10^{-4}$
A-5	2, 3	400	3.3	0	500	2.7* ^b	2.7	2.72	0 (<0.01) ^c	2.7	0 (<0.14) ^c	8.0	1.7	(<0.00) ^c	(<0.017) ^c	(≥2.46) ^c	(≥2.55) ^c
	4	600	3.2	0	0	2.7*	0.9	0.72	400 17 0.19	0.5 1.2 1.0	1200	7.5	1.6	3000 130 1.4	640 27 0.30	2.43 2.66 2.98	2.54 2.77 3.10
A-6	2	400	3.3	0	0.8-1.7	0.098*	0.098	0.62	0 (<0.02)	0.098	0 (<0.01)	8.0	1.7	(<0.16)	(<0.034)	(≥2.42)	(≥2.51)
	5	400	3.3	0	5.9	0.110	0.104	3.27	0.02	0.110	0.012	8.0	1.7	0.16	0.34	2.42	2.51
	7	600	3.3	0	0	0.100	0.04	0.89	23	0.099	5.0	7.3	1.6	168 37 4.0	0.88 144 0.85	2.64 2.91 3.13	2.75 3.02 3.25
A-7	8	800	3.3	0	0	0.04	0.002	0.10	90	0.04	19	6.6	1.6	590	144	3.13	3.25
	2	400	3.3	10	19	2.4	1.95	2.0	0.5	1.0	2.7	8.0	1.7	4.0	0.85	2.84	2.93
A-8	2	600	3.3	0	0.7	0.65*	0.075	0.66	70	0.70	37	7.5	1.6	146	32	2.65	2.76
	5	800	3.3	0	0	0.075	0.015	0.07	7.6 0.71	0.14 0.12	900	6.6	1.6	55 5.2	12 1.1	2.72 2.84	2.83 3.00
A-9	5	600	3.3	140	90-170	9.4*	1.96	1.67	0 (<0.2)	0.015	2000	7.3	1.6	5900 (<1.3)	1400 (<0.32)	2.92 (≥1.7)	3.05 (≥1.8)
	8	400	3.2	4	90-190	6.4*	3.4	3.3	59 2.9	0.6 1.9	2000	7.3	1.6	430 21	94 4.6	2.57 2.79	2.68 2.90
A-10	3	600	3.3	0.2	2-0.2	0.61*	0.02	5.22	2.2 0.043	2.7 3.9	34	8.0	1.7	18 0.34	3.7 0.073	2.16 2.38	2.25 2.47
	6	400	3.3	0	0.5	0.47*	0.32	5.95	25 5.14	0.32 0.14	47	7.3	1.6	180 37	40 8.2	2.63 2.75	2.74 2.86
	11	400	6.7	0	2.8	23.5	22.8	1.91	0.78 0	0.13 0.02	13	4.4	1.3	5.6 1.2	2.88	3.00	
A-11	13	450	6.7	3	2.2	24.2	23.6	0.76	6.5 0.059	0.096 0.44	1.4	8.0	1.7	52 0.47	11 0.10	2.10 2.36	2.19 2.45
	14	600	6.7	3	3	23.6	2.7	0.57	0.006 ^d 0.016 ^d	10.35 23.5	0.34 2.1	4.5	1.4	0.027 0.072	0.008 0.022	2.59 2.47	2.59 2.53
	14	600	6.7	3	3	23.6	2.7	0.57	0.2 0	~12.0 ~12.0	13	4.4	1.3	0.9 0.3	2.50	2.56	
A-12	2	500	6.3	3	2.6-3	6.2	4.5	1.70	0 2.7	1.0 8.6	1200	4.1	1.3	62 20	2.71	2.79	
	3	600	6.3	3	3	4.4	0.64	2.44	0.53 0	3.2 3.0	4.7	4.5	1.3	2.4 0.69	2.61	2.69	
	4	700	6.3	3	3	0.61*	0.047	0.91	9.5 2.8	2.2 1.6	71	4.3	1.3	41 12	12 3.6	2.74 2.83	2.83 2.92
A-13	5	800	6.3	3	3	0.61*	0.047	0.91	0 7.9	0.64 0.14	34	4.1	1.3	100 32	33 10	2.98 3.07	3.07 3.17
	9	600	6.3	3-6	20-30	0.041*	0.009	0.90	55 13	0.018 0.014	3.3	4.0	1.3	220 52	72 17	3.22 3.35	3.32 3.45
	10	400	6.3	0	3.1	9.7	9.5	1.90	0 10	0.21 0.11	5.0	4.3	1.3	43 13	13	2.74	2.82
A-14	13	400	6.3	0	2-3	9.7	9.5	1.90	0.014 ^d 13	9.7 5.2	0.38 210	4.7	1.4	0.066 56	0.020	2.47	2.54
	13	600	6.3	0	0	9.4	0.53	1.56	2.4 0	3.8 0.4	210	4.3	1.3	10 3.1	2.84	2.93	

^a Δp is the increase in iodine burden in the helium produced by desorption at the beginning of the desorption phase; $\Delta p = \frac{-17.6}{T} \sum_{i=1}^n \lambda_{i, m_{no}}$.

^b Asterisks indicate that loading was at steady state at end of preceding phase.

^c Numbers in parentheses are the maximum values for which λ_n could not be distinguished from 0.

^d Desorption rate known to have been limited by gas flow.

where

m_n, m_{n0} = mass of iodine on specimen associated with component curve n at times t and t_0 , μg ;

t = time, s;

λ_n = desorption rate constant, s^{-1} .

Three of the desorption curves from experiment A-13 are shown in Figs. 6.7, 6.8, and 6.9. The rate constants and related data for all the desorptions are reported in Table 6.3. The fact that more than one component curve with $\lambda \neq 0$ was obtained in most cases suggests that the iodine was present in populations having different activation energies for desorption.

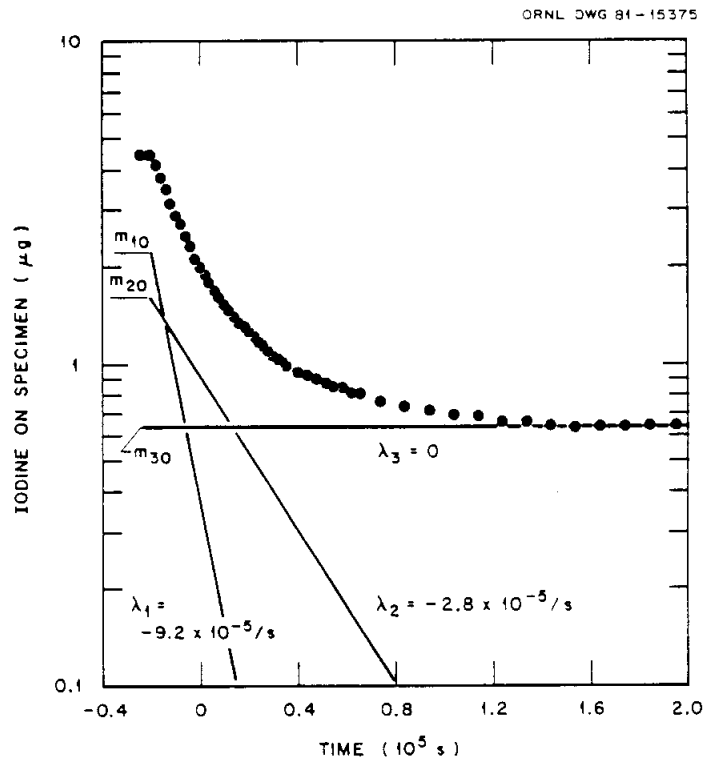


Fig. 6.7. Desorption curve for experiment A-13-3 at 600°C in helium having an iodine burden of 3×10^{-5} Pa.

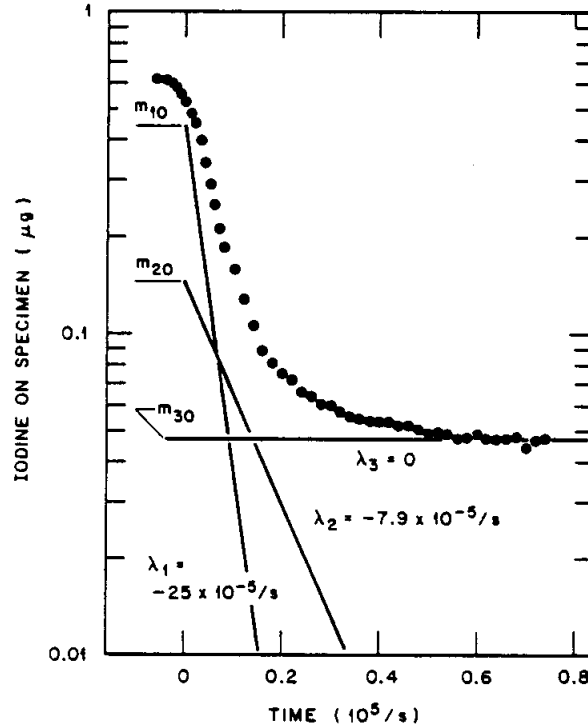


Fig. 6.8. Desorption curve for experiment A-13-4 at 700°C in helium having an iodine burden of 3×10^{-5} Pa.

If there were several such populations, the desorption could be described by the equation

$$\frac{dw}{dt} = C p a_1 S_1 - v w_1 e^{-E'_1/RT} + \dots + C p a_n S_n - v w_n e^{-E'_n/RT}, \quad (18)$$

where the subscripts designate the several populations, and $a_1 \dots a_n$ are the fractions of the surface occupied by sites having activation energies $E'_1 \dots E'_n$ for desorption. Assuming that the sticking coefficients were equal at each temperature,

$$C p \sum_1^n a_n S_n = C p S = \frac{4947 p S}{T^{1/2}}. \quad (19)$$

As the helium passed over the specimen and iodine desorbed into the gas, the iodine burden increased from the inlet to the exit of the specimen.

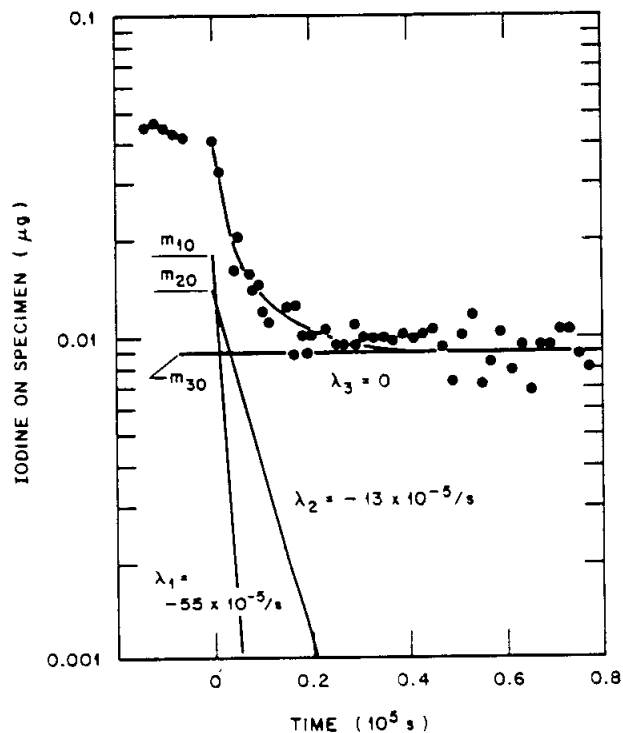


Fig. 6.9. Desorption curve for experiment A-13-5 at 800°C in helium having an iodine burden of 3×10^{-5} Pa.

When this effect is included

$$CpS = C(p_o + f\Delta p)S = \frac{4947}{T^{\frac{1}{2}}} \left(p_o - \frac{17.6 Af}{F} \frac{dw}{dt} \right) S, \quad (20)$$

where

p_o = partial pressure of iodine in helium entering the specimen, Pa;

Δp = change in partial pressure resulting from desorption, Pa;

f = factor to average the increase in pressure over the surface;

$p_o + f\Delta p$ = average pressure over the surface;

A = geometrical area of specimen, cm^2 ;

F = helium flow, $\text{std cm}^2/\text{s}$.

With regard to the desorption curve and its component curves,

$$\begin{aligned} w &= w_1 + \dots + w_n \\ &= w_1' + w_1'' + \dots + w_n' + w_n'' , \end{aligned} \quad (21)$$

and

$$\frac{dw}{dt} = \frac{dw_1'}{dt} + \dots + \frac{dw_n'}{dt} , \quad (22)$$

where w_n' represents the desorbing part and w_n'' represents the steady state part of w_n . Then, Eqs. (18) to (21) combine to give

$$\left(1 + \frac{87,200Afs}{T^{\frac{1}{2}}F} \right) \frac{dw}{dt} = -vw_1'e^{-E_1'/RT} - \dots - vw_n'e^{-E_n'/RT} , \quad (23)$$

and

$$\frac{4947p_o S}{T^{\frac{1}{2}}} - vw_1''e^{-E_1'/RT} - \dots - vw_n''e^{-E_n'/RT} = 0 . \quad (24)$$

Equation (23) can be solved to obtain equations for $w_1' \dots w_n'$ of the form

$$\ln\left(\frac{w_n'}{w_{no}'}\right) = \frac{-v e^{-E_n'/RT}}{1 + \frac{87,200Afs}{T^{\frac{1}{2}}F}} (t - t_o) . \quad (25)$$

It follows that, for $\lambda \neq 0$,

$$\frac{vd e^{-E_n'/RT}}{1 + \frac{87,200Afs}{T^{\frac{1}{2}}F}} = -\lambda_n . \quad (26)$$

The steady state component curve, for which $\lambda = 0$, is represented here by Eq. (24). However, care must be taken in using values from the steady state component, because it may also contain populations for which λ was so small as to have been indistinguishable from 0 when the desorption curve was resolved.

The activation energy for desorption, calculated by use of Eq. (26), for each value of λ_n for each desorption is given in Table 6.3. For purposes of the calculations, values of 1×10^{-3} and 1×10^{-4} were

assigned to the product fS on the basis of the results of the analysis of the adsorption data. The commonly used value of $1 \times 10^{13}/s$ was assigned to ν .³⁵ Except for experiment A-5, the values of $\nu \exp(-E'/RT)$ obtained from the adsorption phases and listed in Table 6.2 are about the same as those obtained from the desorption phases (Table 6.3).

In experiment A-13, desorptions were carried out at 100°C intervals from 400 to 800°C. The relationship between the temperature and the activation energy for desorption of the iodine being desorbed at each temperature is shown in Fig. 6.10.

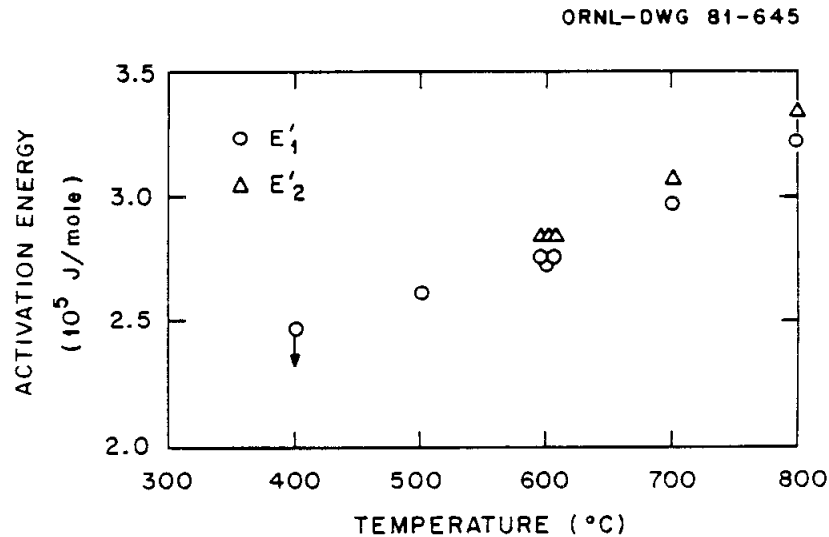


Fig. 6.10. Effect of temperature of desorption on activation energy for desorption of iodine.

The data from all the experiments are consistent in showing that the fractional desorption rate increased with temperature, but less than would be expected if the activation energy were constant. In each case where iodine was desorbed by raising the temperature, the activation energy for the rapidly desorbing component at the higher temperature was equal to or somewhat greater than the activation energy for the slowly desorbing component at the preceding lower temperature. This observation obtains whether the sticking coefficient is assumed to be constant over the temperature range or to decrease from 10^{-3} to 10^{-4} between 400 and 800°C.

We conclude that the data from the experiments provide substantial support for the thesis that the iodine was adsorbed on sites having a range of activation energies for desorption. Assuming that $10^{-3} > S > 10^{-4}$ and $\nu \approx 10^{13}$, the range for iodine adsorbed at 400°C was from about 2.2×10^5 to 3.3×10^5 J/mol. It is not possible to determine the iodine concentration as a function of activation energy, but it appears that about 80% was on sites having activation energies of 2.2×10^5 to 2.8×10^5 J/mol.

These estimates, and the data on which they are based, contain some substantial uncertainties. The activation energies depend on uncertain values for S and ν . The values of λ_n , primarily λ_1 , depend on the extent to which the calculation compensated for readsorption. Values in the Δp column of Table 6.3 show that the iodine burden in the helium leaving the specimen at the beginning of a desorption was often equal to and sometimes, when the temperature was raised, much greater than the burden during the preceding adsorption. This could result in low values for λ_1 and high values for E_1' .

In particular, the values for λ for the desorptions at 400°C in experiments A-12-6, A-12-7, A-12-11, and A-13-12 must be low. The iodine concentration on the specimen had not reached steady state at the end of the adsorption phases. The iodine burden in the helium leaving the specimen was well below the burden in the entering gas. The concentration of iodine on the specimen near the exit must have been considerably lower than the average concentration on the surface.

During the desorption phases, the iodine burden in the helium entering the specimens was near 0. The burdens in the gas leaving the specimens were about the same as they were at the end of the adsorption phases. This implies that the net desorption rate was being controlled by the helium flow rate and the equilibrium between the iodine in the gas and on the surface at the exit of the specimen.

The desorptions in Neill's experiments were carried out in vacuum. Presumably, readsorption was negligible. He found that several desorption coefficients (λ 's) were required to describe each desorption curve.

All the desorptions were carried out at the temperature of the adsorption. Not all the iodine desorbed at temperatures from 316 to 538°C, the range in the experiments. The fraction that desorbed decreased with increasing temperature, but the concentration of iodine remaining on the surface also decreased.

Neill derived a desorption activation energy of 67,000 J/mol (16 kcal/mol) from an Arrhenius-type plot of the λ_1 values from his experiments. This value is close to the free energy for the sublimation of FeI_2 . On this basis he concluded that the iodine was desorbed as FeI_2 .

The values of $\nu \exp(-E_1'/RT)$ for $fS = 10^{-3}$, which is λ_1 "corrected" for the effect of readsorption, from our desorptions at temperatures from 600 to 800°C fit the extension of Neill's data to higher temperature. At lower temperatures, the corrected desorption coefficients from our experiments, except for experiment A-8-8, are much smaller than Neill's. The value of $18 \times 10^{-5}/s$ for A-8-8 fits the data from his experiments.

All the desorptions in Neill's experiments were preceded by adsorptions at an iodine pressure of 5 to 10 Pa. According to the system equilibrium calculations, $\text{FeI}_2(s)$ is stable at the temperature and iodine pressure in Neill's experiments. It seems likely that some iodine would be released as FeI_2 during the desorptions. At the temperature and iodine and hydrogen pressures in our experiments, $\text{FeI}_2(s)$ and $\text{FeI}_2(l)$ (above 587°C) are not stable. The difference in the stability of FeI_2 may, in addition to the effect of readsorption, account for some of the difference between the initial adsorption rates in the two sets of experiments. However, there is evidence that iodine desorbed as FeI_2 at times, seemingly when a large amount was released rapidly, in our experiments. During phase 4 of experiment A-13, about 14 μg of iodine was released from specimen 2 when it was heated rapidly from 400 to 700°C. At least one-third of the iodine condensed in a film on the wall of the furnace tube between the specimen and the charcoal trap. The material could not be recovered for analysis, but there was ample indirect evidence to conclude that it was FeI_2 .

The data from the experiments seem to show that adsorbed iodine resides on the metal surface as FeI_2 . Whether the iodine desorbs as FeI_2 , HI, or I depends on such conditions as the temperature, the composition of the gas phase, and the amount and rate of release.

6.3 Conclusions

Tests were performed to determine the equilibrium loadings of iodine on 2-1/4% Cr-1% Mo steel in the temperature range 400 to 800°C. The tests were characterized by a large scatter in the measured or inferred equilibrium loadings, which we attribute to variations in the condition of the surface. For this reason, one isotherm (400°C) was examined most extensively in order to obtain more complete information for at least one case.

Our tests at 400°C and comparisons with the work of other experimenters lead us to the following conclusions regarding the 400°C isotherm:

1. In helium containing enough hydrogen to prevent significant oxidation of the steel, the surface saturates with chemisorbed iodine at an iodine burden of about 10^{-5} Pa (10^{-10} atm). For our specimens the saturation concentration was 3 to 5 $\mu\text{g}/\text{cm}^2$. Assuming that the surface was covered by one monolayer of adsorbed iodine at saturation, the effective surface area was 30 to 60 times the geometric area.
2. At iodine pressures high enough for $\text{FeI}_2(\text{s})$ to be stable and to accumulate, the concentration of iodine on the surface increases above the chemisorbed saturation level with increasing iodine burden. The iodine burden at which $\text{FeI}_2(\text{s})$ is stable is about 0.4 Pa (4×10^{-6} atm) when the gas contains no hydrogen and increases with increasing hydrogen pressure.
3. The equilibrium concentration of iodine on unoxidized steel falls rapidly with decreasing iodine burden below about 10^{-5} Pa (10^{-10} atm). The few data obtained at the lower pressures suggest that the equilibrium concentration may vary directly with the iodine burden in this regime.

4. The equilibrium concentration of iodine on oxidized steel depends on the degree of oxidation. On a severely oxidized surface, the equilibrium concentration may be as little as 1% of that on an unoxidized surface, which is comparable with measured equilibrium concentrations on Fe_3O_4 .
5. The equilibrium concentration of iodine on steel decreases with increasing temperature above 400°C . The decrease in our experiments was about a factor of 50 for each 200°C increase in temperature. At 800°C the adsorptive capacity of the metal was so small that it was hardly measurable.
6. The data from our experiments and others indicate that the adsorption of iodine on steel is not a thermally activated process. The rate of adsorption decreases with increasing temperature, and the adsorption reactions are not understood. If the adsorption rate is taken as the product of the rate of impingement of iodine on the surface and a sticking coefficient, we obtain values for the sticking coefficient that decrease from $\sim 10^{-3}$ at 400°C to $\sim 10^{-4}$ at 700°C .
7. The desorption of iodine is a thermally activated process. The desorption rate increases with temperature but, in our experiments, does so less rapidly than would be expected if the activation energy were constant. We inferred from this that iodine adsorbed on sites having a range of activation energies for desorption. The range of activation energies was calculated to be from 2.2×10^5 to 3.3×10^5 J/mol if a value of 10^{13} was assigned to ν , the vibration frequency normal to the surface of adsorbed atoms with sufficient energy to desorb. About 80% of the iodine was on sites having activation energies in the range 2.2×10^5 to 2.8×10^5 J/mol. These values provide a basis for estimating desorption rates.
8. Evidence from the experiments seems to indicate that adsorbed iodine resides on the metal surface as FeI_2 . Whether the iodine desorbs as FeI_2 , HI , or I may depend on the temperature, the composition of the gas phase, and the amount and rate of desorption.

7. FUTURE WORK

The results presented in this report have been evaluated with regard to what additional work is needed to complete our understanding of iodine sorption/desorption behavior on low-chromium alloy steel under HTGR conditions. Experiments need to be conducted which are designed to avoid problems or uncertainties experienced in the past and/or to address unanswered questions.

Specimen fabrication and geometry need to be reexamined, with emphasis on eliminating (or at least reducing) the uncertainty in surface area available for gas adsorption by revision of fabrication techniques. A change in specimen geometry which might facilitate data collection and analysis should be considered. Better control of the impurity levels in the helium should be investigated also.

Experiments need to be conducted to measure the equilibrium iodine loadings at 300°C, and the higher temperature data (at 600 to 800°C) need to be supplemented. At least one experiment should be devoted to additional equilibrium measurements at very low iodine burdens, $<10^{-6}$ Pa ($<10^{-11}$ atm). The test sequences should be planned to provide as much additional data as possible on sorption/desorption kinetics. Experiments to investigate desorption upon the injection of controlled amounts of water vapor, and perhaps simulations of other accident scenarios, should be considered.

The above experiments will be considered in the future when financial support is provided.

8. ACKNOWLEDGMENTS

The valuable contributions of many other people to this study are gratefully acknowledged: F. F. Dyer and L. L. Fairchild for assistance in spectrometer calibration and iodine analysis; R. S. Crouse and B. C. Leslie for metallographic examination and interpretation; E. Hoinkis for specimen examination and consultation on iodine sorptive behavior; Betty Drake for preparation of the manuscript; and A. L. Harkey for editing. Technical reviewers were T. M. Besmann, A. D. Kelmers, and J. S. Watson.

9. REFERENCES

1. General Atomic Company, *HTGR Accident Initiation and Progression Analysis Status Report*, GA-A13617 (1976).
2. D. L. Hanson, *A Review of Fission Product Plateout Investigations at General Atomic*, GA-A14555 (1977).
3. E. L. Compere, M. F. Osborne, and H. J. de Nordwall, *Iodine Behavior in an HTGR*, ORNL-TM-4744 (1975).
4. F. E. Vanslager and L. D. Mers, *PAD: A Computer Code for Calculating the Plateout Activity Distribution in a Reactor Circuit*, GA-10460 (January 1971).
5. W. W. Hudritsch and P. D. Smith, *PADLOC: A One-Dimensional Computer Program for Calculating Coolant and Plateout Fission Product Concentrations*, GA-A14401, to be published.
6. E. Hoinkis, *A Review of the Adsorption of Iodine on Metal and Its Behavior in Loops*, ORNL/TM-2916 (1970).
7. C. E. Milstead, W. E. Bell, and J. H. Norman, "Deposition of Iodine on Low Chromium-Alloy Steel," *Nucl. Appl. Technol.* 7, 361-66 (1968).
8. "HTGR Safety Research—Plateout Tests," pp. 1-5 to 1-9 in *HTGR Generic Technology Program Quarterly Progress Report for the Period Ending June 30, 1978*, GA-A15055 (July 1978).
9. F. H. Neill, *Adsorption and Desorption of Iodine on Mild Steel*, ORNL/TM-2763 (1970).
10. K. Watanabe, S. Maeda, T. Yamashina, and A. G. Mathewson, "Changes in Roughness Factors of 304 and 316 L + N Stainless Steels with Ion Bombardment and Discharge Cleaning," *J. Nucl. Mater.* 93 and 94, 679-85 (1980).
11. R. A. Strehlow, Chemistry Division, ORNL, personal communication to M. F. Osborne, 1980.
12. F. H. Neill, D. L. Gray, and T. S. Kress, *Iodine Transport and Deposition in a High Temperature Helium Loop*, ORNL/TM-1286 (1966).

13. J. M. Genco, W. E. Berry, H. S. Rosenberg, and D. L. Morrison, *Fission Product Deposition and Its Enhancement Under Reactor Accident Conditions: Deposition on Primary System Surfaces*, BMI-1863 (March 1969).
14. M. E. Davis, W. W. Browning, Jr., G. E. Creek, and G. W. Parker, *The Deposition of Fission Product Iodine on Structural Surfaces*, CONF-650407 (1965), pp. 730-46.
15. E. Hoinkis, "Surface Interactions of Iodine with Fe_3O_4 ," *Vacuum* 22(11), 525-30 (1972).
16. M. F. Osborne, E. L. Compere, and H. J. de Nordwall, *Studies of Iodine Adsorption and Desorption on HTGR Coolant Circuit Materials*, ORNL/TM-5094 (1976).
17. T. M. Besmann, *SOLGASMIX-PV, A Computer Program to Calculate Equilibrium Relationships in Complex Chemical Systems*, ORNL/TM-5775 (April 1977).
18. R. B. Briggs and M. F. Osborne, *Iodine Adsorption Experiment A-4*, ORNL/GCR-79/8 (October 1979).
19. R. B. Briggs and M. F. Osborne, *Iodine Adsorption Experiment A-5*, ORNL/GCR-79/9 (January 1980).
20. R. B. Briggs and M. F. Osborne, *Iodine Adsorption Experiment A-6*, ORNL/GCR-80/3 (January 1980).
21. R. B. Briggs and M. F. Osborne, *Iodine Adsorption Experiment A-7*, ORNL/GCR-79/5 (October 1979).
22. R. B. Briggs and M. F. Osborne, *Iodine Adsorption Experiment A-8*, ORNL/GCR-80/5 (April 1980).
23. R. B. Briggs and M. F. Osborne, *Iodine Adsorption Experiment A-9*, ORNL/GCR-80/6 (April 1980).
24. R. B. Briggs and M. F. Osborne, *Iodine Adsorption Experiment A-10*, ORNL/GCR-80/4 (April 1980).
25. R. B. Briggs and M. F. Osborne, *Iodine Adsorption Experiment A-11*, ORNL/GCR-80/12 (May 1980).

26. R. B. Briggs and M. F. Osborne, *Iodine Adsorption Experiment A-12*, ORNL/GCR-80/14 (October 1980).
27. R. B. Briggs and M. F. Osborne, *Iodine Adsorption Experiment A-13*, ORNL/GCR-80/21 (October 1980).
28. R. L. Heestand, Metals and Ceramics Division, ORNL, personal communication to M. F. Osborne, 1978.
29. O. P. Chawla, General Atomic Company, San Diego, Calif., personal communication to M. F. Osborne, 1979.
30. J. D. Kintigh, Analytical Chemistry Division, ORNL, personal communication to M. F. Osborne, 1980.
31. B. C. Leslie and R. S. Crouse, Metals and Ceramics Division, ORNL, personal communication to M. F. Osborne, 1980.
32. "Sorption of Iodine on Metal Surfaces (Dynamic Method)," pp. 143-55 in *Public Service Company of Colorado 330-MW(e) High Temperature Gas-Cooled Reactor Research and Development Program, Quarterly Progress Report, Sept. 30, 1967*, USAEC Report GA-8270 (1967).
33. R. E. Honig and H. O. Hook, "Vapor Pressure Data for Some Common Gases," *RCA Rev.* 21, 360-68 (1960).
34. D. O. Hayward and B. M. W. Trapnell, *Chemisorption*, Butterworth & Co., 1964.
35. O. A. Hougen and W. R. Marshall, Jr., "Adsorption of a Component Material from a Fluid Stream Flowing through a Stationary Granular Bed," *Chem. Eng. Prog.* 43(4), 197-99 (April 1947).
36. R. Kelly, "The Diffusion of Attached Inert-Gas Activity," *Can. J. Chem.* 39, 2411 (1961).
37. O. Kubachewski, E. Ll. Evans, and C. B. Alcock, *Metallurgical Thermochemistry*, 4th ed. rev., Pergamon Press, 1967.
38. E. Hoinkis, Han-Meitner-Institut, 1000 Berlin 39, Germany, personal communication to M. F. Osborne, 1979.
39. S. T. Carroll, Jr., Isotopes Division, ORNL, personal communication to M. F. Osborne, 1971.

40. J. G. Knudsen and D. L. Katz, *Fluid Dynamics and Heat Transfer*, McGraw-Hill, New York, 1958, pp. 240-42.
41. *Perry's Chemical Engineers Handbook*, 4th ed., McGraw-Hill, New York, pp. 14-20, 1963.
42. A. P. Malinauskas, "Gaseous Diffusion. The Systems He-Ar, Ar-Xe, and He-Xe," *J. Chem. Phys.* 42, 156 (1965).

10. APPENDIXES

Appendix A. THERMODYNAMIC EQUILIBRIUM CALCULATIONS

Calculations were made by use of the computer program SOLGASMIX-PV¹⁷ to obtain information about the chemical species likely to be present in the chemical systems involved in the adsorption studies. The calculations involved equilibrating specified amounts of iodine, oxygen, and hydrogen in helium with an excess of iron or iron and chromium metal at specified temperatures and pressure. Values for $\Delta H_{f,298}^{\circ}$ and ΔS_{298}° for the various chemical species considered in the calculations are listed in Table A.1. The assumption that $\Delta G_T^{\circ} = \Delta H_{f,298}^{\circ} - T\Delta S_{298}^{\circ}$ was used, as discussed by Kubachewski, Evans, and Alcock.³⁷ The results of the calculations are values for the partial pressures of the various species in the gas and the amounts of any condensed phases that would be present at equilibrium.

Some of the results for the system Fe-Cr-I-H are shown in Figs. A.1 through A.8. Those for the system Fe-I-H are presented in Figs. A.9 through A.14. The pressures of the principal species HI, I, I₂, FeI₂, and CrI₂, when present, are plotted in the figures. FeI₃ and Fe₂I₄ also were calculated to be present in the gas, mostly at pressures that are insignificant in comparison with the principal constituents. The Fe₂I₄ pressure became significant under some conditions in the Fe-I-H system and is included in Figs. A.9 through A.14.

The iodine burden in the figures represents the iodine burden in the gas before equilibration. That is also the iodine burden in the gas after equilibration if no iodine is removed in condensed phases. The hydrogen pressure is the pressure in the gas before equilibration. For all practical purposes, that is the hydrogen pressure after equilibration for those cases in which the initial hydrogen pressure is much greater than the iodine burden in gas. If the iodine burden is of the same or greater magnitude than the initial hydrogen pressure, much of the hydrogen is consumed in the production of hydrogen iodide and the hydrogen pressure is reduced.

Table A.1. Thermodynamic data used in SOLGASMIX-PV calculations

Chemical species	$\Delta H_f^\circ, 298$ (J/mol)	ΔS_{298}° ^a [J/(k·mol)]
He(g)	0.0	0.0
H ₂ (g)	0.0	-1.3057E02
I(g)	1.0685E05	-1.8068E02
I ₂ (g)	6.2442E04	-2.6058E02
O ₂ (g)	0.0	-2.0500E02
H ₂ O(g)	2.0920E04	-2.2754E02
FeI ₂ (g)	8.7900E04	-3.4900E02
FeI ₃ (g)	7.1100E04	-3.9500E02
Fe ₂ I ₄ (g)	8.3700E03	-54350E02
HI(g)	2.6360E04	-2.6048E02
CrI ₂ (g)	1.0000E5	-3.4600E02
I ₂ (l)	1.3520E04	-1.5036E02
FeI ₂ (l)	7.0998E04	-1.9550E02
I ₂ (s)	0.0	-1.1614E02
Fe(s)	0.0	-2.7320E01
Cr(s)	0.0	-2.3620E01
FeI ₂ (s)	-1.0460E05	-1.6760E02
CrI ₂ (s)	-1.5700E05	-1.6400E02
Cr ₂ O ₃ (s)	-1.1347E06	-8.1150E01
FeO(s)	-2.7204E05	-6.0750E01
Fe ₂ O ₃ (s)	-8.2550E05	-8.7400E01
Fe ₃ O ₄ (s)	-1.1209E06	-1.4530E02
FeCr ₂ O ₄ (s)	-1.4443E06	-1.4600E02

^awhere $\Delta G_T^\circ = \Delta H_f^\circ, 298 - T\Delta S_{298}^\circ$.

ORNL DWG 80-1532

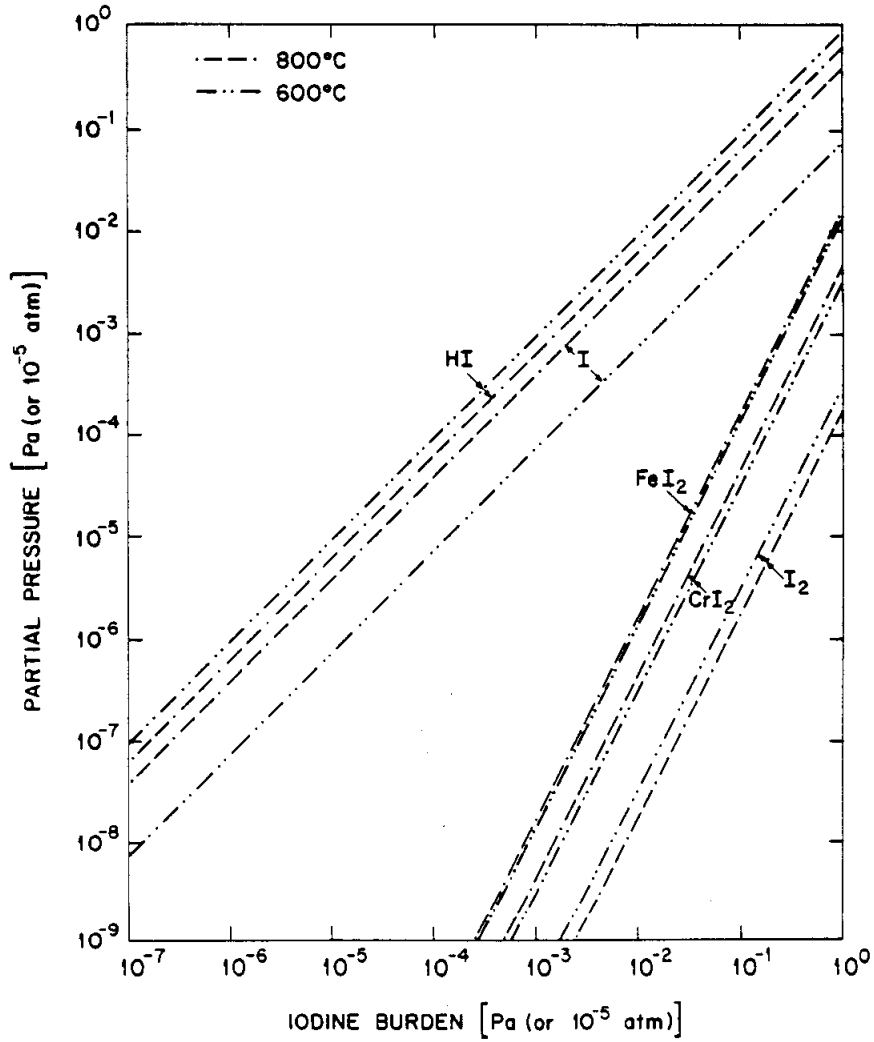


Fig. A.1. Partial pressures of iodine species in equilibrium with chromium and iron at 600 and 800°C in helium containing 50 Pa of hydrogen.

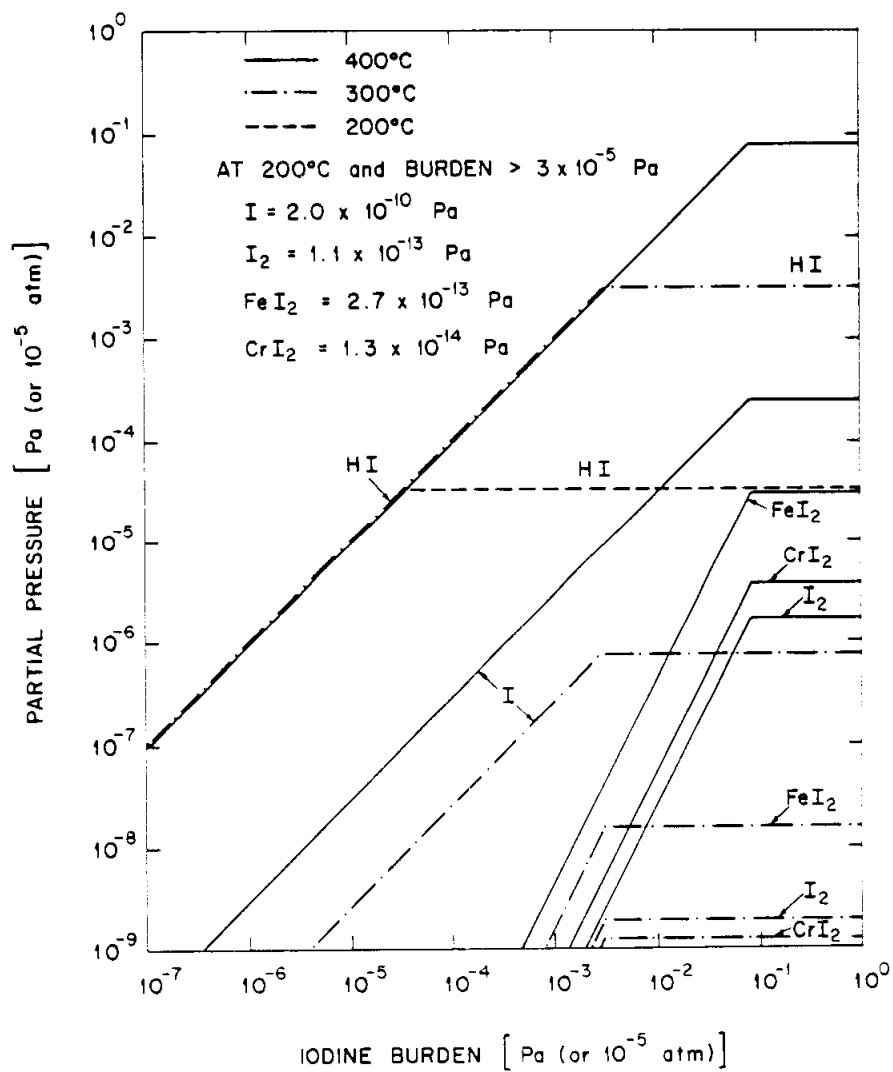


Fig. A.2. Partial pressures of iodine species in equilibrium with chromium and iron at 200, 300, and 400°C in helium containing 50 Pa of hydrogen.

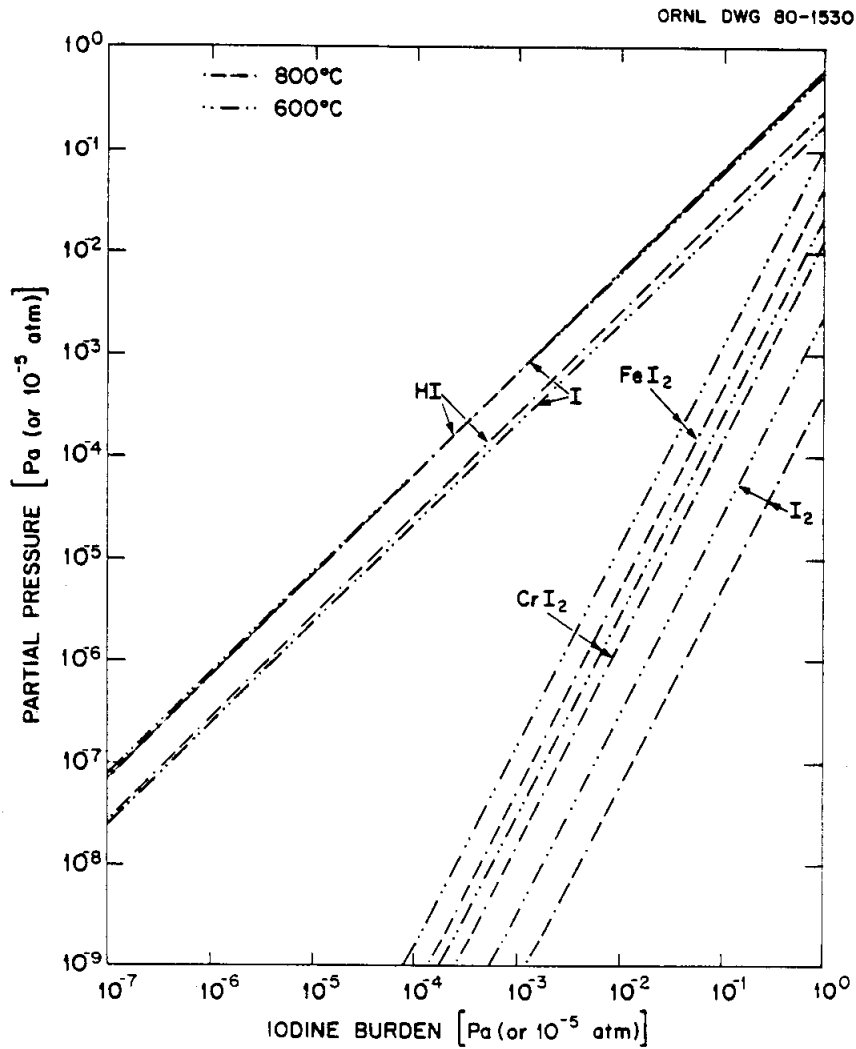


Fig. A.3. Partial pressures of iodine species in equilibrium with chromium and iron at 600 and 800°C in helium containing 3 Pa of hydrogen.

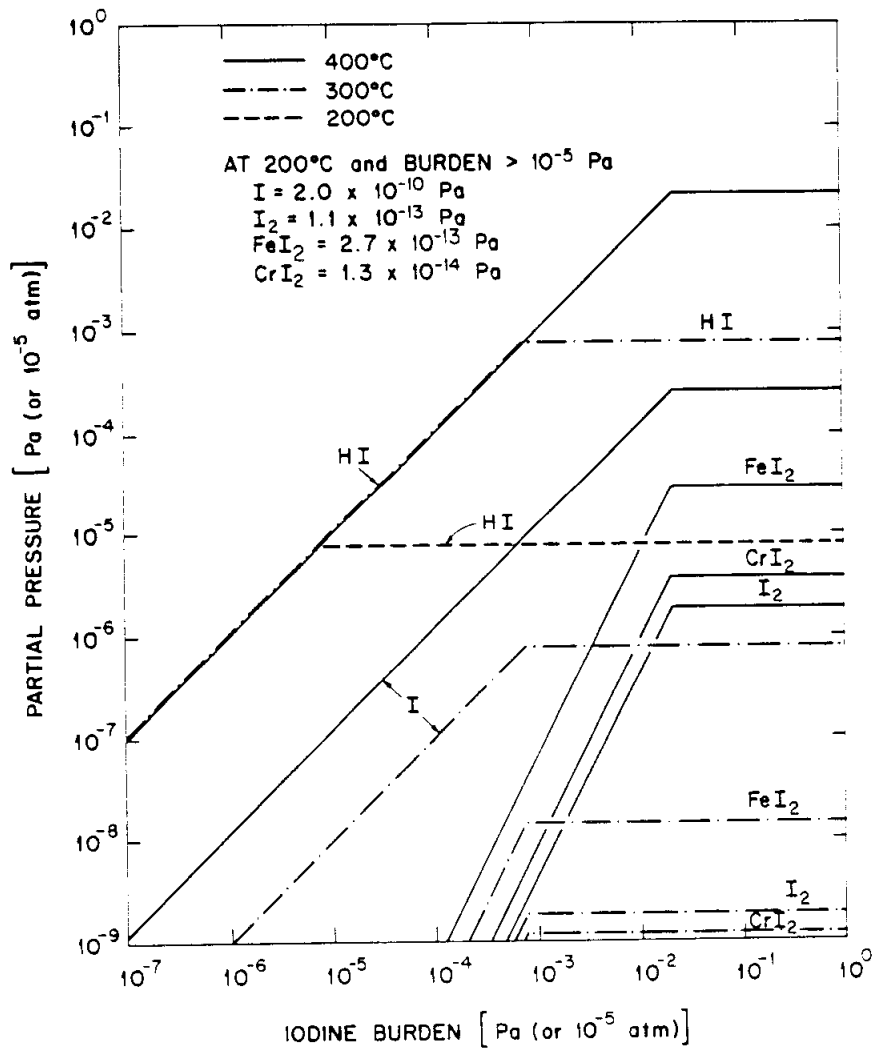


Fig. A.4. Partial pressures of iodine species in equilibrium with chromium and iron at 200, 300, and 400°C in helium containing 3 Pa of hydrogen.

ORNL DWG 80-1534

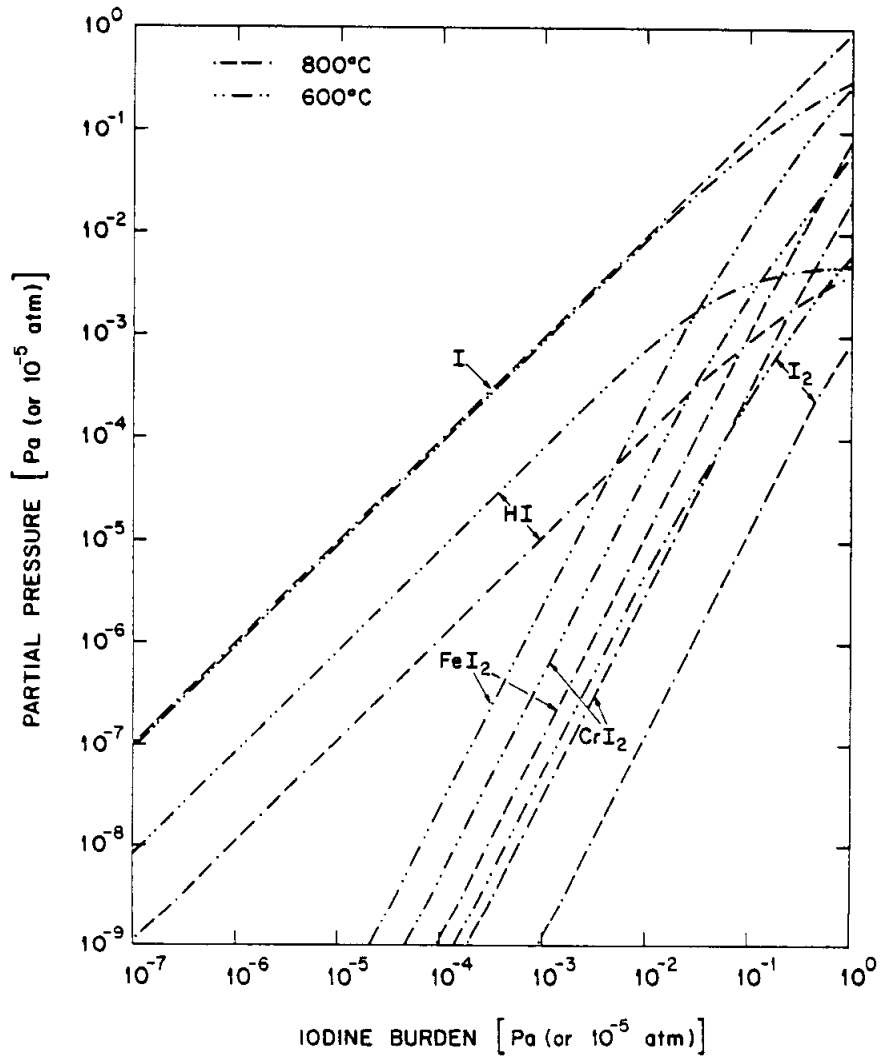


Fig. A.5. Partial pressures of iodine species in equilibrium with chromium and iron at 600 and 800°C in helium initially containing 2.5×10^{-3} Pa of hydrogen.

ORNL DWG 80-1543

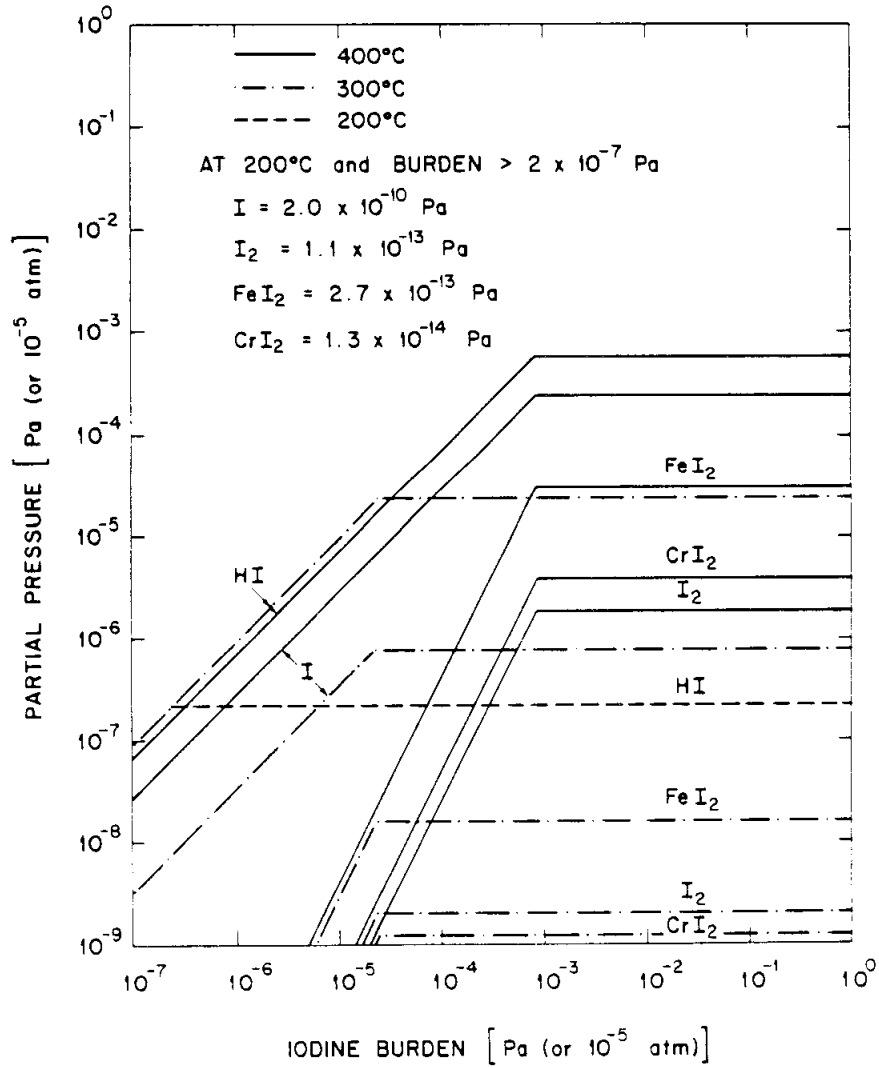


Fig. A.6. Partial pressures of iodine species in equilibrium with chromium and iron at 200, 300, and 400°C in helium initially containing 2.5×10^{-3} Pa of hydrogen.

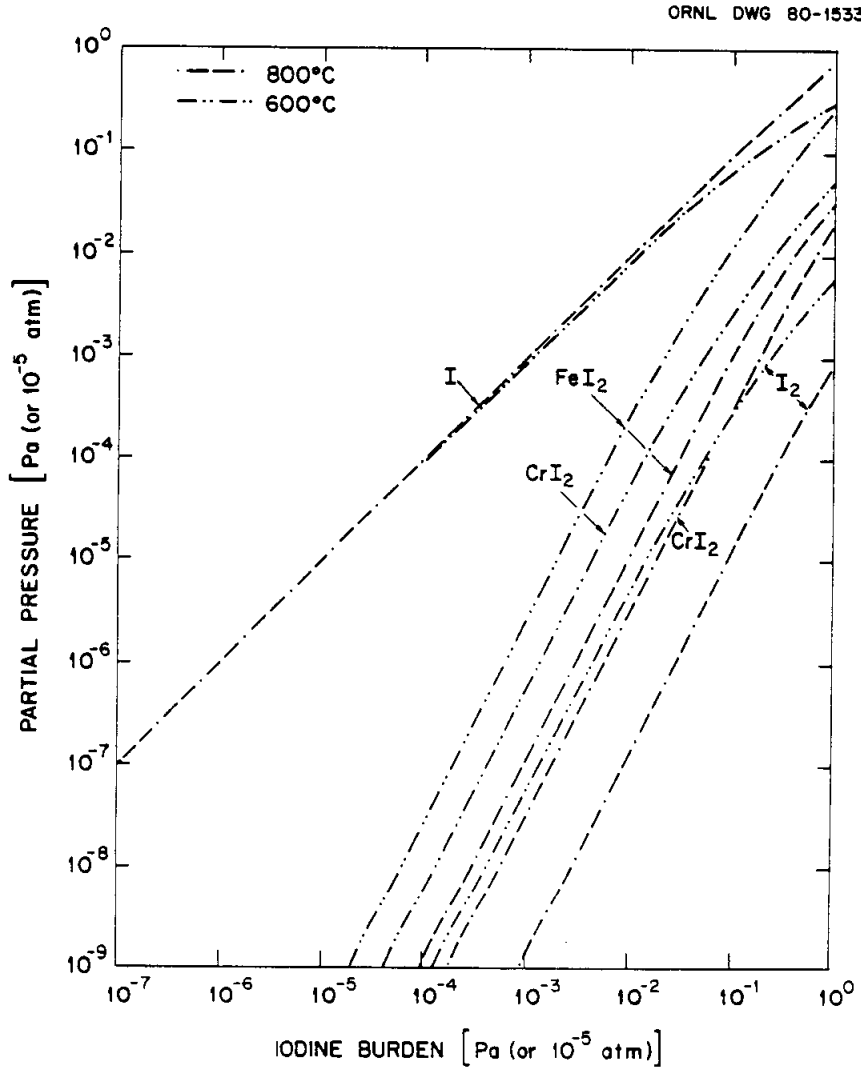


Fig. A.7. Partial pressures of iodine species in equilibrium with chromium and iron at 600 and 800°C in helium.

ORNL DWG 80-1538

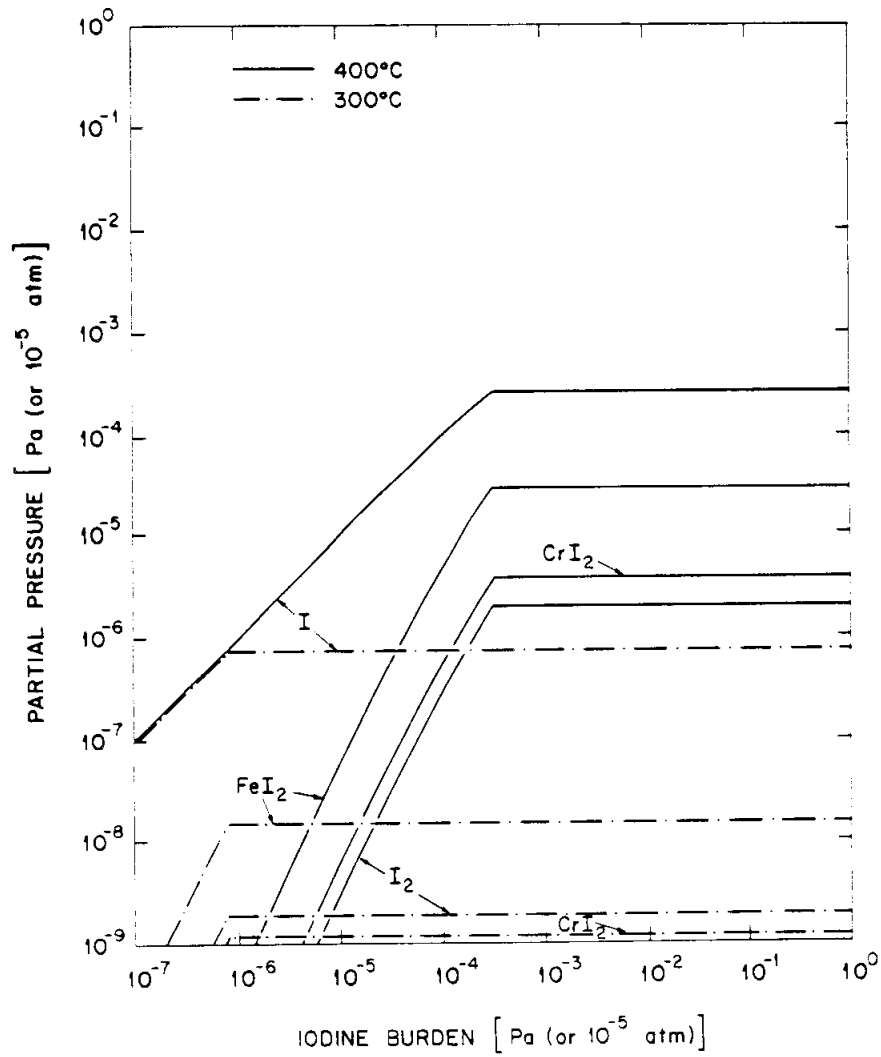


Fig. A.8. Partial pressures of iodine species in equilibrium with chromium and iron at 300 and 400°C in helium.

ORNL DWG 80-1537

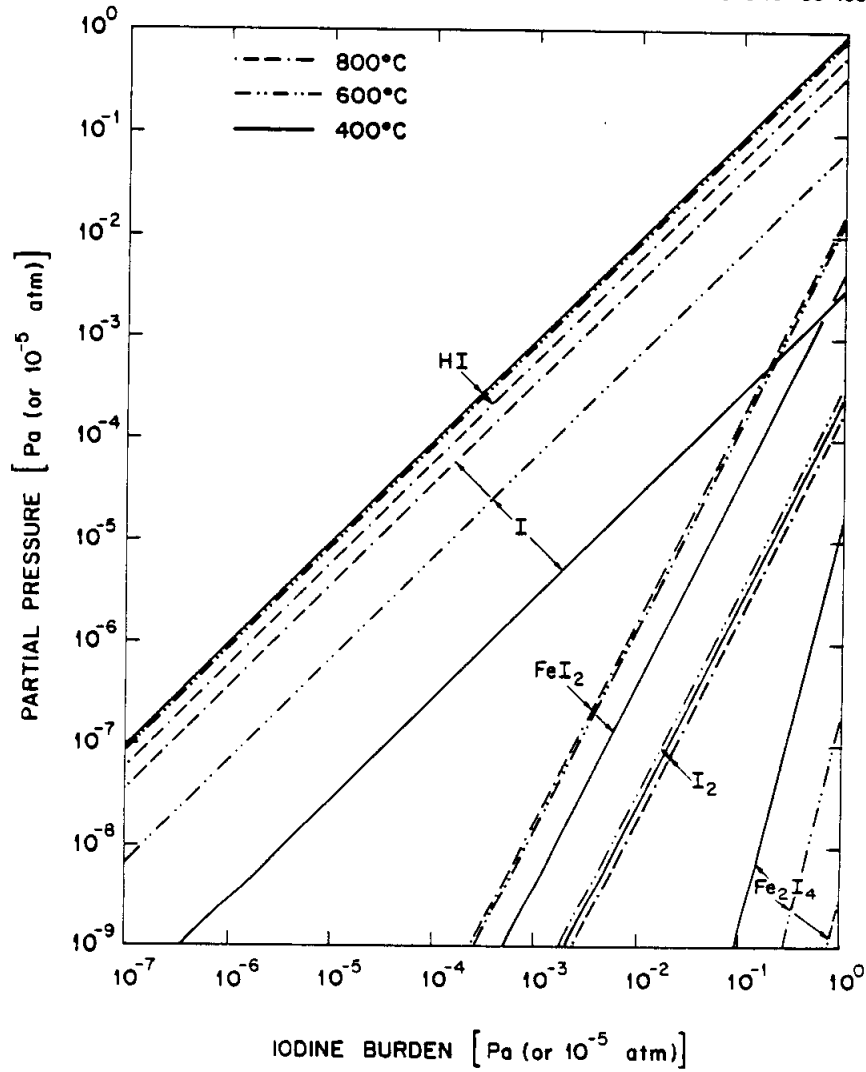


Fig. A.9. Partial pressures of iodine species in equilibrium with iron at 400, 600, and 800°C in helium containing 50 Pa of hydrogen.

ORNL DWG 80-1541

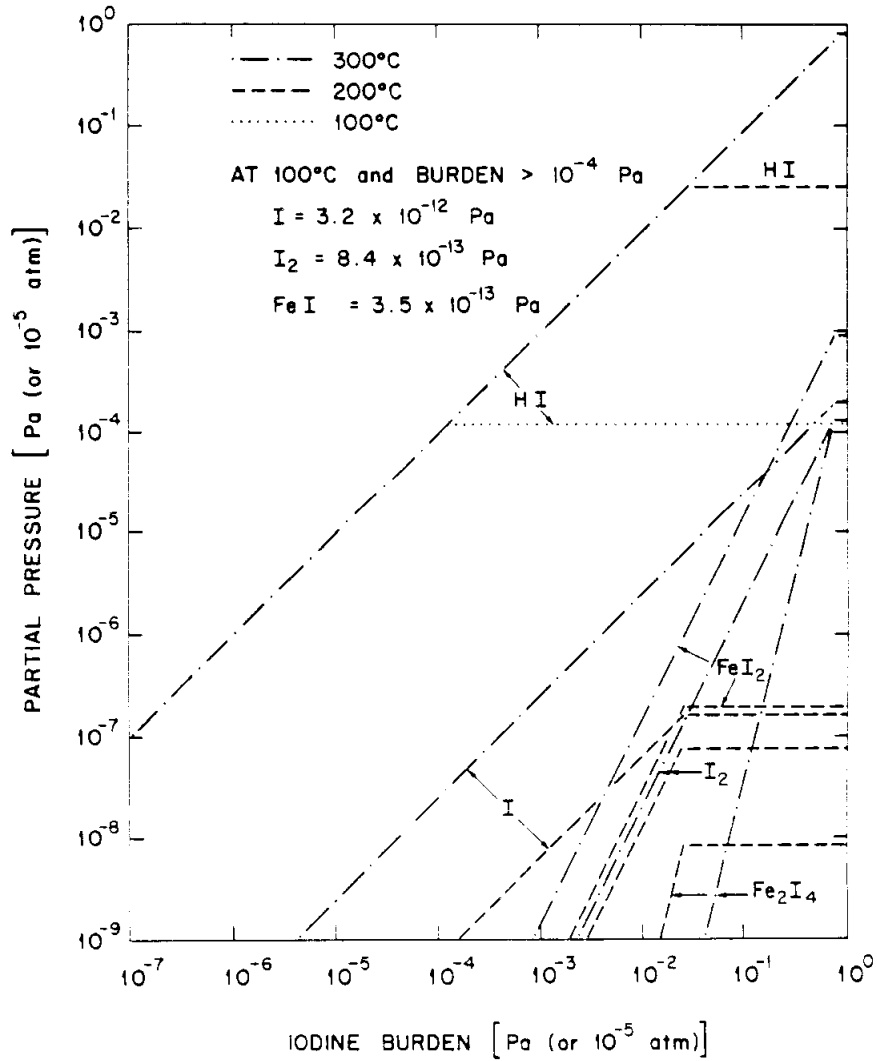


Fig. A.10. Partial pressures of iodine species in equilibrium with iron at 100, 200, and 300°C in helium containing 50 Pa of hydrogen.

ORNL DWG 80-1540

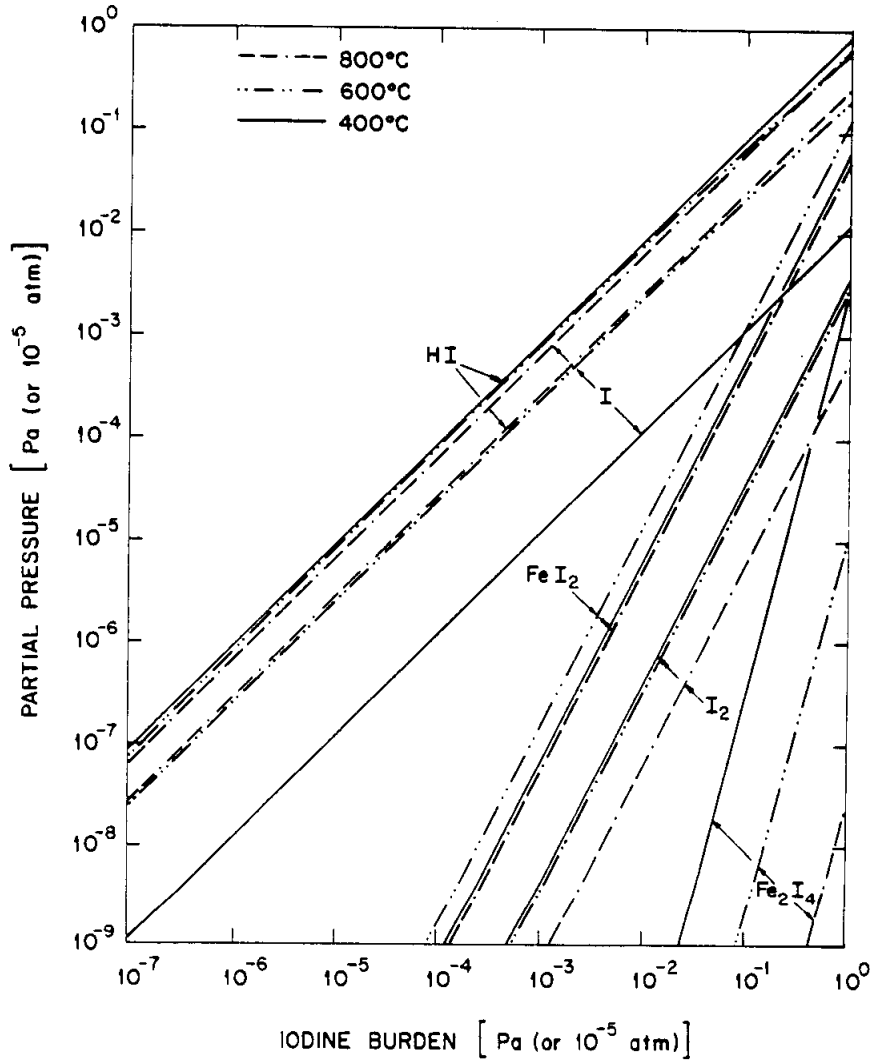


Fig. A.11. Partial pressures of iodine species in equilibrium with iron at 400, 600, and 800°C in helium containing 3 Pa of hydrogen.

ORNL DWG 80-1544

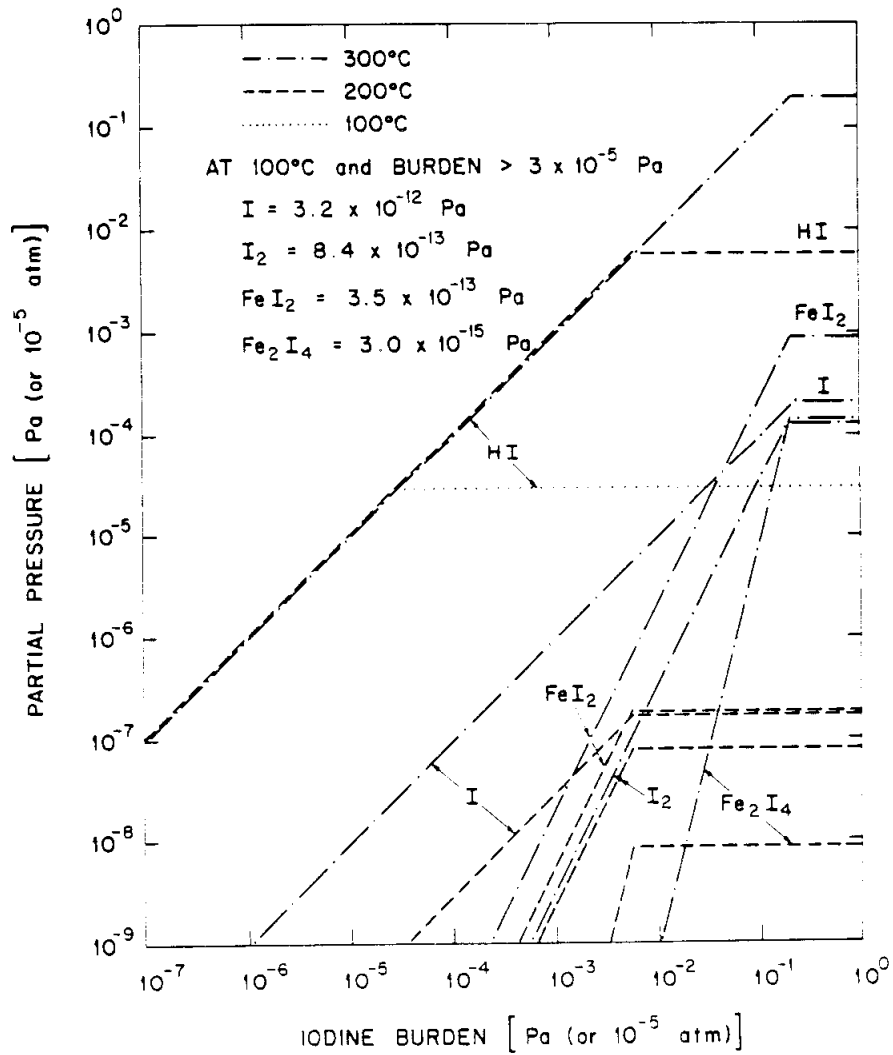


Fig. A.12. Partial pressures of iodine species in equilibrium with iron at 100, 200, and 300°C in helium containing 3 Pa of hydrogen.

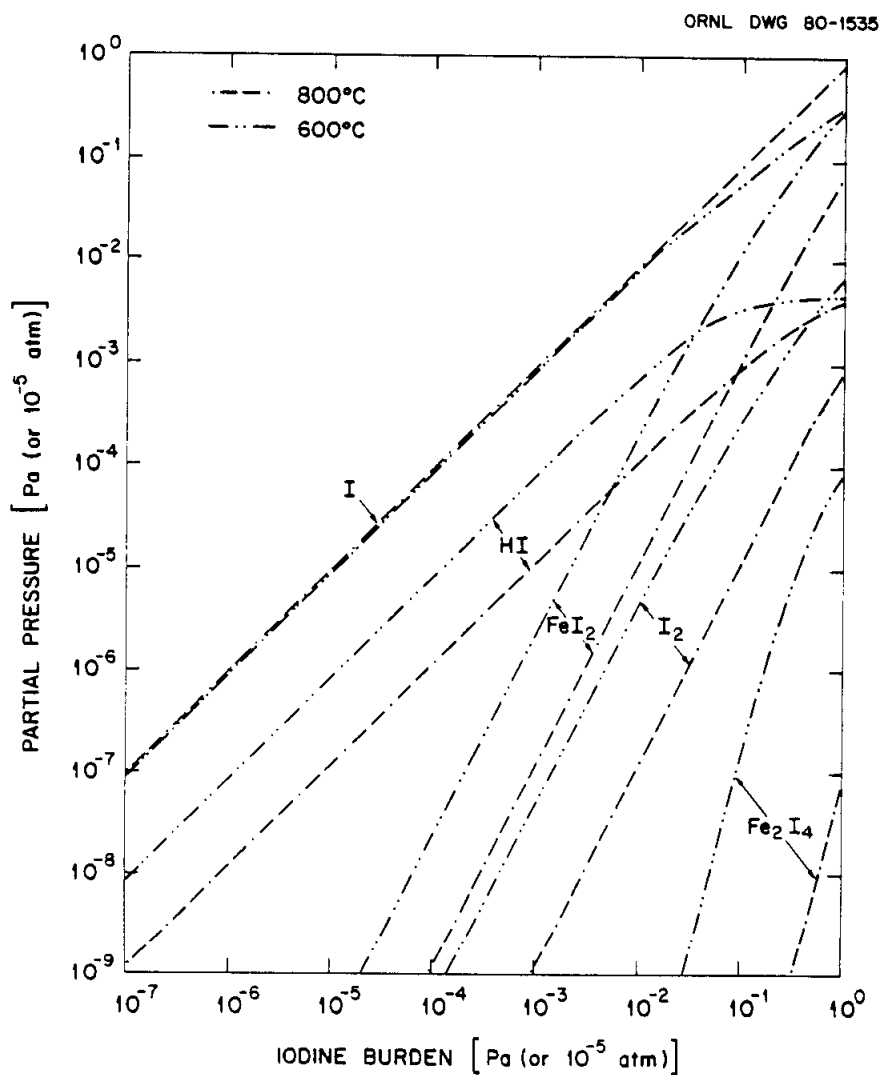


Fig. A.13. Partial pressures of iodine species in equilibrium with iron at 600 and 800°C in helium initially containing 2.5×10^{-3} Pa of hydrogen.

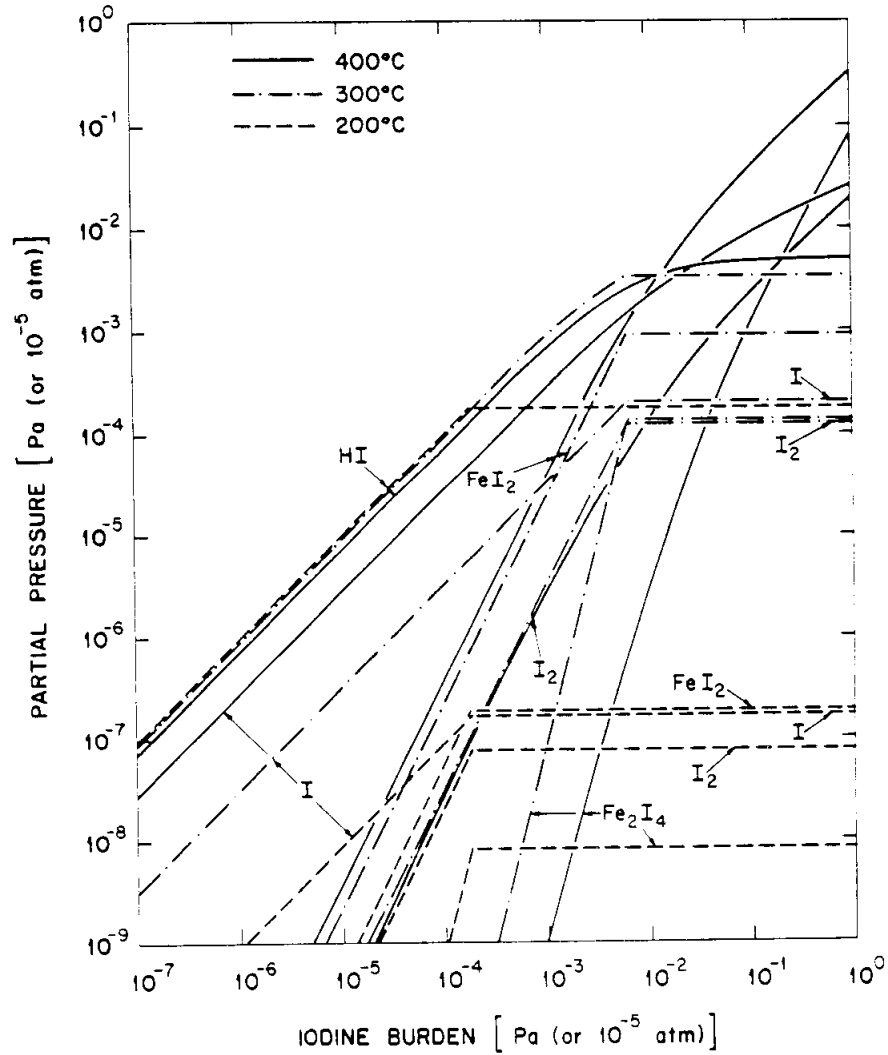


Fig. A.14. Partial pressures of iodine species in equilibrium with iron at 200, 300, and 400°C in helium initially containing 2.5×10^{-3} Pa of hydrogen.

In the systems that contain chromium and iron, $\text{CrI}_2(\text{s})$, or $\text{CrI}_2(\text{l})$ above 856°C , is stable beginning at an iodine burden that depends on the temperature and the hydrogen pressure. $\text{FeI}_2(\text{s})$, or $\text{FeI}_2(\text{l})$ above 587°C , occurs as the condensed phase in the Fe-I-H system. Formation of the condensed phase limits the partial pressures of the iodine species, and the iodine burden in the gas after equilibration, to the values at the iodine burden where condensation begins. In Figs. A.2, A.4, A.6, and A.8 the iodine burden above which the partial pressures of the iodine species remain constant is the iodine burden at which CrI_2 first condenses at the associated temperature. The excess iodine present in gas having a greater initial iodine burden is removed in the condensed CrI_2 . Condensation of FeI_2 produces the similar effect shown in Figs. A.10, A.12, and A.14.

Some of the data for 100 and 200°C that were not included in the figures, but are worth noting, are listed in Table A.2.

Table A.2. Additional data for 100 and 200°C

System	Fe-Cr-I-H					Fe-I-H
Hydrogen pressure (Pa)	50	3	0.0025	0	0	0.0025
Temperature ($^\circ\text{C}$)	100	100	100	100	200	100
Condensed phase	CrI_2	CrI_2	CrI_2	CrI_2	CrI_2	FeI_2
Iodine burden at which condensed phases forms (Pa)	$2.4\text{E}-8$	$5.8\text{E}-9$	$1.7\text{E}-10$	$6.5\text{E}-16$	$2.0\text{E}-10$	$8.1\text{E}-7$
Partial pressures of iodine species over condensed phase (Pa)						
HI	$2.4\text{E}-8$	$5.8\text{E}-9$	$1.7\text{E}-10$	0	0	$8.1\text{E}-7$
I	$6.5\text{E}-16$	$6.5\text{E}-16$	$6.5\text{E}-16$	$6.5\text{E}-16$	$2.0\text{E}-10$	$3.2\text{E}-12$
I_2	$3.5\text{E}-18$	$3.5\text{E}-18$	$3.5\text{E}-18$	$3.5\text{E}-18$	$1.1\text{E}-13$	$8.4\text{E}-13$
FeI_2	$1.5\text{E}-20$	$1.5\text{E}-20$	$1.5\text{E}-20$	$1.5\text{E}-20$	$2.7\text{E}-13$	$3.5\text{E}-13$
Fe_2I_4	$5.3\text{E}-30$	$5.3\text{E}-30$	$5.3\text{E}-30$	$5.3\text{E}-30$	$1.9\text{E}-20$	$3.0\text{E}-15$
CrI_2	$3.3\text{E}-22$	$3.3\text{E}-22$	$3.3\text{E}-22$	$3.3\text{E}-22$	$1.3\text{E}-14$	0

Trace amounts of oxygen in the gas may react with chromium in the Fe-Cr-I-H system to form $\text{CrO}_2(\text{s})$ and with iron in the Fe-I-H system to form $\text{FeO}(\text{s})$. The equilibrium pressure of O_2 over the metal oxide and the ratio $p_{\text{H}_2}/p_{\text{H}_2\text{O}}$ above which reduction of the oxide would occur are listed in Table A.3 for several temperatures.

Table A.3. O_2 pressure and $p_{\text{H}_2}/p_{\text{H}_2\text{O}}$ in gas over CrO_2 and FeO at equilibrium

T (°C)	Over CrO_2		Over FeO	
	p_{O_2} (Pa)	$p_{\text{H}_2}/p_{\text{H}_2\text{O}}$	p_{O_2} (Pa)	$p_{\text{H}_2}/p_{\text{H}_2\text{O}}$
800	5E-23	2E04	5E-15	1.5
600	2E-31	5E05	5E-21	3
400	7E-45	1E08	1E-30	11
200	1E-69	4E12	1E-48	110

Appendix B. CHARACTERIZATION OF METAL ADSORPTION SPECIMENS

The adsorption specimens were composed of thin (0.24-mm-thick) plates of 2-1/4% Cr-1% Mo steel, called alloy T-22. These plates had been fabricated by reducing the thickness of the original 4.76-mm plate (see Sect. 6.2) through a series of rolling and annealing operations. The individual specimen plates, either 2 mm or 51 mm long by 13.3 mm wide, were assembled into holders of the same material (Fig. B.1). Each specimen was composed of ten thin plates plus the thicker side pieces of the holder.

ORNL-DWG 78-355R2

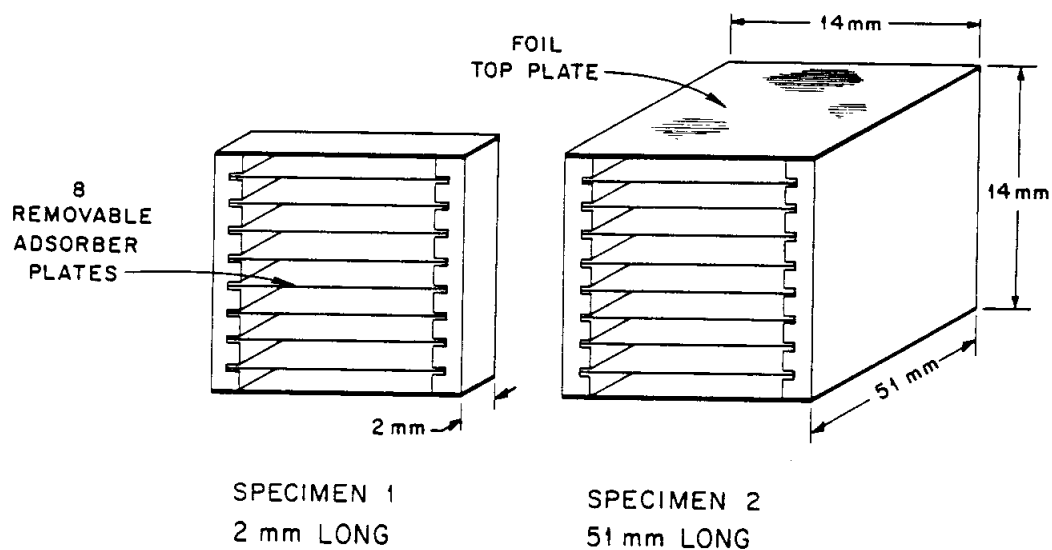


Fig. B.1. Steel adsorption specimens.

Investigation of the surface characteristics of these specimens included determination of (1) surface roughness using the diamond stylus technique, (2) surface area available for gas adsorption using a modified BET method on a large number of the 2-mm-long specimens, (3) metallic composition of the surface by x-ray analysis, (4) surface appearance at 1000 \times using the backscattered electron image technique, and (5) general

appearance at 250 and 1000 \times of sections through the specimens by metallographic examination. The first two methods were applied to control specimens only, but in the latter three analyses, the results of examinations of control (untested) and tested specimens were compared.

A supply of the thin plate material from which the specimens were cut was sent to General Atomic Company for surface roughness measurement and, if desired, for testing in their iodine sorption studies at much higher iodine burdens (0.01 to 100 Pa). This material was reported²⁹ to have a surface roughness of 6.8; that is, the true area was 6.8 times geometric.

A large number (~ 100) of the 2- by 13.3-mm plates were submitted for BET surface area measurement at ORNL. Although the total area was marginal for reliable measurement, the reported value³⁰ was about 140 times geometric, much higher than expected.

Metallographic examination was conducted on ten specimen plates;³¹ two were as-fabricated controls, three had been exposed to slightly oxidizing helium at three different temperatures (200, 500, and 800°C) for several days, and the remaining five plates were selected from five different adsorption tests. Initial examination of the control specimen plates at 250 \times did not reveal any unusual features in the microstructure, and the three plates exposed to slightly oxidizing helium exhibited typical oxide layers, very thin except at 800°C. Upon receipt of the very high surface area measurements by gas adsorption, the control specimens were reexamined at 1000 \times , and numerous small cracks, especially in the sheared edges, were found. Examples of this cracking are shown in Fig. B.2. Thus, it appears likely that these cracks, which probably were produced during the rolling and/or shearing operations in specimen fabrication, could significantly increase the surface area for gas adsorption. Similar cracks were apparent in and near the sheared end of the plate from specimen 1 of test A-9, shown in Fig. B.3. However, there was only slight surface oxidation, in agreement with visual observations and test operating history. Some recrystallization and increase in grain size were the only other apparent test effects.

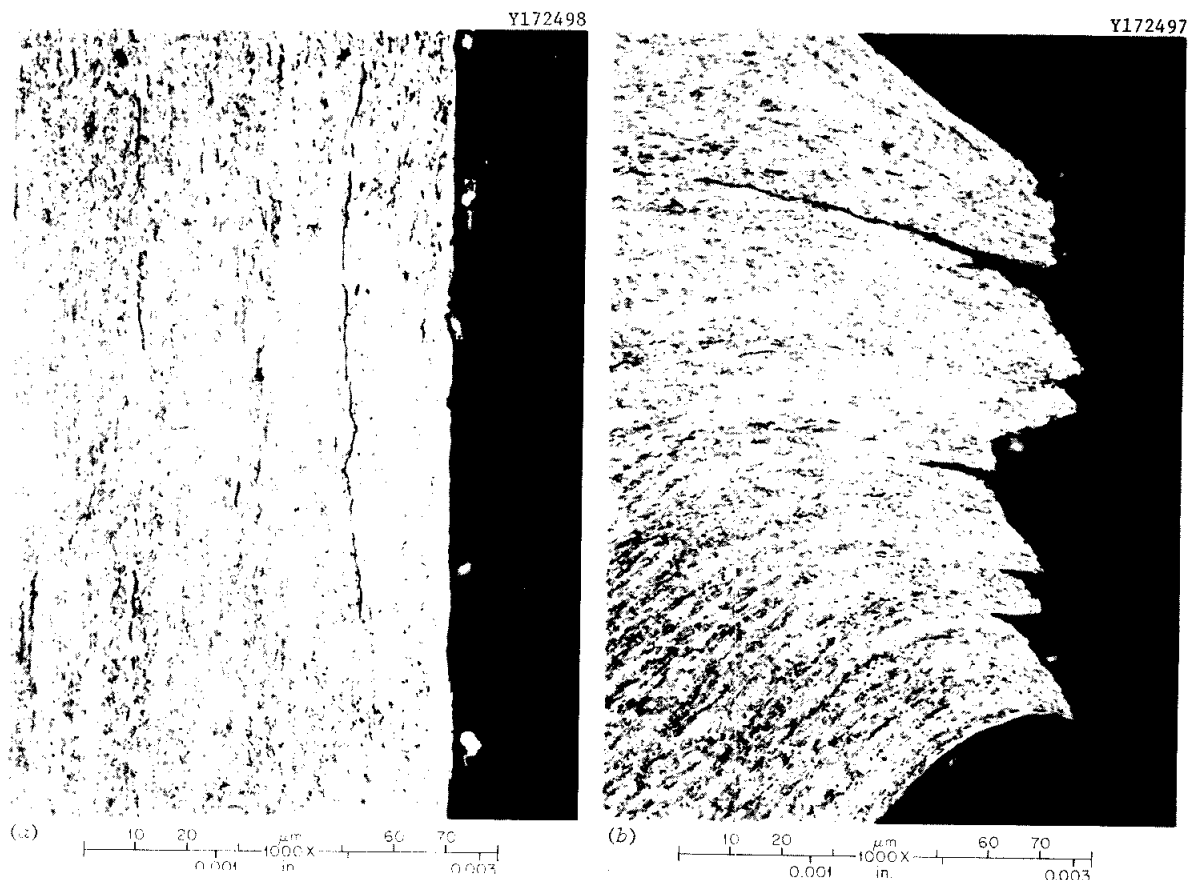


Fig. B.2. Appearance of as-fabricated control specimen plate, etched. Note subsurface longitudinal cracks (a) and distortion and cracks in sheared end (b).

The appearance of unoxidized and oxidized specimens is illustrated in Fig. B.4. Although the plate shown in Fig. B.4 (a) was exposed in test A-9 [>6 weeks at 400 to 600°C in He plus 50 Pa (5×10^{-4} atm) H_2], it is similar in appearance to the untested control specimens. Conversely, the plate from test A-6 [Fig. B.4 (b)] was covered with oxide of quite variable thickness. Such nonuniform oxidation under these conditions would not be unexpected for this alloy. The sheared end of a plate from test A-12 is shown at 250 and 1000 \times in Fig. B.5. Again, appreciable distortion and cracking (presumably resulting from fabrication) were observed. Some carbide-poor regions are shown in the etched view; however, there is no indication that these regions were related to prior cracking or to the sorption testing.



Fig. B.3. Appearance of specimen plate from test A-9, showing cracks penetrating the sheared end (etched condition). Some recrystallization and grain growth is apparent, compared with control plate shown in Fig. B.2.

In summary, these metallographic studies revealed cracking which could have increased specimen surface area significantly. However, this observed cracking hardly seems sufficient to substantiate the very high surface area (140 times geometric) indicated by BET measurements. No other features of the specimen microstructure appeared to be significant in evaluating iodine sorption behavior.

The analysis of metallic surface composition by x ray showed that several areas, before and after testing, were within acceptable ranges for this alloy. Similarly, backscattered electron images of the specimen surfaces revealed no unusual or unexpected features.³⁸

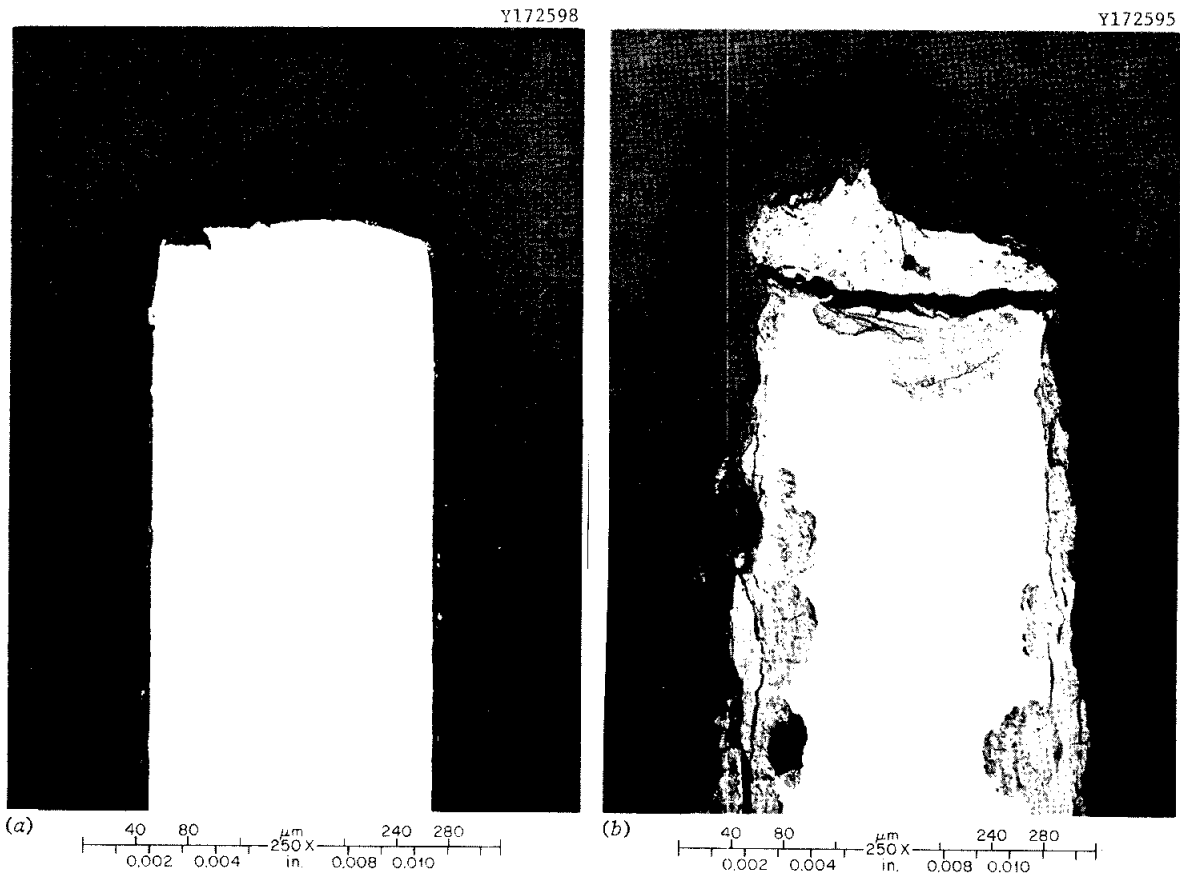


Fig. B.4. Comparison of (a) unoxidized and (b) oxidized specimen plates, as polished. The plate in (a) was exposed in test A-9 but is also typical of control specimens. The plate in (b), from test A-6, exhibits heavy, nonuniform oxidation.

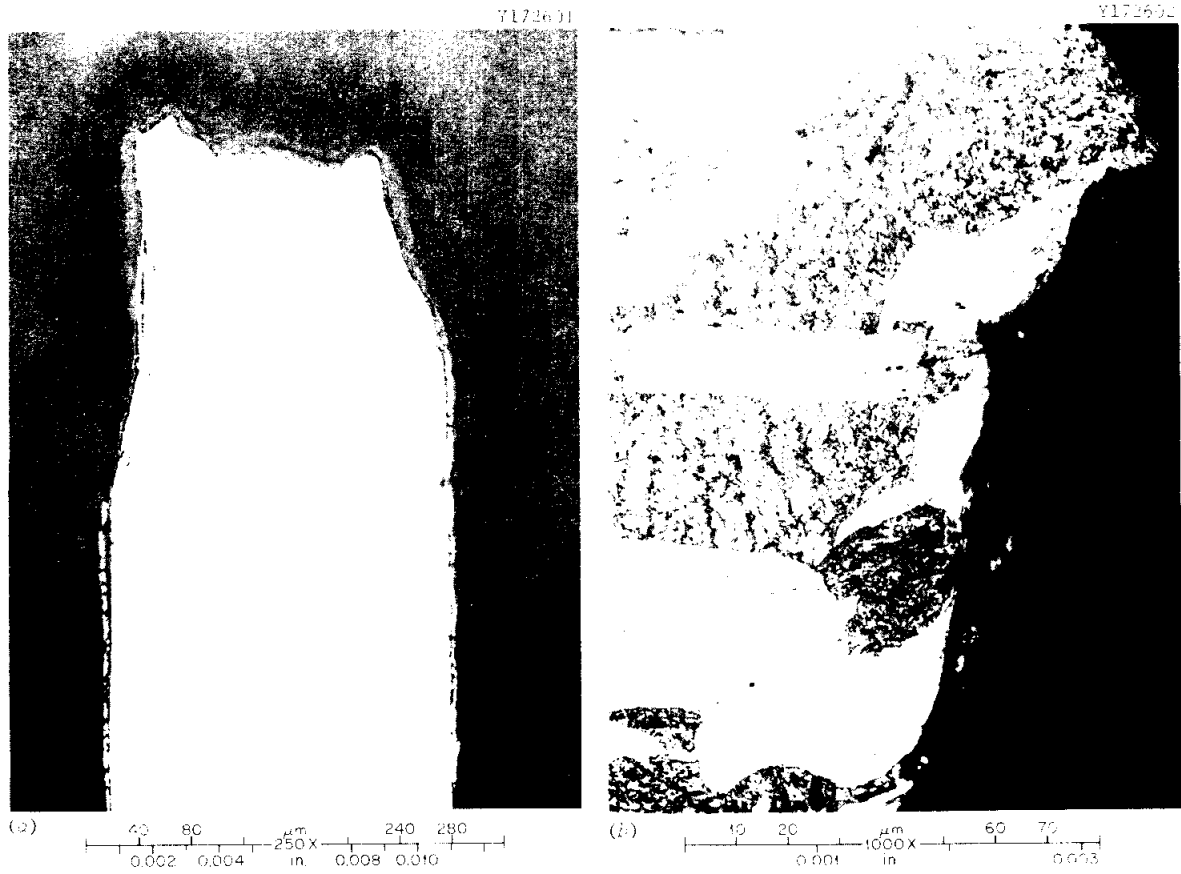


Fig. B.5. Sheared end of plate from test A-12, 250 \times , as polished (a) and 1000 \times , etched (b). Note distortion and crack from shearing (a) and carbide-poor regions in sheared end (b).

Appendix C. PREPARATION OF ELEMENTAL IODINE SOURCE MATERIAL

High-purity elemental iodine containing a specific fraction of ^{131}I tracer was used in these adsorption experiments. A procedure originally developed by Carroll³⁹ and modified by Osborne¹⁶ was used; the principal steps are listed below. Because radiation safety regulations limited the amount of ^{131}I allowable in this preparation to 5 mCi (and 1 mCi per experiment), the amount of normal iodine carrier used was limited to 0.5 to 2 mg, thus providing a specific activity of 2.5 to 10 mCi $^{131}\text{I}/\text{mg I}$ at the beginning of an experiment. The apparatus used in the preparation is shown in Fig. C.1.

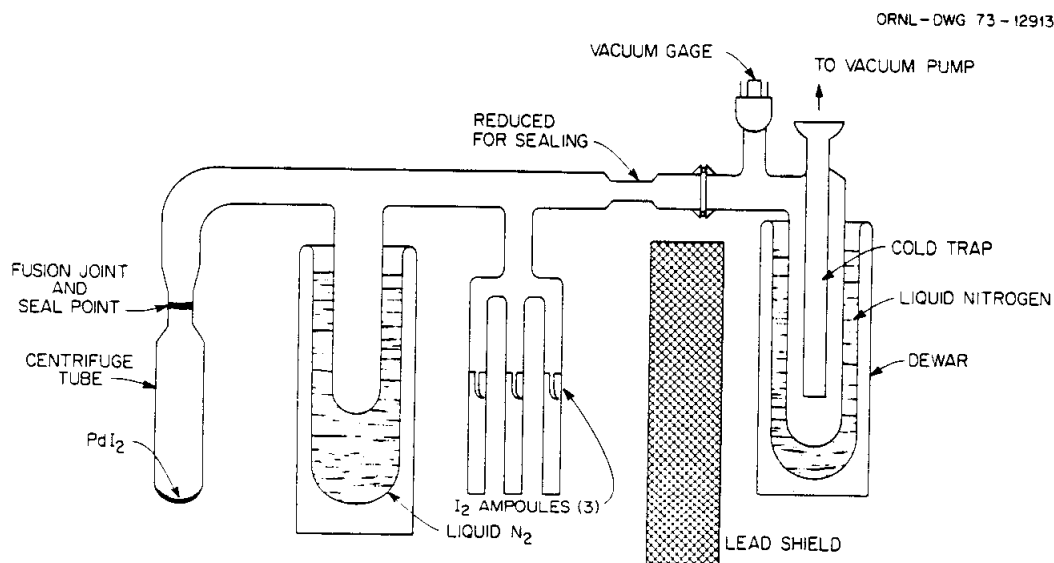


Fig. C.1. Apparatus used to prepare elemental iodine by the decomposition of PdI_2 in vacuum.

1. Obtain carrier-free ^{131}I , normally ~ 5 mCi as NaI in NaOH solution.
2. Add natural I carrier as NaI , using standard solution.
3. Dilute with distilled H_2O to total of 2.00 mL, mix, and withdraw two samples of 0.020 mL each and add to 0.10 mL H_2O in culture tubes. (These samples, each 1% of total, are to be used as counting standards.)

4. Transfer remaining 98% of solution into Vycor centrifuge tube and rinse bottle with ≈ 1 mL H_2O .
5. Add 0.30 mL concentrated $PdCl_2$ solution to precipitate PdI_2 , mix, and wait 10 min.
6. Add 0.030 mL saturated H_3PO_3 solution and mix to precipitate excess Pd.
7. Warm solution slowly with heat lamp (to 80-90°C), being careful not to boil, and wait until solution clears.
8. Dilute with H_2O to 2/3 volume of centrifuge tube and mix thoroughly to wash precipitate.
9. Concentrate PdI_2 by centrifuging and decant solution with long pipette, being careful not to disturb the precipitate.
10. Wash the precipitate four more times and check wash solution with 3 to 4 drops of $AgNO_3$ solution for any evidence of $AgCl$ (or AgI) precipitate in separate tube.
11. Dry precipitate and centrifuge tube with heat lamp. (PdI_2 starts decomposing at 350°C.) Purge tube carefully with vacuum or air.
12. Attach centrifuge tube containing PdI_2 to transfer apparatus and evacuate to <0.01 Pa (<10 μ m Hg) with entire apparatus (except bottom end of centrifuge tube) heated to 300 to 400°C for 1 to 2 h. Use a liquid nitrogen-cooled trap to prevent back diffusion of pump oil.
13. Seal off the apparatus and add liquid nitrogen coolant to intermediate iodine collection tube.
14. Slowly heat the PdI_2 precipitate to decompose it. (Iodine will collect above liquid nitrogen level in intermediate collection tube.) After I_2 has transferred, seal off centrifuge tube.
15. Transfer liquid nitrogen cooling from intermediate collection tube to break-seal ampoules and allow the former to come to room temperature without heating.
16. After more than one hour, iodine should be completely transferred to ampoules. Seal ampoules with torch while cooling iodine.

Appendix D. DETECTOR CALIBRATIONS AND ACTIVITY PROFILES FOR SPECIMENS

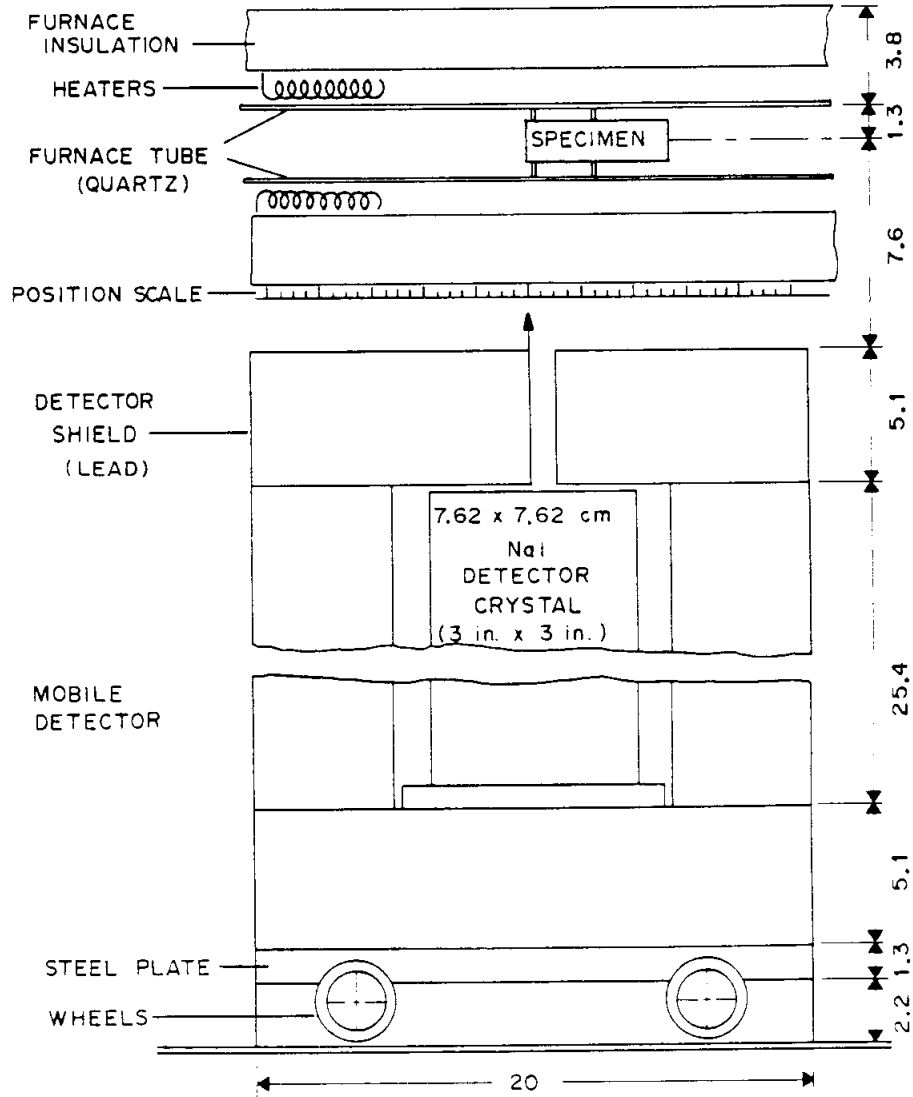
The amounts of iodine adsorbed on the specimens and other adsorbers in these experiments were determined by measuring the ^{131}I tracer activity by use of sodium iodide crystal detectors. The detectors were mounted in lead shields and viewed the specimens through collimator slits 3.2 to 9.5 mm (1/8 to 3/8 in.) wide and 2.5 to 5 cm (1 to 2 in.) long. The output from each crystal was connected to a single-channel analyzer that was adjusted to measure the 365-keV photons from the decay of ^{131}I .

The geometrical relationship between a specimen in the furnace tube and a detector in its shield is shown in Fig. D.1. The shield was mounted on wheels so that it could be moved along a track below the furnace tube. The ability to move the detector enabled us to measure activity on the wall of the furnace tube and on charcoal traps away from the specimens. Movement coupled with the use of narrow collimators offered the possibility of determining the axial distribution of iodine on the 51-mm-long specimens.

Each detector was calibrated before each experiment by measuring the activities of ^{131}I or ^{51}Cr standards which were placed at the entrances to the specimens and the charcoal traps that were to be measured during the experiment. The iodine standards were glass or plastic tubes about 3 mm diam \times 15 mm long that contained an aqueous solution of ^{131}I or solution adsorbed in silver zeolite beads. The ^{51}Cr standard was a 0.5 mm diam \times 10 mm long piece of Nichrome wire. These calibrations could not be repeated during an experiment, so the activities of standards placed at the entrance of the collimators were measured also. These measurements at the collimators were repeated periodically during some of the experiments to monitor the performance of the detectors.

For many of the calibrations, the detector was moved along the track to obtain a curve of activity versus position of the detector relative to that of the standard. Curves for detectors having collimator slit widths of 3.2, 6.4, and 9.5 mm (1/8, 1/4, and 3/8 in.) are shown in Fig. D.2. Some calibrations were made by measuring the activities of

ORNL DWG 80-1503



ALL DIMENSIONS ARE CENTIMETERS.

Fig. D.1. Geometrical relationship of detector to specimen.

ORNL-DWG 80-1494

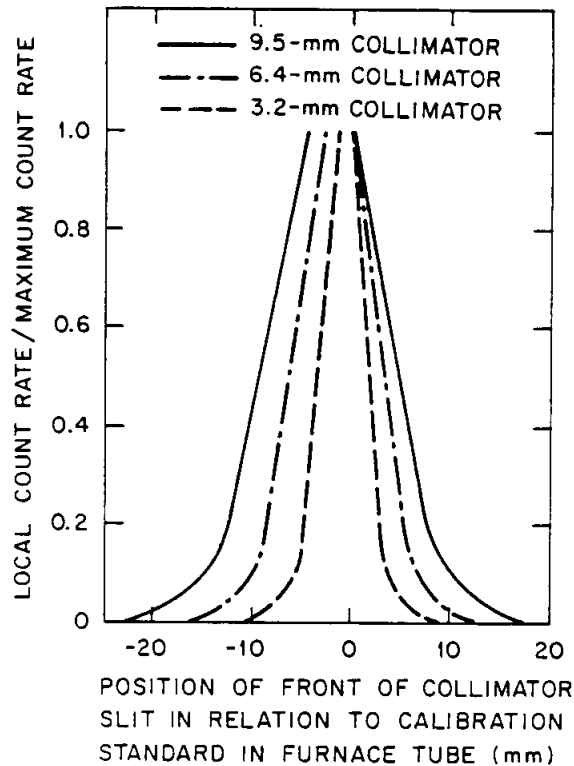


Fig. D.2. Calibration curves for detectors.

the standards with the detectors positioned, on the basis of the curves of Fig. D.3, to obtain a maximum reading. The calibrations obtained were in terms of activity in counts/s per μCi of ^{131}I . These were converted to counts/s per μg of iodine by multiplying by the specific activity, in $\mu\text{Ci } ^{131}\text{I}/\mu\text{g I}$, of the iodine used in the experiment. This latter calibration and the activities measured during the experiment were converted to a common basis by correcting for decay to a time 0 that was established at the beginning of each experiment. Calibrations that were obtained for experiments A-4 through A-13 are shown in Table D.1.

Determining the amount of iodine on a 2-mm-long specimen was straightforward. The detector was positioned so that the entire specimen could be seen by the detector through the collimator. The amount (in micrograms) of iodine on the specimen was simply the measured activity, in counts/s corrected to time 0, divided by the product of the

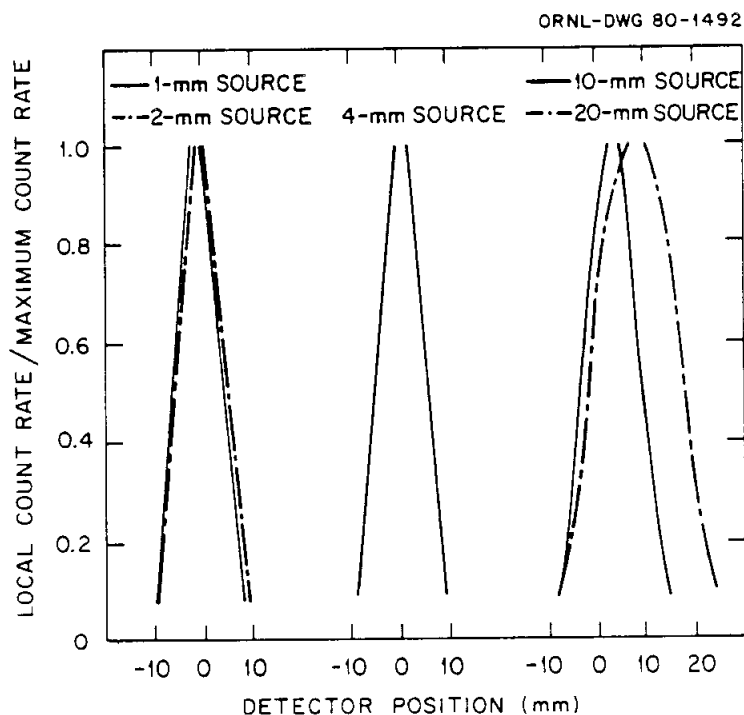


Fig. D.3. Effect of length of uniform source on profile obtained with detector with a 3.2-mm collimator.

calibration factor, in counts/s $\mu\text{Ci } ^{131}\text{I}$, and the specific activity of the iodine in $\mu\text{Ci } ^{131}\text{I}/\mu\text{g I}$.

The part of a 51-mm specimen that could be seen with full efficiency varied from about 3 mm for a 3.2-mm collimator to 9 mm for a 9.5-mm collimator. As long as almost all the activity adsorbed over a length that was fully visible to the detector through the collimator and the detector was positioned properly, the amount of iodine on the specimen could be determined in the manner described above. This was often the case.

When the iodine was adsorbed over a greater length of specimen, the activity registered by the detector did not give a true measure of all the iodine on the specimen. In such cases, it was necessary to obtain an activity profile by moving the detector under the specimen and measuring the activity as a function of position. The total amount of iodine on a specimen was obtained from the profile by use of the following relationship:

Table D.1. Detector calibrations

Experiment	Detector	Collimator width (mm)	Calibration, (counts/s)/ $\mu\text{Ci } ^{131}\text{I}$				
			Specimen	Charcoal trap	Monitor trap	Purge trap Collimator	
A-4	1	3.2	1.45 ^a				
		6.4	2.54 ^a				
		9.5	5.44 ^a				
A-5	1	3.2	12.6				
		6.4	23.6				
		9.5	42.6				
A-6	1	6.4	25.2				
		9.5	48.6				
A-7	1	6.4	22.6				
		9.5	44.3				
A-8	1	6.4	20.2		145	179	
		9.5	40.7			277	
A-9	1	6.4	20.6		130	155	
		2a ^b	9.5	51.9			331
		2b ^b	9.5	(59) ^b			376
A-10	1	9.5	24.4			244	
		2	9.5	41.9			328
		3	9.5		492		318
A-11 and A-12	1	9.5	27.5			238	
		2	9.5	54.5	68.8	290	372
		3	9.5		554		363
A-13	1	9.5	29.9			229	
		2	9.5	46.6	60.9	246	350
		9.5	(37) ^c	(48) ^c			277
		3	9.5		554		350

^aCause for low values is not known but might have been improper adjustment of single-channel analyzer.

^bDetector was replaced during experiment. Calibration at position of specimen was calculated by comparison of calibrations at collimator.

^cCalibration drifted during experiment. These values during latter part were based on change in calibration at collimator.

$$Q = \frac{A_p C_{\max}}{ADS},$$

where

- Q = total amount of iodine, μg ;
 A_p = area under specimen profile, mm;
 C_{\max} = maximum activity for profile, counts/s;
A = area under calibration profile, mm;
= 12 mm for 3.2-mm collimator;
= 18 mm for 6.4-mm collimator;
= 31 mm for 9.5-mm collimator;
D = detector calibration, counts/s $\mu\text{Ci } ^{131}\text{I}$;
S = specific activity, $\mu\text{Ci } ^{131}\text{I}/\mu\text{g I}$.

Although it was necessary for some calculations to know the total amount of iodine on the specimens, the main objective of the experiments was to determine the concentration of iodine on the metal surface when a steady state was reached in helium containing a specified burden of iodine. We learned early during the experiments that the time required to reach an equilibrium loading on more than a 1- or 2-mm length of specimen at 400°C and iodine burdens of $\leq 10^{-5}$ Pa ($\leq 10^{-10}$ atm) was likely to be prohibitive. A short specimen could be used and operated until the amount of iodine adsorbed reached a steady value. Or, a long specimen could be used and operated until the concentration of iodine on a part of the surface, as determined by analysis of the activity profiles, reached a steady value.

Two specimens, each 51 mm long, were used in experiment A-4, the first meaningful experiment, and we attempted to obtain values for the equilibrium loading on the metal by analyzing the activity profiles. We found that the calibration profiles and the profiles for the specimens could not be measured precisely enough to permit a good analysis of the axial distribution of iodine on the specimens. Thereafter, we used one or two, 2-mm-long specimens in the position of specimen 1 for the loading measurements. A 51-mm-long specimen was used in the position of specimen 2, mostly for measurements of the amount of iodine that passed through specimen 1 and for some general information on the adsorption behavior.

In experiment A-4 and again in A-13, some estimates of equilibrium loadings were obtained by comparing the activity profiles for the 51-mm-long specimens with profiles that had been calculated for particular loadings. Figure D.3 shows how the profiles measured with a detector with a 3.2-mm collimator were calculated to change with length of specimen that reaches the equilibrium loading. Figure D.4 shows how the local activity and the ratio of the local activity to the maximum activity change as the length of the saturated zone increases. Figure D.5 shows the profiles that would be obtained with a detector with a 9.5-mm collimator if the concentration of iodine were uniform over various lengths.

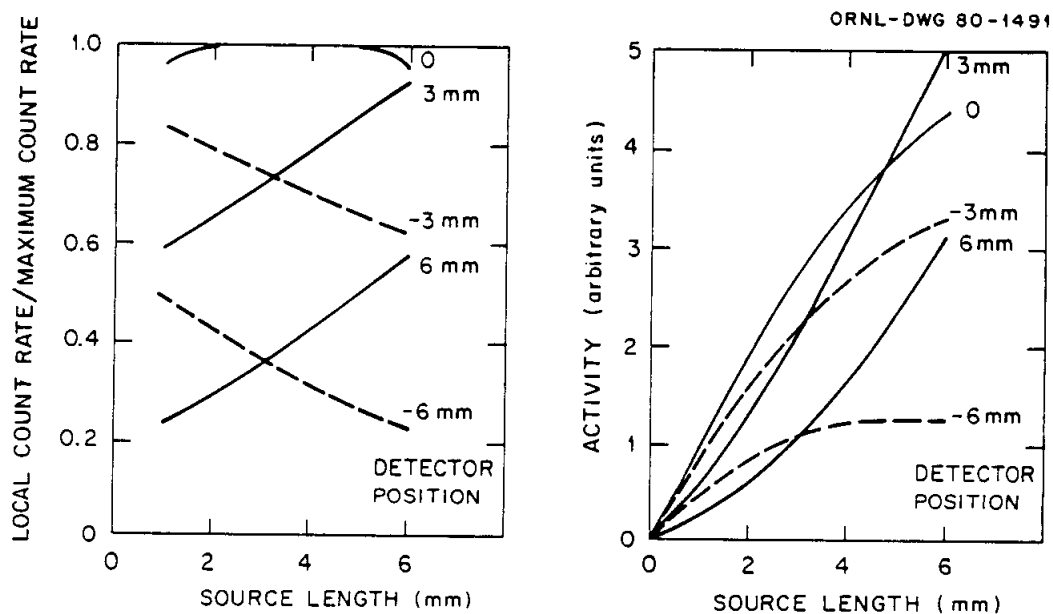


Fig. D.4. Effect of length of uniform source on absolute and normalized activities at several positions of a detector with a 3.2-mm collimator.

The curves in Figs. D.3 and D.4 are based on the assumption that all the iodine is present on the length of specimen that has reached equilibrium. Although the assumption is not quite correct, calculations based on information in Appendixes F and G indicated that, in the range

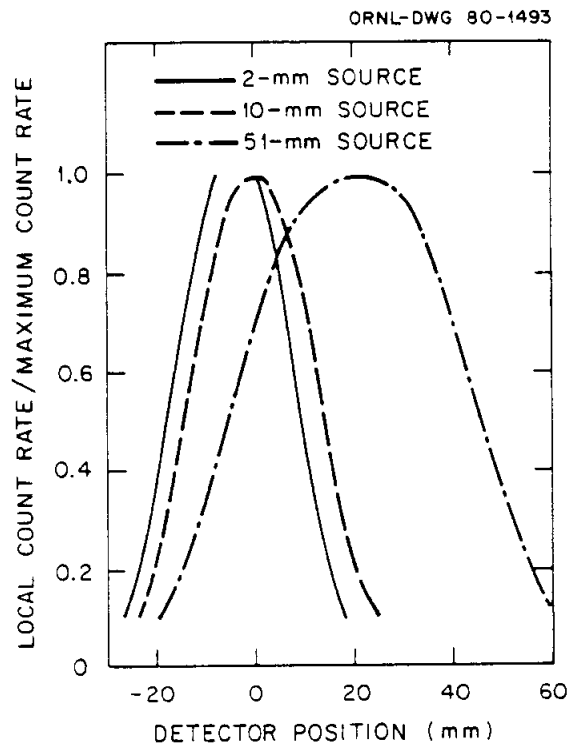


Fig. D.5. Effect of length of uniform source on profile obtained with detector with a 9.5-mm collimator.

of interest, most of the iodine would be in the region of saturation and that the concentration would fall rapidly with distance downstream. Figures D.3 and D.4 were used to estimate the equilibrium loadings on the specimens in experiment A-4. Measured profiles were compared with Fig. D.5 to judge whether the activity on specimen 2 was distributed nearly uniformly over the surface during some phases of experiment A-13.

Appendix E. BRIEF DESCRIPTIONS OF EXPERIMENTS

E.1 Experiment A-4

Experiment A-4 followed a series of preliminary tests and was the first in which a serious attempt was made to determine the equilibrium loading of iodine on type T-22 steel at low iodine burden. Conditions during the several phases of the experiment are reported in Table E.1. The amounts of iodine on the specimens at several times, and estimates of the iodine burdens based on those amounts, are shown in Table E.2. The accumulation of iodine on specimen 1 during phases 1 and 2 is illustrated in Fig. E.1. Activity profiles for the two specimens, each 51 mm long, are shown for several times in Figs. E.2 and E.3.

Phases 1 and 2 differed only in that the flows sometimes fluctuated during phase 2, so the conditions were less steady. During both phases, all the iodine in the gas adsorbed on specimen 1. The distribution of iodine on the specimen was estimated by comparing the measured profiles with the calculated profiles (Appendix D, Figs. D.3 and D.4). We judged that the concentration of iodine on the surface had reached a steady state over a length of 1 to 3 mm from the entrance of the specimen at the end of phase 1. The 23 μg adsorbed, distributed over the 3.5 to 9.5 cm^2 of surface, gave an average concentration of 6.6 to 2.4 $\mu\text{g}/\text{cm}^2$.

At the end of phase 2 (see profile in Fig. E.2), 32 μg of iodine appeared to be distributed over 12 cm^2 of surface within about 4 mm of the entrance with an average concentration of 2.7 $\mu\text{g}/\text{cm}^2$. We inferred from the data that the equilibrium concentration of iodine on the surface was 2 to 3 $\mu\text{g}/\text{cm}^2$ at 400°C in helium having an iodine burden of 2×10^{-4} to 3×10^{-4} Pa (2×10^{-9} to 3×10^{-9} atm) and containing 1200 Pa (1.2×10^{-2} atm) of hydrogen.

The conditions for phases 3 and 4 were the same as for phases 1 and 2 except for the lower partial pressure of hydrogen in the helium. At the beginning of phase 3, about 10% of the iodine desorbed from near the entrance of specimen 1. Then the activity near the entrance remained constant throughout the remainder of the experiment.

Table E.1. Test conditions in each phase of experiment A-4

	I ₂ transfer	1	2a	2b	2c	3	4	5	End
Beginning date	2/1	2/2	2/9	2/10	2/11	2/12	2/20	2/22	2/23
Time (clock)	13:48	10:40	14:30	14:00	~23:00	8:05	11:00	11:00	11:18
Cumulative time (10 ⁵ s)	0	0.748	6.95	7.81	8.96	9.29	16.22	17.95	18.82
Specimen temperature (°C)									
Specimen 1 (51 mm)	400	400	400	400	400	400	400	400	
Specimen 2 (51 mm)	200	200	200	200	200	200	200	200	
Helium flow (cm ³ /min, STP)									
Saturator	3	10	10 to 12	10	10 to 0	10	10	10	
Primary	0	190	190 to 230	190	190 to 0	190	190	190	
Total	3	200	200 to 242	200	200 to 0	200	200	200	
Iodine source									
Temperature (°C)	-95	-86 ± 1	-86	-86	-86	-86	-86	-63	
P _{I₂} at saturator temperature (10 ⁻⁵ Pa)	0.1	~1	1	1	1	1	1	100	
I burden in mixed gas based on P _{I₂} and gas flows (10 ⁻⁵ Pa)		~0.1	~0.1	~0.1	~0.1	~0.1	~0.1	10	
I burden based on adsorption measurements (10 ⁻⁵ Pa)		20 to 30	20 to 30	20 to 30	20 to 30	10 to 20	20	300	
Atmosphere	He with 1200 Pa H ₂	He with 3 Pa H ₂	Pure He (~10 ⁻³ Pa H ₂)	Pure He (~10 ⁻³ Pa H ₂)					

Table E.2. Iodine on specimens and iodine burden determined from activity measurements during experiment A-4

Test phase	Time (10 ⁵ s)	Specimen 1 ^a			Specimen 2 ^b			Charcoal trap		Total iodine (μg)	Adsorption rate (10 ⁻⁵ μg I/s)	Iodine burden (10 ⁻⁴ Pa or 10 ⁻⁹ atm)
		Profile area (mm)	C _{max} (counts/s)	Iodine (μg)	Profile area (mm)	C _{max} (counts/s)	Iodine (μg)	C (counts/s)	Iodine ^c (μg)			
1	4.21	11.9	4.1	9		0	0	1.3	0.7	9		
	6.88	11.9	9.7	23		0	0	1.3	0.7	24	5.3	2.9
3	9.50	14.0	12.5	34		0	0	1.5	0.8 ^d	35	4.2	2.2
	11.09	15.8	12.1	37		0	0	1.1	0.6 ^d	38	1.9	1.0
	16.16	23.9	26.4 ^e	49	38.4	64.4 ^e	8.1	12.0 ^e	1.2 ^d	58	3.9	2.1
4	17.03	24.1	25.5	48	48.8	74.7	12.0	14.0	1.4	61	3.5	1.9
5	18.14	27.4	24.0	52	48.8	103	16.0	13.0	1.3	69		
	18.79	27.2	26.5	57	62.7	189	37.0	126	13.0	107	59.0	32.0

^a Profiles measured with 3.2-mm collimator.

^b Profiles measured with 9.5-mm collimator.

^c Iodine on charcoal trap was obtained directly from activity measured by detector with 9.5-mm collimator.

^d The difference between the values is believed to have resulted from the adjustment to the analyzer and not to adsorption of iodine.

^e Adjustment of the single-channel analyzers at 11.9 × 10⁵ s changed the calibrations and increased the counts/s per μg I.

ORNL DWG 81-15366R

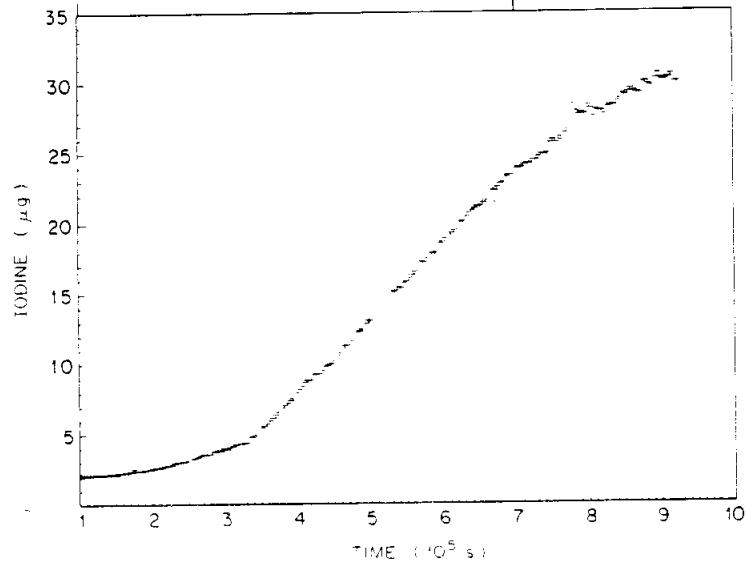


Fig. E.1. Iodine on specimen 1 of experiment A-4 during phases 1 and 2.

ORNL DWG 81-15371

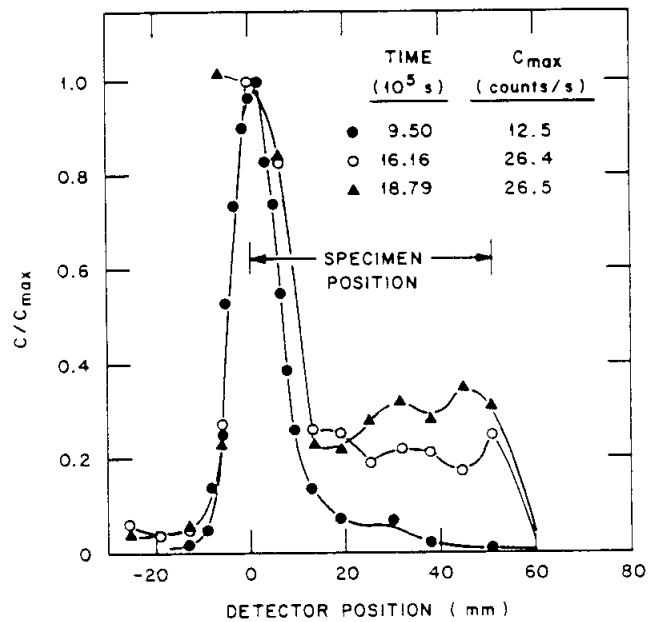


Fig. E.2. Activity profiles for specimen 1, as measured by detector 1 with 3.2-mm collimator and normalized to maximum count rate. These data represent conditions at ends of phases 2, 3, 4, and 5 of experiment A-4.

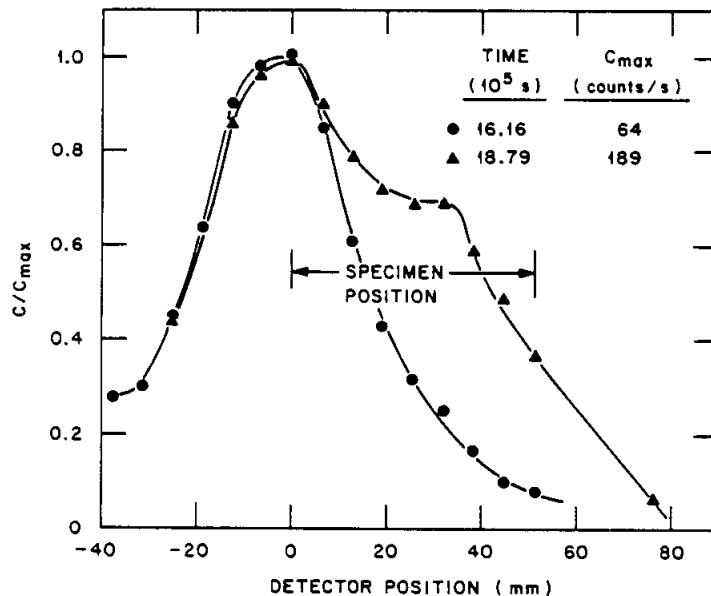


Fig. E.3. Activity profiles for specimen 2, as measured by detector 2 with 9.5-mm collimator. These data represent conditions at ends of phases 3 and 5 of experiment A-4.

The iodine that desorbed from near the entrance adsorbed farther along specimen 1, and all the iodine in the gas continued to adsorb on that specimen until about 11.4×10^5 s. Before the end of phase 3, the amount and distribution of iodine on specimen 1 had become steady, and all the iodine was adsorbing on specimen 2. This situation persisted to the end of phase 4.

An activity profile for specimen 1 at the end of phase 3 is shown in Fig. E.2. Profiles and maximum activities measured during phase 4 were practically the same. The profiles indicate that most of the $32 \mu\text{g}$ of iodine that was present on the surface within 4 mm of the entrance of the specimen at the end of phase 2 remained in place. The $17 \mu\text{g}$ that adsorbed during phase 3 was distributed almost uniformly over the remainder of the specimen. This implies that the concentration of 0.1 to $0.2 \mu\text{g I/cm}^2$ over most of the surface was in equilibrium at 400°C with helium having an iodine burden of 2×10^{-4} Pa (2×10^{-9} atm) and containing 3 Pa (3×10^{-5} atm) of hydrogen.

During phase 5 the temperature of the saturator was increased to raise the iodine burden in the gas. During this phase, 13% of the iodine adsorbed on specimen 1, 55% adsorbed on specimen 2, and 32% adsorbed on the charcoal trap. This was the first time that appreciable iodine reached the charcoal trap. Activity profiles measured at the end of phase 5 are shown in Figs. E.2 and E.3. The period of operation was too short to provide the data needed for estimating an equilibrium concentration of iodine on the metal.

Several factors produce uncertainty in the estimates of the equilibrium values of iodine concentrations derived above. First, the iodine burden calculated from the rate of adsorption of iodine on the specimens in phases 1 through 4 was 200 to 300 times greater than should have been obtained from elemental iodine at the temperature in the saturator. This difference was shown to be much greater than could be attributed to uncertainties in temperature and flow. For lack of other explanation, the high burden was attributed to the presence, in the saturator, of iodine compounds that are more volatile than elemental iodine. Methyl iodide is one such compound.

If such a compound was present, the adsorption was not appreciably inhibited when the helium contained 1200 Pa (1.2×10^{-2} atm) of hydrogen. The iodine adsorbed readily and within a few millimeters of the entrance of specimen 1.

Clearly, reducing the partial pressure of hydrogen to 3 Pa (3×10^{-5} atm) had a drastic effect on the adsorption on specimen 1. Adsorption on the surface near the entrance stopped. When steady state was reached, the concentration on the surface downstream was only 5 to 10% of that which had been reached near the entrance when the hydrogen pressure was high.

The reason for the difference is unclear. The chemical equilibrium data in Appendix A show that almost all the iodine should have been present in the gas as HI at 400°C when the iodine burden was 3×10^{-4} Pa (3×10^{-9} atm) or less and the hydrogen pressure was 3 Pa (3×10^{-5} atm) or greater, if iodine was added to the gas as elemental iodine. The effect of the hydrogen pressure might be explained if the iodine was

added as a compound that had to be reduced by hydrogen to HI before the iodine could adsorb.

Alternatively, the effect might have been related to the ability of the hydrogen to inhibit oxidation of the metal. Examination of the specimens after the experiment revealed that the metal had been oxidized. On specimen 1, the surface within 4 to 5 mm of the entrance was blistered and flaking. The remainder was spotted with oxide. Specimen 2, which had been at 200°C, was oxidized less than specimen 1. It was reddish brown over about the first centimeter and blue over the rest of its length. Red-brown oxide occurred in short stringers over the full length. Presumably, most of the oxidation occurred during phases 3, 4, and 5 when the hydrogen content of the gas was reduced to 3 Pa (3×10^{-5} atm) and then to about 10^{-3} Pa (10^{-8} atm). The oxide has less capacity than the metal for adsorbing iodine.

E.2 Experiment A-5

Experiment A-5 was run with pure helium [$\sim 1 \times 10^{-3}$ Pa ($\sim 1 \times 10^{-8}$ atm) of hydrogen] as the carrier for the iodine. Conditions for phase 1 were the same as those for phase 5 (the final phase) of experiment A-4. Specimen 1 was made 2 mm long so that all the surface would reach the equilibrium concentration more rapidly, and the total amount of deposited iodine could be determined directly from the detector reading obtained with the 6.4-mm collimator.

The test conditions during experiment A-5 are listed in Table E.3. The way in which the amounts of iodine on the specimens and the charcoal trap changed during the experiment is shown in Figs. E.4 and E.5. The amounts shown for specimen 1 and the charcoal trap are the total amounts of iodine on those items. The amount shown for specimen 2 is indicative of the amount of iodine on the part of the specimen that could be seen through the collimator of a detector positioned at the entrance of the specimen. The total amount of iodine on specimen 2 was determined from activity profiles. Several activity profiles, plotted in terms of total rather than normalized activity, are shown in Fig. E.6. Some of the data and calculations are summarized in Table E.4.

Table E.3. Test conditions in each phase of experiment A-5

	I ₂ transfer	1	2	3	4	End
Beginning date	3/2	3/2	3/5	3/6	3/8	3/9
Time (clock)	9:50	14:52	10:30	15:15	14:16	10:23
Cumulative time (10 ⁵ s)	0	0.180	2.61	3.66	5.33	6.05
Specimen temperature (°C)						
Specimen 1 (2 mm)	400	400	400	400	600	
Specimen 2 (51 mm)	200	200	200	200	400	
Helium flow (cm ³ /min, STP)						
Saturator (pure He)		10	10	0	0	
Primary (pure He)		190	190	190	190	
Total		200	200	190	190	
Iodine source						
Temperature (°C)	-100	-63	-95	-95	-95	
P _{I₂} at saturator temperature (10 ⁻⁵ Pa)	0.035	100	0.1	0.1	0.1	
I burden in mixed gas based on P _{I₂} and gas flows (10 ⁻⁵ Pa)		10	0.01	0	0	
I burden based on adsorption measurements (10 ⁻⁵ Pa)		500 to 600				

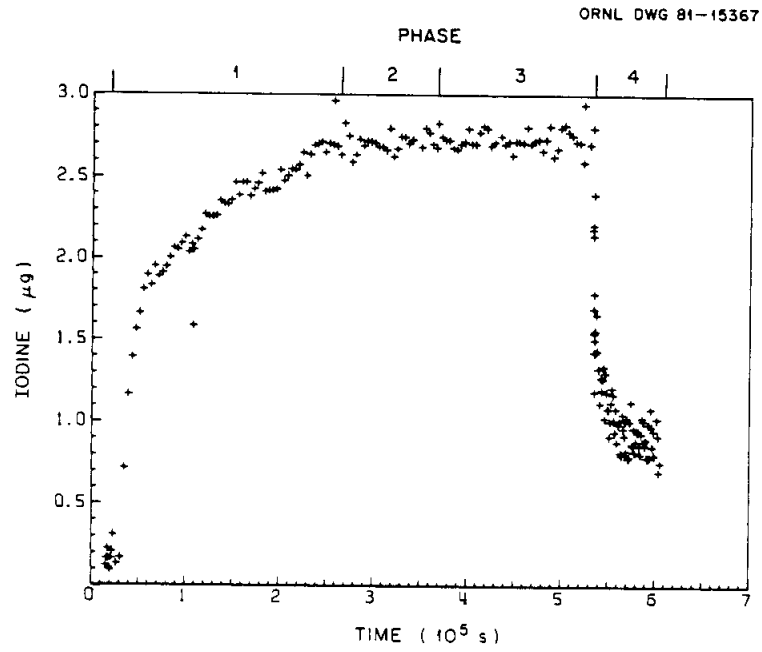


Fig. E.4. Iodine on specimen 1 during experiment A-5.

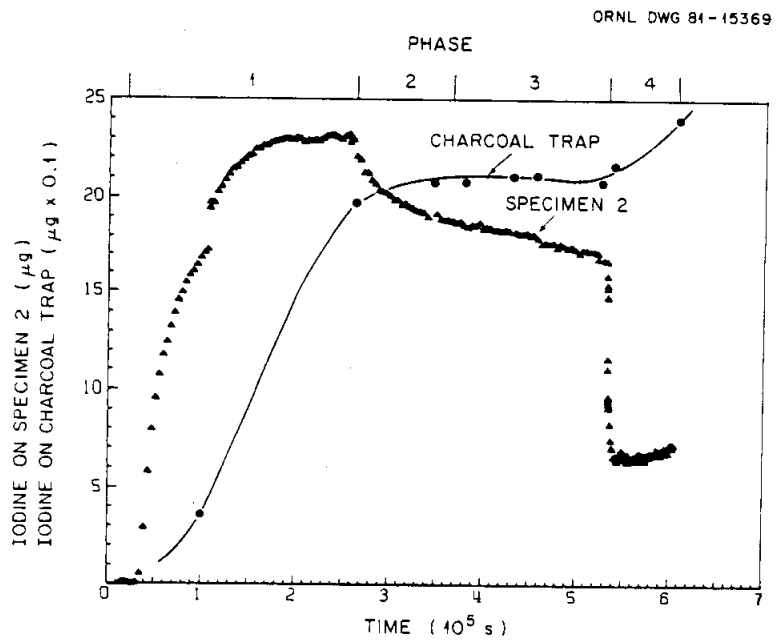


Fig. E.5. Iodine on specimen 2 and charcoal trap during experiment A-5.

ORNL DWG 81-15374

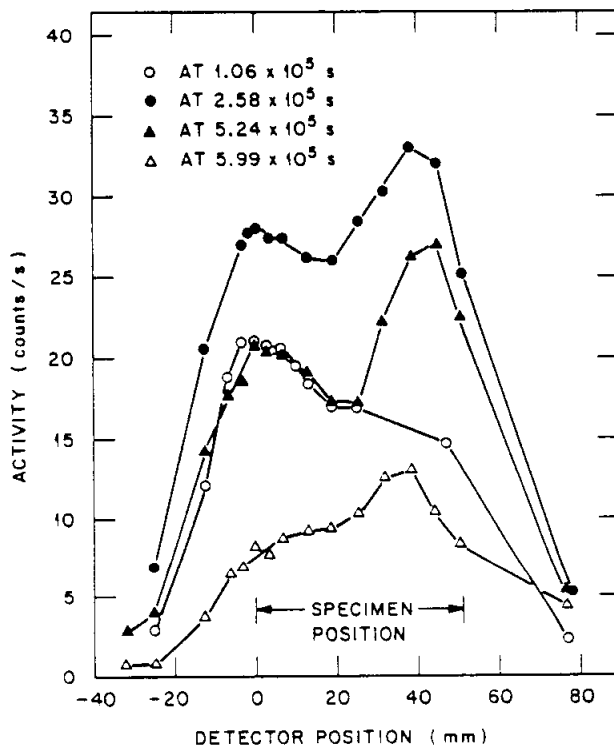


Fig. E.6. Activity profiles for specimen 2 during experiment A-5, as measured by detector with 9.5-mm collimator.

Although it was intended that phase 1, the adsorption phase of the experiment, be carried out at an iodine burden of 1×10^{-4} Pa (1×10^{-9} atm), measurements of the rate of adsorption of iodine on the components show that it was actually 5×10^{-3} to 6×10^{-3} Pa (5×10^{-3} to 6×10^{-8} atm). This was like the experience in experiment A-4. Again, after study of temperatures, flows, and operation of the experiment, the high burden was attributed to the presence of an iodine compound that is more volatile than elemental iodine.

The high iodine burden in helium that contains as little as 10^{-3} Pa (10^{-8} atm) of hydrogen complicates the interpretation of the adsorption data. Although chemical equilibrium, as projected by the figures in Appendix A, would not be expected to exist in the experiment, the data do suggest the following:

Table E.4. Iodine on specimens and iodine burden determined from activity measurements during experiment A-5

Test phase	Time (10 ⁵ s)	Specimen 1		Specimen 2			Charcoal trap		Total iodine (μg)	Adsorption rate (10 ⁻⁵ μg I/s)	Iodine burden (10 ⁻³ Pa or 10 ⁻⁸ atm)
		C (counts/s)	Iodine (μg)	Profile area (mm)	C _{max} (counts/s)	Iodine (μg)	C (counts/s)	Iodine (μg)			
1	0.30	<0.1	<0.1		<0.1	<0.1			<1		
	1.06	1.3	2.0	68	21.0	40.0	40.9	36	78	103	5.5
	2.58	1.7	2.7	72	33.0	66.0	227	197	266	124	6.5
2	3.41	1.7	2.7	68	30.0	57.0	239	208	268		
	4.30	1.7	2.7	71	28.0	56.0	245	213	271		
3	5.24	1.7	2.7	68	27.0	52.0	242	210	265		
	5.99	0.4	0.7	58	13.0	21.0	277	240	262		
Posttest ^a			0.9			16.0		214 ^b	231	101 ^c	5.4

^a Posttest measurements by use of multichannel analyzer

^b Includes 14 μg on furnace tube in vicinity of charcoal trap.

^c Based on assumption that iodine was adsorbed between 0.3×10^5 and 2.58×10^5 s.

1. $\text{CrI}_2(\text{s})$ is stable at iodine burdens $>10^{-3}$ Pa ($>10^{-8}$ atm) at 400°C and $>2 \times 10^{-7}$ Pa ($>2 \times 10^{-12}$ atm) at 200°C . HI and I should have reacted with any chromium that was accessible on specimens 1 and 2 to produce $\text{CrI}_2(\text{s})$.
2. In circumstances where the activity or accessibility of chromium is too low to deplete the gas of iodine, $\text{FeI}_2(\text{g})$ can attain an equilibrium pressure of 10^{-3} Pa (10^{-8} atm) in helium having an iodine burden of 6×10^{-3} Pa (6×10^{-8} atm) at 400°C . At 200°C $\text{FeI}_2(\text{s})$ is stable at iodine burdens $>2 \times 10^{-4}$ Pa ($>2 \times 10^{-9}$ atm). Therefore, HI and I should have reacted with iron on specimen 1 to produce a significant pressure of FeI_2 in the gas. This $\text{FeI}_2(\text{g})$ should have condensed on specimen 2, and additional $\text{FeI}_2(\text{s})$ should have been produced on that part of specimen 2 where the iodine burden was $>2 \times 10^{-4}$ Pa.

The interpretation is further complicated by oxidation of the specimen. Specimen 1 was considerably oxidized and the surface was blistered. The front half of specimen 2 was greenish gray mixed with reddish brown. The downstream half of the specimen was reddish brown. Areas of heavier oxidation appeared as short axial stringers on the surface. Calculations following a later experiment indicated that most of the oxygen probably diffused into the gas through the wall of plastic tubing in the helium lines. The rate was sufficient to give an oxygen pressure of 0.02 to 0.04 Pa (2 to 4×10^{-7} atm). Oxidation would be expected to reduce the availability of the small amount of chromium in the metal for reaction with iodine.

In Fig. E.5 it appears that a steady state loading on specimen 1 had almost been reached at 1.1×10^5 s. At that time, the total loading was $2.0 \mu\text{g I}$. The average concentration was $0.3 \mu\text{g}/\text{cm}^2$. However, the amount of iodine on specimen 1 continued to increase slowly and reached $0.4 \mu\text{g}/\text{cm}^2$ by the end of phase 1.

The amount of iodine on the part of specimen 2 that could be seen by the detector at its monitoring location near the entrance of the specimen reached a steady value at 1.9×10^5 s. According to the activity profile

at 2.58×10^5 s in Fig. E.6, there were regions of higher-than-average activity near the entrance and near the exit of the specimen. Whether a steady state had been reached over the entire specimen is unknown. We estimate that the concentration on the surface near the entrance was not less than $0.4 \mu\text{g}/\text{cm}^2$, the average over the entire surface, or greater than $2 \mu\text{g}/\text{cm}^2$.

We do not consider the steady, or nearly steady, concentrations of iodine on the specimens to be adsorption equilibrium values. Unless access of iodine to chromium and iron was blocked by films of chromium and iron oxides and iodides, there should have been continuing reactions to produce $\text{CrI}_2(\text{s})$ and $\text{FeI}_2(\text{g})$ on specimen 1 and $\text{CrI}_2(\text{s})$ and $\text{FeI}_2(\text{s})$ on specimen 2. Without limited access, it appears that the concentration of iodine on the surface, especially on specimen 2, could have increased indefinitely.

In phases 2 and 3, the specimen temperatures of phase 1 were maintained, and the iodine burden in the gas was reduced to a very low value to investigate desorption. No measurable amount of iodine desorbed from specimen 1. Either the activation energy for desorption was so high, for the sites on which iodine had adsorbed, that the desorption rate was very low, or the iodine was occluded within the metal oxides, and the rate of diffusion to the surface was low. Iodine desorbed readily from specimen 2. We attribute this to the dissociation of FeI_2 when the iodine burden was lowered.

When the temperatures were raised in phase 5, iodine desorbed rapidly from both specimens until new steady values were reached on specimen 1 and near the inlet on specimen 2. At the end of the experiment, iodine activity was found on the wall of the furnace tube downstream of specimen 2. This is an indication that part of the iodine was released as FeI_2 . The average concentration on specimen 1 at 600°C was $0.1 \mu\text{g}/\text{cm}^2$. The concentration on specimen 2 near the entrance at 400°C is estimated to have been 0.1 to $0.4 \mu\text{g}/\text{cm}^2$. We attribute the steady concentrations, in the absence of an appreciable iodine burden in the gas, to the iodine being present on sites having high activation energies for desorption, or to an effect of the metal oxides.

E.3 Experiment A-6

Experiment A-6 was run partly to obtain adsorption data and partly to investigate the behavior of the iodine saturator. Conditions during the many phases of the test are shown in Table E.5. The way in which the amounts of iodine on specimen 1 and near the entrance of specimen 2 changed during phases 1 through 7 is shown in Figs. E.7 and E.8. Some of the data are summarized in Table E.6.

Appreciable iodine reached the specimens during the charging of the saturator. The amount was about 0.06 μg on specimen 1 and 0.10 μg near the entrance of specimen 2 at the beginning of phase 1. When the flow of pure helium through the system was begun, the amount of iodine on specimen 1 rose erratically, peaking at 0.105 μg at 0.79×10^5 s. Then it settled back to 0.096 μg where it remained for the rest of phase 1. The steady concentration of iodine on specimen 1 was 0.014 $\mu\text{g}/\text{cm}^2$.

The amount of iodine on specimen 2 began a rise at about 0.7×10^5 s that continued to the end of phase 1. The activity profile at the end of phase 1 indicated that most of the 0.63 μg of iodine on the specimen was distributed over the first 6 mm. The average concentration was 0.034 $\mu\text{g}/\text{cm}^2$, but the data do not indicate that a steady state had been reached.

Based on the rate of increase of activity on the specimens and the charcoal trap, the iodine burden during phase 1 was 0.9×10^{-5} to 1.7×10^{-5} Pa (0.9×10^{-10} to 1.7×10^{-10} atm). The activity profiles indicated that almost all the iodine on specimen 2 was near the entrance. Yet, about one-third of the iodine passed over the rest of the specimen to the charcoal trap. If the iodine reaching the charcoal trap was in a form not readily adsorbable by the metal, the burden of "adsorbable" iodine was steady at 8×10^{-6} to 9×10^{-6} Pa (0.8×10^{-10} to 0.9×10^{-10} atm) during phase 1. All these burdens are 20 to 40 times the burden that should have produced by iodine at the temperature of the saturator. The higher burden is attributed to an unidentified iodine compound that is more volatile than elemental iodine.

Table E.5. Test conditions in each phase of experiment A-6

	1	2	3	4	5	6	7	8	9	10
Beginning date	4/12	4/17	4/18	4/19	4/20	4/24	4/25	4/26	4/26	4/26
Time (clock)	16:30	16:12	9:34	14:45	16:03	11:03	9:00	9:53	13:45	15:07
Cumulative time (10^5 s)	0.058	4.35	4.97	6.02	6.93	10.20	10.98	11.87	11.97	12.05
Specimen temperature ($^{\circ}$ C)										
Specimen 1 (2 mm)	400	400	400	400	400	400	600	800	800	600
Specimen 2 (51 mm)	200	200	200	200	200	200	400	600	800	800
Helium flow (cm^3/min , STP)										
Saturator	2	0	10	2	0	0	0	0	0	0
Primary	190	195	190	195	196	196	196	196	196	196
Total	192	195	200	197	196	196	196	196	196	196
Iodine source										
Temperature ($^{\circ}$ C)	-83	-83	-83	-75	-83	-83	-83	-83	-83	-83
P_{I_2} at saturator temperature (10^{-5} Pa)	2	2	2	10	2	2	2	2	-83	-83
I burden in mixed gas based on P_{I_2} and gas flows (10^{-5} Pa)	0.04	0	0.2	0.2	0	0	0	0	0	0
I burden based on adsorption measurements (10^{-5} Pa)	0.9 to 1.7		4.4	5.9						
Atmosphere	Pure He	Pure He	Pure He	Pure He	Pure He	He + 50 Pa H ₂				

Table E.5 (continued)

	11	12	13	14	15	16	End
Beginning date	4/27	4/30	5/3	5/4	5/4	5/4	5/4
Time (clock)	11:41	12:12	11:55	9:59	11:07	11:46	12:59
Cumulative time (10^5 s)	12.79	15.35	17.92	18.71	18.75	18.77	18.82
Specimen temperature ($^{\circ}$ C)							
Specimen 1 (2 mm)	400	400	400	600	800	800	
Specimen 2 (51 mm)	400	400	400	600	800	800	
Helium flow (cm^3/min , STP)							
Saturator	2	2	2	0	0	0	
Primary	195	198	198	198	198	198	
Total	197	200	200	198	198	198	
Iodine source							
Temperature ($^{\circ}$ C)	-83	-68	-57.5	-83	-83	-83	
P_{I_2} at saturator temperature (10^{-5} Pa)	2	40	250	2	2	2	
I burden in mixed gas based on P_{I_2} and gas flows (10^{-5} Pa)	0.04	0.8	5	0	0	0	
I burden based on adsorption measurements (10^{-5} Pa)	>0.4	>1.3	>14				
Atmosphere	Pure He	He + 50 Pa H ₂					

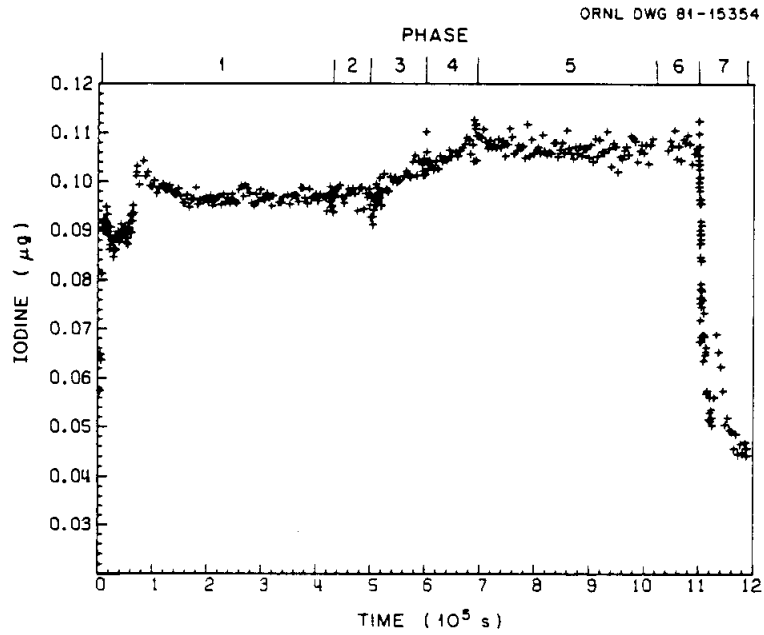


Fig. E.7. Iodine on specimen 1 during phases 1 through 7 of experiment A-6.

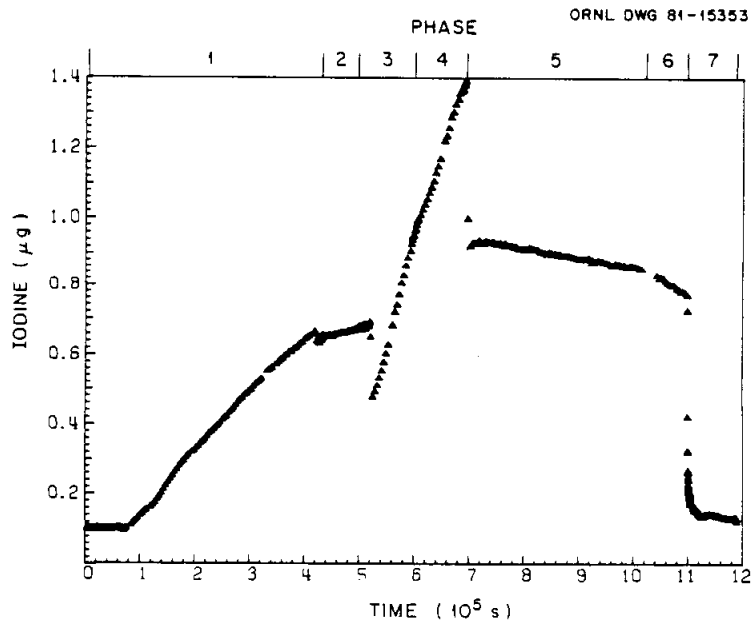


Fig. E.8. Iodine on specimen 2 during phases 1 through 7 of experiment A-6.

Table E.6. Iodine on specimens and iodine burdens determined from activity measurements during experiment A-6

Test phase	Time (10 ⁵ s)	Specimen 1		Profile area (mm)	Specimen 2		Charcoal trap		Total iodine (μg)	Adsorption rate (10 ⁻⁵ μg I/s)	Iodine burden (10 ⁻⁵ Pa or 10 ⁻¹⁰ atm)
		C (counts/s)	Iodine (μg)		C _{max} (counts/s)	Iodine (μg)	C (counts/s)	Iodine (μg)			
1	0.66	3.1	0.105	<i>a</i>	6.4	0.10	11.8	0.19	0.40		
	1.87	2.8	0.096	<i>a</i>	18.0	0.29	24.6	0.39	0.78	0.31	1.7
	3.21	2.9	0.096	<i>a</i>	31.5	0.50	28.0	0.45	1.0	0.20	1.1
	4.08	2.9	0.096	<i>a</i>	39.1	0.63	28.7	0.46	1.2	0.16	0.9
2	4.96	2.8	0.096	<i>a</i>	40.0	0.64	30.4	0.49	1.2		
3	5.90	3.1	0.105	18.0	5.6 ^{<i>b</i>}	1.40	31.5	0.50	2.0	0.83	4.4
4	6.84	3.2	0.110	31.7	12.4 ^{<i>b</i>}	2.46	33.5	0.54	3.1	1.2	5.9
10	12.70	<i>c</i>	0	<i>d</i>	20.0	<i>d</i>	261	4.1	>4.1		
11	15.23	<i>c</i>	0	<i>d</i>	30.0	<i>d</i>	271	4.3	>4.3	>0.08	>0.4
12	17.92	<i>c</i>	0	<i>d</i>	160	<i>d</i>	307	4.9	>4.9	>0.24	>1.3
13	18.67	<i>c</i>	0	<i>d</i>	280	<i>d</i>	434	6.9	>6.9	>2.7	>14

^{*a*}Amount of iodine on specimen 2 was determined directly from activity measured at entrance of specimen by use of a 9.5-mm collimator.

^{*b*}Profile was measured through a 3.2-mm collimator.

^{*c*}Activity was not distinguishable from background.

^{*d*}Specimen had moved and profiles were not complete enough for calculating iodine loading.

Phase 2 was a short interval during which the iodine burden was reduced, presumably to 0, by stopping the flow of gas to the saturator. The activity on specimen 1 did not change appreciably. After the initial sharp decrease (these occurred several times during the experiment and were attributed to upsets in the temperatures attendant to the measurement of activity profiles), the activity on specimen 2 increased, but at a much reduced rate. We assume that the iodine adsorbed on specimen 2 had desorbed from the wall of the furnace tube ahead of the specimen. If, however, it came from a flow of gas through the saturator, as was found to occur in a later experiment, the rate was less than 1 cm^3 (STP)/min.

In phase 3 the flow of gas through the saturator was increased over that of phase 1 by a factor of 5 to see whether the measured iodine burden would increase proportionally. In phase 4 the flow through the saturator was returned to that of phase 1, but the temperature was increased by an amount that would produce a fivefold increase in the vapor pressure of elemental iodine. The changes in flow and temperature increased the iodine burden by factors of about 4 and 6 respectively. Considering the uncertainties in the measurements, the increases obtained were consistent with the changes in flow and temperature. During phases 3 and 4, the amount of iodine on specimen 1 increased slightly. Most of the iodine adsorbed on specimen 2.

Flow of gas through the saturator was turned off to desorb iodine in phases 5 through 10. In phase 5, when the flow reduction was the only change in conditions, iodine desorbed from specimen 1 at the very slow rate of $2.4 \times 10^{-8} \text{ } \mu\text{g/s}$. After an initial loss of iodine when a profile was measured, iodine desorbed from near the entrance of specimen 2 at a rate of $3.5 \times 10^{-7} \text{ } \mu\text{g/s}$.

Changing the gas to helium containing 50 Pa ($5 \times 10^{-4} \text{ atm}$) of hydrogen in phase 6 had no obvious effect on the desorption from specimen 1. However, the rate of desorption from near the entrance of specimen 2 increased to $1.1 \times 10^{-6} \text{ } \mu\text{g/s}$. The reason for this increase in desorption rate is unclear. If the iodine on specimen 2 was in the

form of $\text{FeI}_2(\text{s})$, the increase in hydrogen pressure, from about 10^{-3} Pa in pure helium to 50 Pa, might have increased the rate of desorption by increasing the rate of dissociation of FeI_2 . However, the maximum iodine burden, 6×10^{-5} Pa (6×10^{-10} atm), during phase 4 was not high enough for $\text{FeI}_2(\text{s})$ to have been stable under equilibrium conditions at 200°C unless the helium contained less than about 10^{-4} Pa (10^{-9} atm) of hydrogen.

In phases 7 through 10 the amount of iodine on the specimens was reduced by raising the temperature to 800°C . The final activity on specimen 1 was indistinguishable from background, but a small amount remained on specimen 2.

The adsorption tests in pure helium were resumed in phase 11 under the conditions of phase 1 except that both specimens were at 400°C . In phases 12 and 13, the saturator temperature was increased to raise the iodine burden at the specimens. We found after the test was ended that specimen 2 was displaced downstream from its original position. The profiles obtained after phase 9 were not complete enough to make good estimates of the iodine burdens in the gas during the later phases. We can, however, infer the magnitudes of those burdens from the profiles obtained and the increase in activity on the charcoal trap shown in Table E.6. The iodine burdens during phases 11, 12, and 13 were greater than 4×10^{-6} , 1.3×10^{-5} , and 1.4×10^{-4} Pa respectively.

During phases 11, 12, and 13, there was no appreciable increase in the activity on specimen 1. In phases 14, 15, and 16, the temperature was raised to 800°C and hydrogen was added to the helium. The activity on specimen 1 did not decrease. The specific activity was low at the end of the experiment, but we could easily have discerned a change of $0.02 \mu\text{g}$ ($0.003 \mu\text{g}/\text{cm}^2$) on specimen 1.

Specimen 1 was oxidized, pitted, and had a flaking surface after the end of the experiment. Specimen 2 was covered with a thin reddish brown and blue film characteristic of oxidized steel.

At the beginning of this experiment, we obtained a steady state concentration of $0.014 \mu\text{g}/\text{cm}^2$ on T-22 steel at 400°C in pure helium having

an iodine burden of 0.9×10^{-5} to 1.7×10^{-5} Pa (0.9×10^{-10} to 1.7×10^{-10} atm). When the iodine burden was reduced, this iodine did not desorb at 400°C , but it desorbed readily when the temperature was increased to 600 and 800°C . At the end of the experiment, when the surface was heavily oxidized, $<0.003 \mu\text{g I/cm}^2$ adsorbed at 400°C when the iodine burden was $>1.4 \times 10^{-4}$ Pa ($>1.4 \times 10^{-9}$ atm).

E.4 Experiment A-7

The procedures for this experiment were like those of the preceding ones except that the saturator was purged with helium at the beginning to remove iodine compounds that are more volatile than the element. The purging seemed to help. During most of the tests, the iodine burden in the gas, based on the vapor pressure of iodine at the temperature in the saturator and the gas flows, was in good agreement with that based on the adsorption measurements. Helium containing 50 Pa (5×10^{-4} atm) of hydrogen was the carrier for the iodine in all the tests. Both specimens were at 400°C during the adsorption phases. Under equilibrium conditions, almost all the iodine in the helium would have been present as HI and I during all phases of the experiment. $\text{CrI}_2(\text{s})$ and $\text{FeI}_2(\text{s})$ should not have been stable under any of the conditions. The main stream of helium was passed over type T-22 steel foil at 400°C just before mixing with the stream from the saturator in an effort to reduce the oxidation of the specimens.

Experimental conditions are listed in Table E.7. The manner in which the amount of iodine on the specimens changed during the several phases is shown in Figs. E.9 and E.10. Some of the data are summarized in Table E.8.

Phase 1 began with a small amount of iodine on the specimens. The 0.04 to $0.05 \mu\text{g I/cm}^2$ on specimen 1 did not change during phase 1. Because of difficulties with the detector for specimen 2, which were not corrected until part way into phase 2, we cannot make a good estimate of the iodine burden in phase 1. The data were interpreted to indicate that the burden was less than the intended 2×10^{-5} Pa (2×10^{-10} atm) and probably was greater than 4×10^{-6} Pa (4×10^{-11} atm). We conclude, on a rather

Table E.7. Test conditions in each phase of experiment A-7

	I ₂ transfer	Source purge	1	2	3	4	End
Beginning date	5/17	5/18	5/18	5/22	5/28	6/2	6/6
Time (clock)	15:21	08:50	14:23	14:29	09:55	13:05	10:30
Cumulative time (10 ⁵ s)	0	0.629	0.823	4.273	9.263	13:66	17.01
Specimen temperature (°C)							
Specimen 1 (2 mm)	400	400	400	400	400	400	
Specimen 2 (51 mm)	400	400	400	400	400	400	
Helium flow (std cm ³ /min)							
Saturator (pure He)	2	6	2	2	2	2	
Primary (He + 50 Pa H ₂)	100	100	198	198	198	198	
Total	102	106	200	200	200	200	
Iodine source							
Temperature (°C)	-83	-55/-45	-63	-49	-32	-83	
P _{I₂} at saturator temperature (10 ⁻⁵ Pa)	2	400/2000	100	1000	10 ⁴	2	
I burden in mixed gas based on P _{I₂} and gas flows (10 ⁻⁵ Pa)	<i>a</i>	<i>a</i>	2	20	200	0.04	
I burden based on adsorption measurements (10 ⁻⁵ Pa)			<2	10 to 19	140	4	

^aSpecimens were bypassed during charging of saturator and purging of source.

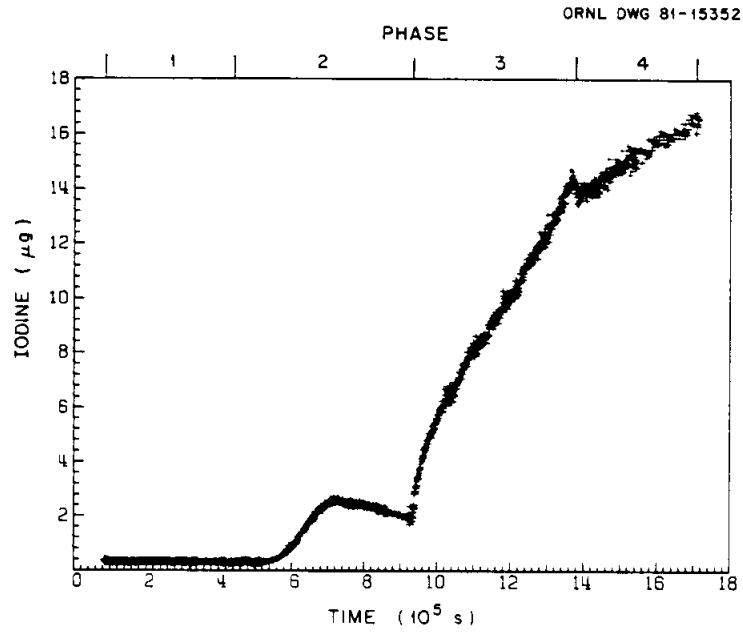


Fig. E.9. Iodine on specimen 1 during experiment A-7.

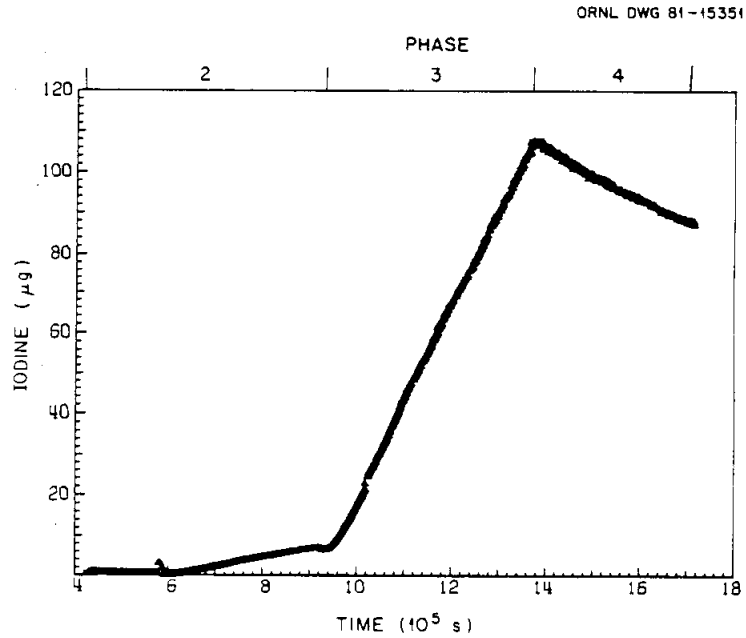


Fig. E.10. Iodine on specimen 2 during experiment A-7.

Table E.8. Iodine on specimens and iodine burdens determined from activity measurements during experiment A-7

Test phase	Time (10 ⁵ s)	Specimen 1		Specimen 2		Total iodine (μg)	Adsorption rate (10 ⁻⁵ μg I/s)	Iodine burden (10 ⁻⁵ Pa or 10 ⁻¹⁰ atm)
		(counts/s)	(μg I)	(counts/s)	(μg I)			
2	6.0	1.2	0.83	2.5	0.88			
	6.5	2.5	1.7	5.1	1.8	1.8	3.6	19
	7.0	3.5	2.4	8.8	3.1	2.0	4.0	
	7.2	3.8	2.6	10.2	3.6	0.7	3.5	
	7.5	3.6	2.4	12.6	4.4	0.6	2.0	
	8.0	3.5	2.4	15.8	5.5	1.1	2.2	10
	8.5	3.2	2.2	18.8	6.6	0.9	1.8	
	9.0	2.9	2.0	22.2	7.8	1.0	2.0	
3	9.3	2.75	1.9	21.8	7.6			
	9.5	5.10	3.5	25.5	8.9	2.9	15.0	80
	10.2	9.0	6.2	70.0	25.0	19.0	27.0	140
	13.1	18.3	12.6	270	95.0	76.0	26.0	140
4	13.7	21.1	14.6	309	108	15.0	25.0	130
	14.0	20.0	13.8	309	108			
	17.0	23.3	16.1	267	108 ^a	2.3	0.8	4
Posttest		19.0		102				

^aBased on activity profiles.

tenuous basis, that the concentration of 0.04 to 0.05 $\mu\text{g}/\text{cm}^2$ was in equilibrium at 400°C with an iodine burden somewhere in the range of 0.4×10^{-5} to 2×10^{-5} Pa (0.4×10^{-10} to 2×10^{-10} atm) in helium containing 50 Pa (5×10^{-4} atm) of hydrogen.

Lack of an increase in activity on specimen 1 led us to raise the saturator temperature to increase the iodine burden for phase 2. Equipment difficulties prevented the saturator from reaching the higher temperature until about 5×10^5 s. The increase in burden produced an almost immediate rise in the amount of iodine on specimen 1 that continued until about 7.2×10^5 s (see Fig. E.9). Thereafter, the amount of iodine decreased slowly until the end of phase 2.

Not much iodine had arrived at specimen 2 by the time the detector was replaced at 5.9×10^5 s. Then, the amount on specimen 2 increased at an almost uniform rate until the end of phase 2 (Fig. E.10). Activity profiles for specimen 2 showed that almost all the iodine on the specimen adsorbed near the entrance in full view of the detector through the 9.5-mm collimator. No significant amount of iodine reached the charcoal trap.

At 7.2×10^5 s, there was 2.6 μg of iodine on specimen 1; the average concentration was $0.4 \mu\text{g}/\text{cm}^2$ and the iodine burden was 1.9×10^{-4} Pa (1.9×10^{-9} atm). Although the concentration had not yet reached steady state, the fraction of the iodine in the gas adsorbing on specimen 1 had decreased to 0.3, so the loading appeared to be nearing a steady value. Then the iodine burden decreased abruptly to 1.0×10^{-4} Pa (1.0×10^{-9} atm), and iodine began to desorb from the specimen. We concluded that the concentration of $0.4 \mu\text{g I}/\text{cm}^2$ would have been in equilibrium at 400°C with an iodine burden between 1.0×10^{-4} and 1.9×10^{-4} Pa.

In phase 3 the saturator temperature was raised again to obtain an iodine burden near 2×10^{-3} Pa (2×10^{-8} atm). The amount of iodine on both specimens increased steadily throughout phase 3. The amount of iodine on the charcoal trap did not increase.

At the end of phase 3, less than 15% of the iodine was adsorbing on specimen 1, and the average concentration was $2.1 \mu\text{g}/\text{cm}^2$. An

activity profile for specimen 2, measured at 12.9×10^5 s, is shown in Fig. E.11. Comparison of this profile with the calculated profiles in Appendix D indicates that the bulk of the iodine was within 4 to 8 mm of the entrance. Other profiles showed that the distribution had not changed much by the end of phase 3, so the average concentration at that time was between 4 and 9 $\mu\text{g}/\text{cm}^2$.

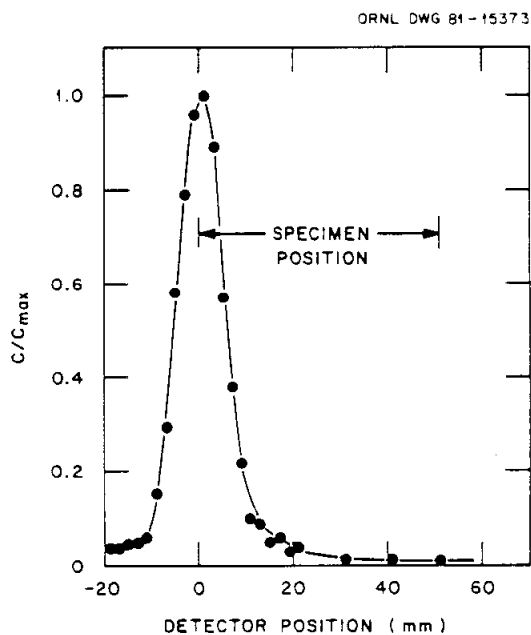


Fig. E.11. Activity profile for specimen 2 in experiment A-7 at 12.9×10^5 s measured by detector 2 with a 3.2-mm collimator.

The numbers above indicate that the equilibrium loading on T-22 steel is at least $4 \mu\text{g}/\text{cm}^2$ at 400°C in helium containing 50 Pa (5×10^{-4} atm) of hydrogen and having an iodine burden of 1.4×10^{-3} Pa (5×10^{-4} atm). Since such a small fraction of the iodine was adsorbing on specimen 1, while the loading was well below the equilibrium value, the surfaces of the specimens must have been considerably different. Based on later observations, we attribute the difference to oxidation of specimen 1.

In phase 4 the temperature of the saturator was lowered to reduce the iodine burden to about 4×10^{-7} Pa (4×10^{-12} atm). Iodine desorbed

from near the entrance of specimen 2, but activity profiles indicated that the iodine just moved along the specimen. There was no significant change in the amount of iodine on specimen 2 or on the charcoal trap.

The amount of iodine on specimen 1 did not decrease but increased at a rate that corresponded to adsorption of all the iodine from gas having a burden of 4×10^{-5} Pa (4×10^{-10} atm). The source of the higher-than-expected iodine pressure might have been desorption from an area at the entrance of the furnace tube. That area was found to contain about 30 μg of iodine at the end of the experiment.

The average concentration of iodine on specimen 1 at the end of phase 4 was $2.3 \mu\text{g}/\text{cm}^2$ and was still rising in gas that was estimated to have an iodine burden of 4×10^{-5} Pa (4×10^{-10} atm). This about six times the equilibrium value of $0.4 \mu\text{g}/\text{cm}^2$ that we assigned to a burden of 1.0×10^{-4} to 1.9×10^{-4} Pa (1×10^{-9} to 1.9×10^{-9} atm) in phase 2. We find no explanation for why all the iodine in the gas seemed to adsorb on specimen 1 during phase 4. Uncertainties in the data and analysis could have obscured the adsorption of some iodine on specimen 2, but not so much that the iodine burden could have exceeded 2×10^{-4} Pa (2×10^{-9} atm). Although we cannot explain the behavior in phase 4, we note that equilibrium loadings of $\sim 4 \mu\text{g}/\text{cm}^2$ at 400°C in helium containing 50 Pa (5×10^{-4} atm) of hydrogen and iodine burdens of 1×10^{-5} to 3×10^{-5} Pa (1×10^{-10} to 3×10^{-10} atm) were estimated from data in later experiments.

Upon disassembly of the apparatus, the specimens were examined and the amounts of iodine on various components were measured. Specimen 1 was oxidized and the surface was flaking, but the extent of oxidation was less than on specimen 1 at the end of experiment A-6. The surface within about 6 mm of the entrance of specimen 2 was mostly covered with tiny mounds of oxide. The remainder of the specimen was coated with a thin film of red-brown oxide containing numerous stringers of thicker oxide. Calculations indicated that oxygen probably was entering the system by diffusion through the wall of plastic tubing in the helium supply lines.

The amount of iodine found on the specimens by use of the multi-channel analyzer was about the same as was indicated by the detectors on the test apparatus at the end of the experiment (see Table E.8). Only 0.2 μg of iodine was found on the charcoal trap.

The following values for steady state concentrations of iodine on type T-22 steel at 400°C versus iodine burdens in helium containing 50 Pa (5×10^{-4} atm) of hydrogen were inferred from the data from this experiment:

Test phase	Iodine burden (10^{-5} Pa or 10^{-10} atm)	Surface concentration ($\mu\text{g I/cm}^2$)
1	0.4-2.0	0.04-0.05
2	10-19	0.4
3	140	>4.0
4	4	>2.3

E.5 Experiment A-8

Several changes in apparatus were made for this experiment. Three specimens, numbered 1A, 1B, and 2, were used. Specimens 1A and 1B were 2 mm long; specimen 2 was 51 mm. The plastic tubing in the helium supply lines were replaced with metal tubing. A trap containing T-22 steel, like that installed earlier in the main helium line, was added to the line to the saturator and operated at 450°C. These modifications helped, for the specimens were only lightly oxidized during this experiment.

Conditions during the experiment are reported in Table E.9. The amount of iodine on the specimens is shown as a function of time in Figs. E.12 through E.15. Data and results of some calculations are summarized in Table E.10.

The furnace tube cracked downstream of specimen 2 during the charging of the saturator, allowing iodine to reach the specimens. Since the crack was outside the furnace, it was sealed with Teflon tape. Phases 1 through 3 of the experiment were devoted to desorbing the iodine from specimens 1A and 1B. The specimens were at 400°C when the iodine was

Table E.9. Test conditions in each phase of experiment A-8

	I ₂ transfer	1	2	3	4	5	6	7	8	End
Beginning date	8/13	8/14	8/15	8/16	8/16	8/22	8/27	8/29	8/31	9/4
Time (clock)	15:42	13:01	13:49	8:19	9:44	13:50	11:43	10:36	14:54	10:55
Cumulative time (10 ⁵ s)	0	0.763	1.65	2.31	2.37	7.62	11.83	13.50	15.34	18.64
Specimen temperature (°C)										
Specimens 1A and 1B (2 mm each)	400	400	600	800	400	400	600	400	400	
Specimen 2 (51 mm)	400	400	400	400	400	400	400	400	400	
Helium flow (std cm ³ /min)										
Saturator (pure He)	14	0	0	0	10	10	10	10	0	
Primary (He + 50 Pa H ₂)	14	100	200	200	190	190	190	190	190	
Total	28 ^a	100	200	200	200	200	200	200	190	
Iodine source										
Temperature (°C)	-83	-83	-83	-83	-75	-63	-63	-63	-80	
P _{I₂} at saturator temperature (10 ⁻⁵ Pa)	2	2	2	2	10	100	100	100	3.9	
I burden in mixed gas based on P _{I₂} and gas flows (10 ⁻⁵ Pa)	0 ^a	0	0	0	1	10	10	10	0	
I burden based on adsorption measurements (10 ⁻⁵ Pa)		<0.7	0	0	0.05 to 0.4	90 to 170	130 to 140	90 to 190	0	

^aFlow was intended to be entirely through purge line. At ~18:00 on 8/13, a crack in the furnace tube allowed some flow over the specimens.

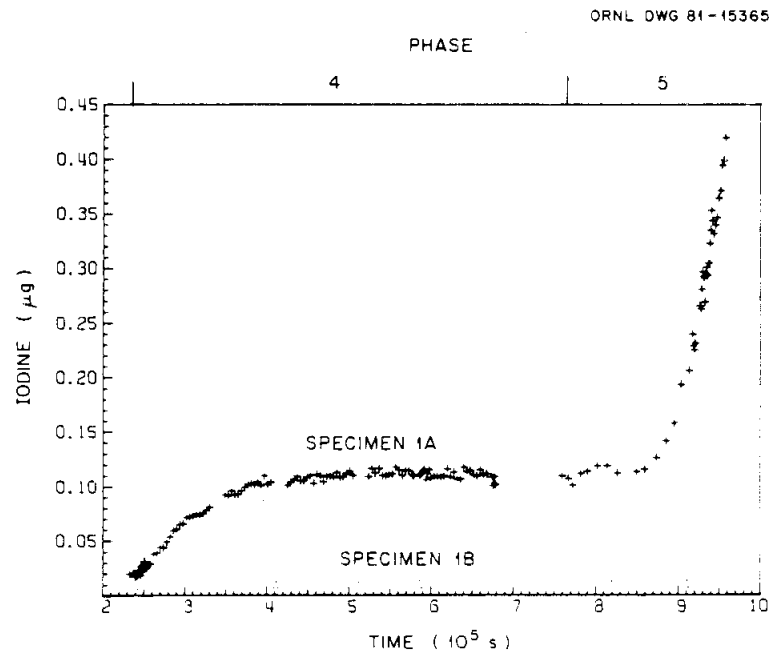


Fig. E.12. Iodine on specimens 1A and 1B during phase 4 and the early part of phase 5 of experiment A-8.

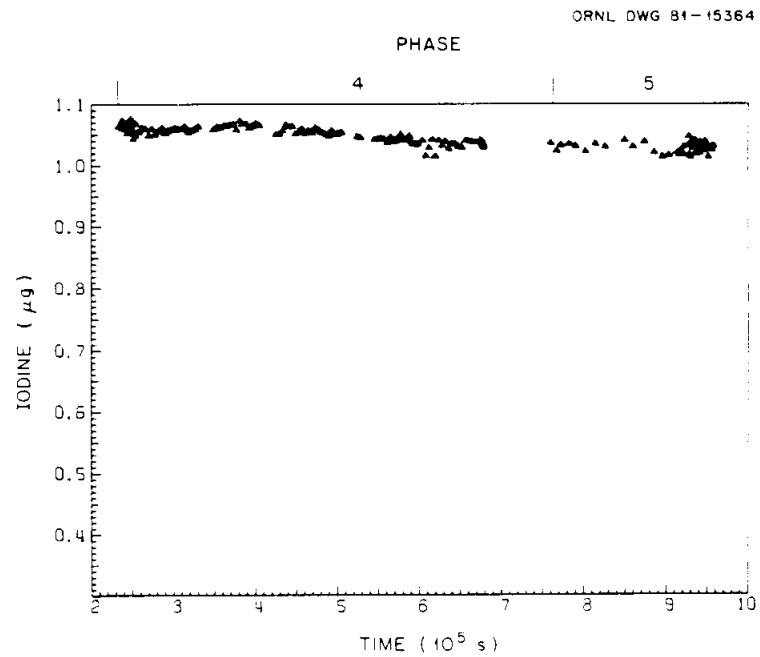


Fig. E.13. Iodine on specimen 2 during phase 4 and the early part of phase 5 of experiment A-8.

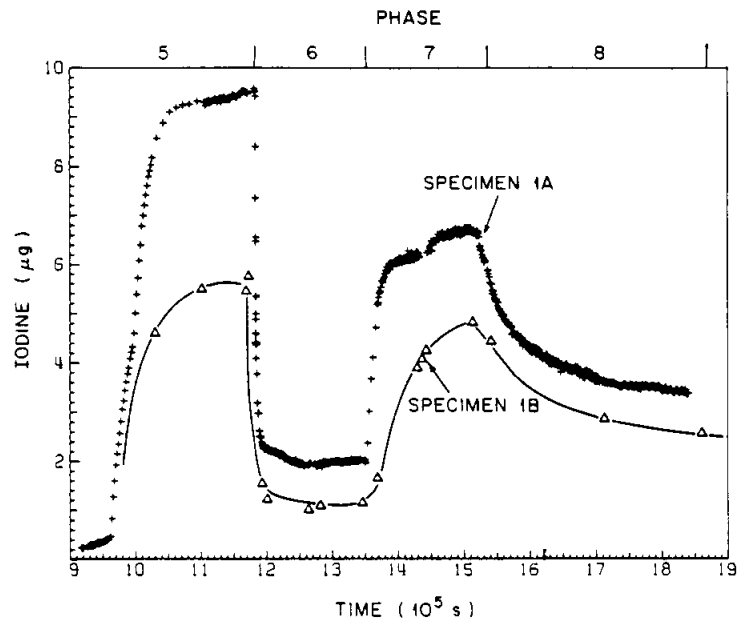


Fig. E.14. Iodine on specimens 1A and 1B during phases 5 through 8 of experiment A-8.

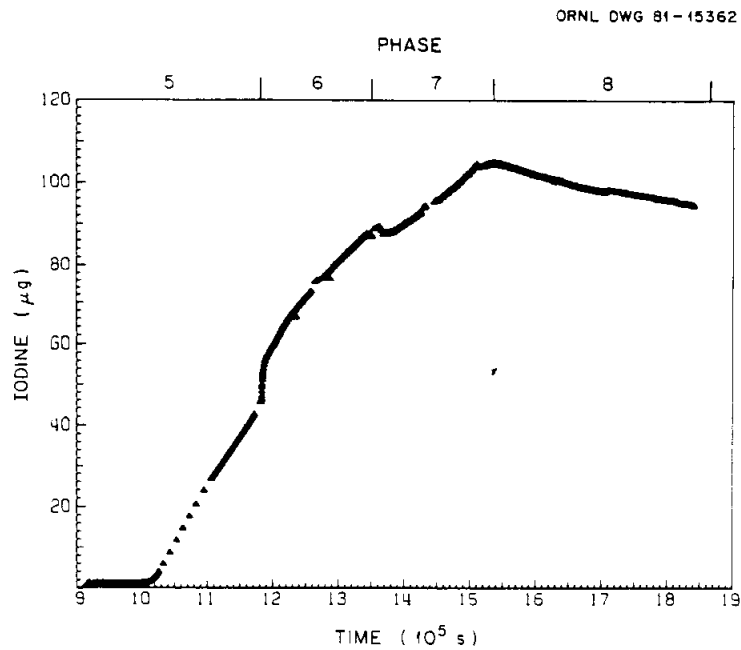


Fig. E.15. Iodine on specimen 2 during phases 5 through 8 of experiment A-8.

Table E.10. Summary of data from experiment A-8

Test phase	Time (10 ⁵ s)	Activity (counts/s)				Iodine adsorbed (µg)				Total	Iodine transport (10 ⁻⁶ µg/s)	Iodine burden (10 ⁻⁵ Pa)	Iodine concentration on surfaces (µg/cm ²)		Specimen 1 temperature (°C)		
		1A	Specimens 1B	2	Charcoal trap	1A	Specimens 1B	2	Charcoal trap				1A	1B			
1	0.77	7.9	4.4	2.6	0.5	0.61	0.34	0.10	0.02	1.07	1.33	0.7	0.087	0.049	400		
	1.60	8.5	4.8	3.5	0.9	0.65	0.37	0.13	0.03	1.18			0.093	0.053			
2	2.30	1.0	0.6	25.8	(0.9) ^a	0.08	0.05	0.96	(0.03)	1.12	0	0	0.011	0.007	600		
3	2.33	0.2	0.1	28.7	0.5	0.02	0.01	1.06	0.02	1.11	0	0	0.003	0.001	800		
4	2.40	0.1	(<0.1)	28.7	(0.5)	0.01	(<0.01)	1.06	(0.02)	1.10	0	0	0.001	<0.001			
	3.34	1.0	0.1	28.7	0.9	0.08	0.01	1.06	0.03	1.18	0.75	0.4	0.013		400		
4.08	1.2	0.1	28.7	0.8	0.09	0.01	1.06	0.03	1.19	0.14	0.07						
7.50	1.2	0.2	28.3	0.5	0.09	0.02	1.05	0.03	1.19	<0.1	<0.05						
5	8.52	1.3	0.1	27.7	0.5	0.10	0.01	1.03	0.02	1.16	3.1	2	1.4	0.81	400		
	9.59	5.5	0.3	27.7	0.6	0.42	0.02	1.03	0.02	1.49							
	10.28	109	59.0	123	0.8	8.4	4.5	4.6	0.03	17.5						230	120
	10.96	120	71.0	655	0.9	9.2	5.5	24.3	0.03	39.0						320	170
	11.76	126	74.0	1190	1.0	9.7	5.7	44.1	0.04	60.0						260	140
6	12.00	29	18.0	1610	(1.0)	2.2	1.4	60.0 ^b	0.04	64.0	170	90	0.29	0.19	600		
	12.60	25	16.0		1.6	1.9	78.0 ^b	0.06	81.0	270	140						
	13.45	26	17.0		1.6	2.0	98.0 ^b	0.06	101	240	130						
7	14.35	80	54.0		1.5	6.2	4.2	107 ^b	0.06	117	180	90	0.96	0.60	400		
	15.12	87	59.0		1.6	6.7	4.5	133 ^b	0.06	144	350	190					
8	18.62	43	34.0		1.7	3.3	2.6	137 ^b	0.06	143	0	0	0.47	0.37	400		
Posttest						2.1	1.9	164	0.03								

^aNumbers in parentheses were assumed on the basis of earlier measured values.

^bValues were calculated by use of the area under an activity profile and the maximum count rate for the profiles.

adsorbed. Simply stopping the flow through the saturator in phase 1 without increasing the temperature of the specimens produced no desorption of iodine. Conversely, the activity increased slightly. Presumably, the iodine in the gas reaching the specimens desorbed from the wall of the furnace tube upstream. The burden might have been as great as 7×10^{-6} Pa (7×10^{-11} atm).

Increasing the temperature in phase 2 resulted in rapid desorption of iodine to steady concentrations of $0.011 \mu\text{g}/\text{cm}^2$ on specimen 1A and $0.007 \mu\text{g}/\text{cm}^2$ on specimen 1B. At 800°C in phase 3, the activity on the specimens was reduced to slightly above background. The iodine concentrations were $0.001 \mu\text{g}/\text{cm}^2$ or less.

In phase 4, the flow through the saturator was restored, the temperature was raised to obtain an iodine burden of 10^{-5} Pa (10^{-10} atm), and the specimens were returned to 400°C . The amount of iodine increased appreciably on specimen 1A only, as shown in Fig. E.12. Based on the rate of increase, the iodine burden was 4×10^{-6} Pa (4×10^{-11} atm) at the beginning and was too low to measure at the end of phase 4.

In phase 5, the temperature was increased again to see whether an appreciable burden could be obtained in the gas. The amount of iodine on the specimens did not change significantly from 7.6×10^5 s, the beginning of phase 5, until about 8×10^5 s when the amount on specimen 1A began to rise slowly. Then, at about 9.5×10^5 s, the amount of iodine on specimen 1A began a very rapid rise that slowed markedly at 10.5×10^5 s as the iodine loading appeared to approach a steady value (see Fig. E.14).

The amount of iodine on specimen 1B was measured only when activity profiles were taken. No increase was seen until after the rapid rise on specimen 1A began. Then, the amount increased to a level that appeared to be steady at about 60% of that on specimen 1A at the end of phase 5.

The amount of iodine on specimen 2 did not begin to increase until the rapid rises on 1A and 1B were about half completed (Fig. E.15). Then, it too began to increase rapidly at a rate that showed no sign of diminishing at the end of phase 5.

Iodine burdens calculated for several intervals during phase 5 are shown in Table E.10. Beginning at the time of the sharp rise in iodine

on specimen 1, the iodine burden was in the range 0.9×10^{-3} to 1.7×10^{-3} Pa (0.9×10^{-8} to 1.7×10^{-8} atm). This was about ten times the burden expected from the gas flows and the vapor pressure of iodine at -63°C .

During tests of the saturator at the end of the experiment, we found that a valve in a bypass between the main helium line and the line to the saturator had been opened accidentally at some time during the experiment. With the valve open, as much as half the helium could have been flowing through the saturator. The higher flow rate was sufficient to account for the higher iodine burden in this experiment. However, there was no evidence that this was the explanation for the high iodine burdens in earlier experiments.

At the end of phase 5, iodine concentrations of $1.4 \mu\text{g}/\text{cm}^2$ on specimen 1A and $0.81 \mu\text{g}/\text{cm}^2$ on specimen 1B appeared to be in equilibrium with an iodine burden of 0.9×10^{-3} to 1.7×10^{-3} Pa (0.9×10^{-8} to 1.7×10^{-8} atm) at 400°C . We note here that specimens 1A and 1B were used in two experiments, A-8 and A-9. The equilibrium activity on specimen 1A was always greater than that on 1B. Whether this was because the specimen with the greater adsorptive capacity happened to be placed in position 1A in both experiments, or whether there is a more subtle reason, is unknown.

In phase 6, the temperature of specimens 1A and 1B was raised to 600°C . Iodine desorbed rapidly and equilibrium concentrations of 0.3 and $0.2 \mu\text{g}/\text{cm}^2$ were obtained on specimens 1A and 1B, respectively, for an iodine burden of 1.3×10^{-3} to 1.4×10^{-3} Pa (1.3×10^{-8} to 1.4×10^{-8} atm) (Fig. E.14).

Then, the temperature of specimens 1A and 1B was lowered to 400°C to see whether the loadings would return to those of phase 5. When the amounts of iodine on the specimens became steady, or nearly so, in phase 7, the iodine concentrations were about $1.0 \mu\text{g}/\text{cm}^2$ on specimen 1A and $0.6 \mu\text{g}/\text{cm}^2$ on specimen 1B. These are about 70% of the concentrations at the end of phase 5. The measurements indicated that the iodine burden had been in the same range, but the measurements were not precise enough

to establish whether the difference in loadings should be attributed to a change in conditions or surfaces.

For phase 8, the temperature of the saturator was reduced to -80°C , and the saturator flow was turned off with the intent of reducing the iodine burden in the gas to zero. However, the flow through the bypass line would not have been stopped. Lowering the temperature should have reduced the burden to about 4×10^{-5} Pa (4×10^{-10} atm). The adsorption measurements indicated that the iodine burden was zero, but they were not accurate enough to distinguish between 4×10^{-5} and 0 Pa (4×10^{-10} and 0 atm).

The amounts of iodine on specimens 1A and 1B decreased rapidly at the beginning of phase 8. The average iodine concentrations had reached about $0.5 \mu\text{g}/\text{cm}^2$ on specimen 1A and $0.4 \mu\text{g}/\text{cm}^2$ on specimen 1B and were decreasing slowly when phase 8 was ended.

At the end of the experiment, specimens 1A and 1B and the front 30 to 35 mm of specimen 2 were uniformly light gray in color, which indicates that they were lightly oxidized. From 35 to 50 mm on specimen 2, the color darkened and changed to the reddish brown typical of heavier oxidation. Presumably, this greater oxidation was produced by oxygen and moisture that entered through the crack in the furnace tube at the beginning of the experiment. Posttest measurements showed about 30% less iodine on specimens 1A and 1B and 20% more iodine on specimen 2 than was indicated by the detectors on the adsorption apparatus. Only about 0.02% of the iodine reached the charcoal trap.

The following values for steady state concentrations of iodine on type T-22 steel in helium containing 50 Pa (5×10^{-4} atm) of hydrogen and various iodine burdens were inferred from the data from this experiment:

Test phase	Temperature (°C)	Iodine burden (10 ⁻³ Pa or 10 ⁻⁸ atm)	Surface concentration (µg I/cm ²)
2	600	0	0.007-0.011
3	800	0	≤0.011
5	400	0.9-1.7	8.0-1.4
6	600	1.3-1.4	0.2-0.3
7	400	0.9-1.9	0.7-1.0
8	400	0-0.04	<0.5

E.6 Experiment A-9

The bypass between the main helium line and the line to the saturator was removed in preparation for experiment A-9. Two short specimens, 1A and 1B, and one long specimen were used in the experiment. Before beginning the adsorption tests, the saturator was purged until there was reasonable agreement between the vapor pressure of elemental iodine at the temperature in the saturator, and the pressure calculated from the gas flow through the saturator and the rate of adsorption of iodine on the purge trap.

Conditions during the experiment are listed in Table E.11. The change with time of the amounts of iodine on the specimens is shown in Figs. E.16 and E.17. Some of the data and calculations are summarized in Table E.12.

Phase 1 was begun under conditions that were intended to provide an iodine burden of 10⁻⁶ Pa (10⁻¹¹ atm). Almost all the iodine adsorbed on specimen 1A. Except for a short interval at the beginning, the iodine burden calculated from the rate of adsorption on the specimens was 2 × 10⁻⁶ Pa (2 × 10⁻¹¹ atm).

Phase 1 came to an abrupt end at about 7.4 × 10⁵ s when the amount of iodine on specimen 1A began to rise very rapidly, as shown in Fig. E.16. In phase 2, the rate of rise was nearly constant for about 1 × 10⁵ s at the higher iodine burden of about 2 × 10⁻⁵ Pa (2 × 10⁻¹⁰ atm). Almost all the iodine adsorbed on specimen 1A. Then the rate of rise on specimen 1A decreased rapidly until the amount of iodine reached a steady level. At

Table E.11. Test conditions in each phase of experiment A-9

	I_2 transfer	Saturator test						Adsorption test						End
		A	B	C	D	E	F	1	2	3	4	5	6	
Beginning date	9/24	9/24	9/25	9/25	9/27	9/27	9/28	9/28	10/3	10/9	10/15	10/15	10/29	11/5
Time (clock)	12:47	14:35	10:30	15:09	9:54	16:30	8:43	14:02	4:40	9:53	11:38	14:45	14:30	13:35
Cumulative time (10^5 s)	0	0.065	0.77	0.94	2.46	2.70	3.28	3.47	7.42	12.79	18.01	18.12	30.15	36.10
Specimen temperature ($^{\circ}$ C)														
Specimens 1A and 1B (2 mm)	400	400	400	400	400	400	400	400	400	600	600	400	400	
Specimen 2 (51 mm)	400	400	400	400	400	400	400	400	400	600	800	400	400	
Helium flow (std cm^3/min)														
Saturator (pure He)	10	10	10	10	10	10	10	2.9	2.9	2.9	2.9	2.9	0	
Primary (He + 50 Pa H_2)	90	90	90	90	90	90	90	197	197	197	197	197	200	
Total	100	100	100	100	100	100	100	200	200	200	200	200	200	
Iodine source														
Temperature ($^{\circ}$ C)	-80	-75	-50	-80	-63	-80	-75	-80	-81	-80	-80	-75	-80	
P_{I_2} at saturator temperature (10^{-5} Pa)	3.9	10	800	3.9	100	3.9	10	3.9	3.0	3.9	3.9	10	3.9	
P_{I_2} in saturator based on adsorption measurements (10^{-5} Pa)				15	190	5.0	18	NA	NA	NA	NA	NA	NA	
I burden in mixed gas based on P_{I_2} and gas flows (10^{-5} Pa)	NA	NA	NA	NA	NA	NA	NA	0.11	0.9	0.11	0.11	0.3	0	
I burden in mixed gas based on adsorption measurements (10^{-5} Pa)	NA	NA	NA	NA	NA	NA	NA	0.2	0.2 to 2.0	0.2	0.2	0.5		

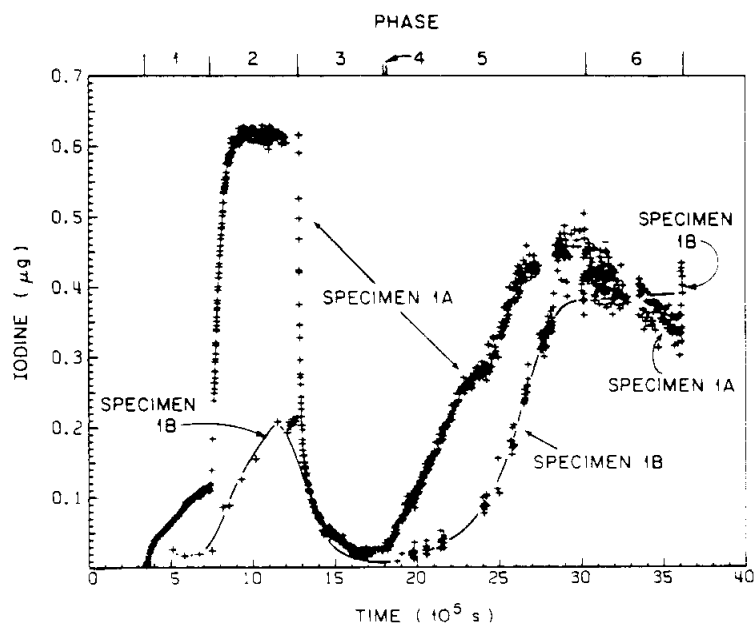


Fig. E.16. Iodine on specimens 1A and 1B during experiment A-9.

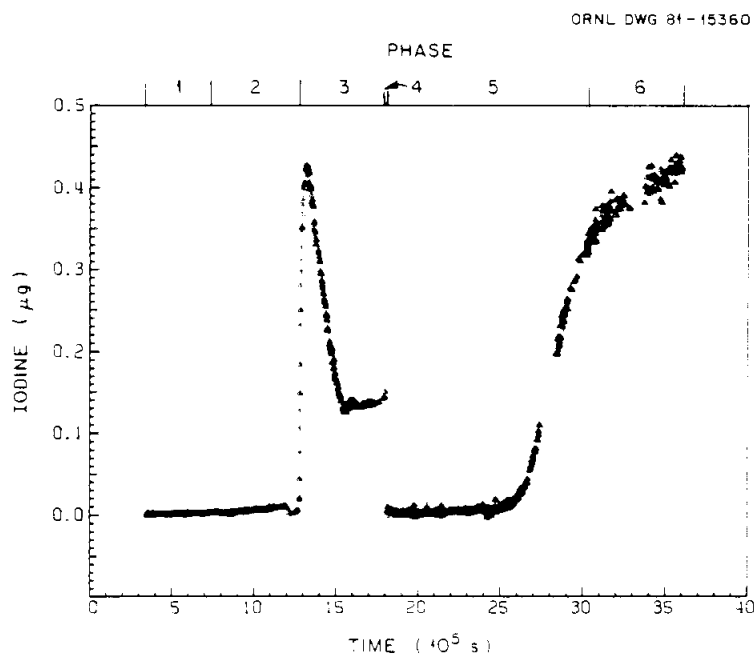


Fig. E.17. Iodine on specimen 2 during experiment A-9.

Table E.12. Summary of data from experiment A-9

Test phase	Time (10 ⁵ s)	Activity (counts/s)				Iodine (µg)				Total (10 ⁻⁷ µg/s)	Iodine transport (10 ⁻⁷ µg/s)	Iodine burden (10 ⁻⁶ Pa)	Iodine concentration (µg/cm ²)		Temperature (°C)	
		1A	1B	2	Charcoal trap	1A	1B	2	Charcoal trap				1A	1B		
1	3.49	0.11	0	0	0	0.004	0	0	0	0.004						
	3.83 ^c	0.98	0	0	0	0.032	0	0	0	0.032	8.2	4				
	4.03	1.24	0	0	0	0.040	0	0	0	0.040	4.2	2				
	6.77	3.36	0.7	0.05	0	0.11	0.023	0.001	0	0.13	3.3	2	0.016	0.003	400	
2	7.64	7.8	1.1	0.15	0	0.25	0.035	0.002	0	0.29						
	8.49	17.9	2.7	0.2	0	0.58	0.087	0.002	0	0.67	45.0	20				
	9.37	19.0	4.1	0.3	0	0.61	0.13	0.003	0	0.74	8.0	4				
	10.25	19.0	4.7	0.5	0	0.61	0.15	0.006	0	0.77	3.4	2				
	12.04	18.9	6.4	0.8	0	0.61	0.21	0.009	0	0.83	3.4	2	0.087	0.030	400	
3	15.33	1.2	0.8		5.5	0.039	0.026	0.82 ^a	0.061	0.95	3.7	2	} 0.003	0.002	600	
	16.25	0.7	0.5		23.0	0.023	0.016	0.71 ^a	0.25	1.00	5.4	3				
	17.25	0.7	0.5		30.0	0.023	0.016	0.71 ^a	0.33	1.08	8.0	4				
	17.91	0.7	0.5		29.8	0.023	0.016	0.71 ^a	0.33	1.08	(4.3)	2) ^b				
4	18.11	0.7	0.7	<1	100	0.02	0.02	<0.01	1.11	1.15						
5	22.40	7.5	1.7	<1	103	0.24	0.05	<0.01	1.14	1.44	6.8	4				
	26.50	13.0	7.4	3	106	0.42	0.24	0.03	1.18	1.87	10.0	5				
	29.95	14.0	12.0	25	103	0.45	0.39	0.28	1.14	2.26	11.0	6	0.064	0.056	400	
											(9.4)	5) ^c				
6	36.00	10.0	12.0		99	0.32	0.39	0.49 ^a	1.10	2.30						
Posttest						0.36	0.42	0.43	0.76							

^aValues obtained from activity profiles.

^bValues are averages for interval from 12.04 × 10⁵ to 17.91 × 10⁵ s.

^cValues are averages for interval from 18.11 × 10⁵ to 29.95 × 10⁵ s.

that time, the iodine burden, based on the rate of adsorption on specimens 1B and 2, had returned to 2×10^{-6} Pa. We could find no reason for the sudden increase in iodine burden or for the rapid return to the burden of phase 1.

At the end of phase 2, the average concentration of iodine on specimen 1A was $0.087 \mu\text{g}/\text{cm}^2$. Because the loading was steady, we assume that the iodine on the surface was in equilibrium with an iodine burden of 2×10^{-6} Pa (2×10^{-11} atm). We found in earlier experiments that iodine adsorbed at 400°C did not always desorb at that temperature when the iodine burden was reduced, so the iodine on the specimen could have been in equilibrium with a higher iodine burden. Since iodine was still adsorbing on specimen 1 during the interval when the burden was falling and averaged 4×10^{-6} Pa (4×10^{-11} atm), the iodine on the surface would not have been in equilibrium with a burden that was $>4 \times 10^{-6}$ Pa.

In phase 3, the specimens were heated to 600°C until the amounts of iodine reached steady levels of $0.003 \mu\text{g}/\text{cm}^2$ on specimen 1A and $0.002 \mu\text{g}/\text{cm}^2$ on 1B. The average iodine burden during phase 3 was 2×10^{-6} Pa (2×10^{-11} atm).

During the interval from 12.79×10^5 to 12.85×10^5 s, the amount of iodine on specimen 1A decreased from 0.61 to 0.33 μg . Assuming that the iodine burden in the gas entering specimen 1A was 2×10^{-6} Pa (2×10^{-11} atm), the average iodine burden in the gas leaving the specimen was 2.5×10^{-4} Pa (2.5×10^{-9} atm). Some of this iodine adsorbed on specimen 1B, and the loading increased from 0.21 to 0.27 μg . Soon thereafter, the iodine loadings on the two specimens became equal and decreased together until the steady loadings were approached. Then the loading on specimen 1B became and stayed less than that on specimen 1A.

In phase 4, specimen 2 was heated to 800°C to desorb most of the iodine that remained at 600°C (see Fig. E.17).

The temperature of the saturator was raised to -75°C to give an iodine burden of 3×10^{-6} Pa (3×10^{-11} atm) for phase 5. The iodine burden obtained from the rate of adsorption on the specimens varied between 4×10^{-6} and 6×10^{-6} Pa (4×10^{-11} and 6×10^{-11} atm) and averaged 5×10^{-6} Pa.

The adsorption conformed to the model in phase 5. At the beginning almost all the iodine adsorbed on specimen 1A. As the concentration on that specimen increased, the fraction that reached and adsorbed on specimen 1B gradually increased. It was not until 8×10^5 s into phase 5 that iodine began to adsorb on specimen 2 at a perceptible rate. By the end of phase 5, the loadings on specimens 1A and 1B had become steady, and all the iodine was adsorbing on specimen 2 near the entrance. Little, if any, of the iodine reached the charcoal trap. The steady concentrations of iodine on specimens 1A and 1B were 0.064 and 0.056 $\mu\text{g}/\text{cm}^2$, respectively, at an iodine burden of 4×10^{-6} to 6×10^{-6} Pa (4×10^{-11} to 6×10^{-11} atm).

At the beginning of phase 6, the temperature of the saturator was lowered, and the flow through the saturator was stopped to lower the iodine burden and to see whether iodine would desorb from the specimens at 400°C. Iodine desorbed from specimen 1A from the beginning and was continuing to desorb at the end of phase 6. As well as we could determine, no iodine desorbed from specimen 1B; the loading on that specimen was higher than on 1A. Specimen 2 adsorbed the iodine that was desorbed ahead of it. The amount of iodine on the charcoal trap did not change significantly.

The measurements indicated that 0.13 μg of iodine desorbed from specimen 1A and 0.21 μg adsorbed on specimen 2 over an interval of 6.0×10^5 s in phase 6. The transfer rates correspond to iodine burdens of 1.2×10^{-6} and 1.9×10^{-6} Pa (1.2×10^{-11} and 1.9×10^{-11} atm) respectively. The difference suggests that the iodine burden in the gas entering specimen 1A might have been as high as 0.7×10^{-6} Pa (0.7×10^{-11} atm). More likely, the difference is indicative of the uncertainty in the measurements.

At the end of the experiment, specimens 1A and 1B were more oxidized than those from experiment A-8, but very much less than specimen 1 from earlier experiments. The specimens in this experiment were exposed almost twice as long as those in A-8. The amounts of iodine on the specimens, as determined by use of the multichannel analyzer, were within 12% of those indicated by the detectors on the apparatus.

The steady state concentrations of iodine on the metal and the iodine burdens that were inferred from the data from this experiment are listed below:

Test phase	Temperature (°C)	Iodine burden (10 ⁻⁶ Pa or 10 ⁻¹¹ atm)	Surface concentration (µg I/cm ²)
2	400	2-4	0.09
3	600	2-4	0.002-0.003
5	400	4-6	0.06

E.7 Experiment A-10

In experiment A-10 our objective was to measure the equilibrium loading of iodine on type T-22 steel at 400°C when exposed to very low iodine burdens, 10⁻⁷ to 10⁻⁶ Pa (10⁻¹² to 10⁻¹¹ atm), in helium containing 50 Pa (5 × 10⁻⁴ atm) of hydrogen. One modification was made to the apparatus. An outlet was installed on the helium line just ahead of the furnace tube so that a small stream of gas could be withdrawn continuously during the experiment (see Fig. 5.1). This stream was passed through a charcoal trap to remove the iodine. A third detector and a third counting channel were added to the data collection system. The rate of increase in activity on the charcoal was measured as a means of monitoring the iodine burden in the gas.

Preparations for the experiment were made in the usual way. The saturator was purged with helium at several temperatures before beginning the adsorption tests. During the purges, the iodine pressure in the saturator was estimated by measuring the rate of adsorption of iodine on a charcoal trap in the purge line. Unexplained changes in the iodine pressure occurred several times during the purges, but, at the end, the pressure inferred from the measurements was within a few percent of the pressure of elemental iodine at the temperature in the saturator.

The adsorption tests were begun with the saturator at the temperature of the final purge test. The flow through the saturator was reduced to provide an iodine burden of 2.8 × 10⁻⁷ Pa (2.8 × 10⁻¹² atm) at the specimens. The system operated steadily for 5.3 × 10⁵ s. About 0.0007 µg of iodine reached the specimens, which corresponds to an iodine burden of

3×10^{-9} Pa (3×10^{-14} atm). The flow through the saturator was increased for 2.7×10^5 s to raise the iodine burden to 1.1×10^{-6} Pa (1.1×10^{-11} atm). Then the temperature of the saturator was raised for 0.7×10^5 s to increase the iodine burden to 1.1×10^{-5} Pa (1.1×10^{-10} atm). The rate at which iodine reached the specimens was not increased by those changes, so the adsorption tests were terminated.

The saturator was tested again at the end of the experiment with anomalous results. Some tests also were made of the procedure for preparing the iodine source and charging the saturator. Those tests indicated that, at low flow rates, iodine could diffuse upstream into the T-22 steel hot trap in the helium line to the saturator and be converted to FeI_2 during the charging. Conversion of much of the 420 μg of iodine in the source to FeI_2 might have caused the difficulties with the source in this test but does not seem to explain all the observations. However, we could find no other explanation.

E.8 Experiment A-11

Because of the difficulties experienced during experiment A-10, the T-22 hot trap was removed from the helium line to the saturator before beginning this experiment. After the iodine was charged, the saturator was subjected to extensive testing and purging before beginning the adsorption test. At the beginning, the results of the tests were confusing. But, it was discovered that, at a given saturator temperature, the rate of delivery of iodine to the purge trap was more sensitive to the main flow of helium than to the flow through the saturator. Apparently, the configuration of the apparatus for purging was such that part of the main flow could backflow into the saturator and pick up iodine before it went on to the purge trap.

This condition was remedied by flowing the gas out through the monitor line during the final purge tests. The iodine pressure in the saturator, based on the gas flow through the saturator and the rate of adsorption on the monitor trap, was in good agreement with the vapor pressure of iodine at the temperature in the saturator.

Phase 1 of the adsorption tests was begun at 8.57×10^5 s after time 0. Specimen 1, 2 mm long, and specimen 2, 51 mm long, were both at 400°C.

Pure helium flowed through the saturator at a rate of 5.7 std cm³/min. The saturator temperature was -81°C. A flow of 394 std cm³/min of helium containing 50 Pa (5×10^{-4} atm) of hydrogen mixed with the gas from the saturator to provide an intended iodine burden of 8.9×10^{-7} Pa (8.9×10^{-12} atm) at the entrance of specimen 1.

These conditions were maintained until 11.23×10^5 s, when the primary flow was reduced to 200 cm³/min to conserve helium. This reduction doubled the iodine burden in the mixed gas. After the helium supply was renewed, the original conditions were restored at 14.44×10^5 s. They were maintained until about 19.5×10^5 s when the helium line cracked near the entrance of the furnace tube, interrupting the flow. The test was terminated at 20.46×10^5 s.

The amounts of iodine on the specimens are shown as a function of time in Fig. E.18. The iodine burdens in the gas, calculated from the

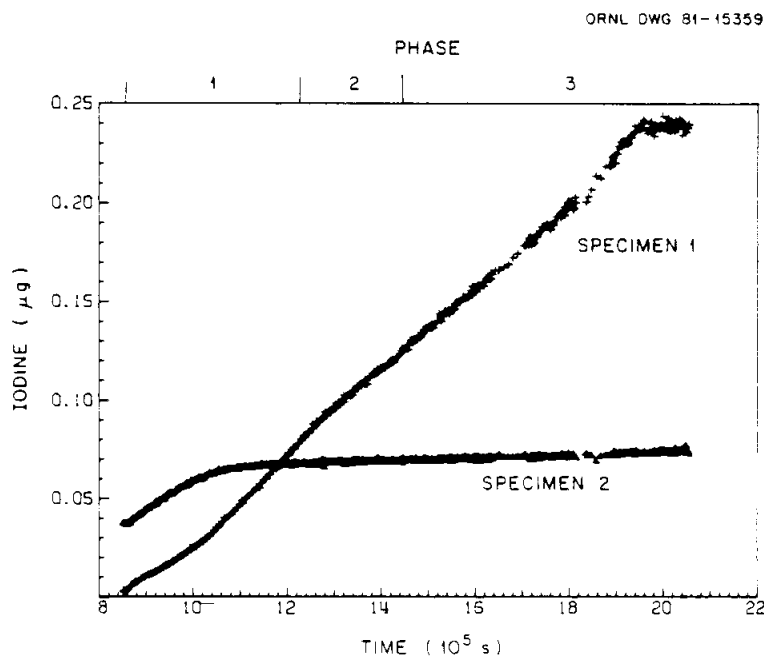


Fig. E.18. Iodine on the specimens during experiment A-11.

rates of accumulation of iodine on the specimens and on the monitor, are shown in Table E.13.

At the beginning of the adsorption test, about half the iodine adsorbed on specimen 1 and half adsorbed on specimen 2 near the entrance. This was surprising because in experiment A-9, under similar conditions, almost all the iodine adsorbed on specimen 1 at the beginning of the test.

By 11.2×10^5 s, the fraction adsorbing on specimen 1 had gradually increased to about 0.95; it remained high throughout the rest of the experiment. None of the monitored operating conditions had changed significantly. The increased adsorption of iodine appears to have resulted from activation of the surface of specimen 1.

At the end of the experiment, 0.24 μg of iodine had adsorbed on specimen 1. The average concentration was 0.034 $\mu\text{g}/\text{cm}^2$. According to the measurements of the iodine on the specimens, the iodine burden varied between 6.0×10^{-7} and 9.6×10^{-7} Pa (6×10^{-12} and 9.6×10^{-12} atm) during the time that the total gas flow was 400 std cm^3/min . This agrees well with the expected burden. The burden calculated from the rate of increase in activity on the monitor was much lower. Only about 3% of the flow passed through the monitor. Being unable to find another cause, we attributed the low burdens obtained from the monitor to the low flow and believed them to be incorrect.

There was no indication that the iodine loadings on specimen 1 was near steady state when the experiment ended. We conclude, in agreement with results of other tests, that the average concentration of 0.034 $\mu\text{g}/\text{cm}^2$ was far below the equilibrium value at 400°C for an iodine burden of about 8×10^{-7} Pa (8×10^{-12} atm) in helium containing 50 Pa (5×10^{-4} atm) of hydrogen.

E.9 Experiment A-12

At the end of experiment A-11, the specimens were removed and the break in the helium line was repaired. New specimens and charcoal traps were installed, and the metal strips in the T-22 hot trap in the main

Table E.13. Iodine burdens calculated from activity measurements during experiment A-11

Test phase	Time (10 ⁵ s)	Specimen 1		Specimen 2		Total iodine adsorption rate (10 ⁻⁷ µg/s)	Iodine burden (10 ⁻⁷ Pa)	Monitor			
		Activity (counts/s)	Iodine (µg)	Activity (counts/s)	Iodine (µg)			Activity (counts/s)	Iodine (10 ⁻³ µg)	Iodine adsorption rate (10 ⁻¹⁰ µg/s)	Iodine burden (10 ⁻⁸ Pa)
1	8.78	1.56	0.0076	16.6	0.0409			161.4	39.4		
	9.98	5.03	0.0245	23.8	0.0586	2.9	7.9	163.2	39.8	33.0	29.0
	10.98	9.57	0.0467	26.6	0.0655	2.9	7.9	164.5	40.1	30.0	27.0
2	11.28	11.0	0.0537	26.7	0.0658			4.1	1.00		
	14.45	25.8	0.1259	28.2	0.0695	2.4	13.0	5.5	1.34	11.0	19.0
3	18.00	41.0	0.2000	29.2	0.0719	2.2	6.0	6.5	1.59	7.0	6.2
	18.42	42.1	0.2054	29.2	0.0719				1.61		
	19.45	49.1	0.2395	29.8	0.0734	3.5	9.6	6.9	1.68	6.8	6.0

helium line were replaced. Although we realized that the iodine source might have been contaminated by air and moisture, experiment A-12 was undertaken while awaiting a new supply of iodine. The saturator was purged before beginning the adsorption tests. At the end of the purging, the iodine pressure in the saturator, based on the rate of adsorption on the purge trap, was 4×10^{-4} Pa (4×10^{-9} atm). This compares with 10^{-3} Pa for iodine at the temperature in the saturator.

The conditions during the adsorption tests are given in Table E.14. The change with time of the amount of iodine on the specimens is shown in Figs. E.19 and E.20. Some of the data and calculations are summarized in Table E.15.

Phase 1 was begun with the intent of obtaining a steady concentration of iodine on specimen 1 at 400°C in helium having an iodine burden of 3×10^{-5} Pa (3×10^{-10} atm). This was a region where data were lacking, but, based on data from earlier experiments, we expected the steady concentration to be $<1.0 \mu\text{g}/\text{cm}^2$ and to be reached in 8 to 10 days.

The adsorption proceeded about as it had in experiment A-11. At the beginning only half the iodine in the gas adsorbed on specimen 1. Then, over a period of about 4-1/2 days, the fraction adsorbed on specimen 1 increased until it exceeded 0.95.

During phase 1, the iodine burden inferred from the rate of adsorption on the specimens ranged from 2.4×10^{-5} to 2.7×10^{-5} Pa (2.4×10^{-10} to 2.7×10^{-10} atm). The burden indicated by adsorption on the charcoal trap in the monitor line was lower by a factor of 5.5 at the beginning. The flow through the monitor was increased from 12 to $24 \text{ cm}^3/\text{min}$ during phase 1. Thereafter, the agreement was better although the monitor continued to provide lower values. We found no reason for the difference but believe that the burdens based on adsorption on the specimens are more accurate.

After almost 7 days of steady operation in phase 1, the average concentration of iodine on specimen 1 had reached $0.62 \mu\text{g}/\text{cm}^2$, and 97% of the iodine was still adsorbing on that specimen. So, in phase 2, we reduced the iodine burden by one-half or more to see whether the

Table E.14. Test conditions in each phase of experiment A-12

	Source		Adsorption tests														End	
	A	B	1a	1b	2	3	4	5	6	7	8	9	10	11	12	13		14
Beginning date	3/13	3/14	3/17	3/19	3/24	3/25	3/28	3/28	4/1	4/5	4/7	4/10	4/12	4/14	4/16	4/21	4/21	4/22
Time (clock)	16:11	13:12	11:35	14:14	10:15	9:34	8:45	16:01	8:39	9:47	9:09	9:48	11:00	9:24	14:32	9:07	15:53	8:19
Cumulative time (10 ⁵ s)		0	2.53	4.34	8.51	9.35	11.90	12.61	15.10	18.75	20.45	23.03	24.83	26.49	28.40	32.52	32.78	33.35
Specimen temperature (°C)																		
Specimen 1 (2 mm)	400	400	400	400	400	400	400	400	400	400	400	400	400	400	400	450	600	
Specimen 2 (51 mm)	400	400	400	400	400	400	400	400	400	400	400	400	400	400	400	450	600	
Helium flow (std cm ³ /min)																		
Saturator (pure He)	5.72	1.43	5.72	5.72	2.3	11.5	5.72	2.3	0	0	5.72	2.3	5.72	0	5.72	5.72	5.72	
Primary (He + 50 Pa H ₂)	15	50	394	394	398	389	394	398	400	100	394	398	394	400	394	394	394	
Total	20	51	400	400	400	400	400	400	400	100	400	400	400	400	400	400	400	
Purge line	20	0	0	0	0	0	0	0	0	0	0	0	0	0	0	0	0	
Monitor line	0	51	12	24	24	24	24	24	24	5.7	24	24	24	24	24	24	24	
Furnace tube	0	0	388	376	376	376	376	376	376	94	376	376	376	376	376	376	376	
Total out	20	51	400	400	400	400	400	400	400	100	400	400	400	400	400	400	400	
Iodine source																		
Temperature (°C)	-63	-62.5	-62.5	-62.5	-62.5	-62.5	-62.5	-62.5	-62.5	-62.5	-52	-62.5	-62.5	-62.5	-62.5	-62.5	-62.5	
P _{I₂} at temperature in saturator (10 ⁻⁵ Pa)	96	105	105	105	105	105	105	105	105	105	590	105	105	105	105	105	105	
I burden in mixed gas based on P _{I₂} and gas flows (10 ⁻⁵ Pa)	55	5.9	3.0	3.0	1.2	6.0	3.0	1.2	0	0	17	1.2	3.0	0	3.0	3.0	3.0	
I burden in mixed gas based on adsorption measurements (10 ⁻⁵ Pa)		2.2	2.4 to 2.7	2.4 to 2.7	1.3	5.6		0.62			15	0.68	2.8		2.2			

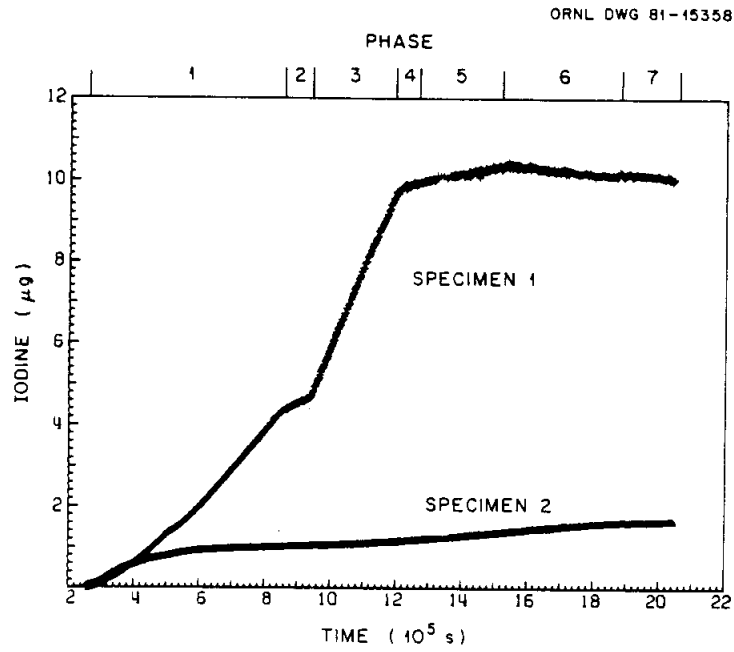


Fig. E.19. Iodine on specimens during phases 1 through 7 of experiment A-12.

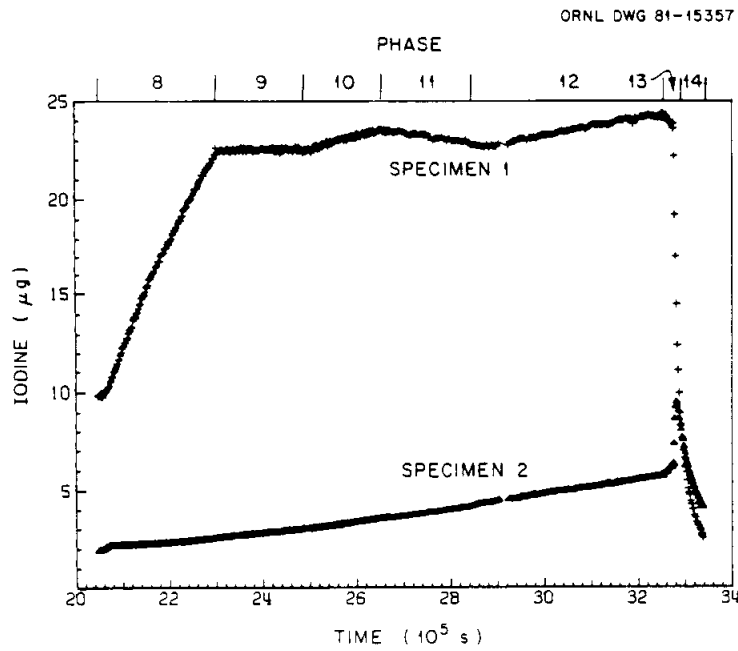


Fig. E.20. Iodine on the specimens during phases 8 through 14 of experiment A-12.

Table E.15. Summary of adsorption data from experiment A-12

Test phase	Time (10 ² s)	Iodine adsorption rates						Iodine burden ^d				S-2 adsorbed	M burden	S-1 burden	Average iodine concentration on S-1 (µg/cm ²)			
		Specimen 1 (counts/s) (10 ⁻⁸ µg l/s)	Specimen 2 (counts/s) (10 ⁻⁸ µg l)	Specimen 3 (counts/s) (10 ⁻⁸ µg l/s)	Monitor (counts/s) (10 ⁻⁸ µg l/s)	S-1 (10 ⁻⁶ Pa)	S-2 (10 ⁻⁶ Pa)	Monitor (10 ⁻⁶ Pa)	Specified (10 ⁻⁶ Pa)	Total adsorbed	S-1 burden					Specified burden		
1a	0.00	1.6	0.037	4.8	0.13	53.9	0.146											
	4.30	8.1	0.440	4.8	0.48	17.5	0.48	5.0	2.4	12.0	4.4	3.0	0.50	0.18	0.80	0.06		
1b	4.50	17.3	0.940	6.3	0.70	25.5	0.70	5.0	2.5	7.6	4.4	3.0	0.30	0.18	0.81	0.13		
	5.00	45.3	1.90	7.0	0.91	33.3	0.91	1.5	2.4	69.6	0.189	25.0	0.18	0.46	0.80	0.27		
2	6.00	44.0	2.39	9.4	0.93	33.9	0.93	74.0	0.201							0.34		
	6.50	36.3	4.36	9.4	1.00	36.3	1.00	101	0.274	35.0	2.7	0.93	1.0	0.03	0.56	0.90	0.62	
3	7.45	87.0	4.73	4.4	1.02	37.3	1.02	105	0.285	13.0	1.3	0.68	5.7	1.0	0.05	0.44	1.08	0.68
	7.60	95.0	5.16			37.7	1.03	110	0.288								0.74	
4	11.00	153	8.42	10.0	1.06	39.5	1.06	164	0.444	91.0	5.7	0.37	40.0	0.0	0.0	0.70	0.99	1.2
	11.50	177	9.62	10.0	1.13	41.1	1.13	190	0.515	100	5.5	2.0	44.0	6.0	0.04	0.60	0.92	1.4
5	12.50	156	10.0			42.7	1.17	101	0.545								1.4	
	13.10	191	10.4	1.5	0.69	42.3	1.15	211	0.571	10.0	0.67	1.9	4.4	1.2	0.31	0.71	0.52	1.5
6	13.50	196	10.4			50.5	1.38	210	0.575								1.5	
	14.05	197	10.2	-0.64	0.70	53.5	1.63	211	0.576	0.99	0	2.0	0.4	0			1.5	
7	19.40	189	10.1	-0.57	0.23	60	1.64	211	0.577	0	0	2.6	0	0			1.4	
	21.00	225	11.2			72	2.14	160	0.705								1.7	
8	23.10	417	22.7	50.0	2.0	93	2.55	499	1.34	300	15.0	5.6	160	17.0	0.04	0.87	0.88	3.2
	24.20	417	22.7	0	2.4	104	2.76	503	1.36	12		6.8	5.3	1.7	1.0	0.78 ^b	0.57 ^b	3.1
10	25.50	417	23.6	6.5	3.5	139	3.55	516	1.45	53	2.8	9.9	23.0	3.0	0.35	0.82	0.93	3.4
	27.00	413	23.5			133	3.64	541	1.47								3.4	
11	28.50	413	23.0	-1.6	3.9	153	4.19	541	1.47	0	0	11.0	0	0			3.3	
	29.00	412	23.0			163	4.47	545	1.48								3.3	
14	32.00	417	24.3	0.3	3.0	103	5.56	598	1.62	47	2.2	10.0	21.0	3.0	0.45	0.95	0.73	3.5
	33.50	50	2.8			471	20.0 ^e	616	1.7									
Posttest			2.76			16.3		1.69										

^aThe iodine burden at S-1 was calculated from the sum of the adsorption rates on S-1 and S-2. The burdens at S-2 and the monitor were calculated from the adsorption rates on S-2 and the monitor respectively. The specified burden was that calculated from the gas flows and the vapor pressure of iodine at the temperature in the saturator.

^bValues are S-2 burden/specified burden and M burden/S-2 burden.

^cValue determined from activity profile.

concentration was near steady state for the lower burden. It was not; about 95% of the iodine adsorbed on specimen 1 at the lower burden.

Then followed several phases in which the iodine burden was raised to add iodine to specimen 1 more rapidly, and lowered to see whether the concentration on the surface equaled or exceeded the steady state concentration (Fig. E.19). In phase 3, the burden was increased to about 6×10^{-5} Pa (6×10^{-10} atm). When the average concentration reached $1.4 \mu\text{g}/\text{cm}^2$, the iodine burden was reduced to 3×10^{-5} Pa (3×10^{-10} atm) in phase 4 and to 0.6×10^{-5} to 1.2×10^{-5} Pa (0.6×10^{-10} to 1.2×10^{-10} atm) in phase 5. Phase 4 was run just long enough to see that almost all the iodine was adsorbing on specimen 1. In phase 5, about 70% of the iodine adsorbed on specimen 1.

In phases 6 and 7 the flow of gas to the saturator was stopped to make sure that iodine would desorb from specimen 1 if the iodine burden was reduced sufficiently, since desorption was to be used as evidence that the steady state concentration had been exceeded. Iodine did desorb.

In phase 6 the helium flow was $400 \text{ std cm}^3/\text{min}$; in phase 7 the flow was reduced to $100 \text{ std cm}^3/\text{min}$. Although the result was not definitive, we interpreted the data as showing that the rate of desorption decreased in proportion to the decrease in flow. The calculations reported in Table E.15 show that the iodine burden in the gas reaching specimen 2 was about the same during phases 6 and 7 (2.6×10^{-6} and 2.0×10^{-6} Pa respectively) as it was during phase 5 [1.9×10^{-6} Pa (1.9×10^{-11} atm)]. This seems to indicate that the iodine burden in the gas was in equilibrium with the concentration of iodine on the surface at the exit of specimen 1, and the rate of desorption was limited by the helium flow rate.

In phase 8 the iodine burden was increased to 1.5×10^{-4} to 1.7×10^{-4} Pa (1.5×10^{-9} to 1.7×10^{-9} atm) to load the surface again (Fig. E.20). When the concentration reached $3.2 \mu\text{g}/\text{cm}^2$, the burden was reduced to 0.7×10^{-5} to 1.2×10^{-5} Pa (0.7×10^{-10} to 1.2×10^{-10} atm) in phase 9. Iodine neither adsorbed on nor desorbed from specimen 1.

In phase 10 the iodine burden was increased to 3×10^{-5} Pa (3×10^{-10} atm). Then, only 65% of the iodine adsorbed on specimen 1.

In phase 11 the iodine burden was reduced to zero again. Iodine desorbed, and the burden in the gas leaving specimen 1 was 1.1×10^{-5} Pa (1.1×10^{-10} atm). This was about the same as in phase 10. We interpret the data as indicating that the desorption rate was limited by the helium flow and that the lowest concentration on the surface, the concentration at the outlet, was in equilibrium with an iodine burden at least as high as 10^{-5} Pa (10^{-10} atm).

In phase 12 the test was continued for several days until the average concentration on the surface reached $3.5 \mu\text{g}/\text{cm}^2$. The fraction of the iodine adsorbing on specimen 1 was 0.55, but had changed little, if any, during phase 12. At this point, the experiment was ended by raising the temperature of the specimens to 450°C and then to 600°C for short times. Iodine desorbed from specimen 1 at both temperatures. The desorption was not carried to steady state, but the steady concentration on specimen 1 at 600°C would have been $<0.4 \mu\text{g}/\text{cm}^2$ (probably 0.1 to $0.2 \mu\text{g}/\text{cm}^2$).

The specimens were examined visually after they were removed from the furnace tube. Only the ends of the plates and the outer surface of the holders could be seen well. The front half (1 mm or less) of specimen 1 was coated with a black scale, presumably mostly iron oxide. The scale was not tightly adherent because a substantial fraction flaked off during handling of the specimen. The remainder of specimen 1 was light gray. Specimen 2 was gray in color, light gray at the front and somewhat darker along its length.

The metal strips from the T-22 hot trap in the main helium stream were lightly oxidized over the front 1 to 2 cm of length. The remaining 8 cm appeared to be in the original condition.

At the end of the test, activity profiles were measured for specimens 1 and 2 and for the furnace tube up to the charcoal trap. A final measurement was made of the activity of the monitor trap. After removing the specimens and the charcoal trap, an activity profile was measured for the empty furnace tube. Finally, the amounts of iodine on the separate

components were determined from activity measurements made with a multi-channel analyzer.

The profile measurements in the vicinity of specimen 1 confirmed the measurements made from the normal position of detector 1 during the experiment. The activity with the specimen removed was at background level, so there was no significant amount of iodine on that region of the furnace tube. The posttest multichannel analyzer measurement, reported in Table E.16, was in good agreement with the in situ measurement.

The activity profiles for the region of specimen 2 and the charcoal trap are shown in Fig. E.21. During phases 1 through 13, iodine that passed specimen 1 adsorbed on specimen 2 near the entrance where all the activity could be measured by the detector in its normal monitoring position. The amount of iodine on the specimen could be determined directly from the measured activity without the use of profiles.

During phase 14, the iodine spread along specimen 2, and some desorbed. The amount of iodine on the specimen at the end of the experiment was determined from the activity profile.

The activity in the region of specimen 2 with the specimen removed was at background level. The amount of iodine on the specimen as determined from the profile was in reasonable agreement with that obtained by use of the multichannel analyzer.

The profile obtained with the specimens and the charcoal trap removed showed that some iodine had deposited on the wall of the furnace tube near the charcoal trap, presumably as FeI_2 . The in situ measurements indicated the presence of 2.9 μg of iodine on the charcoal trap and at least 1.7 μg on the wall of the furnace tube. The multichannel analyzer measurements indicated 4.35 μg on the charcoal trap and 3.27 μg on the furnace tube.

The adsorptive capacity of specimen 1 proved to be so great that a steady state concentration of iodine could not be obtained at 400°C in a reasonable time. Based on observation of whether iodine adsorbed or desorbed at various iodine burdens at 400°C, we concluded that the steady state concentration was not greater than 3.2 $\mu\text{g}/\text{cm}^2$ at a burden of 0.7×10^{-5} to 1.2×10^{-5} Pa (0.7×10^{-10} to 1.2×10^{-10} atm) in helium containing 50 Pa (5×10^{-4} atm) of hydrogen. But, it was greater than

Table E.16. Posttest measurements on components from experiment A-12

	Multichannel analyzer measurements		Detectors on apparatus	
	$\mu\text{Ci } ^{131}\text{I}^a$	$\mu\text{g I}$	Counts/s ^b	$\mu\text{g I}$
Specimen 1	26.64	2.95	52	2.8
Specimen 2	164.7	18.3		20 ^c
Charcoal trap	39.25	4.35	136 ^d (216) ^d	2.9 (4.6)
Monitor trap A-12-B	15.23	1.69	616	1.7
Furnace tube	29.48	3.27	80	1.7
Purge trap A-12-A	0.813	0.090	18.2	0.094
Purge line wash	6.26	0.69		
Iodine used in experiment	282	28.4		
Iodine remaining in saturator	3130	347		

^aIodine activity measurements were normalized to 9:04 on 2-13-80. The corresponding specific activity is 9.02 $\mu\text{Ci } ^{131}\text{I}/\mu\text{g I}$.

^bIodine activity measurements were normalized to time 0 for this experiment.

^cAmount of iodine was determined from activity profile.

^dThe value 216 counts/s was the corrected total count rate that included any activity on the wall of the furnace tube. The value 136 counts/s was obtained by subtracting the 80 counts/s measured on the furnace tube after the charcoal trap and the specimens were removed.

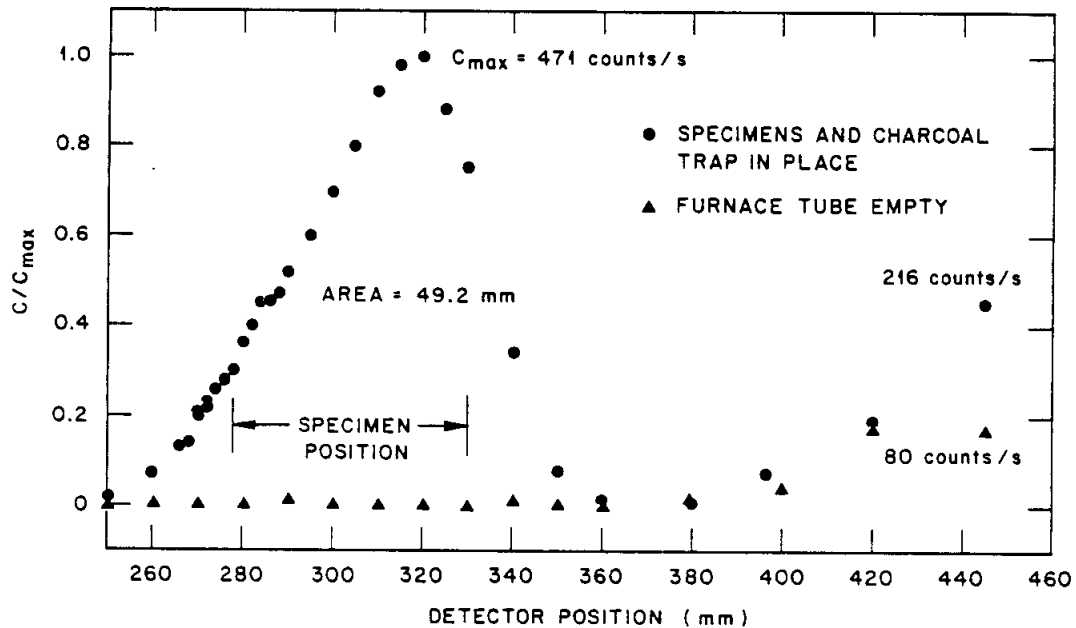


Fig. E.21. Activity profiles in region of specimen 2 and charcoal trap at end of experiment A-12.

$3.5 \mu\text{g}/\text{cm}^2$ at a burden of 2.2×10^{-5} to 3×10^{-5} Pa (2.2×10^{-10} to 3×10^{-10} atm). At 600°C the steady concentration obtained by desorption would have been $<0.4 \mu\text{g}/\text{cm}^2$ and possibly 0.1 to $0.2 \mu\text{g}/\text{cm}^2$ at a burden of 2.2×10^{-5} to 3×10^{-5} Pa (2.2×10^{-10} to 3×10^{-10} atm).

E.10 Experiment A-13

In experiment A-13, we undertook to measure the steady state concentration of iodine on type T-22 steel at temperatures from 400 to 800°C when exposed to an iodine burden of 3×10^{-5} Pa (3×10^{-10} atm) in helium containing 50 Pa (5×10^{-4} atm) of hydrogen. In experiments A-11 and A-12, only about half the iodine in the gas adsorbed on specimen 1 at the beginning. Over a few days, the fraction increased to 0.95 or more, indicating that the surface had become more active. This behavior was observed in experiments after the T-22 metal hot trap was removed from the helium line to the saturator. No other changes had been made in the specimens, equipment, or procedures. The hot trap was restored before this experiment to see whether the adsorption behavior would be affected.

The conditions during the experiment are recorded in Table E.17. The way in which the amount of iodine on the specimens changed with time and with changes in conditions is shown in Figs. E.22 through E.25. The curves for specimen 2 give an indication of the progress of the adsorption or desorption on the specimen but not of the total amount of iodine that was present. The detector could not see the entire specimen from its normal monitoring position at the entrance, and the measurements were not fully corrected for changes in calibration. The data from the several phases of the experiment and some of the calculations are summarized in Tables E.18 through E.23.

Phase 1 was carried out with the specimens at 400°C and an iodine burden of 3×10^{-5} Pa (3×10^{-10} atm) in the gas. These were also the conditions of phase 1 of experiment A-12. This time the adsorption behavior was model. At the beginning, almost all the iodine adsorbed on specimen 1. The fraction passing to specimen 2 increased with time as the loading on specimen 1 increased. Although the difference in adsorption behavior appears to have been related to use of the T-22 metal hot trap in the helium line to the saturator, we cannot be certain of the cause.

Phase 1 was ended after the adsorption behavior was established and while the specific activity of the iodine was still high enough to be able to measure the low iodine loadings expected at higher temperatures. The average concentration on the surface of specimen 1 at the end of phase 1 was $0.83 \mu\text{g}/\text{cm}^2$, and 31% of the iodine was in the gas leaving the specimen.

The concentration of iodine on specimen 1 was far from being at steady state, but a steady state value of $\sim 4 \mu\text{g}/\text{cm}^2$ was estimated by use of a method described in the paper by Hougen and Marshall³⁵ that was the basis for Appendix F. By means of charts included in the paper, one can use measurements of the rate of change in the fraction of the adsorbate remaining in the gas leaving the specimen to obtain estimates of the mass transfer coefficient and the equilibrium concentration of adsorbate on the surface. Based on the results of experiment A-12, the $\sim 4 \mu\text{g}/\text{cm}^2$ appears to be of the correct magnitude, but the uncertainty is large.

Table E.17. Test conditions in each phase of experiment A-13

	I ₂ transfer	Source purge			Adsorption tests					Adsorption tests							End	
		A	B	C	1	2	3	4	5	6	7	8	9	10	11	12		13
Beginning date	4/30	4/30	5/1	5/1	5/5	5/14	5/20	5/19	5/20	5/21	5/22	5/23	5/26	5/27	5/27	6/9	6/11	6/13
Time (clock)	10:50	15:55	15:40	15:44	9:44	13:07	12:50	8:59	10:28	11:41	10:33	13:35	9:30	10:24	16:06	10:03	15:04	10:34
Cumulative time (10 ⁶ s)	0	0.160	1.052	1.092	4.250	12.161	14.864	16.301	17.212	18.115	18.913	19.900	22.333	23.221	23.424	34.404	36.302	37.861
Specimen temperature (°C)																		
Specimen 1 (2 mm)	400	400	400	400	400	500	500	700	800	800	700	600	600	600	400	400	600	
Specimen 2 (51 mm)	400	400	400	400	400	400	400	700	500	800	700	600	600	800	400	400	600	
Helium flow (std cm ³ /min)																		
Saturator (pure He)	11.4	11.4	5.72	1.43	5.72	5.72	5.72	5.72	5.72	8.58	8.58	8.58	5.72	5.72	5.72	0	5.72	
Primary (He + 50 Pa H ₂)	20.6	28.6	14.3	4.9	3.94	3.94	3.94	3.94	3.94	3.92	3.92	3.92	3.94	3.94	3.94	4.00	3.94	
Total in	40	40	20	5.0	4.00	4.00	4.00	4.00	4.00	4.00	4.00	4.00	4.00	4.00	4.00	4.00	4.00	
Purge line	40	40	0	0	0	0	0	0	0	0	0	0	4.00	4.00	4.00	4.00	4.00	
Monitor line	0	0	20	5.0	12	12	24	24	24	24	12	12	24	24	24	0	24	
Furnace tube	0	0	0	0	3.88	3.88	3.76	3.76	3.76	3.76	3.88	3.88	3.76	3.76	3.76	3.76	3.76	
Total out	40	40	20	5.0	4.00	4.00	4.00	4.00	4.00	4.00	4.00	4.00	4.00	4.00	4.00	4.00	4.00	
Iodine source																		
Temperature (°C)	-54	-52	-63	-63	-62.5	-62.5	-62.5	-62.5	-62.5	-51	-51	-51	-62.6	-62.5	-62.5	-81	-62.5	
P ₂ at saturator temperature (10 ⁻⁶ Pa)	430	590	96	96	100	100	100	100	100	690	690	690	100	100	100	3.1	100	
I burden in mixed gas based on P ₂ and gas flows (10 ⁻⁶ Pa)	NA	34 ^d	55	5.5	3	3	3	3	3	31	31	31	3	3	3	0	3	
I burden in mixed gas based on adsorption measurements (10 ⁻⁶ Pa)		34 ^d	16 ^d	4.5 ^d	2.6 to 3	3	3	3	3	20 to 30	20 to 30	20 to 30	3 to 6	3 to 6	3.1	0	2 to 3	

^dValues at end of purge phases.

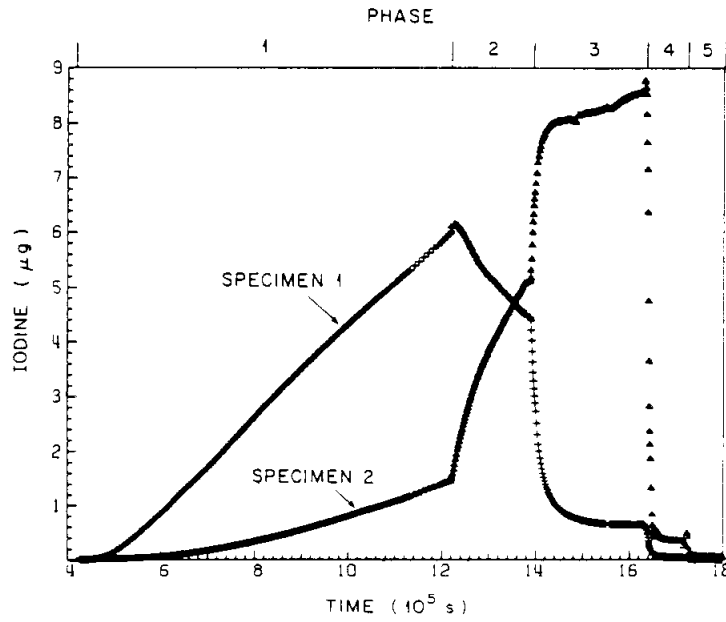


Fig. E.22. Iodine on specimens during phases 1 through 5 of experiment A-13.

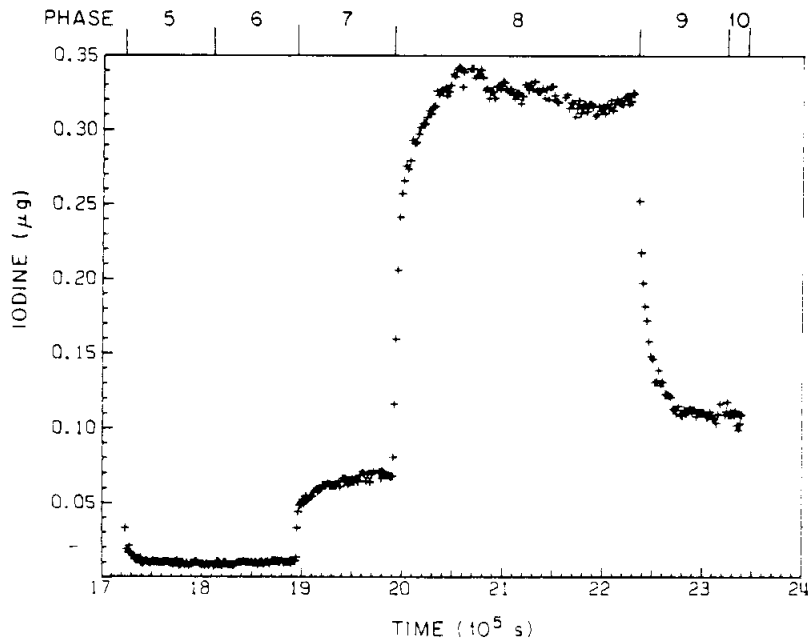


Fig. E.23. Iodine on specimen 1 during phases 5 through 10 of experiment A-13.

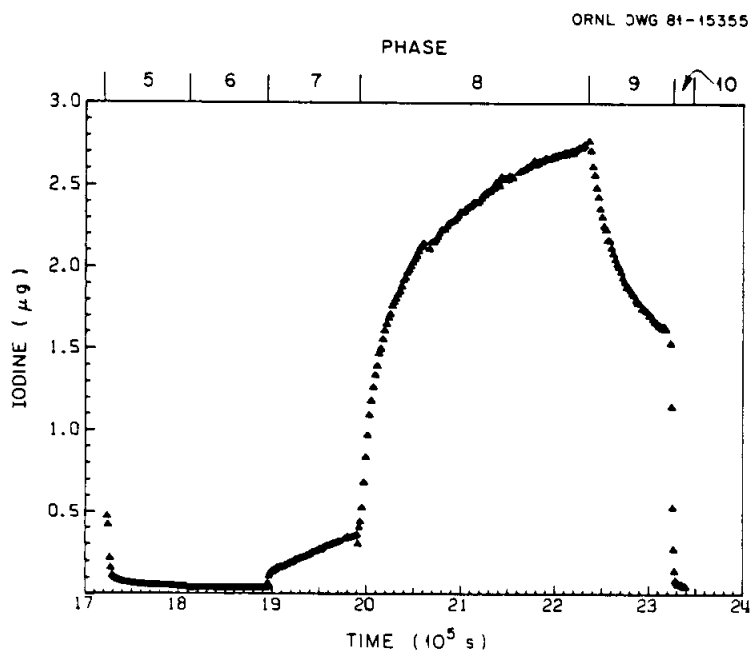


Fig. E.24. Iodine on specimen 2 during phases 5 through 10 of experiment A-13.

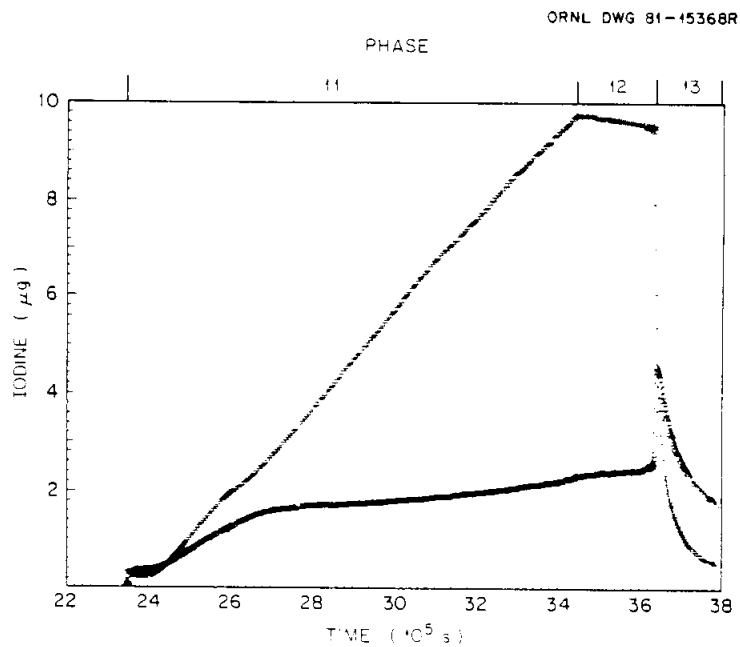


Fig. E.25. Iodine on specimens during phases 11 through 13 of experiment A-13.

Table E.18. Summary of data and calculations from phase 1 of experiment A-13

Time (10 ⁵ s)	Specimen 1			Iodine adsorption rates Specimen 2			Monitor			Iodine burden ^d (10 ⁻⁵ Pa or 10 ⁻¹⁰ atm)			S-2 adsorbed Total adsorbed
	(counts/s)	($\mu\text{g I}$)	(10 ⁻⁶ $\mu\text{g I/s}$)	(counts/s)	($\mu\text{g I}$) ^b	(10 ⁻⁶ $\mu\text{g I/s}$)	(counts/s)	($\mu\text{g I}$)	(10 ⁻⁷ $\mu\text{g I/s}$)	Entering S-1	Entering S-2	Monitor	
4.30	0.83	0.0072		0.06	0.00038		7.3	0.0034					
4.50	2.12	0.0183	0.56	0.20	0.00127	0.045	27.2	0.0126	4.6	0.16	0.012	4.1	0.07
5.00	18.6	0.160	2.8	1.51	0.00962	0.17	59.2	0.0274	3.0	0.82	0.046	2.6	0.056
5.50	55.0	0.474	6.3	3.70	0.0236	0.28	84.0	0.0388	2.3	1.8	0.076	2.0	0.043
6.00	99.9	0.861	7.7	7.90	0.0503	0.54	108	0.0497	2.2	2.3	0.15	1.9	0.065
6.50	151	1.30	8.0	14.8	0.0943	0.88	132	0.0611	2.3	2.6	0.24	2.0	0.091
7.00	199	1.71	8.2	24.3	0.155	1.2	152	0.0702	1.8	2.6	0.33	1.6	0.13
7.50	253	2.18	9.4	35.5	0.226	1.4	174	0.0805	2.1	3.0	0.39	1.8	0.13
8.00	307	2.64	9.3	48.8	0.311	1.7	196	0.0907	2.0	3.0	0.46	1.8	0.15
8.50	359	3.09	8.9	63.4	0.404	1.9	216	0.0996	1.8	2.9	0.51	1.6	0.17
9.00	409	3.53	8.7	80.2	0.511	2.1	237	0.109	1.9	3.0	0.58	1.7	0.20
9.50	456	3.93	8.1	98.9	0.630	2.4	259	0.120	2.0	2.9	0.65	1.8	0.23
10.00	502	4.33	8.0	119	0.757	2.5	280	0.130	2.0	2.9	0.69	1.8	0.24
10.50	540	4.73	8.0	140	0.890	2.7	300	0.139	1.9	2.9	0.73	1.6	0.25
11.00	592	5.10	7.4	160	1.020	2.6	314	0.145	1.3	2.7	0.71	1.1	0.26
11.50	635	5.48	7.4	184	1.173	3.1	344	0.159	2.7	2.9	0.83	2.4	0.29
11.98	677	5.84	7.5	209	1.334	3.3	367	0.169	2.1	3.0	0.91	1.9	0.31

^dThe iodine burden entering S-1 was calculated from the total rate of adsorption of iodine on S-1 and S-2. The burden entering S-2 was calculated from the rate of adsorption on S-2. The burden at the monitor was calculated from the rate of adsorption on the monitor trap. The amount of iodine that passed through specimen 2 to the charcoal trap was too little to measure.

^bValues were corrected for change in detector calibration.

Table E.19. Summary of data and calculations from phases 2 through 5 of experiment A-13

Phase and S-1/S-2 Temperatures (°C)	Time (10 ³ s)	Iodine adsorption and desorption								Iodine burden (10 ⁻⁵ Pa or 10 ⁻¹⁰ atm)						
		Specimen 1		Specimen 2		Charcoal trap		Monitor		Leaving ^a S-1	Entering ^b S-2	Leaving ^c S-2	Entering ^d charcoal trap	Monitor		
		(counts/s)	($\mu\text{g I}/10^{-4}$ $\mu\text{g I/s}$)	(counts/s)	($\mu\text{g I}/10^{-4}$ $\mu\text{g I/s}$)	($\mu\text{g I}/10^{-4}$ $\mu\text{g I/s}$)	($\mu\text{g I}/10^{-4}$ $\mu\text{g I/s}$)	(counts/s)	($\mu\text{g I}/10^{-4}$ $\mu\text{g I/s}$)							
2 500/400	12.40	696	6.00		349	2.28			395	0.183						
	12.80	625	5.39	-1.51	522	3.48	1.00		420	0.194	2.75	7.2	8.2			2.4
	13.20	578	4.99	-1.00	632	4.30	2.05		439	0.203	2.25	5.7	5.6			2.0
	13.60	536	4.62	-0.93	727	5.08	1.95		459	0.212	2.25	5.5	5.3			2.0
	12.40	696	6.00		349	2.28			395	0.183						
3 600/400	13.80	518	4.47	-1.09		6.8 ^e	3.21	0.003	471	0.218	2.50	6.0	8.8			2.2
	0.90	442	3.81					0.003								
	14.00	290	2.50	-13.1					479	0.221						
	0.10	205	1.77	-7.30								40				
	0.20	161	1.39	-3.80								24				
4 700/700	0.40	118	1.02	-1.85					519	0.240	3.80					
	0.60	99	0.854	-0.83									8.2			1.7
	0.80	88	0.762	-0.46									5.4			
	0.84												4.3			
	15.20	78	0.677	-0.21		12.3 ^e	5.31									
	0.52								594	0.274	4.25	3.6	15			
	0.60	75	0.647	-0.075		13.5 ^e	1.77							5.0		1.9
	16.00	74	0.619	-0.020									3.2			
	0.30	74	0.619	0		14.3 ^e	1.03		693	0.320	4.18	3.1				
	0.30	74	0.619	0		14.3 ^e		(0.01)	693	0.320		3.0	2.9			1.8
5 800/800	16.31	74	0.639													
	0.36	60.5	0.521	-2.34					693	0.320						
	0.42	28.9	0.249	-4.53												9.6
	0.48	14.6	0.126	-2.05												16.0
	0.54	9.5	0.081	-0.75												8.8
	0.60	7.7	0.066	-0.25												5.1
	0.70	6.4	0.055	-0.11												3.7
	0.90	5.7	0.049	-0.030												3.3
	17.16	4.9	0.042	-0.028												3.1
	0.19					1.00 ^e	-15.1	13.8 ^e	15.7	796	0.368	5.65				3.1
5 800/800	17.19															
	0.22	4.7	0.041						1.00 ^e					48		44
	0.23	3.8	0.032	-0.90												
	0.24	2.1	0.018	-1.40												
	0.26	1.9	0.016	-0.10												
	0.30	1.6	0.014	-0.050												
	0.35	1.4	0.012	-0.040												
	0.40	1.2	0.010	-0.040												
	0.55	1.2	0.010	0												
	0.85	1.1	0.0095	-0.002												
18.10	1.0	0.0086	-0.004		0.10 ^e	-0.99	16.6 ^e	3.1	950	0.439	7.61				3.0	3.4

^a Calculated from the rate that iodine reached S-1 in the helium (0.1×10^{-4} $\mu\text{g I/s}$) plus the rate of desorption from S-1.

^b Calculated from the rate of adsorption on S-2.

^c Calculated from the sum of the rates that iodine reached S-1, desorbed from S-1, and desorbed from S-2.

^d Calculated from rate of adsorption on the charcoal trap and the furnace tube ahead of the trap.

^e Calculated from activity profiles.

Table E.20. Summary of data and calculations from phases 6 through 10 of experiment A-13

Phase and S-1/S-2 temperatures (°C)	Time (10 ⁵ s)	Iodine adsorption and desorption								Iodine burdens (10 ⁻⁵ Pa or 10 ⁻¹⁰ atm)				
		Specimen 1		Specimen 2		Charcoal trap		Monitor		Leaving ^b S-1	Leaving ^c S-2	Entering ^d charcoal trap	Monitor	
		(counts/s) (μg I)	(10 ⁻⁵ μg I/s)	(μg I) ² (10 ⁻⁵ μg I/s)	(μg I) ² (10 ⁻⁵ μg I/s)	(counts/s)	(μg I) (10 ⁻⁷ μg I/s)							
6 800/800	18.10	1.0	0.0086	0.10		16.6		950	0.439					
	0.30	0.99	0.0085											
	0.50	1.16	0.0100											
	0.70	1.22	0.0105											
	0.86	1.17	0.0101					1681	0.777	44.5			19.6	
	0.91		0.0101	0.002	0.14	0.049	22.5	7.28			30.0	29.8	20.5	
7 700/700	18.91		0.0101	0.14		22.5								
	0.93	1.3	0.011					1757	0.812					
	0.95	3.8	0.033	1.1						27.0				
	0.97	5.6	0.049	0.80						27.8				
	19.00	5.9	0.051	0.067						29.8				
	0.10	6.3	0.054	0.030						29.9				
	0.20	7.1	0.061	0.070						29.8				
	0.40	7.5	0.065	0.020					2022	0.935	26.2			23.0
	0.60	8.1	0.070	0.025							29.9			
	0.74				1.53	1.67	29.6	8.55	2252	1.037	30.0			26.5
	0.80	8.1	0.070	0.000							30.0	25.3	23.3	
8 600/600	19.92	13.5	0.116					2314	1.069					
	0.95	23.9	0.206	3.00							21.8			
	0.99	29.8	0.257	1.28				2352	1.087	25.7	26.5			
	20.05	31.8	0.274	0.28							29.2		22.7	
	0.15	34.5	0.298	0.24				2457	1.135	30.0	29.3		26.5	
	0.31	36.6	0.316	0.11							29.7			
	0.51	39.0	0.336	0.10				2686	1.241	29.4	29.7		26.0	
	0.64				7.15		32.3							
	21.01	38.3	0.330	-0.012				2972	1.373	26.4	30.0		23.3	
	0.51	37.5	0.323	-0.014				3246	1.500	25.4	30.0		22.4	
	0.58				9.28	2.27	38.8	6.70						
	22.30	37.5	0.323	0				3659	1.691	24.2	30.0	23.8	18.3	
	0.33				9.96	0.91	42.6	5.07						21.3
9 600/600	22.33					9.96	42.6							
	0.36	29.2	0.252					3654	1.689					
	0.38	25.2	0.217	1.75							7.8			
	0.40	22.8	0.197	-1.00							5.7			
	0.44	19.9	0.172	-0.63							4.7			
	0.50	16.9	0.146	-0.43				3698	1.709	14.3	4.2		12.6	
	0.70	13.0	0.113	-0.17							3.5			
	0.90	11.0	0.113	0				3746	1.731	5.5	3.0		4.9	
	21.16	12.3	0.106	-0.03				3779	1.746	5.8	3.1		5.1	
	0.21				6.72	-3.68	49.1	7.39				13.7	20.1	5.7
	10 600/800	23.21	12.3	0.106		6.72	49.1		3780	1.747				
23.41		12.1	0.104	0	0.23	-32.5	53.8	23.5	3810	1.761	7.0	3.0	91.4	64.0

^aValues were determined from activity profiles

^bCalculated from the rate at which iodine arrived at S 1 in the helium minus the rate of adsorption or plus the rate of desorption on S 1.

^cCalculated from the rate at which iodine arrived at S 2 minus the rate of adsorption or plus the rate of desorption of iodine on S 2.

^dCalculated from the rate of adsorption on the charcoal trap and the furnace tube downstream of S 2.

Table E.21. Summary of data and calculations from phase 11 of experiment A-13

Time (10 ⁵ s)	Iodine adsorption rates						Iodine burdens (10 ⁻⁵ Pa or 10 ⁻¹⁰ atm)			
	Specimen 1		Specimen 2		Monitor		Entering ^b S-1	Entering ^c S-2	Monitor	S-2 adsorbed Total adsorbed
	(counts/s)($\mu\text{g I}$)	(10 ⁻⁵ $\mu\text{g/s}$)	($\mu\text{g I}^a$)	(10 ⁻⁵ $\mu\text{g/s}$)	(counts/s)($\mu\text{g I}$)	(10 ⁻⁷ $\mu\text{g/s}$)				
24.05				0.59						
24.200	37	0.32								
25.800	211	1.82	0.94		3879	1.79				
25.83				1.89	0.73		4152	1.92	7.9	4.7
27.597	378	3.26	0.80							2.1
27.63				2.47	0.32		4381	2.02	5.8	3.2
29.380	592	5.10	1.03							0.9
29.41				2.60	0.073		4599	2.13	5.7	3.1
30.902	770	6.64	1.01							0.2
30.92				2.71	0.073		4809	2.22	6.4	3.1
34.200	1107	9.54	0.88							0.2
34.37				3.43	0.21		5225	2.42	5.9	3.1
										0.6
										2.6
										0.19

^aValues were determined from activity profiles.

^bCalculated from the rate of adsorption on S-1 and S-2.

^cCalculated from the rate of adsorption on S-2.

Table E.22. Summary of data and calculations for phases 12 and 13 of experiment A-13

Phase and S-1/S-2	Temperature (°C)	Time (10 ⁵ s)	Iodine adsorption and desorption						Iodine burden (10 ⁻⁵ Pa or 10 ⁻¹⁰ atm)					
			Specimen 1		Specimen 2		Charcoal trap		Monitor		Leaving S-1	Entering S-2	Leaving S-2	Entering charcoal trap
			(counts/s)	($\mu\text{g l}^{-1}$) (10 ⁻⁵ $\mu\text{g/s}$)	($\mu\text{g l}^{-1}$) ^d (10 ⁻⁵ $\mu\text{g/s}$)	($\mu\text{g l}^{-1}$) ^d (10 ⁻⁵ $\mu\text{g/s}$)	($\mu\text{g l}^{-1}$) ^d (10 ⁻⁵ $\mu\text{g/s}$)	(counts/s)	($\mu\text{g l}^{-1}$) (10 ⁻⁷ $\mu\text{g/s}$)					
12 400/400		34.37			3.43		54.4							
		34.501	1172	9.76				5250	2.426					
		36.050	1108	9.55	-0.134			5254	2.428	0.13	0.38 ^b			0.06
		36.09				3.71	0.181	53.1	-0.84			0.51 ^c		
13 600/600		36.09			3.71		53.1							
		36.302	1105	9.53				5250	2.426					
		36.400	625	5.39	-42.2						122 ^d			
		36.500	405	3.49	-19.0						57			
		36.600	292	2.52	-9.77						31			
		36.800	190	1.64	-4.37						15			
		37.000	141	1.21	-2.15			5321	2.46	4.73	9.1			2.1
		37.305	95.6	0.82	-1.27						6.6			
		37.755	69.6	0.60	-0.50			5408	2.50	5.30	4.4			2.3
		37.83			(-5.14) ^e	7.03	1.91	63.0	5.69		(18) ^g		12 ^f	16

^d Values were calculated from activity profiles.

^b Calculated from rate of desorption from S-1.

^c Calculated from rate of adsorption on S-2.

^d Values for phase 13 were calculated from rate of arrival of iodine at S-1 (1.07×10^{-5} $\mu\text{g/s}$ for burden of 3×10^{-5} Pa) plus rate of desorption from S-1.

^e Average values for phase 13.

^f Calculated from rate of iodine at S-2 minus rate of adsorption on S-2.

Table E.23. Iodine on specimen 2 and region of charcoal trap from activity profiles of experiment A-13

Test phase	Time (10 ⁵ s)	Specimen 2				Charcoal trap and furnace tube			
		Profile area (mm)	C _{max} (counts/s)	Corrected calibration (counts/s.µg I)	Iodine ^a (µg)	Profile area (mm)	C _{max} (counts/s)	Corrected calibration (counts/s.µg I)	Iodine (µg)
2	13.80	36.8	811	141	6.8				
3	14.84	39.6	1330	137	12.3				
	15.52	41.2	1370	134	13.5				
	16.30	41.0	1440	132	14.3				
4	17.19	62.7	72	145	1.00	61.5	1330	190	13.8
5	18.10	68.0	6.8	149	0.10	38.7	2610	195	16.6
6	18.91	60.0	11	152	0.14	40.3	3460	199	22.5
7	19.74	46.7	150	147	1.53	43.6	4070	192	29.6
8	20.64	62.3	519	145	7.15	45.4	4210	190	32.3
	21.58	56.8	734	144	9.28	47.0	4840	188	38.8
	22.33	54.8	811	143	9.96	48.4	5130	187	42.6
9	23.21	54.6	545	142	6.72	49.1	5800	186	49.1
10	23.41	59.0	17	142	0.23	40.6	7690	186	53.8
11	24.05	51.9	50	142	0.59	39.0	7960	186	53.5
	25.83	44.6	188	142	1.89	38.0	8160	186	53.4
	27.63	42.4	258	142	2.47	37.7	8180	186	53.1
	29.41	41.3	279	142	2.60	38.2	8230	186	54.2
	30.92	40.5	297	142	2.71	38.2	8260	186	54.4
	34.37	41.2	369	142	3.43	37.8	8350	186	54.4
12	35.40	b	383	142		b	8170	186	
	36.09	40.3	417	142	3.79	37.6	8200	186	53.1
13	37.83	55.3	563	142	7.03	39.5	9260	186	63.0
Post-test	37.99					36.0	3930 ^d	186	24.4
	38.04					39.8	9130 ^d	186	62.6
	38.04					33.0	7090 ^e	186	40.3

$$\mu\text{g I} = \frac{\text{Profile area in mm} \times C_{\text{max}} \text{ in counts/s}}{31.2 \text{ mm} \times \text{corrected calibration in counts/s.}\mu\text{g I}}$$

^b Too few points to estimate area.

^c Furnace tube alone.

^d Furnace tube and charcoal trap.

^e Furnace tube subtracted from furnace tube and charcoal trap.

The method depends on the equilibrium concentration of iodine on the surface being proportional to the concentration in the gas over the range involved in the calculation. We have not established that the relationship is linear.

The value for mass transfer coefficient obtained as part of the calculation was 7.4 cm/s. In Appendix G, Table G.2, we calculated values of ~ 45 cm/s for transport of HI and I at 400°C. The large difference implies that the rate of adsorption in phase 1 of this experiment was limited by reactions at the surface rather than diffusion through the gas. This difference would invalidate the estimate of the equilibrium concentration, unless the controlling reactions were found to be first order.

In phases 2 and 3, the temperature of specimen 1 was raised to 500 and 600°C respectively. Both specimens were raised to 700°C in phase 4 and to 800°C in phase 5. We thought that the steady state concentrations at 700 and 800°C might be low enough for the entire surface of specimen 2 to reach steady state.

Some of the data and calculations for phases 2 through 5 are summarized in Table E.19. The calculations were made to obtain values of desorption rates and iodine burdens at various locations in the furnace tube. We assumed that the iodine burden in the gas entering specimen 1 was 3×10^{-5} Pa (3×10^{-10} atm). That the burden was of that magnitude was generally verified by the monitor.

Calculation of the iodine burden in the gas leaving specimen 1 took into account the iodine that desorbed from specimen 1. The iodine burden in the gas entering specimen 2 was calculated from the amount of iodine adsorbed on specimen 2 and only for conditions when practically all the iodine in the gas entering specimen 2 adsorbed on the specimen. The iodine burdens were averages for the intervals over which they were calculated. Where the intervals were the same for specimens 1 and 2, the burden in the gas leaving specimen 1 should have been the same as that in the gas entering specimen 2. Differences between the two reflect uncertainties in the value assumed for the iodine burden in the gas entering specimen 1 and in the measurements of the amounts of iodine on the specimens.

The iodine burden in the gas leaving specimen 2 was calculated for those cases in which iodine desorbed from the specimen. The burden was obtained between measurements on specimen 2, to gas having an initial burden of 3×10^{-5} Pa (3×10^{-10} atm). The iodine burden in the gas entering the charcoal trap was calculated from the amount of iodine deposited on the charcoal and the furnace tube between specimen 2 and the charcoal trap. Again, differences between the iodine burden in the gas leaving specimen 2 and that entering the charcoal trap reflect uncertainties in the data and assumptions.

Since we concluded that the concentration on the surface of specimen 1 at the end of phase 1 was far from the steady state concentration at 400°C , our primary interest in phase 2 was to see whether there would be much desorption on raising the temperature only 100°C ; there was. However, the steady state concentration was approached slowly, so we began phase 3 well before reaching steady state. At the end of phase 2, the average concentration of iodine on specimen 1 was $0.64 \mu\text{g}/\text{cm}^2$. We judged from the shape of the desorption curve that the steady state concentration would have been 0.3 to $0.5 \mu\text{g}/\text{cm}^2$.

At 600°C in phase 3, the iodine desorbed rapidly, as shown in Fig. E.22. A steady concentration of $0.091 \mu\text{g}/\text{cm}^2$ was reached on specimen 1 in about 2×10^5 s.

In phase 4, at 700°C , the amounts of iodine on both specimens appeared to be steady in less than 1×10^5 s. The average concentration on specimen 1 was $0.0060 \mu\text{g}/\text{cm}^2$.

Activity profiles for specimen 2 and the furnace tube through the charcoal trap, measured at the end of phase 3 ($t = 16.30 \times 10^5$ s) and the end of phase 4 ($t = 17.19 \times 10^5$ s) are shown in Fig. E.26.* Specimen 2 extended from about 280 to 330 mm. The front of the charcoal trap, where practically all the activity is found when it is adsorbed by the charcoal, was at about 445 mm.

* Only a few points were taken for the profile at $t = 16.30 \times 10^5$ s because it was expected to be like that taken at $t = 15.52 \times 10^5$ s. The points from both profiles are shown in Fig. E.26. The profiles end at detector position 450 mm because the detector could not be moved beyond that point.

At the end of phase 3, the bulk of the activity on specimen 2 was near the entrance. The profile at the end of the desorption at 700°C in phase 3 indicates that the iodine on the specimen was distributed nearly uniformly along the length. If the concentration had been uniform, the profile should have peaked at 300 mm and fallen off to about 0.7 at 280 mm and 0.4 at 330 mm.[†]

The profile indicates that the iodine concentration increased toward the outlet of the specimen. Possibly the increase was real and was produced by a slightly lower temperature near the outlet. Or, the appearance of an increase might have resulted from distortion of the profile by contributions from the much greater activity on the wall of the furnace tube between the specimen and the charcoal trap. If, while recognizing the uncertainties, we assume that the concentration of iodine on the surfaces of specimen 2 was uniform, that concentration was 0.0065 µg/cm², about the same as on specimen 1.

Before phase 4, practically all the iodine in the gas adsorbed on the specimens. There was no detectable iodine on the furnace tube and not more than 0.01 µg on the charcoal trap downstream of specimen 2. During phase 4, approximately 14 µg of iodine passed from specimen 2 into the furnace tube. According to the profile, one-third to one-half of that iodine was on the wall of the furnace tube, and the remainder was on the charcoal trap at the end of phase 4.

Presumably, the iodine on the furnace tube was in the form of CrI₂ and FeI₂. According to Table E.19, the average iodine burden in the gas leaving specimen 2 was 4.8×10^{-4} Pa (4.8×10^{-9} atm) during phase 4. However, 85% of the iodine desorbed during the first 17% of phase 4, so the iodine burden during that interval was 2×10^{-3} to 3×10^{-3} Pa (2×10^{-8} to 3×10^{-8} atm). Thermodynamic equilibrium calculations in Appendix A show that CrI₂(s) and FeI₂(s) are not stable at 400°C in an iodine burden of 3×10^{-5} Pa (3×10^{-10} atm) nor at 700°C in an iodine

[†]The detector position is referenced to the front of the collimator slit, so the profile is offset from the position of the center of the slit.

burden of 3×10^{-3} Pa (3×10^{-8} atm) in helium containing 50 Pa (5×10^{-4} atm) of hydrogen. Solid CrI_2 and FeI_2 should not have been present on the surface of specimen 2 before or during the desorption at 700°C in phase 4.

However, the deposit on the wall of the furnace tube is substantial evidence that much of the iodine was released from specimen 2 as CrI_2 and FeI_2 , probably mostly as FeI_2 . The amount on the wall indicates that the pressure of metal iodides in the gas must have been 5×10^{-4} Pa or greater during the early part of phase 4. At that pressure, FeI_2 would have begun to condense at about 275°C and would have been mostly removed from the gas at 225°C . The temperature at the exit of specimen 2, 330 mm, would have been near 700°C , and that at the entrance of the charcoal trap, 445 mm, would have been below 150°C . The iodine deposit on the wall of the furnace tube was centered near 410 mm, where the temperature would have been in the range 200 to 300°C .

On raising the temperature of the specimens to 800°C in phase 5, most of the remaining iodine desorbed very rapidly. At the end of the desorption, the measured activity on specimen 1 was only about 0.1 count/s above a background of 0.6 count/s. The inferred concentration of iodine on specimen 1 was $0.0012 \mu\text{g}/\text{cm}^2$.

The maximum activity on specimen 2 was about 1 count/s above a background of 0.7 count/s. The profile for specimen 2 is shown in Fig. E.26. We interpret the profile as indicating that the iodine was distributed nearly uniformly over the specimen. The abnormally high relative activities beyond detector position 320 mm are attributed to contributions from iodine on the furnace tube beyond the specimen. Assuming that the iodine distribution on specimen 2 was uniform, the steady state concentration was $0.007 \mu\text{g}/\text{cm}^2$.

The activity profile for the region downstream of specimen 2 shows that most of the iodine on the wall of the furnace tube at the end of phase 4 moved near to or onto the charcoal trap during phase 5. With the iodine burden reduced to 3×10^{-5} Pa (3×10^{-10} atm) and the pressure of metal iodides at a low level in the gas, the metal iodides should have migrated to a region of lower temperature or dissociated and released the iodine to the charcoal trap.

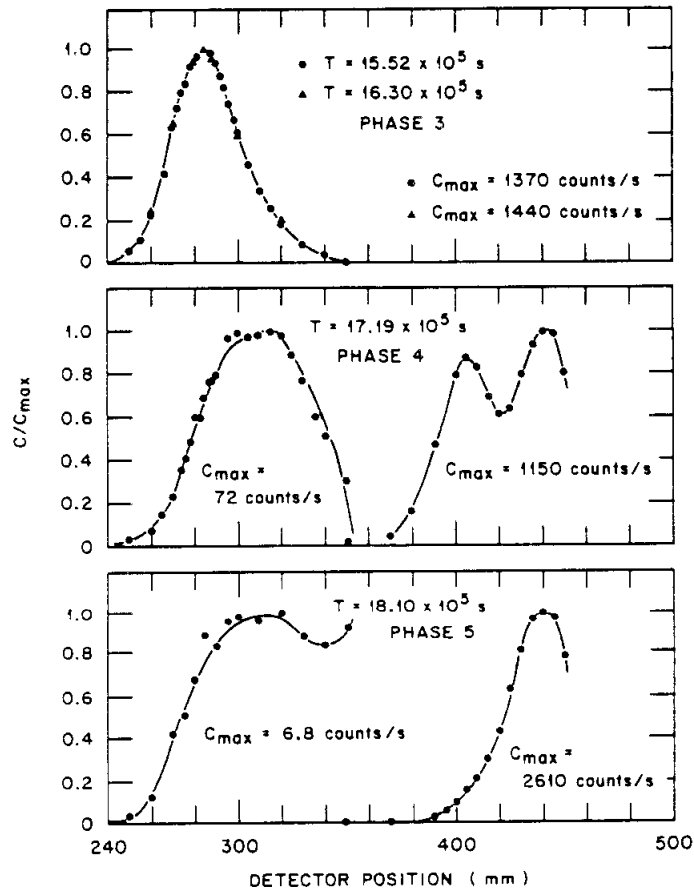


Fig. E.26. Activity profiles for region of specimen 2 and the charcoal trap during phases 3, 4, and 5 of experiment A-13.

The amounts of radioiodine on the specimens at 800°C and 3×10^{-5} Pa (3×10^{-10} atm) were so small that the measurements were not very accurate. So, we decided to hold the temperature and determine the steady state concentration on the surface for an iodine burden of 3×10^{-4} Pa (3×10^{-9} atm). This was done in phase 6 with the results shown in Figs. E.23 and E.24 and Table E.20.

As well as we could measure, the amount of iodine on specimen 1 increased from 0.0086 to 0.0101 μg , raising the surface concentration to 0.0014 $\mu\text{g}/\text{cm}^2$. The activity profile for specimen 2 at the end of phase 6 (Fig. E.27) was distorted as at the end of phase 5. Assuming that the

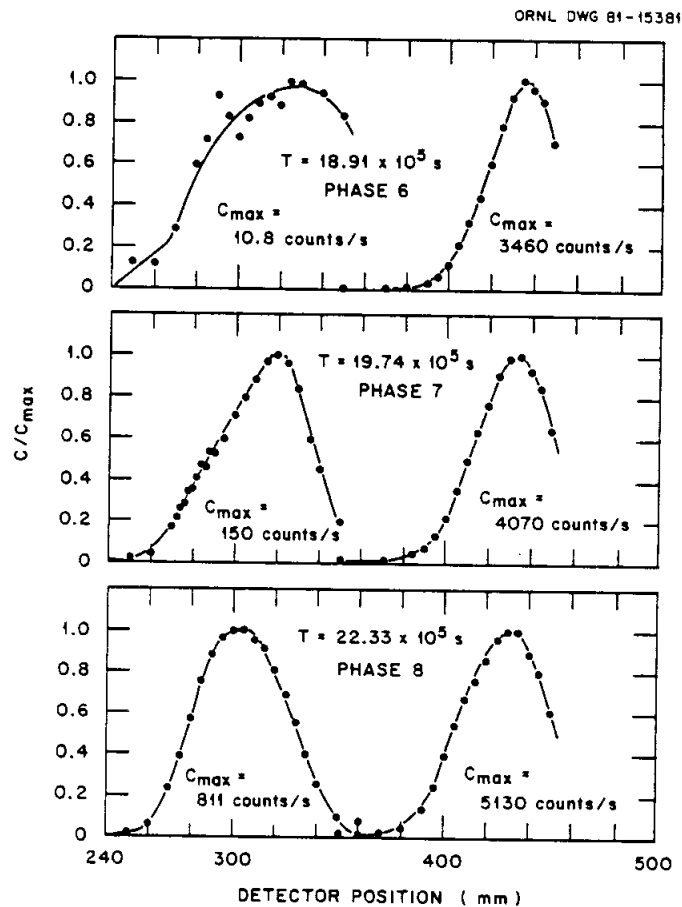


Fig. E.27. Activity profiles for specimen 2 at ends of phases 6, 7, and 8 of experiment A-13.

activity was distributed uniformly over the surface, the concentration increased from $0.0007 \mu\text{g}/\text{cm}^2$ at the end of phase 5 to $0.0009 \mu\text{g}/\text{cm}^2$ at the end of phase 6.

Since the increase of a factor of 10 in the iodine burden produced only a slight increase in the concentration of iodine on the surfaces of the specimens at 800°C , we lowered the temperature to 700°C in phase 7 and then to 600°C in phase 8, while holding the iodine burden at $3 \times 10^{-4} \text{ Pa}$ ($3 \times 10^{-9} \text{ atm}$).

At the end of phase 7 at 700°C , the steady state concentration on specimen 1 was $0.010 \mu\text{g}/\text{cm}^2$. This compares with $0.0060 \mu\text{g}/\text{cm}^2$ at the

end of phase 4 when the iodine burden was only one-tenth as great. The average concentration on specimen 2 at the end of phase 7 was $0.010 \mu\text{g}/\text{cm}^2$, but the activity profile shows that the concentration of iodine near the outlet of the specimen was substantially greater than that near the inlet. Also, Fig. E.24 shows that the activity near the entrance of the specimen had not reached a steady value at the end of phase 7, so the $0.010 \mu\text{g}/\text{cm}^2$ was not a steady state concentration for specimen 2.

At the end of phase 8 at 600°C , the steady state concentration on specimen 1 was $0.046 \mu\text{g}/\text{cm}^2$. This is only half the concentration that was measured at the end of phase 3 when the iodine burden was one-tenth as great. The amount of iodine on the region of specimen 2 being monitored was nearly steady. The profile was nearly identical to that calculated for a uniform concentration over the entire surface of the specimen. The average concentration of $0.065 \mu\text{g}/\text{cm}^2$ on specimen 2 was equal to, or very close to steady state concentration.

Since the steady state concentrations of iodine on the specimens at 600°C and $3 \times 10^{-4} \text{ Pa}$ ($3 \times 10^{-9} \text{ atm}$) were lower than those that had been measured earlier at $3 \times 10^{-5} \text{ Pa}$ ($3 \times 10^{-10} \text{ atm}$), the question arose as to the cause. In phase 9 we reduced the iodine burden to $3 \times 10^{-5} \text{ Pa}$ ($3 \times 10^{-10} \text{ atm}$) while maintaining the temperature at 600°C . Iodine desorbed from both specimens, as shown in Figs. E.23 and E.24. The concentration on specimen 1 reached a steady value of $0.015 \mu\text{g}/\text{cm}^2$. That on specimen 2 had reached $0.044 \mu\text{g}/\text{cm}^2$ and was still falling at the end of phase 9.

It appeared that the surfaces of the specimens had been changed by the prolonged heating at up to 800°C . We decided to return to 400°C at an iodine burden of $3 \times 10^{-5} \text{ Pa}$ ($3 \times 10^{-10} \text{ atm}$) to determine the adsorptive capacity of the changed surface under the conditions of phase 1. Before doing this, we heated specimen 2 to 800°C , in phase 10, to desorb most of the iodine so that the normal monitoring of the specimen would provide a more sensitive measure of the amount of iodine that passed specimen 1.

Phase 11 of the experiment was begun at $23.424 \times 10^5 \text{ s}$ when the temperature of both specimens was reduced to 400°C . Iodine began to

adsorb on both specimens immediately. The manner in which the amount of iodine on the specimens changed with time is shown in Fig. E.25. Some of the data and calculations are summarized in Table E.21.

Shortly after phase 11 began, the supply of liquid nitrogen to the cold traps in the helium supply lines was interrupted. The traps warmed and permitted the small amount of moisture that had accumulated to be passed through the system. The effect on the accumulation of iodine on the specimens and on the monitor is shown in Fig. E.28. From 23.43×10^5 s until 23.51×10^5 s, a total of $0.33 \mu\text{g}$ of iodine adsorbed on the two specimens. The average rate of adsorption was $4.1 \times 10^{-5} \mu\text{g/s}$, which corresponds to the removal of all the iodine from helium having an iodine burden of

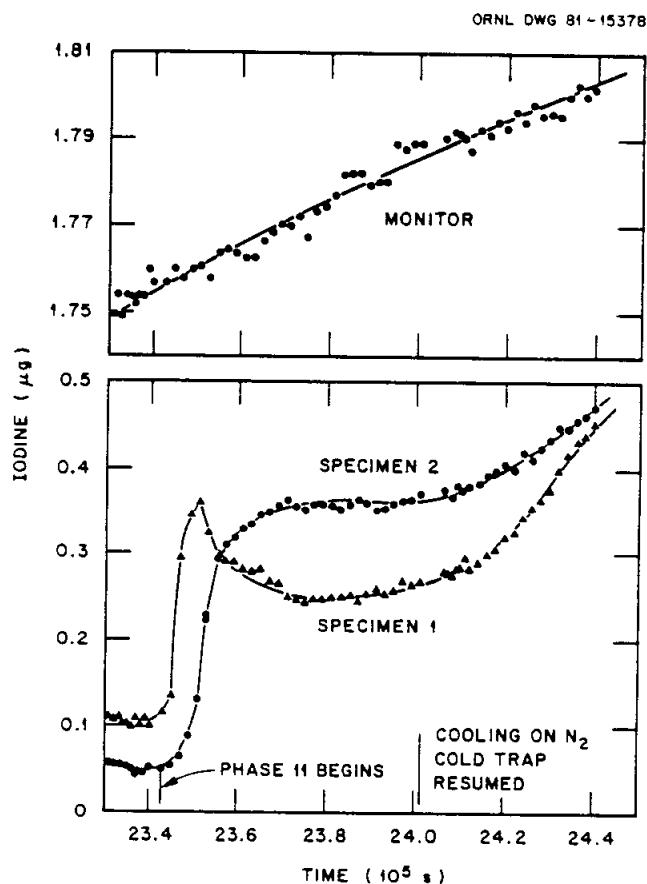


Fig. E.28. Iodine on specimens and monitor during interruption of cooling of the moisture traps in helium lines during experiment A-13.

about 11×10^{-5} Pa (11×10^{-10} atm). Then iodine began to desorb from specimen 1 but continued to adsorb on specimen 2. By 23.71×10^5 s, when the desorption on specimen 1 and the adsorption on specimen 2 had ceased for a time, a total of 0.45 μg had adsorbed on the two specimens. The average adsorption rate from 23.51×10^5 to 23.71×10^5 s was 2.2×10^{-5} $\mu\text{g/s}$, corresponding to an average iodine burden of 6.3×10^{-5} Pa (6.3×10^{-10} atm). Thereafter, the amounts of iodine on the specimens changed little (there appears to have been a little adsorption on specimen 1) until the liquid nitrogen cooling on the moisture traps was restored at 24.014×10^5 s.

During the entire time, iodine was adsorbing on the monitor at a rate of 5×10^{-7} $\mu\text{g/s}$, which corresponds to an iodine burden of 2.2×10^{-5} Pa (2.2×10^{-10} atm). Since the monitor values usually are low, we assume that the burden was about the intended 3×10^{-5} Pa (3×10^{-10} atm). Calculations based on the activity profiles indicated that no measurable amount of iodine passed specimen 2.

It appears to us that release of a small amount of moisture from the cold traps into the helium first caused iodine to desorb from the apparatus ahead of the specimens. Initially, much of this iodine adsorbed on specimen 1. Later, the moisture effect reached specimen 1 and resulted in some desorption from that specimen. At most, the effect on specimen 2 was to distribute iodine along the specimen. Practically all the iodine reaching specimen 2 in the gas adsorbed on the specimen.

It appears that all the moisture had been evaporated from the traps into the helium and passed through the system by about 23.75×10^5 s. Then, for a while, most of the iodine in the helium adsorbed on walls ahead of the specimens to replace some of the iodine that had desorbed. Gradually, the amount reaching and adsorbing on the specimens increased. During the interval from 24.2×10^5 to 24.4×10^5 s, the combined adsorption rate was 1.05×10^{-5} $\mu\text{g/s}$, which corresponds to the intended iodine burden of 3×10^{-5} Pa (3×10^{-10} atm). Whether the increase in the rate of adsorption on the specimens began when cooling was restored to the cold traps, or shortly before that time, is unclear.

During the interval from 24.2×10^5 to 25.8×10^5 s, after the upset, about 56% of the iodine in the gas adsorbed on specimen 1 and 44% was in the gas leaving the specimen. The fraction in the gas leaving the specimen decreased to 0.07 by 29.4×10^5 s. It then increased gradually and was above 0.2 at the end of phase 11.

The behavior during phase 11 was similar to that observed at the beginning of experiments A-11 and A-12. It appears that the surface was activated and the adsorptive capacity increased during the first few days of operation at 400°C . At the end of phase 11, the iodine concentration on specimen 1 was $1.4 \mu\text{g}/\text{cm}^2$, and less than 30% of the iodine remained in the gas leaving the specimen. The initial behavior was such that the method used to estimate the steady state concentration for phase 1 cannot be applied to phase 11. However, the data indicate that the steady state concentration probably would have been at least as great as the $4 \mu\text{g}/\text{cm}^2$ estimated for phase 1.

At the beginning of phase 12, the temperature of the saturator was reduced to -81°C , and the flow through the saturator was stopped. This condition was maintained for about 1.9×10^5 s. Iodine desorbed from specimen 1 at a rate of about $0.13 \times 10^{-5} \mu\text{g}/\text{s}$ and adsorbed on specimen 2 at a rate of $0.18 \times 10^{-5} \mu\text{g}/\text{s}$ (see Table E.22). These rates correspond to iodine burdens in the gas leaving specimen 1 and entering specimen 2 of 4×10^{-6} and 5×10^{-6} Pa (0.4×10^{-10} and 0.5×10^{-10} atm) respectively. As well as we could determine, the amounts of iodine in the gas entering specimen 1 and leaving specimen 2 were insignificant. The difference reflects uncertainty in the measurements.

At the end of phase 11, the iodine burden in the gas leaving specimen 1 was about 6×10^{-6} Pa (0.6×10^{-10} atm) as shown in Table E.21. This burden is not much different from those obtained above for phase 12. This fact may simply indicate, as observed before, that the iodine burden in the gas leaving specimen 1 was close to being in equilibrium with the concentration of iodine on the surface of the specimen at the outlet. If this was the condition, the desorption rate measured in phase 12 would reflect the gas flow rate rather than the reaction rates on the surface.

In phase 13 the iodine burden was returned to the nominal 3×10^{-5} Pa (3×10^{-10} atm), and the temperature of both specimens was raised to 600°C . Initially, iodine desorbed from specimen 1 and adsorbed on specimen 2 near the entrance. During this time, the iodine burden at the exit of specimen 1, as calculated in Table E.22, was greater than 10^{-3} Pa (10^{-8} atm). As the rate of desorption from specimen 1 decreased, the point was reached at which iodine began to desorb from near the entrance of specimen 2. This desorption was continuing at the end of phase 13. However, the numbers in Table E.22 show that the total amount of iodine on specimen 2 increased considerably during phase 13.

The concentration of iodine on specimen 1 had not quite reached a steady state when the experiment was ended (Fig. E.25). Comparison of the data from phase 13 with that from phase 3 suggests that the steady state concentration would have been 0.06 to $0.07 \mu\text{g}/\text{cm}^2$. This compares with $0.11 \mu\text{g}/\text{cm}^2$ measured at the end of phase 3 and 0.018 at the end of phase 9, both at 600°C and 3×10^{-5} Pa (3×10^{-10} atm).

Figure E.25 shows that iodine was desorbing from specimen 2 at the end of phase 13. The activity profile indicate that the iodine was distributed along the entire length of the specimen with the lowest concentration near the inlet. This implies that the average concentration on the surface was above the steady state value. At the end of phase 13, the average concentration was $0.046 \mu\text{g}/\text{cm}^2$.

After phase 13 was ended, the apparatus was examined visually, and measurements were made to determine the distribution of iodine. Specimen 1 was uniformly gray. Plates from specimen 2 were gray-brown over the first two millimeters. Then they lightened, becoming light tan to silver over the center of the specimen and light blue near the outlet end. There was a very thin deposit on the furnace tube in the region of 420 to 435 mm, between the outlet of specimen 2 at 330 mm and the entrance of the charcoal trap at 444 mm.

The bundles of T-22 steel strips were removed from the hot traps in the helium lines and were inspected. The metal that was removed from the main line was lightly oxidized over the entire length of about 7 cm. The

metal from the line to the saturator was similarly oxidized, but over only the front 3 cm.

Activity profiles were made for the furnace tube after the specimens were removed. They are shown in Fig. E.29. One was made with the charcoal trap in place. Another was made of the furnace tube alone. A third, for the charcoal trap alone, was calculated from the difference between measurements at each of the data points. The profiles show the presence of a substantial iodine activity on the wall of the furnace tube in the vicinity of 420 to 425 mm, the region of the thin film.

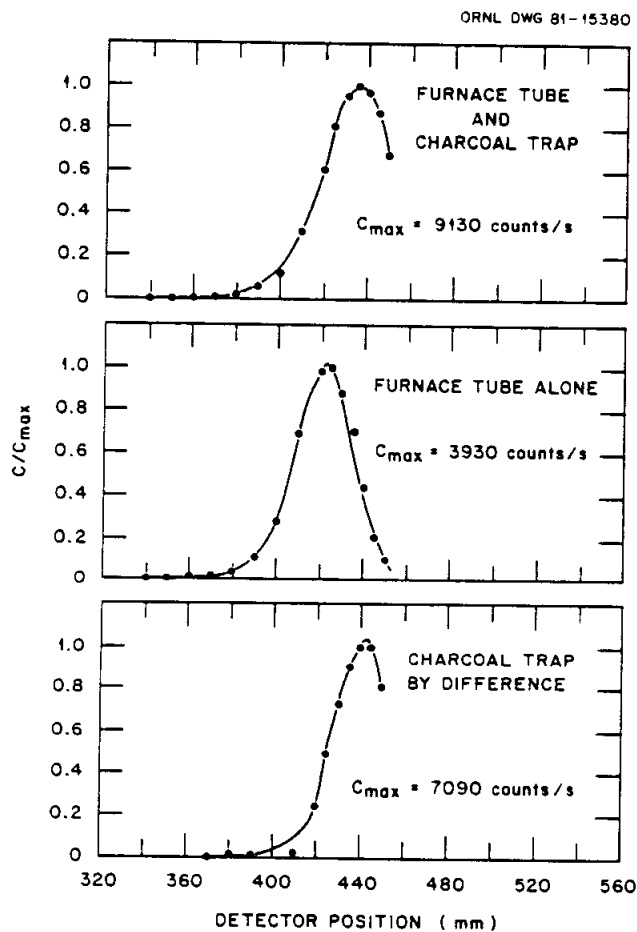


Fig. E.29. Activity profiles in region of charcoal trap at end of experiment A-13.

Measurements, by use of a multichannel analyzer, of the amounts of iodine on various components from the experiment are reported in Table E.24. Measurements on components that were made during and after the experiment by use of detectors on the apparatus are listed for comparison. The post-test measurements account for 3064 of the 3093 μCi of iodine measured to be in the source ampoule prior to the experiment. The ratio gives a material balance of 0.99.

The steady state concentrations or estimates for experiment A-13 are summarized in Table E.25.

Table E.24. Posttest measurements on components from experiment A-13

	Multichannel analyzer measurements		Detectors on apparatus	
	($\mu\text{Ci } ^{131}\text{I}$) ^a	($\mu\text{g I}$)	(counts/s) ^b	($\mu\text{g I}$)
Specimen 1	5.43	0.64	62.6	0.54
Specimen 2	46.5	5.5		7.0 ^c
Charcoal trap	382	45.1		39.0 ^c
Backup charcoal trap	6.77	0.80		
Monitor trap D	25.5	3.01	5405	2.50
Inlet tubes to saturator	18.1	2.13		
Saturator - source L-1	1986	234		
Connector tube to furnace tube	3.54	0.42		
Furnace tube - inlet end	0.79	0.094		
Furnace tube - outlet end	206	24.3		24.0
Monitor line wash	2.45	0.29		
Purge line wash	0.032	0.004		
Purge and monitor lines after wash	0.62	0.074		
Purge trap from evacuation at shutdown	1.03	0.12		
Purge trap A - iodine transfer	21.9	2.58	2240	2.3
Purge trap B - purge A	110	13.0	6390	6.7
Ampoule after transfer of source L-1	243	28.6		
Monitor trap C - purges B and C	3.89	0.46	897	0.41
	3064	361		

^aMeasurements were corrected to 10:30 on 4/21/80.

^bMeasurements were corrected to time 0.

^cValues were determined from activity profiles.

Table E.25. Summary of steady-state concentration data from experiment A-13^a

Test phase	Starting time (10 ⁵ s)	Specimen temperature (°C)		Iodine burden (10 ⁻⁵ Pa or 10 ⁻¹⁰ atm)		Final loading on S-1 ^b (μg I/cm ²)	Equilibrium loading (μg I/cm ²)
		S-1	S-2	Predicted	Observed		
1	4.27	400	400	3.0	2.9	0.83	~4 ^c
2	12.16	500	400	3.0	2.2 ^d	0.64	0.3-0.5 ^e
3	13.86	600	400	3.0	1.8 ^d	0.091	0.091
4	16.30	700	700	3.0	2.5 ^d	0.0060	0.006 ^f
5	17.21	800	800	3.0	3.4 ^d	0.0012	0.0007-0.0012 ^f
6	18.11	800	800	30	20	0.0014	0.0009-0.0014 ^f
7	18.93	700	700	30	26	0.010	0.010
8	19.90	600	600	30	24	0.046	0.046-0.065 ^f
9	22.33	600	600	3.0	~5.0 ^d	0.015	0.015
11	23.42	400	400	3.0	~3.1	1.4	>4
12	34.40	400	400	0	0	1.4	1.4
13	36.30	600	600	3.0	2.3	0.086	0.06-0.07 ^e
End	37.86						

^a Tests were run in He containing 50 Pa of H₂ at a total flow of 400 cm³/min.

^b Loading is based on geometric area.

^c Inferred from rate of increase in fraction of iodine in gas leaving S-1.

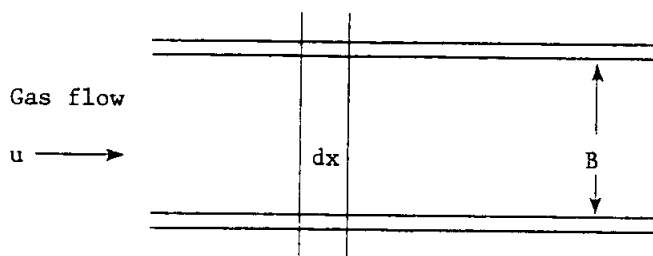
^d Values were obtained from monitor. Monitor values usually lower than those obtained from adsorption on specimens.

^e Inferred from shape of desorption curve.

^f Values obtained from specimens 1 and 2.

Appendix F. CALCULATION OF THE CONCENTRATION OF IODINE IN THE GAS
AND ON THE SURFACES OF THE SPECIMENS FOR THE CONDITION
THAT THE EQUILIBRIUM CONCENTRATION ON THE SURFACE
IS PROPORTIONAL TO THE CONCENTRATION IN THE GAS

A section of a specimen can be represented by two parallel plates as shown below.



Over the element of length dx and unit width, the material balance is

$$uBcd\tau - uB \left[c + \left(\frac{\partial c}{\partial x} \right) dx \right] d\tau - 2dx \left(\frac{\partial c_s}{\partial \tau} \right) d\tau - Bdx \left(\frac{\partial c}{\partial \tau} \right) d\tau = 0, \quad (1)$$

where

- u = average velocity of gas, m/s;
- c = concentration of adsorbate in gas, mol/m³;
- c_s = concentration of adsorbate on surface, mol/m²;
- B = plate spacing, m;
- τ = time, s;
- x = axial distance from entrance, m.

Equation (1) reduces to

$$\frac{\partial c}{\partial x} + \frac{2}{uB} \frac{\partial c_s}{\partial \tau} + \frac{1}{u} \frac{\partial c}{\partial \tau} = 0. \quad (2)$$

In a flow process $\partial c / \partial \tau$ becomes negligible if the volume between the plates is small in comparison with the flow volume, and the material balance becomes

$$\frac{\partial c}{\partial x} + \frac{2}{uB} \frac{\partial c_s}{\partial \tau} = 0. \quad (3)$$

For a gas adsorption process in which the resistance to diffusion of the adsorbate through the gas is the controlling factor, the rate of adsorption

can be expressed as

$$N = k_G A (c - c^*) , \quad (4)$$

where

N = rate of transfer to surface, mol/s;

A = surface area, m^2 ;

c^* = concentration of adsorbate in gas in equilibrium with the concentration on the surface, mol/ m^3 .

Then,

$$\frac{\partial c}{\partial \tau} = k_G (c - c^*) , \quad (5)$$

and, substituting in Eq. (3):

$$- \frac{\partial c}{\partial x} = \frac{2k_G}{uB} (c - c^*) . \quad (6)$$

An analytical solution of Eqs. (5) and (6) has been provided by Hougen and Marshall³⁵ for the case of isothermal adsorption in which

$$c^* = m c_s ,$$

c is constant for all values of τ at $x = 0$,

$c_s = 0$ for all values of x at $\tau = 0$.

Equations (5) and (6) become

$$\frac{\partial c}{\partial \tau} = k_G m \left(\frac{c}{m} - c_s \right) = b \left(\frac{c}{m} - c_s \right) , \quad (7)$$

and

$$- \frac{\partial c}{\partial x} = \frac{2k_G}{uB} (c - m c_s) = a (c - m c_s) , \quad (8)$$

where b equals $k_G m$ and a equals $2k_G/uB$. The solution in terms of the dimensionless groups c/c_0 , c_s/c_{s0} , ax , and $b\tau$ is

$$\frac{c}{c_0} = 1 - e^{-b\tau} \int_0^{ax} e^{-ax} J_0 [2i(b\tau ax)^{\frac{1}{2}}] d(ax) ; \quad (9)$$

$$\frac{c_s}{c_{s0}} = e^{-ax} \int_0^{b\tau} e^{-b\tau} J_0[2i(axb\tau)^{\frac{1}{2}}] d(b\tau) , \quad (10)$$

where

$$i = (-1)^{\frac{1}{2}},$$

J_0 = Bessel function of the first kind and zero order,

c_0 = concentration of adsorbate in entering gas,

c_{s0} = concentration of adsorbate on surface in equilibrium with the entering gas.

Hougen and Marshall presented solutions to Eqs. (9) and (10) in the form of charts in their paper. The charts showed c/c_0 and c_s/c_{s0} as functions of $b\tau$ for a range of values of ax . Figures F.1 and F.2 show c/c_0 and c_s/c_{s0} as functions of ax for various values of $b\tau$. These plots, which show the theoretical distribution along the surfaces at various times, were derived from Hougen and Marshall's charts³⁵ and were more suited to our purposes.

Although the equations were solved and the charts were prepared for the limited case that $c_s = 0$ at $\tau = 0$ and the rate of adsorption is controlled by the resistance to transport of adsorbate through the gas, they have broader application. By substituting $(c - c'_0)/(c_0 - c'_0)$ for c/c_0 and $(c_s - c'_{s0})/(c_{s0} - c'_{s0})$ for c_s/c_{s0} , the solutions apply to the case in which c'_{s0} is a uniform concentration of adsorbate on the surface at $\tau = 0$ and c'_0 is the concentration of adsorbate in the gas in equilibrium with c'_{s0} . The equations and solutions apply also to cases in which reactions at the surface of the metal provide an appreciable resistance to adsorption if the reactions are of first order. In this case an overall transfer coefficient, k_M , is substituted for k_G in the equations, and

$$\frac{1}{k_M} = \frac{1}{k_G} + \frac{1}{k_S} ,$$

where k_S is a rate coefficient, in consistent units, for the surface reactions.

ORNL DWG 80-1487

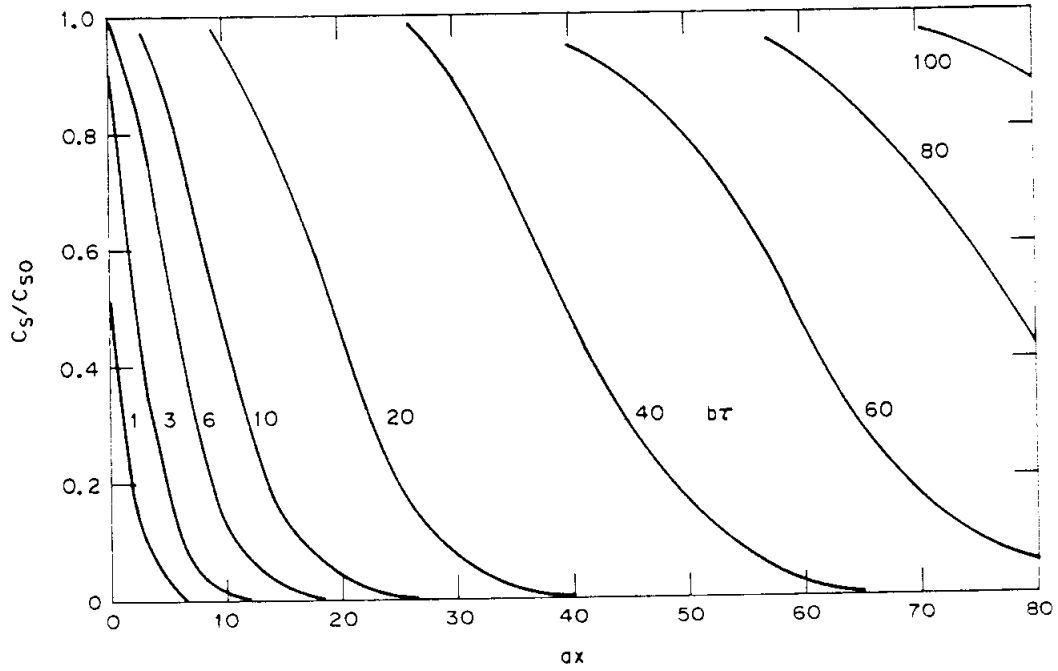


Fig. F.1. Fraction of saturation of surface.

ORNL DWG 80-1486

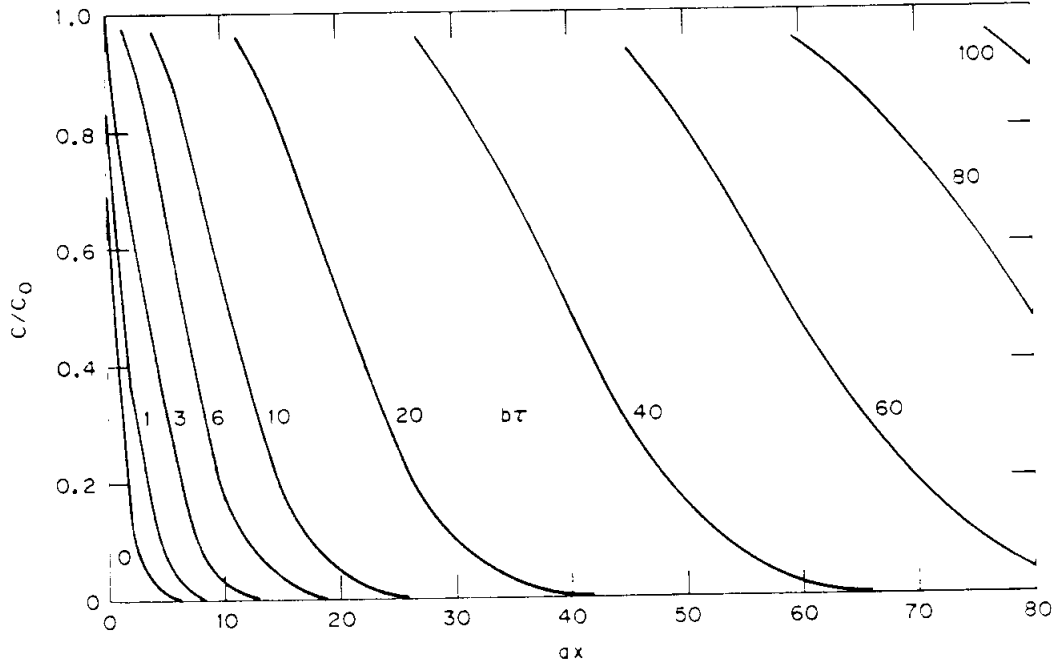


Fig. F.2. Fraction of adsorbate remaining in gas.

Appendix G. MASS TRANSPORT ANALYSIS FOR ADSORPTION SPECIMENS

The specimens used in the adsorption and desorption experiments consisted of ten type T-22 steel plates in the configuration shown in Fig. G.1. Two specimens in series were used in most of the experiments. At first, both specimens were 51 mm (2 in.) long, but in most of the experiments, specimen 1 was 2 mm long and specimen 2 was 51 mm long. The surface area of the 2-mm-long specimen was 7 cm², including the ends. That of the long specimens was 3 cm²/mm of length. The specimens were set in 15-mm-square holes in quartz partitions in the furnace tube. The partitions supported and positioned the specimens in the tube and caused most of the gas to flow through the channels in the specimens.

ORNL-DWG 80-1502

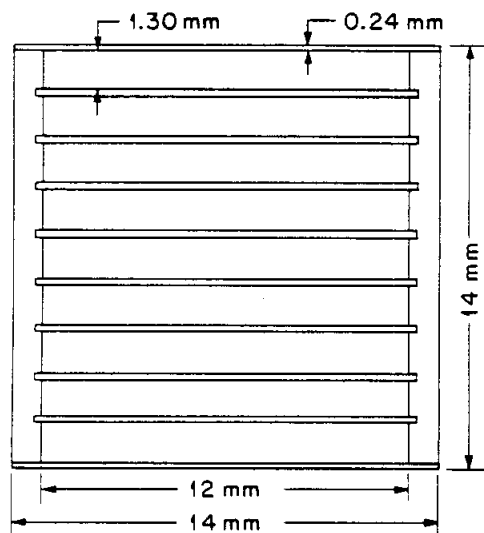


Fig. G.1. Configuration of specimens in adsorption and desorption experiments.

The total cross sectional area for flow of gas was $(9 \times 1.30 \text{ mm} \times 12 \text{ mm}) + (2 \times 1 \text{ mm} \times 14.5 \text{ mm}) = 170 \text{ mm}^2$. For the purposes of this analysis, it is acceptable to assume that the flow velocity was the same through all channels inside and outside the specimens. On this basis, 83% of the

gas passed through and 17% passed around each specimen. The experiments were run at atmospheric pressure, so the average flow velocity was

$$u = 3.3 \times 10^{-5} qT ,$$

where

u = linear velocity, cm/s;

q = gas flow, std cm³/min (at 1 atm and 298 K);

T = temperature, K .

Typically, q was 200 std cm³/min, T was 673 K, and u was 4.5 cm/s.

Flow through the specimens was laminar under the conditions of all phases of the experiment. For a typical experiment having a flow of 200 std cm³/min at 673 K,

u = gas velocity = 4.5 cm/s = 0.045 m/s;

ρ = gas density = 0.724×10^{-4} g/cm³ = 0.0724 kg/m³;

μ = gas viscosity = 0.083 lb/ft·h = 3.43×10^{-5} Pa·s;

D_e = equivalent diameter of channel = 2 × plate spacing
= 2.6 mm = 0.0026 m;

and the Reynolds' number

$$N_{Re} = \frac{0.0026 \text{ m} \times 0.045 \text{ m/s} \times 0.00724 \text{ kg/m}^3}{3.43 \times 10^{-5} \text{ Pa}\cdot\text{s}} = 0.25 .$$

In none of the experiments did the Reynolds' number exceed 1, and it was not less than 0.1 in the adsorption or desorption phases of experiments considered in this report.

The distance downstream from the entrance at which the velocity profile for laminar flow between parallel plates is fully developed is given by the relationship⁴⁰

$$(Le/2B) = 0.00648 N_{Re} ,$$

where

Le = entrance length,

B = plate spacing.

For the specimens

$$Le = 0.00648 N_{Re} \times 2.6 \text{ mm} = 0.017 N_{Re} \text{ mm} .$$

In our experiments, the velocity profile would have been fully developed in less than 0.02 mm.

In the entrance region, the heat transfer and mass transfer coefficients are greater than they are downstream where the velocity and temperature or concentration profiles are fully developed. Although the entrance lengths for heat and mass transfer may be greater than for the transfer of momentum, it is safe to assume that neither would exceed 0.1 mm for the specimens and conditions of our experiment. Since this is a small fraction of the lengths of the specimens, we need consider only the relationships for fully developed profiles in the analysis of the transport of iodine from the gas to the metal surfaces of the specimens.

In laminar flow downstream of the entrance region, the heat transfer coefficient is constant with a value that is independent of the velocity but depends on the properties of the fluid, the configuration of the channel, and whether the heat flux is constant or varies with distance along the channel. Transfer of mass is an analogous process, and mass transfer coefficients can be obtained by substituting values for the appropriate properties into relationships that have been obtained for transfer of heat. The following relationships⁴⁰ apply to the transfer of heat downstream from the entrance region when the fluid is in laminar flow in a rectangular channel having a ratio of thickness to width of 0.1, as in our specimens. For uniform heat flux

$$N_{Nu} = 7 ,$$

and for constant wall temperature

$$N_{Nu} = 6 .$$

N_{Nu} is the Nusselt number, the heat transfer coefficient multiplied by the equivalent diameter of the channel and divided by the thermal conductivity of the fluid.

For mass transfer, the Sherwood number replaces the Nusselt number:

$$N_{Sh} = \frac{k_G D}{D v} ,$$

where

- k_G = mass transfer coefficient, m/s;
 D_e = equivalent diameter of channel, m;
 D_v = diffusivity of the species being transferred in the carrier gas, m^2/s .

For uniform mass flux

$$N_{Sh} = 7 ,$$

and for constant concentration of adsorbate at the wall

$$N_{Sh} = 6 .$$

Neither of these conditions quite applies to our specimens during the experiments, but the difference between the values for N_{Sh} is small and unimportant to the analysis of the data that were obtained.

Thermodynamic equilibrium calculations reported in Appendix A indicated that the predominant iodine species in the helium in our experiments would have been HI when 50 Pa of hydrogen was present, and iodine atoms at 673 K and above if no hydrogen was present. Appreciable FeI_2 and I_2 could have been present when the iodine burden was abnormally high during parts of some experiments.

In the absence of measured values, diffusivities can be estimated by use of the equation⁴¹

$$D_G = \frac{BT^{3/2} \sqrt{(1/M_1) + (1/M_2)}}{Pr_{12}^2 I_D} ,$$

where

D_G = gas diffusivity, cm^2/s ;

M_1, M_2 = molecular weights of components 1 and 2;

$B = [10.7 - 2.46 \sqrt{(1/M_1) + (1/M_2)}] \times 10^{-4}$;

T = temperature, K;

P = absolute pressure, atm;

r_{12} = collision diameter, \AA

$$= \frac{(r_o)_1 + (r_o)_2}{2} ;$$

$$r_o = 1.18 V_o^{1/3} ;$$

V_o = molal volume of liquid at normal boiling point, $\text{cm}^3/\text{g-mol}$;

I_D = collision integral for diffusion, a function of kT/ϵ_{12} ;

$$\frac{\epsilon_{12}}{k} = \sqrt{\left(\frac{\epsilon_1}{k}\right)\left(\frac{\epsilon_2}{k}\right)} .$$

Values for the parameters in the equation (see ref. 14) and the diffusivities calculated by use of the equation are shown in Table G.1. The calculated diffusivity of $2.2 \text{ cm}^2/\text{s}$ for iodine atoms at 673 K compares with a value of $2.18 \text{ cm}^2/\text{s}$ for xenon obtained by use of an equation based on experimental data.⁴²

If we now assume a value of 6 for N_{Sh} , we obtain the values in Table G.2 for the mass transfer coefficients for the several iodine species in the channels.

Table G.1. Diffusivities of iodine species and values for parameters in equation for calculating diffusivities

	He	I	HI	I ₂	FeI ₂
M	4	127	128	254	310
$\sqrt{(1/M_1) + (1/M_2)}$		0.508	0.508	0.504	0.503
B		9.45E-4	9.45E-4	9.46E-4	9.46E-4
P	1				
V_o		37	41	71.5	82
r_o	2.70	3.9	4.1	4.98	5.1
r_{12}		3.3	3.4	3.8	3.9
ϵ/k	6.03	300	300	550	1600
ϵ_{12}/k		43	43	58	98
kT/ϵ_{12} at 673 K		16	16	12	17
at 1073 K		25	25	19	11
I_D at 673 K		0.35	0.35	0.37	0.40
at 1073 K		0.32	0.32	0.34	0.37
D_G at 673 K		2.2	2.1	1.6	1.4
at 1073 K		4.8	4.6	3.4	3.0

Table G.2. Calculated values for mass transfer coefficient

	k_G (m/s)	
	673 K	1073 K
I	0.47	1.0
HI	0.45	0.99
I ₂	0.34	0.73
FeI ₂	0.30	0.64

INTERNAL DISTRIBUTION

- | | | | |
|--------|----------------|--------|---|
| 1. | J. T. Bell | 28. | A. P. Malinauskas |
| 2-4. | R. B. Briggs | 29-33. | M. F. Osborne |
| 5. | D. O. Campbell | 34. | G. W. Parker |
| 6. | E. L. Compere | 35. | R. L. Pearson |
| 7. | W. Davis, Jr. | 36. | P. L. Rittenhouse |
| 8. | B. C. Drake | 37. | R. L. Towns |
| 9. | A. L. Harkey | 38. | D. B. Trauger |
| 10. | F. J. Homan | 39. | S. K. Whatley |
| 11. | M. J. Kania | 40-41. | R. P. Wichner |
| 12-21. | P. R. Kasten | 42. | M. E. Wadsworth (consultant) |
| 22. | T. S. Kress | 43-44. | Central Research Library |
| 23. | C. E. Lamb | 45. | ORNL-Y-12 Technical Library
Document Reference Section |
| 24. | T. B. Lindemer | 46-47. | Laboratory Records Department |
| 25. | R. A. Lorenz | 48. | Laboratory Records, ORNL R.C. |
| 26. | A. L. Lotts | 49. | ORNL Patent Section |
| 27. | J. C. Mailen | | |

EXTERNAL DISTRIBUTION

50. Director, Office of Nuclear Power Systems, U.S. Department of Energy (NE-540, GTN), Washington, D.C. 20545
51. G. A. Newby, Director, High-Temperature Reactor Program, Office of Nuclear Power Systems, U.S. Department of Energy (NE-540, GTN), Washington, D.C. 20545
52. J. E. Fox, High-Temperature Reactor Program, Office of Nuclear Power Systems, U.S. Department of Energy (NE-540, GTN), Washington, D.C. 20545
53. Assistant Manager for Energy Research and Development, U.S. Department of Energy, Oak Ridge Operations Office, Oak Ridge, TN 37830
54. Senior Program Coordinator, U.S. Department of Energy, San Francisco Operations Office - San Diego, 110 West A Street, Suite 460, San Diego, CA 92101
55. M. J. Steindler, Argonne National Laboratory, Chemical Engineering - Bldg. 205, Argonne, IL 60439
56. M. Blumeier, General Atomic Company, P. O. Box 81608, San Diego, CA 92138
57. O. P. Chawla, General Atomic Company, P. O. Box 81608, San Diego, CA 92138
58. W. E. Bell, General Atomic Company, P. O. Box 81608, San Diego, CA 92138

59. R. D. Burnette, General Atomic Company, P. O. Box 81608,
San Diego, CA 92138
60. A. W. Barsell, General Atomic Company, P. O. Box 81608,
San Diego, CA 92138
61. D. L. Hanson, General Atomic Company, P. O. Box 81608,
San Diego, CA 92138
62. L. R. Zumwalt, Nuclear Engineering Department, North Carolina
State University, Raleigh, NC 27607
63. E. M. Page, Detroit Edison, 2000 Second Avenue, Detroit, MI 48226
64. M. Plys, Room NW12-311, 138 Albany Street, Cambridge, MA 02139
65. P. R. Rowland, UKAEA, AEE, Winfrith, Dorchester, Dorset DT2,
Great Britian
66. H. J. de Nordwall, Avenue Francois Peeters 31, 1150 Bruxelles,
Belgium
67. E. Hoinkis, Hahn-Meitner-Institut, Glienicker Str. 100,
1000 Berlin 39, Germany
68. H. F. E. Feuerstein, Kernforschungszentrum Karlsruhe,
Postfach 3640, 7500 Karlsruhe, West Germany
69. H. Albrecht, Kernforschungszentrum Karlsruhe, Postfach 3640,
7500 Karlsruhe, West Germany
70. K. Münchow, KFA - Jülich, Postfach 1913, D5170 Jülich 1,
West Germany
71. B. Thiele, KFA - Jülich, Postfach 1913, D5170 Jülich 1,
West Germany
72. W. Nowak, BBC Aktiengesellschaft, Brown, Boveri, and Cie,
CH-4501 Baden/Schweiz, Switzerland
73. H. Nagao, NAIG Nuclear Research Laboratory, Nippon Atomic
Industry Group, Ltd., 4-1, Ukishima-cho, Kawasaki, Japan
- 74-223. Given distribution as shown in TID-4500 under Gas-Cooled
Reactor Technology category UC-77